LÁZARO MORATELLI JUNIOR

INTEGRATED CONTROLLER BASED ON HYBRID CONCEPT AND GEOMETRIC CONTROL FOR DYNAMICALLY POSITIONED VESSELS

SÃO PAULO
2015

LÁZARO MORATELLI JUNIOR

INTEGRATED CONTROLLER BASED ON HYBRID CONCEPT AND GEOMETRIC CONTROL FOR DYNAMICALLY POSITIONED VESSELS

Doctoral Thesis submitted for the partial fulfilment of the requirements for the degree of philosophiae doctor

SÃO PAULO
2015

LÁZARO MORATELLI JUNIOR

INTEGRATED CONTROLLER BASED ON HYBRID CONCEPT AND GEOMETRIC CONTROL FOR DYNAMICALLY POSITIONED VESSELS

Doctoral Thesis submitted for the partial fulfilment of the requirements for the degree of philosophiae doctor

Research Area:
Naval Architecture and Ocean Engineering

Supervisor: Prof. Ph.D. Hélio Mitio Morishita

SÃO PAULO
2015

Este exemplar foi revisado e corrigido em relação à versão original, sob responsabilidade única do autor e com a anuência de seu orientador.

São Paulo, 03 de Julho de 2015.

Assinatura do autor _____

Assinatura do orientador _____

Catalogação-na-publicação

Moratelli Junior, Lázaro

Integrated controller based on hybrid concept and geometric control for dynamically positioned vessels / L. Moratelli Junior. – versão corr. – São Paulo, 2015.

233 p.

Tese (Doutorado) – Escola Politécnica da Universidade de São Paulo. Departamento de Engenharia Naval e Oceânica.

1. Sistemas de posicionamento dinâmico (Controle) 2. Navios (Projeto) I. Universidade de São Paulo. Escola Politécnica. Departamento de Engenharia Naval e Oceânica II. t.

DEDICATION

To my parents Cleide and Lázaro, my sister Thaís and my brother Tiago.

ACKNOWLEDGMENTS

First and foremost, I would like to thank God for providing me health and necessary conditions to obtain the degree of Doctor of Philosophy.

I am grateful to my supervisor Prof. PhD Hélio Mitio Morishita for his teaching and guidance since 2003.

I would also like to thank Prof. PhD Eduardo Aoun Tannuri for allowing me joining to his teamwork and for his friendship.

I am thankful to Prof. PhD Alexandre Nicolaos Simos and Prof. PhD André Luis Condino Fujarra for the support that they have given to me about hydrodynamic issues.

I am also grateful to my uncles Estevo and José Bittencourt for the support that have given to me.

The financial support of the CAPES [1] scholarship from federal program of Brazilian government to incentive formation of human resources is gratefully acknowledged.

I want to thank Prof. António Manuel Santos Pascoal, Prof. PhD José Jaime da Cruz, Prof. PhD Pedro Aladar Tonelli, Prof. PhD Jessé Rebello de Souza Junior and again Prof. PhD Hélio Mitio Morishita for participating my doctoral defence and for giving me suggestions and recommendations to improve my research and the text of the thesis.

Last but not least, I am extremely grateful to my teacher Paul-Gerhard Woolcock for his text proofreading.

[1] Coordenação de Aperfeiçoamento de Pessoal de Nível Superior (CAPES)

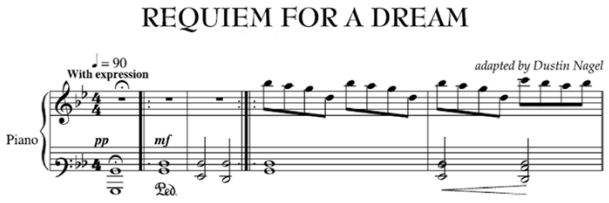

(Adapted by Dustin Nagel)
translated freely

”Whatever position you have in life, a very high or lower social condition, have always a lot of strength, determination and always do everything with love and with faith in God that one day you get there. Somehow you get there.”

(Ayrton Senna)
translated freely

”When a human being awakens to a great dream about it and throws the full force of his soul, all the universe conspires in your favor.”

(Johann Wolfgang von Goethe)
translated freely

”Stay hungry. Stay foolish.”

(Steward Brand)

ABSTRACT

The hybrid control concept is applied to the offloading operation by means of a Floating, Production, Working, Storage and Offloading (FPWSO) vessel and a Shuttle Tanker (ST). Both vessels are able to maintain their position and heading as a result of the Dynamic Positioning System (DPS). The vessels are in tandem configuration connected by a hawser. The offloading operation lasts approximately 24 hours. During this period, the sea condition may change and the drafts are being constantly altered. Hybrid controller is designed to permit modification of the controller/observer parameters should a significant sea state alteration and/or draft variation occur. The main goal of the controllers is to maintain relative positioning between vessels in order to avoid dangerous proximity or excessive hawser tension. With that in mind, a new control strategy is proposed based on differential geometry that acts integrally in both vessels. Nonlinear observers based on passivity are used to estimate position, velocity and external force ranging from calm to extreme seas. The criterion for changing the controller/observer law is based on draft and sea state. The draft is assumed to be known and sea state is estimated by tracking the peak-frequency of the first-order vessel motion spectrum. A perturbation-based model is proposed to find the number of hybrid system controllers. The equivalence between the geometric control approach and the Lagrange Multiplier (LM) - based control is demonstrated. Taking some assumptions as given, the equivalence between geometric and PD-like controllers is regarded as having also been demonstrated. The performance of the new strategy is assessed by means of numerical simulations and compared to a Proportional-Derivative (PD)-like control. The results present a very good performance as regards the proposed main goal. Result comparison of the geometric approach and the PD-like control shows very similar behavior between geometric and PD-like controllers.

Keywords: dynamic positioning, geometric control, hybrid systems

RESUMO

O conceito de controle híbrido é aplicado à operação de alívio entre um FPWSO e um navio aliviador. Ambos os navios mantêm suas posições e aproamentos pelo resultado da ação do seu Sistema de Posicionamento Dinâmico (SPD). O alívio dura cerca de 24 horas para ser concluído. Durante este período, o estado de mar pode se alterar e os calados estão sendo constantemente alterados. Um controlador híbrido é projetado para permitir modificaccões dos parâmetros de controle/observação se alguma alteração significante do estado de mar e/ou calado das embarcações ocorrer. O principal objetivo dos controladores é manter o posicionamento relativo entre os navios com o intuito de evitar perigosa proximidade ou excesso de tensão no cabo. Com isto em mente, uma nova estratégia de controle que atue integradamente em ambos os navios é proposta baseda em geometria diferencial. Observadores não lineares baseados em passividade são aplicados para estimar a posição, a velocidade e as forças externas de mares calmos até extremos. O critério para troca do controle/observação é baseado na variação do calado e no estado de mar. O calado é assumido conhecido e o estado de mar é estimado pela frequência de pico do espectro do movimento de primeira ordem dos navios. Um modelo de perturbação é proposto para encontrar o número de controladores do sistema híbrido. A equivalência entre o controle geométrico e o controlador baseado em Multiplicadores de Lagrange é demonstrada. Assumindo algumas hipósteses, a equivalência entre os controladores geométrico e o PD é também apresentada. O desempenho da nova estratégia é avaliada por meio de simulações numéricas e comparada a um controlador PD. Os resultados apresentam muito bom desempenho em função do objetivo proposto. A comparação entre a abordagem geométrica e o controlador PD aponta um desempenho muito parecido entre eles.

Palavras-chave: posicionamento dinâmico, controle geométrico, sistemas híbridos

Contents

List of Figures

List of Tables

Acronyms and Abbreviations

CAPES Coordenação De Aperfeiçoamento De Pessoal De Nível Superior.

CTAN Comprehensive TEXArchive Network.

DOF Degrees Of Freedom.

DPS Dynamic Positioning System.

FPWSO Floating, Production, Working, Storage And Offloading.

I/O Input-to-Output.

ISS Input-to-State Stability.

KF Kalman Filter.

LM Lagrange Multiplier.

MIMO Multiple-Input-Multiple-Output.

PD Proportional-Derivative.

PID Proportional-Integral-Derivative.

SISO Single-Input-Single-Output.

SNAME Society Of Naval Architects And Marine Engineers.

SPD Sistema De Posicionamento Dinâmico.

ST Shuttle Tanker.

Notation

In order to reduce the math symbology and make the reading easily, the variables, vectors and matrices are written in the following notation:

$\mathbf{M}$ is a capital bold letter that stands for matrix instead of [M].

$\boldsymbol{\nu}$ is a lower-case bold letter that stands for vector instead of $\{\vec{\nu}\}$.

$\mathbf{f}(\cdot)$ is a bold letter that stands for function of dim>1.

f$(\cdot)$ is a letter that stands for function of dim=1.

Other letters stand for variable or constant.

The text presents some variables, matrices and other math elements with the lower index i. This index refers to the vessels and the index $i = 1$ refers to the FPWSO vessel and the index $i = 2$ refers to the shuttle tanker.

The sets of the numbers are expressed as the trivial symbols such as:

$\mathbb{N}$ means the natural number set

$\mathbb{Z}$ means the integer number set

$\mathbb{R}$ means the real number set

$\mathbb{C}$ means the complex number set

The ship motions are named according to Society of Naval Architects and Marine Engineers (SNAME) convention as follows:

Degree of Freedom	Motion
1	surge (x-direction translation)
2	sway (y-direction translation)
3	heave (z-direction translation)
4	roll (x-direction rotation)
5	pitch (y-direction rotation)
6	yaw (z-direction rotation)

This thesis have been written in LaTeX with TeXnicCenter©. The bibliography style is based on AbnTeX2 from Comprehensive TeXArchive Network (CTAN).

List of Symbols

Greek Lower-case Letter

α_{c_i}	Relative angle between the current incidence angle and the vessel heading
α_{n_i}	Thruster angles of the actuator n_i
$\boldsymbol{\alpha}(\boldsymbol{x})$	Smooth function
$\boldsymbol{\alpha}_i(\boldsymbol{x})$	Smooth function
$\boldsymbol{\beta}(\boldsymbol{x})$	Smooth function
$\boldsymbol{\beta}_{ij}(\boldsymbol{x})$	Smooth function
γ	Function of class $\mathscr{K}$
γ_{w_i}	Relative angle between the wind incidence angle and the vessel heading
ϵ	Small parameter related to draft variation
$\boldsymbol{\eta}$	Global position and heading vector
$\boldsymbol{\eta}_1$	FPWSO global position and heading vector
$\boldsymbol{\eta}_2$	Shuttle tanker global position and heading vector
$\boldsymbol{\eta}_i$	Global position and heading vector for the vessel i
$\boldsymbol{\eta}_r$	Reference vector
$\boldsymbol{\eta}_w$	First-order horizontal vessel motion vector
$\boldsymbol{\eta}_0$	Set-point vector
$\boldsymbol{\lambda}$	Lagrange Multiplier vector
λ	Constant non-negative forgetting factor

$\boldsymbol{\mu}_p$ Monitoring signal

$\boldsymbol{\nu}$ Vessel velocity vector

$\boldsymbol{\nu}_1$ FPWSO velocity vector

$\boldsymbol{\nu}_2$ Shuttle tanker velocity vector

$\boldsymbol{\nu}_c$ Current vector

$\boldsymbol{\nu}_i$ Vessel velocity vector for the vessel i

$\boldsymbol{\nu}_r$ Relative velocity vector

$\boldsymbol{\nu}_{T_i}$ Translational velocity vector for the vessel i

$\boldsymbol{\xi}_1$ Internal variable vector

$\boldsymbol{\xi}_2$ Internal variable vector

ρ Process switching signal

ρ_w Water density

ρ_{air} Air density

σ Switching signal

σ_i Wave intensity parameter

ς_i Relative damping ratio

ς_{n_r} Parameter of the linear reference model

ς_{ni} Damping factor

$\varsigma_{c_{n_i}}$ Control parameter

$\overline{\boldsymbol{\tau}}_{p_i}$ External force and moment vector

$\boldsymbol{\tau_1}$ FPWSO external force and moment vector

$\boldsymbol{\tau_2}$ Shuttle tanker external force and moment vector

$\boldsymbol{\tau_c}$ Control vector with respect to body-fixed frame, named local control vector

$\boldsymbol{\tau_d}$ Force and moment vector due to the yaw damping

$\boldsymbol{\tau_e}$ Environmental force and moment vector

$\boldsymbol{\tau_h}$ Hawser force and moment vector

$\boldsymbol{\tau_i}$ External force and moment vector for the vessel i

$\boldsymbol{\tau}$	External force and moment vector
$\boldsymbol{\tau}_q$	Control output vector
$\boldsymbol{\tau}_{c_i}$	Local control vector of the vessel i
$\boldsymbol{\tau}_{cur}$	Current force and moment vector
$\boldsymbol{\tau}_d$	Demanded thrust vector
$\boldsymbol{\tau}_p$	Real thrust vector
$\boldsymbol{\tau}_{q_i}$	Switching system control vector
$\boldsymbol{\tau}_{sw}$	Force and moment vector due to the captive model
$\boldsymbol{\tau}_{wave}$	Second-order wave force and moment vector
$\boldsymbol{\tau}_{wind}$	Wind force and moment vector
χ	Mapping between σ and ρ (switching control)
ψ_1	FPWSO heading
ψ_2	Shuttle tanker heading
ψ_{10}	Set-point
ψ_{20}	Set-point
$\psi_{hf}(s)$	Transfer function of the high-pass frequency filter
ψ_i	Heading for the vessel i
ω	Vessel motion frequency
ω_{0i}	Dominating wave-frequency
ω_{ci}	Filter cut-off frequency
ω_{n_i}	Control parameter
$\omega_{r_{n_r}}$	Parameters of the linear reference model
ω_p	Peak-frequency spectrum

Greek Capital Letter

Γ	Nonlinear observer matrix

$\mathbf{\Sigma}_2$	Nonlinear observer matrix
$\Delta(x)$	Smooth distribution on manifold M
Φ	coordinate transformation
Ψ	Diagonal scaling matrix
$\mathbf{\Omega}$	Nonlinear observer matrix
$\mathbf{\Omega}_{21}$	Nonlinear observer matrix
$\mathbf{\Omega}_{22}$	Nonlinear observer matrix

Roman Lower-case Letter

$ad_f^k g(x)$	Lie bracket of order k
$\bar{\boldsymbol{b}}$	Smooth function
$\boldsymbol{b}$	External force and moment vector
$\boldsymbol{d}$	Zero-mean Gaussian white measurement noise
d	Horizontal distance between vessels
d_0	Distance set-point
d_r	Reference distance
$\mathbf{e}_p$	Error of the estimator p
d_0	Positioning error vector
$\boldsymbol{f}(\boldsymbol{x})$	Smooth vector field
$f(p)$	Tangent vector
f	Function
$f_1(\boldsymbol{x})$	Smooth function
$f_2(\boldsymbol{x})$	Smooth function
$f_3(\boldsymbol{x})$	Smooth function
$f_4(\boldsymbol{x})$	Smooth function
$\boldsymbol{g}(\boldsymbol{x})$	Smooth vector field

$\boldsymbol{g}_i(\boldsymbol{x})$ Smooth vector field

$\boldsymbol{h}$ Draft vector

$\boldsymbol{h}_i(\boldsymbol{x})$ Smooth function

h Positive constant of the hysteresis

h_i Draft of the vessel i

$h_w^i(s)$ Transfer function between a white noise signal and wave-frequency vessel motion

i Number of the vessel, being 1 for the FPWSO and 2 for shuttle tanker

k_i Offloading rate for the vessel i

k_{1i} Nonlinear observer matrix entry

k_{2i} Nonlinear observer matrix entry

k_{3i} Nonlinear observer matrix entry

l Hawser length

m_i Rigid body mass for the vessel i

m_{11_i} Surge added mass for the vessel i

m_{22_i} Sway added mass for the vessel i

m_{26_i} Sway-yaw coupled added mass for the vessel i

m_{62_i} Yaw-sway coupled added mass for the vessel i

m_{66_i} Yaw added inertia for the vessel i

$\boldsymbol{n}$ Zero-mean Gaussian white noise vector

n Controller plus observer number of the switching control

n_f Number of the filters in cascade

p Number of the estimator

q Number of the controller

r_i Relative degree

r_1 FPWSO yaw velocity

r_2 Shuttle tanker yaw velocity

r_i Yaw velocity for the vessel i

t	Time
$\boldsymbol{u}_\lambda$	Lagrangian control vector
$\boldsymbol{u}_{G_p}$	Switching system geometric control vector
$\boldsymbol{u}_G$	Geometric control law
$\boldsymbol{u}_{PD_i}$	Switching system PD-like control vector
$\boldsymbol{u}_{PD}$	PD-like control vector
$\mathbf{u}$	Control vector of the switching system
u_1	FPWSO surge velocity
u_2	Shuttle tanker surge velocity
u_i	Surge velocity for the vessel i
$\boldsymbol{v}_{\boldsymbol{T}i}$	Switching system new control vector
$\boldsymbol{v}(t)$	Control vector
$\boldsymbol{v}_i$	Switching system new control vector
$\mathbf{v}$	Input for the injected system
v_1	FPWSO sway velocity
v_2	Shuttle tanker sway velocity
v_i	Sway velocity for the vessel i
$\overline{\boldsymbol{w}}$	Disturbance vector
$\boldsymbol{w}$	Zero-mean Gaussian white noise vector
$\mathbf{w}$	Disturbance of the process (switching control)
w_h	Hawser weight per unit length
w_{n_i}	Entry of the weighting thruster matrix
$\mathbf{x}$	State space of the process
$\mathbf{x}_p$	State vector of the model set
$x(t, \epsilon)$	Solution of the perturbation model
x_1	FPWSO longitudinal position with respect to body-frame
x_2	Shuttle tanker longitudinal position with respect to body-frame

x_i	Longitudinal position with respect to body-frame for the vessel i
x_{g_i}	Longitudinal position of the gravity center for the vessel i
x_{n_i}	Longitudinal position of the actuator of the vessel i
$\boldsymbol{y}_r$	Output vector of the reference model
$\mathbf{y}$	Process output
$\mathbf{y}_p$	Output vector of the process p
y_1	FPWSO transverse position with respect to body-frame
y_2	Shuttle tanker transverse position with respect to body-frame
y_i	transverse position with respect to body-frame for the vessel i
y_{g_i}	transverse position of the gravity center for the vessel i
y_{n_i}	Transverse position of the actuator of the vessel i
$\bar{\boldsymbol{z}}_0$	System input of the reference model
$\boldsymbol{z}$	State-space vector of the linearized system
$\boldsymbol{z}_0$	Relative set-point vector
$\boldsymbol{z}_{1r}$	Internal variables of the reference model
$\boldsymbol{z}_{2r}$	Internal variables of the reference model
$\boldsymbol{z}_r$	State-space vector of the reference model
$\mathbf{z}_q$	State vector of the controller q

Roman Capital Letter

$\overline{\boldsymbol{A}}_i$	Generalized inverse matrix of the vessel i
$\boldsymbol{A_1}$	Matrices of the linear reference model
$\boldsymbol{A_2}$	Matrices of the linear reference model
$\boldsymbol{A_3}$	Matrices of the linear reference model
$\boldsymbol{A}$	MIMO linearization procedure matrix
$\boldsymbol{A}_r$	Matrices of the linear reference model

$\boldsymbol{A}_{LF}$ Switching system matrix

$\mathbf{A}_p$ Function or a matrix of the estimator p

$\mathbf{A}_{\rho\sigma}$ Functions of the injected system

A_h Cross-section of the hawser

A_{L_i} Longitudinal area projected to wind for the vessel i

A_{T_i} transverse area projected to wind for the vessel i

$\overline{\boldsymbol{B}}_i$ Actuator configuration matrix

$\boldsymbol{B}$ MIMO linearization procedure matrix

$\boldsymbol{B}_r$ Matrices of the linear reference model

$\boldsymbol{B}_{LF}$ Switching system matrix

$\boldsymbol{B}_q$ Switching system matrix

$\boldsymbol{C}_{A_1}$ FPWSO centripetal and Coriolis matrices of added inertia matrix

$\boldsymbol{C}_{A_2}$ Shuttle tanker centripetal and Coriolis matrices of added inertia matrix

$\boldsymbol{C}_{A_i}$ Centripetal and Coriolis matrices of added inertia matrix for the vessel i

$\boldsymbol{C}_A$ Centripetal and Coriolis matrices of added inertia matrix

$\boldsymbol{C}_p$ Switching system matrix

$\boldsymbol{C}_{RB_1}$ FPWSO centripetal and Coriolis matrices of rigid body matrix

$\boldsymbol{C}_{RB_2}$ Shuttle tanker centripetal and Coriolis matrices of rigid body matrix

$\boldsymbol{C}_{RB_i}$ Centripetal and Coriolis matrices of rigid body matrix for the vessel i

$\boldsymbol{C}_{RB}$ Centripetal and Coriolis matrices of rigid body matrix

$\mathscr{C}$ Family of controllers

$\mathscr{C}(\boldsymbol{\eta})$ Constraint function

$\mathscr{C}(\boldsymbol{\eta}, \boldsymbol{z}_{1_r})$ Constraint function

$\mathscr{C}_q$ Controller of the process p

$\mathbf{C}_p$ Function of the estimator p

C^∞ Atlas

C_{1i} Current force model coefficient of the vessel i

C_{2i} Current force model coefficient of the vessel i

C_{3i} Current moment model coefficient of the vessel i

C_{Ni} Wind moment model coefficient of the vessel i

C_{Xi} Wind force model coefficient of the vessel i

C_{Yi} Wind force model coefficient of the vessel i

$\boldsymbol{D}$ Linear damping matrix

$\boldsymbol{D}_k$ Matrix calculated in draft range k

$\boldsymbol{D}_1$ FPWSO linear damping matrix

$\boldsymbol{D}_2$ Shuttle tanker linear damping matrix

$\boldsymbol{E}_p$ Switching system matrix

$\boldsymbol{E}_{LF}$ Switching system matrix

E The Young modulus of the hawser

E_{max} Maximum error in the perturbation model

$\mathbf{F}_q$ Function of the controller q

$\mathbf{F}_{\rho\sigma}$ Functions of the injected system

F_{ψ_i} Yaw moment for the vessel i

F_{x_i} Surge force for the vessel i

F_{y_i} Sway force for the vessel i

$\mathbf{G}_q$ Function of the controller q

H_h Horizontal tension component of the hawser

I_{z_i} Yaw inertia of the rigid body for the vessel i

$\boldsymbol{J}(\boldsymbol{\psi}_1, \boldsymbol{\psi}_2)$ Euler angle transformation matrix

$\boldsymbol{J}_1(\boldsymbol{\psi}_1)$ FPWSO Euler angle transformation matrix

$\boldsymbol{J}_2(\boldsymbol{\psi}_1)$ Shuttle tanker Euler angle transformation matrix

$\boldsymbol{J}_i(\boldsymbol{\psi}_i)$ Euler angle transformation matrix for the vessel i

$\overline{\boldsymbol{K}}_d$ Gain matrices

$\overline{\boldsymbol{K}}_p$ Gain matrices

$\boldsymbol{K_1}$ Nonlinear observer matrix

$\boldsymbol{K_2}$ Nonlinear observer matrix

$\boldsymbol{K_3}$ Diagonal positive and the error matrix

$\boldsymbol{K_4}$ Diagonal positive and the error matrix

$\boldsymbol{K_{2_T}}$ Nonlinear observer for extrema seas matrix

$\boldsymbol{K_{2_{Ts}}}$ Switching system nonlinear observer matrix

$\boldsymbol{K_{3_T}}$ Nonlinear observer for extrema seas matrix

$\boldsymbol{K_{3_{Ts}}}$ Switching system nonlinear observer matrix

$\boldsymbol{K_{4_T}}$ Nonlinear observer for extrema seas matrix

$\boldsymbol{K_{4_{Ts}}}$ Switching system nonlinear observer matrix

$\boldsymbol{K}$ Gain matrix of feedback state

$\boldsymbol{K}_d$ Gain matrix

$\boldsymbol{K}_p$ Gain matrix

$\boldsymbol{K}_{1_s}$ Switching system nonlinear observer matrix

$\boldsymbol{K}_{2_s}$ Switching system nonlinear observer matrix

$\boldsymbol{K}_{3_s}$ Switching system nonlinear observer matrix

$\boldsymbol{K}_{4_s}$ Switching system nonlinear observer matrix

$\boldsymbol{K}_{d_k}$ Gain matrices

$\boldsymbol{K}_{LF_s}$ Switching system nonlinear observer matrix

$\boldsymbol{K}_{p_k}$ Gain matrices

$\boldsymbol{K}_{p_s}$ Switching system nonlinear observer matrix

$\mathscr{L}(\boldsymbol{\eta}, \dot{\boldsymbol{\eta}})$ Lagrangian equation

L_1 Length of the FPWSO

L_2 Length of the ST

$L_f g(x)$ Lie derivative

L_i Length of the vessel i

$\boldsymbol{M}$ Total inertia system matrix

$\boldsymbol{M}_k$	Matrix calculated in draft range k
$\boldsymbol{M}_{A_1}$	FPWSO Added inertia matrix
$\boldsymbol{M}_{A_2}$	Shuttle tanker added inertia matrix
$\boldsymbol{M}_{A_i}$	Added inertia matrix for the vessel i
$\boldsymbol{M}_A$	Total added inertia matrix
$\boldsymbol{M}_{RB_1}$	FPWSO rigid-body inertia matrix
$\boldsymbol{M}_{RB_2}$	Shuttle tanker rigid-body inertia matrix
$\boldsymbol{M}_{RB_i}$	Rigid-body inertia matrix for the vessel i
$\boldsymbol{M}_{RB}$	Total rigid-body inertia matrix
$\mathscr{M}$	Family of estimators
$\mathscr{M}_p$	Estimator of the process p
M	Manifold
N_{c_1}	FPWSO current moment
N_{c_2}	Shuttle tanker current moment
N_{c_i}	Current moment of the vessel i
N_{w_1}	FPWSO wind moment
N_{w_2}	Shuttle tanker wind moment
N_{w_i}	Longitudinal wind moment of the vessel i
$\mathscr{P}$	Set of estimators
$Pmax_{n_i}$	Maximum power of the actuator
$\mathscr{Q}$	Set of controllers
Q	Configuration manifold
Sr	Response spectra of vessel motion
$\boldsymbol{T}$	Diagonal matrix of time constants
$\boldsymbol{T}_d$	Diagonal matrix of time constants
T^*M	Cotangent space
T_pM	Tangent space

TM Tangent bundle

T Total kinetic energy of the vessels

T_f Cut-off high-frequency

$T_i(\dot{\boldsymbol{\eta}})$ Kinetic energy of the vessels

$Tmax_{n_i}$ Maximum thrust of the actuator

$\boldsymbol{U_{c_i}}$ Current velocity vector of the vessel i

U Open set

U_{c_i} Current velocity

U_{w_i} Wind velocity for the vessel i

V Open set

$\overline{\boldsymbol{W}}_i$ Weighting diagonal matrix

$\boldsymbol{W}$ Jacobian matrix of the constraint with respect to $\boldsymbol{\eta}$

$\boldsymbol{W}_{z_{1_r}}$ Jacobian matrix of the constraint with respect to $\boldsymbol{z}_{1_r}$

X Topological space

X_1 Longitudinal axis for FPWSO

$X_1Y_1Z_1$ Body-fixed frames for the FPWSO

X_2 Longitudinal axis for shuttle tanker

$X_2Y_2Z_2$ Body-fixed frames for the shuttle tanker

X_{10} Set-point of the FPWSO

X_{1r} Longitudinal reference of the FPWSO

X_{20} Set-point of the ST

X_{2r} Longitudinal reference of the ST

X_{c_1} FPWSO longitudinal current force

X_{c_2} Shuttle tanker longitudinal current force

X_{c_i} Longitudinal current force of the vessel i

X_{w_1} FPWSO longitudinal wind force

X_{w_2} Shuttle tanker longitudinal wind force

X_{w_i} Longitudinal wind longitudinal of the vessel i

Y Topological space

Y_1 transverse axis for FPWSO

Y_2 transverse axis for shuttle tanker

Y_{10} Set-point of the FPWSO

Y_{1r} Transverse reference of the FPWSO

Y_{20} Set-point of the ST

Y_{2r} Transverse reference of the ST

Y_{c_1} FPWSO transverse current force

Y_{c_2} Shuttle tanker transverse current force

Y_{c_i} transverse current force of the vessel i

Y_{w_1} FPWSO transverse wind force

Y_{w_2} Shuttle tanker transverse wind force

Y_{w_i} transverse wind force of the vessel i

Z_2 Vertical axis for shuttle tanker

Z_1 Vertical axis for FPWSO

Chapter 1

Introduction

1.1 General

Oil and gas play a strategic role in the economy of Brazil as they represent approximately 50% of total global energy consumption. Brasil has been involved in oil and gas exploration since 1950. The latest finds are located in deep waters increasingly further from the coast. As a result of this, the Brazilian offshore oil and gas industries are increasing activity. This new activity involves the use of a huge number of ocean vehicles and stationary floating units.

Distance, harsh seas, requirements for environmental damage constraints, increasing operational range and performance requirements, as well as the complexity of operations, have all challenged engineers to design the most appropriate vessels and floating units.

Semi-submersibles and vessel-like stationary floating units such as FPSOs are used for exploiting and storing oil and gas. Most of them are positioned by mooring lines. Certain units require more than one vessel to complete some of their tasks. For instance, those units receive supplies from auxiliary vessels and transfers oil to the shuttle tanker that transports it to the shore. The main concern when two or more vessels operate together is to avoid collision. Figure 1.1 shows a typical offloading operation from a FPSO to a shuttle tanker. At least one of these units possesses DPS, which is responsible for ensuring safe operation.

A DPS is a closed-loop control system that maintains vessel position and heading by means of thruster action. Although in essence simple, its design presents some challenges. The vessel dynamics mathematical model is multivariable, nonlinear and stochastic. Many vessels are overactuated and require a specific control logic to define a demanded thrust actuator. Vessel motion presents two distinct frequencies, low- and wave. The former is due to current, wind, second order forces and thrust actuators, and the latter to first-order wave forces. The controller should, in principle, suppress low-frequency motion only. Thus, the control loop needs a wave-frequency filter to feed the controller with a noiseless position and heading feedback signals.

Figure 1.1: Offloading with DP shuttle tanker (TRELLEBORG, 2012)

Up to now, DPS design has been based on single vessel operation without considering other vessel position. As a consequence, during an operation involving more than one vessel, the vessel controller only takes its own position into account, without considering those of other vessels.

A joint operation is more intricate when all vessels are controlled dynamically. In Brazil, offloading operations from a DP-FPWSO to a DP shuttle tanker have already been performed. To improve both the safety of this kind of operation and control system performance, some authors have investigated the application of cooperative control (LAPIERRE; SOETANTO; PASCOAL, 2003a; GHABCHELOO, 2007; IHLE, 2006). New system modeling to cooperative controllers by the use of Lagrangian formalism (IHLE; JOUFFRY; FOSSEN, 2006; MORATELLI JR et al., 2013) has also been investigated.

DPS observer and controller parameters are set up based on a given environmental condition

and some vessel parameters. However, during an offloading operation, typically lasting about 24 hours, sea conditions can change dramatically and vessel draft constantly vary. Both variations may materially affect vessel dynamical response. A new approach to dealing with these variations is the use of supervisory control.

1.2 Literature Review

Dynamically positioned vessels first appeared in the 1960s. Proportional-Integral-Derivative (PID) controllers with low-pass or notch filters were used to avoid wave-frequency motion counteraction (FOSSEN, 1994). Subsequently, Balchen, Jenssen and Sælid (1976) proposed low-frequency vessel motion estimation using the Kalman Filter (KF). This approach was extended by Grimble, Patton and Wise (1980), Balchen, Jenssen and Sælid (1980) and Sælid, Jenssen and Balchen (1983). However, the state estimator based on KF requires a linear model of the vessel motion equations around a set of constant yaw angles. As a consequence, the tuning of the control parameters is a time-consuming procedure and global stability can not be proved. Fossen and Strand (1999) proposed a passive nonlinear observer for vessels to overcome the linearization problem of a state estimator based on KF. This observer, in combination with a controller based on backstepping methodology, was proposed by Aarset, Strand and Fossen (1998), and Zakartchouk Jr and Morishita (2009). For the purposes of controlling DP vessels, new control approaches other tahn PID controllers have been proposed: sliding mode controller Tannuri, Donha and Pesce (2001), Tannuri (2002), Agostinho (2009), Tannuri et al. (2010); H$\propto$ (KATEBI et al., 1997; NAKAMURA; KAJIWARA, 1997; TANNURI; DONHA, 2000); and adaptive controller (TANNURI; KUBOTA; PESCE, 2006).

In recent years, the theory of cooperative control has attracted the attention of researchers around the world. This type of control allows elements, for instance cars in traffic, to exchange information. A special case of cooperative control is the formation control where many elements share the same objective of maintaining the relative formation. Observation of nature has been a great source of study and development in the establishment of state of the art formation control. For instance, the V-shaped formation of birds like ducks and geese reduces the animals' energy consumption resulting in improved aerodynamics. In addition, the formation can lead

to better communication and coordination. Some studies of attempts to reduce flight formation drag have been based on observation of the birds in flight (BADGEROW; HANSWORTH, 1981; HOERNER, 1958; WEIMERSKIRCH et al., 2001). Other animals, shoals of fish being an example, also increase locomotive efficiency by changes in their formation. Vicsek et al. (1995) applied some of these animal behavior rules in control system theory.

The use of formation control is widespread in spatial research (BEARD; LAWTON; HADAEGH, 2001; WANG; HADAEGH, 1996; REN; BEARD, 2004), aviation (PACHTER; D′AZZO; DARGAN, 1994; PACHTER; D′AZZO; PROUD, 2001) and (GIULETTI; POLLINI; INNOCENTI, 2000), military tasks (BUZOGANY; PACHTER; D′AZZO, 1993), transportation, maritime area, and robotics. General studies of the formation control can be found in Nijmeijer and Angelez (2003), Spry and Hedrick (2004), Kumar, Leonard and Morse (2005) and Børhaug (2008). Fax and Murray (2004) studied the stability of information flow with regard to the cooperative control of vehicles by use of a graph model. Girard and Hedrick (2003) proposed a surface sliding control for vehicle formation control using hybrid formalism. Behavior models can be seen in both Antonelli and Chiaverini (2004) and Stilwell and Bishop (2002).

As regards transportation on land, Sheikholeslam and Desoer (1992) studied decentralized control laws for highway congestion problems sourcing leader dynamics' information and the distance between vehicles. Aguiar et al. (1995) studied autonomous mobile robots to understand traffic control design. Bender (1991) studied Automated highway systems. The cooperative box/pushing load problem was discussed by Brock, Montana and Ceranowics (1992).

In marine applications, formation control is applied in both icebreaker escort and coordinated transportation (IHLE, 2006). Skjetne (2005) presented a maneuvering review including the theoretical aspects concerning of control objectives. Ihle (2006), Ihle, Jouffry and Fossen (2005) and Ihle, Jouffry and Fossen (2006) presented a path-following design for marine crafts using a multibody model via Lagrange Multipliers. Encarnação and Pascoal (2001) proposed an autonomous underwater vehicle obliged to track the motion of an autonomous surface craft. Breivik (2010) presented a marine craft formation control scheme in order to track targets in a leader-follower framework. Skjetne, Moi and Fossen (2002), Lapierre, Soetanto and Pascoal (2003a), Lapierre, Soetanto and Pascoal (2003b) and Skjetne, Flakstad and Fossen (2003) have all contributed marine formation control studies.

Formation control application is associated with a multibody system comprising a collection of subsystems (bodies) connected by some type of joint. A pioneer reference on multibody dynamics was presented by Wittenburg (1977). The multibody concept has many applications in the fields of aerospace exploration and robotics. Aircraft and robot equations of motion are typically derived by applying either the Newton-Euler algorithm (BALAFOUTIS; PATEL, 1991; FEARTHRSTONE, 1987; LUH; ZHENG, 1987; STEPANENKO; VUKOBRATOVIC, 1976) or Lagrange′s equations (KAHN, 1969). Some applications are also based on Hamilton′s equations (SOUZA, 2008).

Differential geometry has resulted in great innovations in the control of nonlinear mechanical systems. Sussmann (1987) presented the algebra of this theory based on Jacobi-Lie brackets which describe the vectorial fields of the dynamics equations. Abraham and Marsden (1978), Arnold (1989) and Sattinger and Weaver (1986) established a connection between mechanics and differential geometry. This link is known as Geometric Mechanics. Spivak (1999), Marsden (2004) carried out a deep analysis of differential geometry. Using the new tools based on differential geometry, Isidori (1995) and Respondek (2002) developed techniques for nonlinear feedback linearization of Single-Input-Single-Output (SISO) and Multiple-Input-Multiple-Output (MIMO) systems. Many publications concerning geometric control of mechanical systems have appeared int the last few years (SONTAG, 1998; SASTRY, 1999; JAKUBCZYK, 2001; TALMAN, 2007; OLIVA, 2002; MONFORTE, 2002; BULLO; LEWIS, 2010).

It is interesting to apply the hybrid system concept where there is some variation in plant operational conditions. A hybrid system is a dynamical system where discrete and continuous variables interac. Initial hybrid model applications were specific to the needs of the proposed problem., i.e, there was no overarching theory. Some proposals aiming to generalize the models have been presented by (YE; MICHEL; ANTSAKLIS, 1995; SCHAFT; SCHUMACHER, 2000).

The first work on hybrid systems was presented by Witsenhausen (1966). A hybrid systems and application overview can be found in Svakin and Evans (2002), Schaft and Schumacher (2000) and Sun and Ge (1989). Some articles have presented a mnore general picture of hybrid systems, such as Antsaklis (2000) and Davoren and Nerode (2000). A relevant thesis was presented by Branicky (1995) where a wide discussion of modeling, analysis and control of hybrid systems

was presented. Another significant contribution to the literature on hybrid dynamical systems can be found in Goebel, Sanfelice and Teel (2012).

The study of hybrid systems has been applied to computational science in order to control continuous processes (BAKKER et al., 1992; BENVENISTE; BERRY, 1991; HALBWACHS, 1993). Hybrid systems have been applied in process control, automated vehicles and highways (VARAIYA, 1993) and corporate planning (NAYLOR, 1982; ROSENKRANZ, 1970). Hybrid systems have also been investigated within biological and medical system contexts (AIHARA; SUZUKI, 2000).

The supervisory control is a specific application based on hybrid theory. This control is responsible for switching the hybrid system dynamic based on some type of estimator (HESPANHA, 1998; KOUTSOUKOS et al., 2000). Liberzon (2003) presented a significant review of the subject of switching systems, including stability analysis and systems with large modeling uncertainty. Switching between controllers can cause instability in some applications (LIBERZON; MORSE, 1999). Stability issues in hybrid dynamical systems are found in Decarlo et al. (2000), Michel and Wang (1995), Or and Ames (2001), Sanfelice, Goebel and Teel (2007) and Ye, Michel and Hou (1998). In marine applications, Smogeli, Sorensen and Fossen (2004) developed a hybrid controller to control those thrusters that combine different operational loads. Dong (2005) proposed a hybrid controller for vessels with dynamic positioning systems.

1.3 Objective of the Thesis

Consider a DP-FPWSO and a DP-shuttle tanker in tandem configuration during an offloading operation. The objective is to propose a new control strategy by designing an integrated hybrid controller for a multibody system consisting of both vessels. This means that the control law for each DPS is defined by considering the dynamics of the whole system. The controller integration is established by means of the geometric control theory where the control law is found via Input-to-Output (I/O) exact linearization for Multiple-Input-Multiple-Output (MIMO).

A comprehensive time-varying low-frequency model for the 6 DOF multibody system (horizontal motions of two vessels) is developed by applying Kirchhoff equations. The main concern of this

model is to best express the draft influence on both vessel inertia and environmental forces and moments. Controller design is facilitated by means of a simplified dynamical model.

Controller design is preceded by an analysis of some control approach alternatives. These alternatives based on geometric control, Lagrangian and conventional PD-like controller are analytically compared. As a result of this comparison, the equivalence between the Lagrangian based and differential geometric approaches is proved when the Lagrange formalism constraint is equal to the geometric control output. Furthermore, the similarity between the differential geometry controller and the PD-like structure is demonstrated in the case of low-speed vessel motions and the constant reference. For the purposes of observing and filtering, the wave-frequency vessel motions are filtered and the system state vector is estimated by a nonlinear state observer where the sea state is calm to moderate. In case of extreme seas, nonlinear observer for extreme seas without wave-frequency model is applied.

The hybrid concept is used in the evaluation of performance degradation of both observer and controller. This degradation occurs due to huge variations in draft vessel and changing sea condition parameters during the offloading operation. Vessel drafts and sea condition parameters need to be estimated in order to retune controller and observer parameters. This is not a gain schedule problem since the nonlinear observer model has its structure modified as a function of sea conditions (wave-frequency model or extreme sea observer).

Retuning only occurs in the case of a discrete variation in observer parameters. A perturbation based algorithm is proposed to determine the number of draft ranges. Sea conditions are evaluated by the wave peak-frequency of the sea spectrum. As the on-board measurement of this parameter is quite difficult, the peak-frequency of the wave-frequency vessel motions is estimated through spectral analysis.

Assessment of hybrid controller performance is carried out by means of numerical simulations. The main results analyzed are relative distance between vessels and hybrid controller performance (switch between controllers). Results obtained from the PD-like controller are also presented for comparison purposes.

1.4 Organization of the Text

Chapter 1 presents the main reasons for studying the control of two vessels during an offloading operation. The literature review presents the state of the art as regards dynamic positioning systems, geometric control, hybrid dynamics and multibody systems. Thesis objectives are summarized in Section 1.3.

Chapter 2 describes the time-varying plant mathematical model. The model comprises the kinematic and dynamic equations for low-frequency motions as well as a time-series for the wave-frequency vessel motions. The models employed in the calculation of environmental forces and moments are presented here.

Chapter 3 discusses the hybrid control concept's hierarchical structure. The main goal is to describe both the supervisory control operation and the hybrid concept elements, such as the multi-estimator-based supervisor, switching logic and hysteresis logic.

Chapter 4 presents the well-known dynamic positioning system and its subsystems. The non-linear observers to be used are here presented in detail. The control strategy for the offloading operation between the FPWSO and the shuttle tanker is established. The geometric approach, the Lagrange Multiplier-based controller and PD-like control are dealt with here. The equivalence between geometric and Lagrangian strategies is demonstrated. On some assumptions, the geometric and PD-like controllers are considered to have had their equivalence demonstrated. The thrust allocation logic and the thruster dynamics are introduced in this section.

Chapter 5 presents the hybrid control concept applied to the control strategy discussed in Chapter 4. The reference is made to the observer models based on sea conditions (wave-frequency model and extreme sea). A discussion as to how best to determine the number of controllers in the control set, by means of the perturbation method, can be found here. This is followed by a presentation of how the wave-peak frequency tracker and draft survey monitoring are used in supervisory control.

Chapter 6 presents the designed hybrid control results when used in Brazilian waters. Geometric controller and PD-like performance is evaluated by means of the set-point and relative distance change. Some short-term environmental scenarios are established for assessing hybrid controller

performance when vessel drafts are constant. One long-term environmental scenario is used to evaluate the control strategy performance for a complete offloading operation.

Final conclusions and suggestions for further research are presented in Chapter 7.

Chapter 2

Ship Kinematics and Dynamics

Vessel motions can be described by 3-DOF[3] with respect to global and/or local frames. Using vessel kinematics and dynamics based on those 3-DOF, mathematical model is obtained for specific purposes. Sørensen (2005) discusses two different purposes: plant model and control model. The former model tries to approximate system dynamics as closely as possible to the real system mechanics. In the latter model, some simplifications are assumed to facilitate control design.

Chapter 2 presents plant model construction using the vessels' kinematics and dynamics. The resultant system dynamics is well-known and has been discussed by Fossen (1994), Lewandowski (2004) and Sørensen (2005). However, the vessels intended to be modeled here have a certain peculiarity. During offloading, their drafts will vary due to the oil transfer process. From a mechanics perspective, the vessels are described as variable mass systems. Recently, variable mass system mechanics has been the subject of considerable academic research. The dynamics of variable mass systems is addressed by Irschik and Holl (2004),Pesce, Tannuri and Casetta (2006), Pesce and Casetta (2007), Casetta (2008) and Pesce (2013).

The vessels' mass (FPWSO and ST) is assumed to be time-dependent and their dynamics are modeled using the Kirchhoff equation. The resultant dynamics is written as a unified model regarding both vessels as a multibody system. This interpretation is proposed by Ihle (2006).

[3]Degrees of Freedom (DOF)

2.1 Kinematics

Consider two vessels (FPWSO and shuttle tanker) in tandem configuration connected by a hawser as presented in Figure 2.1. Vessel motions are described with respect to both global and local frames. Kinematics equations are used to transform the body-fixed coordinates into Earth-fixed coordinates or vice versa. There are three frames, one Earth-frame and two body frames as follows:

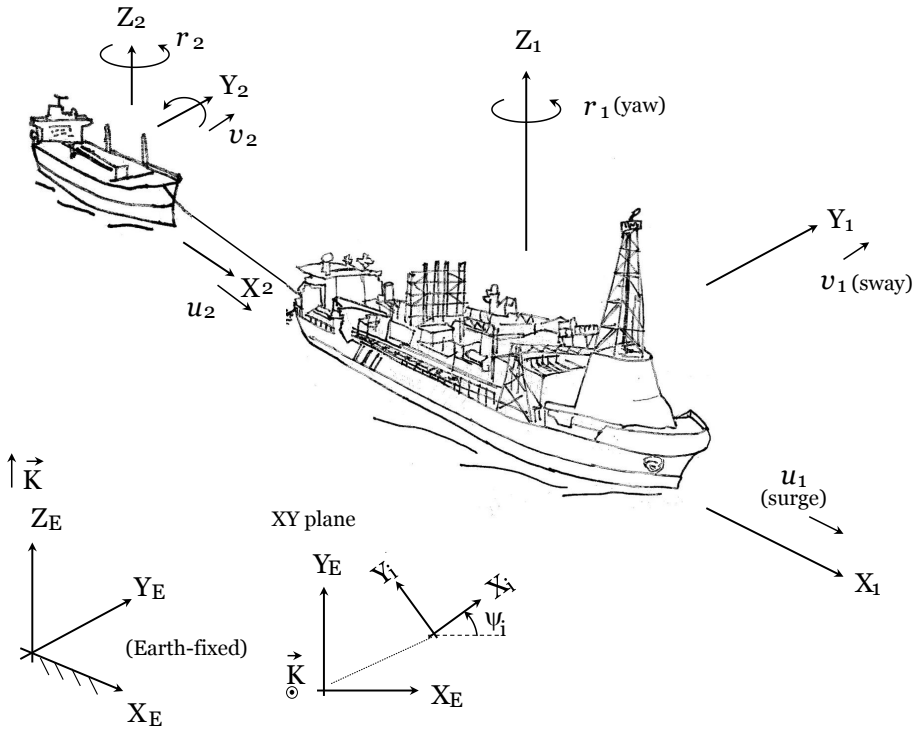

Figure 2.1: Reference frames for vessels

Earth-fixed reference frame: The Earth-fixed reference frame is written as $X_E Y_E Z_E$, defined as positively-oriented orthonormal and assumed to be inertial.

Body-fixed frames: Let $X_1 Y_1 Z_1$ and $X_2 Y_2 Z_2$ be the body-fixed frames for the FPWSO and the shuttle tanker, fixed in the gravity center of each vessel, respectively. The longitudinal axes X_1 and X_2 are directed from aft to fore. The transverse axes Y_1 and Y_2 are directed to port side. The normal axes Z_1 and Z_2 to the $X_1 Y_1$ and $X_2 Y_2$ planes are directed from bottom to top.

The total global position and heading vector $\boldsymbol{\eta} \in \mathbb{R}^6$ are defined as $\boldsymbol{\eta} = [\ \boldsymbol{\eta}_1^T \quad \boldsymbol{\eta}_2^T\ ]^T$, where

$\boldsymbol{\eta}_i = [\ x_i \quad y_i \quad \psi_i\ ]^T$ with $i = 1, 2$ being the FPWSO and shuttle tanker, respectively, and x_i, y_i and ψ_i being the horizontal positions and heading, respectively.

The total local velocity vector $\boldsymbol{\nu} \in \mathbb{R}^6$ is defined as $\boldsymbol{\nu} = [\ \boldsymbol{\nu}_1^T \quad \boldsymbol{\nu}_2^T\ ]^T$, where $\boldsymbol{\nu}_i = [\ u_i \quad v_i \quad r_i\ ]^T$ with u_i, v_i and r_i being the surge and sway velocities and the yaw velocity, respectively. The Euler angle transformation matrix $\boldsymbol{J}(\boldsymbol{\psi}_1, \boldsymbol{\psi}_2) \in \mathbb{R}^{6x6}$ that transforms local velocity vectors into the global velocity vectors is described as follows

$$\dot{\boldsymbol{\eta}} = \boldsymbol{J}(\boldsymbol{\psi}_1, \boldsymbol{\psi}_2)\boldsymbol{\nu} = \begin{bmatrix} \boldsymbol{J}_1(\boldsymbol{\psi}_1) & \mathbf{0}_{3x3} \\ \mathbf{0}_{3x3} & \boldsymbol{J}_2(\boldsymbol{\psi}_2) \end{bmatrix} \boldsymbol{\nu} \tag{2.1}$$

The transformation matrix $\boldsymbol{J}_i(\boldsymbol{\psi}_i) \in \mathbb{R}^{3\times3}$ of the special orthogonal group $\boldsymbol{SO}(3)$ is described as

$$\boldsymbol{J}_i(\boldsymbol{\psi}_i) = \begin{bmatrix} c\psi_i & s\psi_i & 0 \\ -s\psi_i & c\psi_i & 0 \\ 0 & 0 & 1 \end{bmatrix} \tag{2.2}$$

where c·=cos(·) and s·=sin(·).

2.2 Vessel Dynamics

The offloading operation is very slow taking 24h to complete. The vertical motion here is not a dynamical response on the part of the vessel, but a quasi-static draft variation with a very low rate. Hence, added inertia has been calculated by assuming it to be dependent on draft only. This means that occasional temporal and draft variation influences were not considered in its calculation. Hence, the kinetic energy of the systems can be written in quasi-coordinates (MEIROVITCH, 1970; FOSSEN, 1994) as

$$T = \frac{1}{2}\boldsymbol{\nu}^{\boldsymbol{T}}\boldsymbol{M}(t)\boldsymbol{\nu} = \frac{1}{2}\boldsymbol{\nu}^{\boldsymbol{T}}\left[\boldsymbol{M}_{RB}(t) + \boldsymbol{M}_A(t)\right]\boldsymbol{\nu} \tag{2.3}$$

where T is the total kinetic energy of the vessels, $\boldsymbol{M}(t) \in \mathbb{R}^{6\times6}$ is the total inertia matrix of systems, $\boldsymbol{M}_{RB}(t) \in \mathbb{R}^{6\times6}$ is the inertia of the rigid body, $\boldsymbol{M}_A(t) \in \mathbb{R}^{6\times6}$ is the added inertia

matrix and t is the time. The rigid body inertia matrix is described as

$$\boldsymbol{M}_{RB}(t) = \begin{bmatrix} \boldsymbol{M}_{RB_1}(t) & \mathbf{0}_{3x3} \\ \mathbf{0}_{3x3} & \boldsymbol{M}_{RB_2}(t) \end{bmatrix} \tag{2.4}$$

$$\boldsymbol{M}_{RB_i}(t) = \begin{bmatrix} m_i(t) & 0 & -m_i(t).y_{g_i} \\ 0 & m_i(t) & m_i(t).x_{g_i} \\ -m_i(t).y_{g_i} & m_i(t).x_{g_i} & I_{z_i}(t) \end{bmatrix} \tag{2.5}$$

where $\boldsymbol{M}_{RB_i}(t) \in \mathbb{R}^{3\times3}$ is the rigid body inertia matrix, $m_i(t)$ and $I_{z_i}(t) \in \mathbb{R}$ being the rigid body mass and yaw inertia of the rigid body, respectively. The variables x_{g_i} and y_{g_i} are the longitudinal and transverse positions of the gravity center. The longitudinal center of the vessels has a little variation so it is considered constant and fixed at the midship. Due to the ships' symmetry, transverse position of the gravity center is considered to be at the centerline. The added inertia matrix is described as

$$\boldsymbol{M}_{A}(t) = \begin{bmatrix} \boldsymbol{M}_{A_1}(t) & \mathbf{0}_{3x3} \\ \mathbf{0}_{3x3} & \boldsymbol{M}_{A_2}(t) \end{bmatrix} \tag{2.6}$$

$$\boldsymbol{M}_{A_i}(t) = \begin{bmatrix} m_{11_i}(t) & 0 & 0 \\ 0 & m_{22_i}(t) & m_{26_i}(t) \\ 0 & m_{62_i}(t) & m_{66_i}(t) \end{bmatrix} \tag{2.7}$$

where $\boldsymbol{M}_{A_i}(t) \in \mathbb{R}^{3\times3}$ is the added inertia for the vessel, $m_{11_i}(t)$, $m_{22_i}(t)$, $m_{26_i}(t)$, $m_{62_i}(t)$ and $m_{66_i}(t)$ are the added mass to surge, sway, sway-yaw coupled, yaw-sway coupled, yaw added inertia, respectively. These variables depend on the motion frequency. Due to the fact that DPS needs to act upon only the second-order effects, the added inertia matrix is assumed to be calculated with vessel motion frequency $\omega \to 0$. For low velocities, $m_{26_i}(t)$ is assumed to be equal to $m_{62_i}(t)$. To obtain ship dynamics, consider the following Kirchhoff equations

$$\frac{d}{dt}\left(\frac{\partial T}{\partial \boldsymbol{\nu}_{T_i}}\right) + \boldsymbol{r}_i \times \frac{\partial T}{\partial \boldsymbol{\nu}_{T_i}} = \begin{bmatrix} F_{x_i} & F_{y_i} \end{bmatrix}^T \tag{2.8}$$

$$\frac{d}{dt}\left(\frac{\partial T}{\partial \boldsymbol{r}_i}\right) + \boldsymbol{r}_i \times \frac{\partial T}{\partial \boldsymbol{r}_i} + \boldsymbol{\nu}_{T_i} \times \frac{\partial T}{\partial \boldsymbol{\nu}_{T_i}} = F_{\psi_i} \tag{2.9}$$

where $\boldsymbol{\nu}_{T_i} = \begin{bmatrix} x_i & y_i \end{bmatrix}^T$ is the translational velocity vector. The variables F_{x_i}, F_{y_i} and $F_{\psi_i} \in \mathbb{R}$ are the surge and sway external forces and the yaw moment, respectively. Replacing (2.3) with (2.8) and (2.9), considering a linear damping due to the relative velocity between current and

vessel, and neglecting terms of second-order yields

$$\boldsymbol{M}(t)\dot{\boldsymbol{\nu}} + (\dot{\boldsymbol{M}}_{RB}(t) + \boldsymbol{C}_{RB}(t))\boldsymbol{\nu} + (\dot{\boldsymbol{M}}_{A}(t) + \boldsymbol{C}_{A}(t)(\boldsymbol{\nu}_r))\boldsymbol{\nu}_r = \boldsymbol{\tau} = \boldsymbol{\tau}_e + \boldsymbol{\tau}_h + \boldsymbol{\tau}_c \tag{2.10}$$

where $\boldsymbol{C}_{RB}(t)$ and $\boldsymbol{C}_{A}(t) \in \mathbb{R}^{6\times6}$ are the centripetal and Coriolis matrices of rigid body and added inertia, respectively. The vector $\boldsymbol{\nu}_r \in \mathbb{R}^6$ is relative velocity vector. The external force vector is $\boldsymbol{\tau} = [\ \boldsymbol{\tau}_1^T \quad \boldsymbol{\tau}_2^T\ ]^T \in \mathbb{R}^6$ where $\boldsymbol{\tau}_i = [\ F_{x_i} \quad F_{y_i} \quad F_{\psi_i}\ ]^T$. The vectors $\boldsymbol{\tau}_e$, $\boldsymbol{\tau}_h$ and $\boldsymbol{\tau}_c \in \mathbb{R}^6$ are the environmental force and moment, the hawser force and moment and the local control vectors, respectively. The centripetal and Coriolis matrices and the relative velocity vector are defined as

$$\boldsymbol{C}_{RB}(t) = \begin{bmatrix} \boldsymbol{C}_{RB_1}(t) & \boldsymbol{0}_{3x3} \\ \boldsymbol{0}_{3x3} & \boldsymbol{C}_{RB_2}(t) \end{bmatrix} \tag{2.11}$$

$$\boldsymbol{C}_{RB_i}(t) = -\begin{bmatrix} 0 & 0 & -m_i(t)(x_{g_i}.r_i + v_i) \\ 0 & 0 & m_i(t).u_i \\ m_i(t)(x_{g_i}.r_i + v_i) & -m_i(t).u_i & 0 \end{bmatrix} \tag{2.12}$$

$$\boldsymbol{C}_{A}(t) = \begin{bmatrix} \boldsymbol{C}_{A_1}(t) & \boldsymbol{0}_{3x3} \\ \boldsymbol{0}_{3x3} & \boldsymbol{C}_{A_2}(t) \end{bmatrix} \tag{2.13}$$

$$\boldsymbol{C}_{A_i}(t) = -\begin{bmatrix} 0 & 0 & (m_{22_i}(t)v_i + m_{26_i}(t)r_i) \\ 0 & 0 & -m_{11_i}(t)u_i \\ -(m_{22_i}(t)v_i + m_{26_i}(t)r_i) & m_{11_i}(t)u_i & 0 \end{bmatrix} \tag{2.14}$$

$$\boldsymbol{\nu}_r = \boldsymbol{\nu} - \boldsymbol{\nu}_c \tag{2.15}$$

where $\boldsymbol{C}_{RB_i}(t)$ and $\boldsymbol{C}_{A_i}(t) \in \mathbb{R}^{3\times3}$ and $\boldsymbol{\nu}_c \in \mathbb{R}^6$ are the centripetal and Coriolis rigid bodies matrix, the centripetal and Coriolis added inertia matrix and the current vector, respectively.

Let us suppose that oil mass flow rate during offloading is time-invariant and that the waterline plane of the vessels does not change with the drafts. Hence, the draft variation can be written $dh_i/dt = k_i$, where k_i is the offloading rate and $h_i(t)$ is the vessel draft. Thus, the time-derivative of the rigid body and the added inertia matrices can be written as

$$\dot{\boldsymbol{M}}_{RB_i}(t) = \frac{\partial \boldsymbol{M}_{RB_i}(t)}{\partial h_i}\frac{dh_i}{dt} \tag{2.16}$$

$$\dot{\boldsymbol{M}}_{A_i}(t) = \frac{\partial \boldsymbol{M}_{A_i}(t)}{\partial h_i}\frac{dh_i}{dt} \tag{2.17}$$

The partial derivatives in (2.16) and (2.17) can be found from the curves of the matrix elements $\boldsymbol{M}_{RB}(h)$ and $\boldsymbol{M}_{A}(h)$ with respect to draft. These curves of the matrix elements are shown in Appendix A.

The control model assumes that vessel motion velocities are very low. Thus, the centripetal and Coriolis matrices can be neglected and a linear damping is assumed. The inertia time-derivative and damping matrices are both assumed to be null. So, the control model is written as

$$\boldsymbol{M}\dot{\nu} + \boldsymbol{D}\nu = \boldsymbol{\tau}_e + \boldsymbol{\tau}_h + \boldsymbol{\tau}_c \tag{2.18}$$

$$\boldsymbol{D} = \begin{bmatrix} \boldsymbol{D}_1 & \boldsymbol{0}_{3x3} \\ \boldsymbol{0}_{3x3} & \boldsymbol{D}_2 \end{bmatrix} \tag{2.19}$$

where $\boldsymbol{D} \in \mathbb{R}^{6\times6}$ is the linear damping matrix of the system. The matrix entries $\boldsymbol{D}_1$ and $\boldsymbol{D}_2$ are calculated as presented in Appendix A. It is pointed out that both the inertia and damping matrices are assumed to be constant for some draft ranges.

Due to the low draft variation of the vessels, control model of the system with a constant matrix is reasonable within a certain draft range. The matrices $\boldsymbol{M}$ and $\boldsymbol{D}$ are used by the hybrid control to generate the control model for a specific state observer and control law. When positioning error exceeds a certain predefined limit, the inertia and damping matrices are updated in observer and control laws. Chapter 5 presents the hybrid concept applied to offloading operation.

2.3 Wave-Frequency Motion

The first-order horizontal vessel motions $\boldsymbol{\eta}_w \in \mathbb{R}^{6x6}$ are simulated by the time realization of the response spectra Sr derived from the cross spectrum. These motions are calculated using the RAO (RAO) and sea spectrum (LEWIS, 1990). See details in Appendix C.

2.4 Environmental and External Forces

The WMO (World Meteorological Organization) recommendations have been adopted. The notation of the waves obeys the following orientation:

- Wind and wave direction indicates where the wind and wave come from (True North origin; clockwise rotation).
- Current direction indicates flow direction (same North as before)
- North is associated with 0° direction and East with 90°.

The environmental force and moment vector $\boldsymbol{\tau}_e \in \mathbb{R}^6$ includes forces and moments that come from the action of current, second-order wave effect and wind such as

$$\boldsymbol{\tau_e} = \boldsymbol{\tau_{cur}} + \boldsymbol{\tau_{wave}} + \boldsymbol{\tau_{wind}} \tag{2.20}$$

where $\boldsymbol{\tau}_{cur}$, $\boldsymbol{\tau}_{wave}$ and $\boldsymbol{\tau}_{wind} \in \mathbb{R}^6$ are the current, second-order wave and wind force and moment vectors, respectively. Despite the fact that the FPWSO is connected to a riser, the forces and moments of this connection are not included in the model.

2.4.1 Current

The model of the forces and moments due to current is proposed by Leite et al. (1998). The current force and moment model used here also considers the model that was extended from Leite et al. (1998) by Simos et al. (2001) for the purposes of including terms of damping caused by yaw. The current force and moment vector $\boldsymbol{\tau_{cur}} \in \mathbb{R}^6$ is written as

$$\boldsymbol{\tau_{cur}} = \boldsymbol{\tau_{sw}} + \boldsymbol{\tau_d} \tag{2.21}$$

where $\boldsymbol{\tau}_{sw}$ and $\boldsymbol{\tau}_d \in \mathbb{R}^6$ are the force and moment vectors due to the captive model and yaw damping, respectively. The vector $\boldsymbol{\tau}_d$ is calculated using the model proposed by Simos et al.

(2001). The forces and moments from the captive model are calculated according to

$$\boldsymbol{\tau_{sw}} = [\ X_{c_1} \quad Y_{c_1} \quad N_{c_1} \quad X_{c_2} \quad Y_{c_2} \quad N_{c_2}\ ]^T \tag{2.22}$$

$$X_{c_i}(\alpha_{c_i}) = \frac{1}{2}\rho_w h(t) L_i C_{1i}(\alpha_{c_i}) U_{c_i}^2 \tag{2.23}$$

$$Y_{c_i}(\alpha_{c_i}) = \frac{1}{2}\rho_w h(t) L_i C_{2i}(\alpha_{c_i}) U_{c_i}^2 \tag{2.24}$$

$$N_{c_i}(\alpha_{c_i}) = \frac{1}{2}\rho_w h(t) L_i C_{3i}(\alpha_{c_i}) U_{c_i}^2 \tag{2.25}$$

$$\boldsymbol{U_{c_i}} = U_{c_i}.[cos(\alpha_{c_i})\vec{i} + sin(\alpha_{c_i})\vec{j}] \tag{2.26}$$

where X_{c_i}, Y_{c_i} and $N_{c_i} \in \mathbb{R}$ and are longitudinal and transverse current forces and the moment with respect to body-frame. The relative angle $\alpha_{c_i} \in \mathbb{R}$ is the angle between the current incidence angle and the vessel heading. The variables $U_{c_i} \in \mathbb{R}$, $\boldsymbol{U_{c_i}} \in \mathbb{R}^2$, ρ_w and $L_i \in \mathbb{R}$ are current velocity, current velocity vector, water density and ship length. The current force and moment coefficients C_{1i}, C_{2i} and $C_{3i} \in \mathbb{R}$ are defined by Leite et al. (1998).

2.4.2 Wind

The wind force and moment vector $\boldsymbol{\tau_{wind}} \in \mathbb{R}^6$ is calculated in line with proposals made by OCIMF (1977) according to

$$\boldsymbol{\tau_{wind}} = [\ X_{w_1} \quad Y_{w_1} \quad N_{w_1} \quad X_{w_2} \quad Y_{w_2} \quad N_{w_2}\ ]^T \tag{2.27}$$

$$X_{w_i} = \frac{1}{2}\rho_{air} A_{T_i}(t) C_{Xi}(\gamma_{w_i}) U_{w_i}^2 \tag{2.28}$$

$$Y_{w_i} = \frac{1}{2}\rho_{air} A_{L_i}(t) C_{Yi}(\gamma_{w_i}) U_{w_i}^2 \tag{2.29}$$

$$N_{w_i} = \frac{1}{2}\rho_{air} A_{L_i}(t) C_{Ni}(\gamma_{w_i}) U_{w_i}^2 \tag{2.30}$$

where X_{w_i}, Y_{w_i} and N_{w_i} $\mathbb{R}$ are the longitudinal and transverse wind forces and the moment with

respect to body-frame. The relative angle $\gamma_{w_i} \in \mathbb{R}$ is the angle between the wind incidence angle and the vessel heading. The variables U_{w_i}, ρ_{air}, A_{L_i} and $A_{T_i} \in \mathbb{R}$ are wind velocity, air density and projected lateral and transverse areas. These areas are presented in Appendix A. The wind force and moment coefficients C_{Xi}, C_{Yi} and $C_{Ni} \in \mathbb{R}$ are defined by OCIMF (1977).

2.4.3 Second-Order Wave Forces and Moments

The second-order wave forces and moment play an important role in the DP system. They induce low-frequency vessel motions that need to be taken into account by the DP controller. These forces and moments are composed of slow-drift and mean-drift forces and moments as well as wave-drift damping effects (result of wave-current interaction). These effects are calculated in accordance with Aranha and Fernandes (1995) and Aranha (1996).

2.4.4 Hawser Forces and Moments

Forces and moments resulting from the hawser connected between the vessels are estimated by a catenary equation. In order to estimate this, horizontal distance is related to hawser tension as follows (IRVINE, 1981)

$$d = \frac{H_h l}{E A_h} + 2\frac{H_h}{w_h} sinh^{-1}(\frac{w_h l/2}{H_h}) \tag{2.31}$$

where d and $H_h \in \mathbb{R}$ are the horizontal distance between vessels and the horizontal tension component, respectively. The variables w_h and $l \in \mathbb{R}$ are the hawser weight per unit length and hawser length, respectively. The Young modulus and the cross-section are the variables E and $A_h \in \mathbb{R}$, respectively.

Chapter 3

Hybrid Control Concept

3.1 General

Hybrid systems are dynamical systems with discrete and continuous variables interacting. The proposal is to use the hybrid controller, known as the switching control system (HESPANHA, 2002), in order to change the controller and the observer laws of two DP vessels. The switching control monitors some continuous system variables, and commands a switcher that changes controller by means of a discrete signal. For the offloading operation, sea state and draft variations are used to switch controller parameters and observer models. To introduce hybrid control, the basic concepts of switching systems are presented, including required system properties, hysteresis logic and stability issues. Important decisions to be made when designing the hybrid controller are the number of controllers and observers that will be available to the switching control. A perturbation model is proposed to address this controller and observer number issue.

3.2 Basic concepts

The switching control is a set of dynamical subsystems responsible for changing the controller of a system when some important event occurs. The switching controller is composed of a

set of controllers (known as the multi-controller) which is supervised by a superior controller (supervisor) that compares the some estimates to the plant. A switching signal included in the supervisor chooses the best controller to control the process. This idea is presented in Figure 3.1.

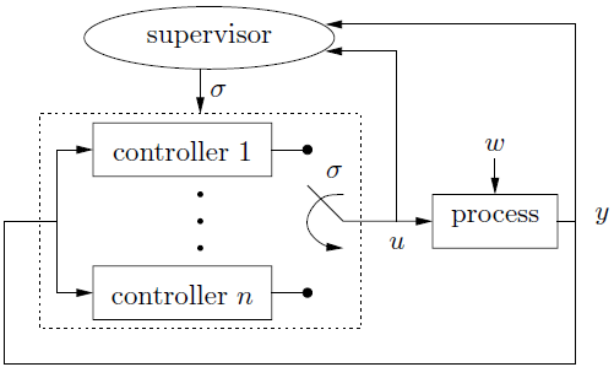

Figure 3.1: Hybrid control concept

The supervisor controller consists of estimators (multi-estimator) that estimates each output of the n controllers plus observers. Each estimate is compared to the process output $\mathbf{y}$. The multi-estimator is a set that describes a family

$$\mathscr{M} := \bigcup_{p \in \mathscr{P}} \mathscr{M}_p \tag{3.1}$$

$$\mathscr{M}_p := \{\dot{\mathbf{x}}_p = \mathbf{A}_p(\mathbf{x}_p, \mathbf{u}, \mathbf{y}), \mathbf{y}_p = \mathbf{C}_p(p, \mathbf{x}_p, \mathbf{u}, \mathbf{y}) : p \in \mathscr{P}\} \tag{3.2}$$

where $\mathscr{P}$ is the set of estimators ($\mathbb{E}$) and p is the number of the estimator. The state vector of the model set is $\mathbf{x}_p$, $\mathbf{y}_p$ is the estimated vector of the p^{th} estimator, $\mathbf{u}$ is the control vector and $\mathbf{A}_p$ and $\mathbf{C}_p$ are functions. The family of the estimators is $\mathscr{M}$ with $\mathscr{M}_p$ estimators. Controller switching is performed by a switcher that receives the switching signal σ from the supervisory control. Similarly to the multi-estimator, the controller set defines a family as

$$\mathscr{C} := \bigcup_{q \in \mathscr{Q}} \mathscr{C}_q \tag{3.3}$$

$$\mathscr{C}_q := \{\dot{\mathbf{z}}_q = \mathbf{F}_q(\mathbf{z}_q, \mathbf{y}), \mathbf{u} = \mathbf{G}_q(\mathbf{z}_q, \mathbf{y}) : q \in \mathscr{Q}\} \tag{3.4}$$

where $\mathscr{Q}$ is the set of controllers and q is the number of the controller. The state vector of the controller is $\mathbf{z}_q$ with $\mathbf{F}_q$ and $\mathbf{G}_q$ being functions. The family of the controllers is $\mathscr{C}$ with $\mathscr{C}_q$ controllers. There is a process switching signal ρ which determines the selected control model in the supervisor. The switching signal σ from the supervisory control may be different from the signal ρ. Hence, there is a mapping $\sigma = \chi(\rho) \in \mathscr{Q}$, $\rho \in \mathscr{P}$. This means that the controller number could be different from the observer number. This work assumes the mapping $\sigma = \rho \in \mathscr{P} \equiv \mathscr{Q}$ which means that each ensuing pair is made up of one controller and one observer. The formal definition of a switched system is presented as follows.

Definition 3.1 Switched system − (HESPANHA, 2002). The switched system includes the process, controller set, and the estimator set

$$\dot{\mathbf{x}} = \mathbf{A}_\sigma(\mathbf{x}, \mathbf{w}) \tag{3.5}$$

$$\mathbf{e}_p = \mathbf{C}_p(\mathbf{x}, \mathbf{w}), \quad \rho \in \mathscr{P} \tag{3.6}$$

where $\mathbf{x}$ denotes the state of the process and $\mathbf{w}$ is the disturbance. The supervisor possesses both process switching ($\mathbb{PS}$) and switching logic ($\mathbb{S}$) in order to generate the signal σ to switch to the best controller. Switching logic prevents chattering (high frequency of σ changing) of the switching signal. Process monitoring is presented in Figure 3.2, where $\mathbf{y}_p$ is the output of the estimator p, $\mathbf{e}_p$ is the error of the estimator p and $\boldsymbol{\mu}_p$ is the monitoring signal of the estimator p.

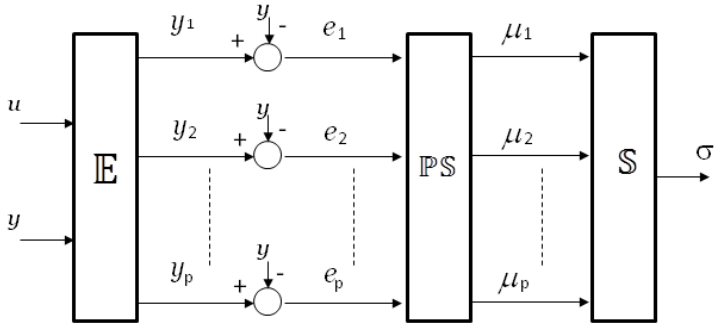

Figure 3.2: Monitoring signal process

3.3 Supervisory Properties

To guarantee correct switching between controllers, Hespanha (2002) presented two important properties of the switching system: matching and detectability. The matching property means there is an estimator with output $\mathbf{y}_p$ that provides a good approximation of the output of the process p. Detectability means that the switching system must be detectable with respect to $\mathbf{e}_p$ for each controller $\chi(p) \in \mathscr{Q}$. These properties are summarized as

Matching: a good approximation of y_p needs to be provided by the multi-estimator, i.e., $\mathbf{e}_p$ needs to be small whenever the process $\mathscr{M}_p \in \mathscr{M}$.

Detectability: The error between the current and initial system states may be occasionally small, as long as system detectability is guaranteed, no matter what its initial state. Each estimator requires detectability related to the error estimator $\mathbf{e}_p$ when a switching signal is fixed at $\sigma = \chi(\rho) \in \mathscr{Q}$.

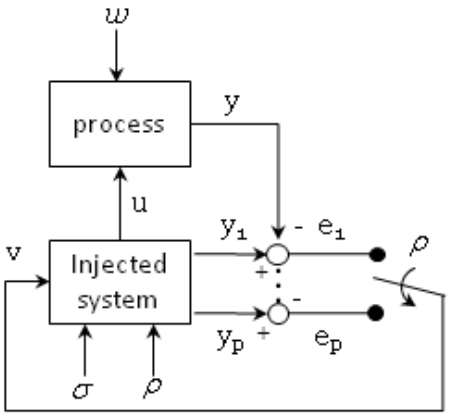

Figure 3.3: Injected system in cascade (HESPANHA,2002)

The signal σ is generated by the switching logic. The switching control needs to have other properties such as small error and non-destabilization.

Small error: For a process switching signal ρ which satisfies $\sigma = \chi(\rho)$, the boundedness of the error vector $\mathbf{e}_\rho$ must be guaranteed by the switching logic. The error vector $\mathbf{e}_\rho$ is the smallest sub-vector of the error vector $\mathbf{e}_p$ under any norm.

Non-destabilization: The system must be stable permanently in order to maintain detectability. Switching stopping in finite time can be guaranteed by means of a scale-independent hystere-

sis switching logic. This logic can be applied for linear and nonlinear observers and controllers.

3.4 Hysteresis Switching Logic

The error between the output $\mathbf{y}_p$ of the estimators and the system output $\mathbf{y}$ is evaluated to select the best controller. The error vector $\mathbf{e}_p$ is written as the difference between the estimate $\mathbf{y}_p$ and the output $\mathbf{y}$. The best controller has the smallest element of the error vector. However, the error vector can present with two or more of its entry close to each other. So, chattering can occur because two or more controllers could be selected. The scale-independent hysteresis switching logic guarantees that chattering will not occur and that the non-destabilization property is maintained (HESPANHA, 2002). Scale-independent hysteresis means that the switching signal will not change since the current monitoring signal $\boldsymbol{\mu}_p$ will be less than others within certain comparative scales. The hysteresis logic diagram is presented in Figure 3.4. The monitoring signal vector $\boldsymbol{\mu}_p$ is defined as follows

Definition 3.2 Monitoring Signal − (HESPANHA, 2002).

$$\dot{\mu}_p = -\lambda\mu_p + \gamma(\|\mathbf{e}_p\|), p \in \mathscr{P} \tag{3.7}$$

where λ denotes a constant non-negative forgetting factor, γ is a class $\mathscr{K}$ function (Lima (2009)) and $\|.\|$ is any norm. The initial value of the monitoring signal is $\mu(0) > 0$.

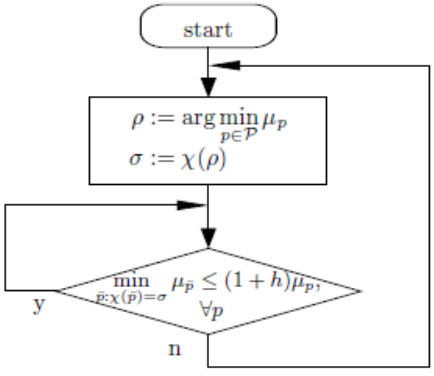

Figure 3.4: Scale-independent hysteresis switching logic (HESPANHA, 2002)

For the purposes of introducing the switching logic, let the positive constant of the hysteresis be h and consider the index of the minimum value of the μ_p that comes from arg min μ_p. The logic operates in the following way: start by taking ρ = arg min μ_p and do $\sigma = \rho$. When $\mu_\rho <= (1+h)\mu_p$ is false for each $p \in \mathscr{P}$, maintain $\sigma = \rho$, else, update the index ρ = arg min μ_p and restart $\sigma = \rho$. Hence, in the next step, reset the algorithm. The inequation will be true when some μ_ρ is the lowest compared with each $(1+h)\mu_p$. More information about this process can be found in (HESPANHA, 2002).

3.5 Stability Analysis

The *Matching*, *Detectability*, *Small error* and *Non-destabilization* properties need to be guaranteed for the application of the switching system. The *Matching* property can be obtained if the applied observer can be proved stable. As regards the *Detectability* property, if the injected system is proved to be stable, the switching system is detectable. The injected system is described as follows

$$\dot{\mathbf{x}} = \mathbf{A}_{\rho\sigma}(\mathbf{x}, \mathbf{v}), \tau_q = \mathbf{F}_{\rho\sigma}(\mathbf{x}, \mathbf{v}), \mathbf{y}_p = \mathbf{C}_p(\mathbf{x}), p \in \mathscr{P} \tag{3.8}$$

where $\mathbf{v} = \mathbf{e}_p = \mathbf{y}_p$ - $\mathbf{y}$ is the input for the injected system. The control output is $\boldsymbol{\tau}_q$ with $\mathbf{A}_{\rho\sigma}$ and $\mathbf{F}_{\rho\sigma}$ being functions for a pair ρ and σ. To prove the stability of the injected system, the following theorem is taken into account.

Theorem 3.1 Certainty Equivalent Stabilization − (HESPANHA, 2002). Let the process be detectable and take a fixed pair $\rho = p \in \mathscr{P}$ and $\sigma = q \in \mathscr{Q}$. Then, if the injected system is Input-to-State Stable (Input-to-State Stability (ISS)), the switched system will be detectable.

The scale-independent hysteresis switching logic ensures that *non-destabilization* and *small error* properties can be guaranteed. More details can be found in (HESPANHA, 2002).

3.6 Controller and Observer Numbers

The previous section presented some properties and conditions for using a control based on hybrid concept. However, an important problem when designing the switching control is the determination of the number of controllers to be included in the controller set. This number depends on the system performance which can be affected by significant parameter. When determining the number of controllers and observers, a criterion to establish parameter range is required.

To determine the controller number, vessel dynamics is described as $\dot{\boldsymbol{x}} = \boldsymbol{f}(t, \boldsymbol{x}, \epsilon)$ in the perturbation model, where ϵ is a small parameter related to draft variation. So, a function set from the Taylor series is used to approximate the solution $\boldsymbol{x}(t, \epsilon)$ as follows

$$x(t, \epsilon) = \sum_{k=0}^{N-1} x_k(t)\epsilon^k + \epsilon^N R_x(t, \epsilon) \tag{3.9}$$

Comparing the response of the approximation of $\boldsymbol{x}(t, \epsilon)$ to the response of $\boldsymbol{x}(t, 0)$, an error E is defined as

$$E = max\|(\sum_{k=0}^{N-1} x_k(t)\epsilon^k + \epsilon^N R_x(t, \epsilon)) - \boldsymbol{x}(t, 0)\| \tag{3.10}$$

Once the maximum error E_{max} is defined, the small variation ϵ is found and subsequently the draft variation is determined. Appendix B presents this model in detail.

To determine the observer number, evaluation of the vessels' wave-frequency motion is done through calculation of the response motion spectrum. This analysis studies the cut-off frequency ranges for the observers. Appendix C presents this analysis in detail.

Chapter 4

Dynamic Positioning System

4.1 General

Dynamic Positioning Systems are closed-loop control systems that maintain vessel position and heading by means of thrusters. The DPS is composed of the following main subsystems: controller, observer, thrusters and sensor subsystem. The controller commands the thrusters in order to counteract the environmental forces and moment and, as consequence, to maintain the vessel set-point. The control law requires a noiseless estimates of vessel positioning and velocity. These estimates are calculated by a state observer that receives the sensor measurement and control vector. An allocation logic is used to distribute the thrust commanded by the controller to the thrusters. Figure 4.1 illustrates this closed-loop control system and its main subsystems.

A new positioning strategy is here proposed to control two DP vessels in offloading operation. The hybrid control concept is used to choose the best controller law and state observer in order to improve the performance of the vessels' positioning. Both nonlinear observers with wave-frequency model and extreme seas are used. In the following section, these models are described in a 6DOF system composed of two vessels. A control law based on the geometric theory is applied to control the DP vessels. The DP control law obtained from the Lagrangian formalism is presented and its equivalence to the geometric controller is demonstrated. PD-like control is

also used and its performance is compared to geometric control performance. Assuming that vessel velocity is low and set-point is constant, the similar performance between the PD-like control and geometric approach is investigated.

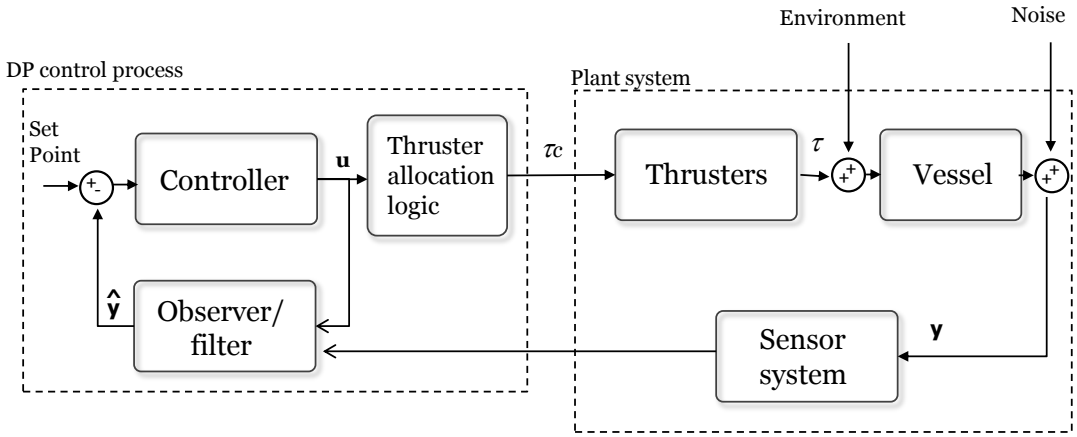

Figure 4.1: Block diagram for a dynamic positioning system

4.2 State Observers

The observer models are applied to DPS vessels in order to provide vessels' velocity and position estimates without disturbance or/and wave-frequency motion influence. Depending on the dominating wave frequency of the sea condition, the wave-frequency motion is not required to be filtered by the observer. External forces and moments are also important to be estimated by observers in order to facilitate vessel through the addition of the feed-forward term to the control law. These external force and moment estimate can be done by a white noise or a Markov process model. The following sections present two state observers applied here.

4.2.1 Nonlinear Observer with Wave-frequency Vessel Motion

A nonlinear observer proposed by Fossen and Strand (1999) is considered. The plant model (2.18) for this observer can be rewritten as

$$\boldsymbol{M}\dot{\nu} + \boldsymbol{D}\nu = \boldsymbol{\tau}_c + \boldsymbol{J}^T(\boldsymbol{\psi})\boldsymbol{b} \tag{4.1}$$

where $\boldsymbol{\tau}_c \in \mathbb{R}^6$ is the local control vector and $\boldsymbol{\tau}_c = \boldsymbol{J}(\psi)^T\boldsymbol{u}$. In this model, the external forces and moments are based on the Markov process as follows

$$\dot{\boldsymbol{b}} = -T^{-1}\boldsymbol{b} + \boldsymbol{\Psi}\boldsymbol{n} \tag{4.2}$$

where $\boldsymbol{b} \in \mathbb{R}^6$ is the external force vector, $\boldsymbol{n} \in \mathbb{R}^6$ is a zero-mean Gaussian white noise vector, $\boldsymbol{T} \in \mathbb{R}^{6\times6}$ is a diagonal matrix of time constants and $\Psi \in \mathbb{R}^{6x6}$ is a diagonal scaling matrix.

In order to evaluate the wave-frequency vessel motion, a second-order model of the wave-induced motion was proposed by Balchen, Jenssen and Sælid (1976) using harmonic oscillators. A extension of this work was presented by Sælid, Jenssen and Balchen (1983) who included an additional term for the damping. To describe this model, let $h_w^i(s)$ be

$$h_w^i(s) = \frac{\sigma_i s}{s^2 + 2\varsigma_i\omega_{0i}s + \omega_{0i}^2} \tag{4.3}$$

where $h_w^i(s)$ is the transfer function between a white noise signal and wave-frequency vessel motion, ω_{0i} is the dominating wave-frequency, ς_i is the relative damping ratio and σ_i is a wave intensity parameter. The indices $i = 1, ..., 6$ refer to FPWSO and shuttle tanker degrees of freedom. The state model for 6DOF yields

$$\begin{bmatrix} \dot{\boldsymbol{\xi}}_1 \\ \dot{\boldsymbol{\xi}}_2 \end{bmatrix} = \begin{bmatrix} \boldsymbol{0}_{6x6} & \boldsymbol{I}_{6x6} \\ \boldsymbol{\Omega}_{21} & \boldsymbol{\Omega}_{22} \end{bmatrix} \begin{bmatrix} \boldsymbol{\xi}_1 \\ \boldsymbol{\xi}_2 \end{bmatrix} + \begin{bmatrix} \boldsymbol{0}_{6x6} \\ \boldsymbol{\Sigma}_2 \end{bmatrix} \boldsymbol{w} \tag{4.4}$$

$$\boldsymbol{\eta}_w = \begin{bmatrix} \boldsymbol{0}_{6x6} & \boldsymbol{I}_{6x6} \end{bmatrix} \begin{bmatrix} \boldsymbol{\xi_1} \\ \boldsymbol{\xi_2} \end{bmatrix} \tag{4.5}$$

where $\boldsymbol{\xi}_1$ and $\boldsymbol{\xi}_2 \in \mathbb{R}^6$ are internal variable vectors, $\boldsymbol{w} \in \mathbb{R}^6$ is a zero-mean Gaussian white noise vector and $\boldsymbol{\eta}_w \in \mathbb{R}^6$ is the wave-frequency vessel motion vector. The matrices $\boldsymbol{\Omega}_{21}$, $\boldsymbol{\Omega}_{22}$ and $\boldsymbol{\Sigma}_2$

$\in \mathbb{R}^{6x6}$ in (4.4) are written as

$$\boldsymbol{\Omega}_{21} = -diag\{\ \omega_{01}^2 \quad ... \quad \omega_{06}^2\ \} \tag{4.6}$$

$$\boldsymbol{\Omega}_{22} = -2.diag\{\ \varsigma_1\omega_{01} \quad ... \quad \varsigma_6\omega_{06}\ \} \tag{4.7}$$

$$\boldsymbol{\Sigma}_2 = diag\{\ \sigma_1 \quad ... \quad \sigma_6\ \} \tag{4.8}$$

The vessels' position and heading measurement vector $\boldsymbol{y} \in \mathbb{R}^6$ can be written as

$$\boldsymbol{y} = \boldsymbol{\eta} + \boldsymbol{\eta}_w + \boldsymbol{d} \tag{4.9}$$

where $\boldsymbol{d} \in \mathbb{R}^6$ is zero-mean Gaussian white measurement noise. To obtain the complete observer model, the following assumptions are necessary (FOSSEN; STRAND, 1999)

A.1 - $\boldsymbol{M} = \boldsymbol{M}^T$: the inertia matrix is symmetry

A.2 - $\boldsymbol{n} = \boldsymbol{w} = 0$: estimation error drives the estimator states and those terms are omitted

A.3 - $\boldsymbol{d} = 0$: this term is small compared to first-order wave disturbance

A.4 - $\boldsymbol{J}(\boldsymbol{\eta}) = \boldsymbol{J}(\boldsymbol{y})$: the heading is known with good accuracy

Under assumptions $A.1$ to $A.4$ and using (4.1) to (4.9), the complete observer model yields

$$\boldsymbol{M}\dot{\nu} + \boldsymbol{D}\nu = \boldsymbol{\tau}_c + \boldsymbol{J}^T(\boldsymbol{y})\boldsymbol{b} \tag{4.10}$$

$$\dot{\boldsymbol{\eta}} = \boldsymbol{J}(\boldsymbol{y})\boldsymbol{\nu} \tag{4.11}$$

$$\dot{\boldsymbol{\xi}} = \boldsymbol{\Omega}\boldsymbol{\xi} \tag{4.12}$$

$$\dot{\boldsymbol{\eta}} = \boldsymbol{J}(\boldsymbol{y})\boldsymbol{\nu} \tag{4.13}$$

$$\dot{\boldsymbol{b}} = -T^{-1}\boldsymbol{b} \tag{4.14}$$

$$\boldsymbol{M}\dot{\nu} = -\boldsymbol{D}\nu + \boldsymbol{J}^T(\boldsymbol{y})\boldsymbol{b} + \boldsymbol{\tau}_c \tag{4.15}$$

$$\boldsymbol{y} = \boldsymbol{\eta} + \boldsymbol{\eta}_w = \boldsymbol{\eta} + \boldsymbol{\Gamma\xi} \tag{4.16}$$

where $\boldsymbol{\Omega} \in \mathbb{R}^{12\times12}$ and $\boldsymbol{\Gamma} \in \mathbb{R}^{6\times12}$ are written as follows

$$\Omega = \begin{bmatrix} \mathbf{0}_{6x6} & \boldsymbol{I}_{6x6} \\ \boldsymbol{\Omega}_{21} & \boldsymbol{\Omega}_{22} \end{bmatrix} \tag{4.17}$$

$$\Gamma = \begin{bmatrix} \mathbf{0}_{6x6} & \boldsymbol{I}_{6x6} \end{bmatrix} \tag{4.18}$$

Using (4.10) - (4.16), the nonlinear observer is

$$\dot{\hat{\boldsymbol{\xi}}} = \boldsymbol{\Omega}\hat{\boldsymbol{\xi}} + \boldsymbol{K_1}.\tilde{\boldsymbol{y}} \tag{4.19}$$

$$\dot{\hat{\boldsymbol{\eta}}} = \boldsymbol{J}(\boldsymbol{y})\hat{\boldsymbol{\nu}} + \boldsymbol{K_2}.\tilde{\boldsymbol{y}} \tag{4.20}$$

$$\dot{\hat{\boldsymbol{b}}} = -T^{-1}\hat{\boldsymbol{b}} + \boldsymbol{K_3}.\tilde{\boldsymbol{y}} \tag{4.21}$$

$$\boldsymbol{M}\dot{\hat{\nu}} = -\boldsymbol{D}\hat{\nu} + \boldsymbol{J}^T(\boldsymbol{y})\hat{\boldsymbol{b}} + \boldsymbol{\tau}_c + \boldsymbol{J}(\boldsymbol{y})^T\boldsymbol{K_4}\tilde{\boldsymbol{y}} \tag{4.22}$$

$$\hat{\boldsymbol{y}} = \hat{\boldsymbol{\eta}} + \boldsymbol{\Gamma}\hat{\boldsymbol{\xi}} \tag{4.23}$$

where $\tilde{\boldsymbol{y}} = \boldsymbol{y}$ - $\hat{\boldsymbol{y}} \in \mathbb{R}^6$ is the estimator error, $\hat{\boldsymbol{\xi}} \in \mathbb{R}^{12}$, $\hat{\boldsymbol{\eta}}$ and $\hat{\nu} \in \mathbb{R}^6$. The hat symbol ($\hat{}$) denotes estimate vector. The matrices $\boldsymbol{K_3}$ and $\boldsymbol{K_4} \in \mathbb{R}^{6\times6}$ are diagonal positive and the error matrices $\boldsymbol{K_1} \in \mathbb{R}^{12\times6}$ and $\boldsymbol{K_2} \in \mathbb{R}^{6\times6}$ are written as follows

$$\boldsymbol{K}_1 = \begin{bmatrix} k_{11} & 0 & 0 & 0 & 0 & 0 \\ 0 & k_{12} & 0 & 0 & 0 & 0 \\ 0 & 0 & k_{13} & 0 & 0 & 0 \\ 0 & 0 & 0 & k_{14} & 0 & 0 \\ 0 & 0 & 0 & 0 & k_{15} & 0 \\ 0 & 0 & 0 & 0 & 0 & k_{16} \\ k_{21} & 0 & 0 & 0 & 0 & 0 \\ 0 & k_{22} & 0 & 0 & 0 & 0 \\ 0 & 0 & k_{23} & 0 & 0 & 0 \\ 0 & 0 & 0 & k_{24} & 0 & 0 \\ 0 & 0 & 0 & 0 & k_{25} & 0 \\ 0 & 0 & 0 & 0 & 0 & k_{26} \end{bmatrix} \tag{4.24}$$

$$\boldsymbol{K}_2 = \begin{bmatrix} k_{31} & 0 & 0 & 0 & 0 & 0 \\ 0 & k_{32} & 0 & 0 & 0 & 0 \\ 0 & 0 & k_{33} & 0 & 0 & 0 \\ 0 & 0 & 0 & k_{34} & 0 & 0 \\ 0 & 0 & 0 & 0 & k_{35} & 0 \\ 0 & 0 & 0 & 0 & 0 & k_{36} \end{bmatrix} \tag{4.25}$$

The entries of these matrices are calculated as (FOSSEN; STRAND, 1999)

$$k_{1i} = -2\omega_{ci}(\varsigma_{ni} - \varsigma_i)\frac{1}{\omega_{0i}} \tag{4.26}$$

$$k_{2i} = 2\omega_{0i}(\varsigma_{ni} - \varsigma_i) \tag{4.27}$$

$$k_{3i} = \omega_{ci} \tag{4.28}$$

where ς_{ni} is the damping factor and ω_{ci} is the filter cut-off frequency.

4.2.2 Nonlinear Observer for Extreme Seas

The nonlinear observer for extreme sea is presented by Sorensen, Strand and Nyberg (2002). This model does not estimate the wave-frequency vessel motion. Hence, the measurement vector is $\boldsymbol{y} = \boldsymbol{\eta}_T = \boldsymbol{\eta} + \boldsymbol{\eta}_w \in \mathbb{R}^6$. The extreme sea observer model is written as follows

$$\dot{\hat{\boldsymbol{\eta}}}_T = \boldsymbol{J}(\boldsymbol{y})\hat{\boldsymbol{\nu}}_T + \boldsymbol{K_{2T}}.\tilde{\boldsymbol{y}} \tag{4.29}$$

$$\dot{\hat{\boldsymbol{b}}}_T = -T^{-1}\hat{\boldsymbol{b}}_T + \boldsymbol{K_{3T}}.\tilde{\boldsymbol{y}} \tag{4.30}$$

$$\boldsymbol{M}\dot{\hat{\boldsymbol{\nu}}}_T = -\boldsymbol{D}\hat{\boldsymbol{\nu}}_T + \boldsymbol{J}^T(\boldsymbol{y})\hat{\boldsymbol{b}}_T + \boldsymbol{\tau}_c + \boldsymbol{J}(\boldsymbol{y})^T\boldsymbol{K_{4T}}.\tilde{\boldsymbol{y}} \tag{4.31}$$

$$\hat{\boldsymbol{y}} = \hat{\boldsymbol{\eta}}_T \tag{4.32}$$

where $\hat{\boldsymbol{\eta}}_T \in \mathbb{R}^6$ is the total estimated motion, $\hat{\boldsymbol{\nu}}_T$ and $\hat{\boldsymbol{b}}_T \in \mathbb{R}^6$. The matrices $\boldsymbol{K_{2_T}}$, $\boldsymbol{K_{3_T}}$ and $\boldsymbol{K_{4_T}} \in \mathbb{R}^{6\times6}$ are similar to the nonlinear observer with wave-frequency model.

4.3 Control Theory

4.3.1 Geometric Control Theory

4.3.1.1 Mathematical Tools

This section brings the mathematical tools applied to the geometric control. A briefly notion about Differential Geometric and Geometric Mechanics is presented to write and discuss the DP control laws.

Basic Concepts in Differential Geometry

The Differential Geometry is a theory composed of elements of topology, differential calculus and linear algebra. The system dynamics in this context is based on the description of vector fields that represent ordinary differential equations (ODE). The Differential Geometry tools allow to associate the state space of the dynamical systems with a topological space. Here, some important concepts are presented such as manifolds, vector field and Lie algebra.

Manifolds

Definition E.1 (GEMIGNANI, 1972) Let f be a function from a topological space X, p to a space Y, q. The function f is said to be a homeomorphism if f is one-one, onto, and continuous, and if f^{-1} is continuous.

For the definition of topological space, see Gemignani (1972). A coordinate transformation Φ that represents $\mathbb{R}^n$-real function on n variables is a diffeomorphism if Φ is invertible and both the transformation and its inverse are smooth mappings. If the mapping is defined on $\mathbb{R}^n$, the diffeomorphism is global. If the mapping is defined on neighborhood of a point, the diffeomorphism is local.

A *manifold* is a topological space where each $p \in M$ with an open set U of p and an integer number $n \geq 0$ such that exits a homeomorphism Φ that parametrizes U to $\mathbb{R}^n$ (SPIVAK, 1999).

A *coordinate chart* on a manifold M is a pair (U,ϕ), where U is an open set of M and ϕ a

homeomorphism of U onto an open set of $\mathbb{R}^n$ (ISIDORI, 1995). Two coordinate charts (U,ϕ) and (V,ψ) are C^∞-*compatible* if, whenever $U \cap V \neq 0$, the coordinates transformation $\psi \circ \phi^-1$ is a diffeomorphism, i.e., *y(x)* and *x(y)* are both C^∞ maps (ISIDORI, 1995). A C^∞ *atlas* on a manifold M is a collection $\mathscr{A} = \{(U_i,\phi_i) : i \in I\}$ of pairwise C^∞-compatible coordinate charts, with the property that $\bigcup_{i\in I} U_i = M$.. An atlas is *complete* if not properly contained in any other atlas.

Definition E.2 (ISIDORI, 1995) A *smooth* or C^∞ manifold is a manifold with a complete C^∞ atlas.

A submanifold of a manifold M is a subset S which itself has the structure of a manifold, and a inclusion map $S \rightarrow M$ satisfies certain properties. See Isidori (1995) for more details.

Vectorial and Tangent Spaces

Definition E.3 (ISIDORI, 1995): Let M be a smooth manifold. A *tangent space* to M at p, written T_pM, is the set of all tangent vectors at p.

Theorem E.1 (ISIDORI, 1995): Let M be a smooth manifold of dimension n. Let p be any point of M. The tangent space T_pM to M at p is a n-dimensional vector space over the field $\mathbb{R}$. If (U,ϕ) is a coordinate chart around p, then the set of tangent vectors $(\frac{\partial}{\partial\phi_1})_p, ..., (\frac{\partial}{\partial\phi_n})_p$ form a basis of T_pM, where $(\frac{\partial}{\partial\phi_n})_p$ is the directional derivative related to ϕ_n in p.

Definition E.4 (ISIDORI, 1995): Let M be a smooth manifold, of dimension n. A *vector field* f on M is a mapping assigning to each point $p \in M$ a tangent vector $f(p)$ in T_pM. A vector field f is smooth if for each $p \in M$ there exits a *coordinate chart* (U,ϕ) about p and n real-valued smooth function $f_1, \ldots, f_n$ defined on U such that, for all $q \in U$

$$f_q = \sum_{i=1}^{n} f_i(q)(\frac{\partial}{\partial\phi_i})_q \tag{4.33}$$

A *tangent bundle* TM is a $2n$-dimensional manifold composed by tangent space union T_pM for each point $p \in M$

$$TM = \bigcup_{p\in M} T_pM \tag{4.34}$$

A vectorial field f assigns $f : M \to TM : p \to (p, v_p)$. Similarly, a dual space to tangent space T_pM can be defined a *cotangent space* T^*M. The vectors into cotagent space are called *covectors*. Once defined a point p on M, the space T_p^*M has a basis $dx_1|_p, ..., dx_n|_p$. A *cotangent bundle* T^*M is defined analogous to TM.

Let be M and N be two manifolds and a diffeomorfism $f : M \to N : m \to f(m) = n$ for $m \in M$ an $n \in N$. A tangent mapping is $T_mf : T_mM \to T_{f(m)}N$ transforms vectors $v \in T_mM$ in $u \in T_pN$. Figure 4.2 presents the spacial relationship between vector space and their mapping. This concept is important to manipulate coordinate transformation and understand forces in the Geometric Mechanics context.

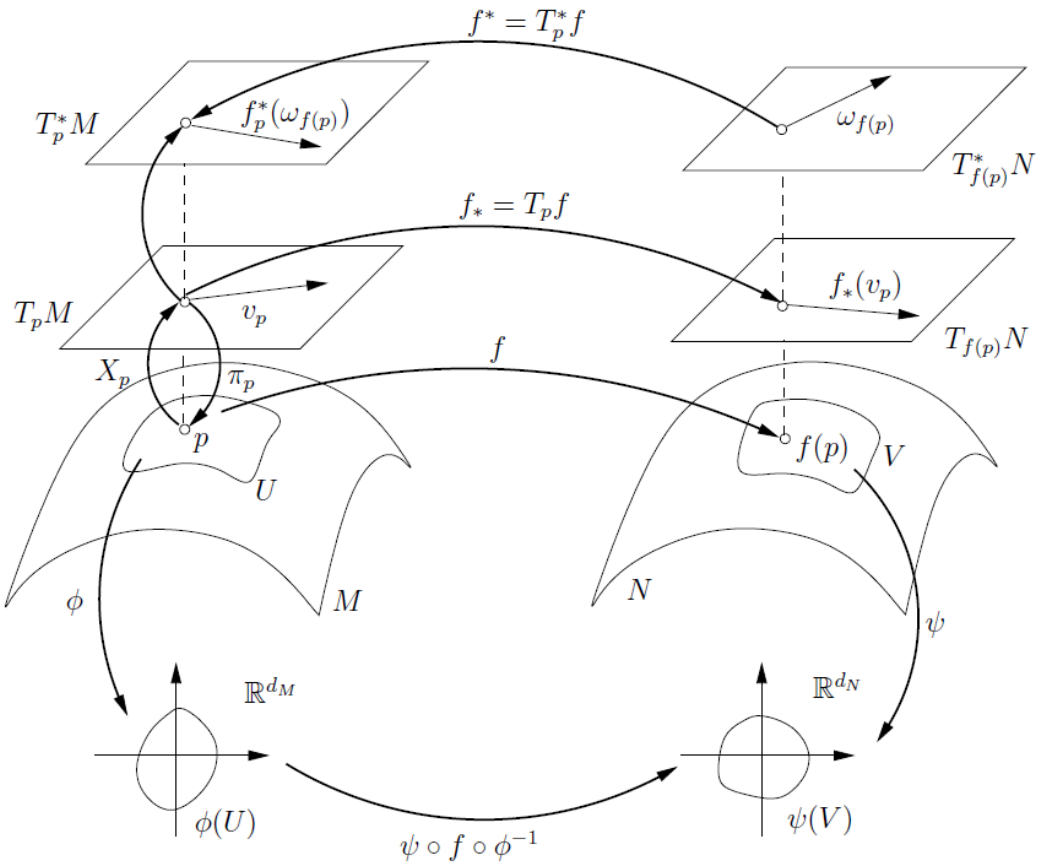

Figure 4.2: Mapping between manifolds (SOUZA, 2008)

Lie Algebra and Distributions

Let $X \subset \mathbb{R}^n$ be a manifold and $f(x)$ and $g(x)$ two vector fields with x on X. The Lie derivative $L_f g(x)$ is given by

$$L_f g(x) = \frac{\partial g}{\partial x}(x) f(x) \tag{4.35}$$

This is the notion of the derivative of g along f. The notation $L_f^k g(x)$ means the k^{th} Lie derivative as follows

$$L_f^k g(x) = \frac{\partial (L_f^{k-1} g)}{\partial x} f(x) \tag{4.36}$$

The Lie bracket of $f(x)$ on $g(x)$ is another vector field on X defined as follows

$$[f, g](x) = \frac{\partial g}{\partial x}(x) f(x) - \frac{\partial f}{\partial x}(x) g(x) \tag{4.37}$$

where $\partial f/\partial x$ and $\partial g/\partial x$ are the Jacobian matrices of $f(x)$ and $g(x)$. Similar to the Lie derivative, $ad_f^k g(x) = [f, ad_f^{k-1} g](x)$ where $ad_f^0 g(x) = g(x)$.

Let M be a manifold on $\mathbb{R}^n$ and $f_1, ..., f_m$ be vector fields described by smooth functions on M. These fields at a fixed point x span a vector space (a subspace of $\mathbb{R}^n$) defined as

$$\Delta(x) = span\{f_1, ..., f_m\} \tag{4.38}$$

where $\Delta(x)$ is a smooth distribution on M. A distribution is involutive if the Lie bracket $[f_i, f_j]$ of any pair f_i and f_j with $i \neq j$ and $i, j = 1, ..., m$ belongs to Δ.

Geometric Mechanics

A configuration is a generalization of the system position and attitude in terms of differential geometry. The configuration manifold Q with q elements has the velocity vectors of the system within the tangent space $T_q Q$. The total external force f is a mapping C^∞ into the cotangent space $T_q^* Q$. Figure 4.3 illustrates this configuration.

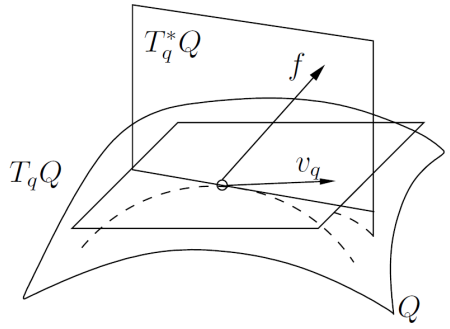

Figure 4.3: Manifold of a configuration (SOUZA, 2008)

Dynamic systems with holonomic constraints without external forces have the constraint forces perpendicular to the velocity vector (see Figure 4.4). This means that the distribution is integrable in the sense of Frobenius theorem (BULLO; LEWIS, 2010; SOUZA, 2008). A constraint of dynamical system is said to be holonomic or integrable if there is a real-valued function $h(x)$ (x understood as generalized coordinates of that system) such that the constraint can be rewritten as $h(x) = k$, where k is a constant. Thus, the system configuration is actually constrained to be a submanifold of the system configuration manifold. This holonomic condition is equivalent to the integrability of the Frobenius theorem (BLOCH et al., 2003). Hence, to find the constraint force into the cotangent space is equivalent to resolve the Lagrangian$-\lambda$ method of the constrained dynamical system. More about this method can be found in Meirovitch (1970), Lanczos (1986), Lima (2009).

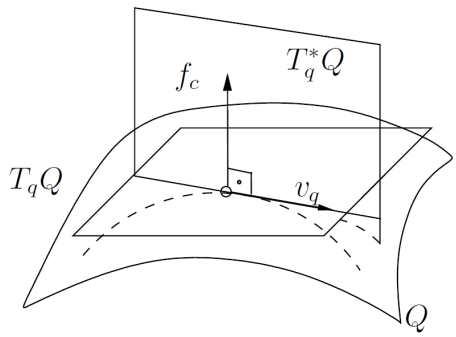

Figure 4.4: Manifold with a constraint force (SOUZA, 2008)

4.3.1.2 Multiple-Input- Multiple-Output Linearizarion

Consider the following system

$$\dot{\boldsymbol{x}}(t) = \boldsymbol{f}(\boldsymbol{x}) + \sum_{i=1}^{m} \boldsymbol{g}_i(\boldsymbol{x})\boldsymbol{u}_i \tag{4.39}$$

$$\begin{aligned} \boldsymbol{y}_1 &= \boldsymbol{h_1}(\boldsymbol{x}) \\ &... \\ \boldsymbol{y}_m &= \boldsymbol{h_m}(\boldsymbol{x}) \end{aligned} \tag{4.40}$$

where $\boldsymbol{f}(\boldsymbol{x})$ and $\boldsymbol{g}_i(\boldsymbol{x})$ with $i = 1, ..., m$ are smooth vector fields, $\boldsymbol{h}_i(\boldsymbol{x})$ is a smooth function $\in \mathbb{R}^n$. Let $\boldsymbol{x}(t) = [\ \boldsymbol{x}_1(t),\ \ ...,\ \ \boldsymbol{x}_n(t)\ ]^T$ be the state space vector, $\boldsymbol{u}(t) = [\ \boldsymbol{u}_1(t),\ \ ...,\ \ \boldsymbol{u}_m(t)\ ]^T$ be the control vector and $\boldsymbol{y}(t) = [\ \boldsymbol{y}_1(t),\ \ ...,\ \ \boldsymbol{y}_m(t)\ ]^T$ be the observation vector. Then, (4.39) and (4.40) can be rewritten as

$$\dot{\boldsymbol{x}}(t) = \boldsymbol{f}(\boldsymbol{x}) + \boldsymbol{g}(\boldsymbol{x})\boldsymbol{u} \tag{4.41}$$

$$\boldsymbol{y} = \boldsymbol{h}(\boldsymbol{x}) \tag{4.42}$$

where $\boldsymbol{g}(\boldsymbol{x})$ is a $n\ x\ m$-matrix and $\boldsymbol{h}(\boldsymbol{x})$ is a m-vector. It is possible to find a control law $\boldsymbol{u}$ in order to linearize the output $\boldsymbol{y}$. This process is called Input-to-Output (I/O) exact linearization for Multiple-Input-Multiple-Output (MIMO) (ISIDORI, 1995). The control law that linearizes the system is

$$\boldsymbol{u}_i = \boldsymbol{\alpha}_i(\boldsymbol{x}) + \sum_{j=1}^{m} \boldsymbol{\beta}_{ij}(\boldsymbol{x})\boldsymbol{v}_j \tag{4.43}$$

where $\boldsymbol{\alpha}_i(\boldsymbol{x})$ and $\boldsymbol{\beta}_{ij}(\boldsymbol{x})$ for $1 \leq i, j \leq m$ are smooth functions $\in \mathbb{R}^n$. The new control vector is defined as $\boldsymbol{v}(t) = [\ \boldsymbol{v}_1(t),\ \ ...,\ \ \boldsymbol{v}_m(t)\ ]^T$. Rewritten (4.43) in condensed way results

$$\boldsymbol{u}_G = \boldsymbol{\alpha}(\boldsymbol{x}) + \boldsymbol{\beta}(\boldsymbol{x})\boldsymbol{v} \tag{4.44}$$

where $\boldsymbol{u}_G$ is the geometric control law. Substituting (4.44) into (4.41) yields

$$\dot{\boldsymbol{x}}(t) = \boldsymbol{f}(\boldsymbol{x}) + \boldsymbol{g}(\boldsymbol{x})\boldsymbol{\alpha}(\boldsymbol{x}) + \boldsymbol{g}(\boldsymbol{x})\boldsymbol{\beta}(\boldsymbol{x})(\boldsymbol{v}) \tag{4.45}$$

If some conditions are satisfied, for an initial state $\boldsymbol{x}^{\circ}$ on $\mathscr{M}$, there is a coordinate transformation $\boldsymbol{z} = \Phi(\boldsymbol{x})$ (section 4.3.1.1), a matrix $\boldsymbol{A} \in \mathbb{R}^{n\times m}$ and a matrix $\boldsymbol{B} \in \mathbb{R}^{n\times m}$ such that

$$\left[\frac{\partial \Phi}{\partial \boldsymbol{x}}(\boldsymbol{f}(\boldsymbol{x}) + \boldsymbol{g}(\boldsymbol{x})\boldsymbol{\alpha}(\boldsymbol{x}))\right]_{x=\Phi_{-1}(z)} = \boldsymbol{A}\boldsymbol{z} \tag{4.46}$$

$$\left[\frac{\partial \Phi}{\partial \boldsymbol{x}}(\boldsymbol{g}(\boldsymbol{x})\boldsymbol{\beta}(\boldsymbol{x}))\right]_{x=\Phi_{-1}(z)} = \boldsymbol{B} \tag{4.47}$$

where the rank$[\ \boldsymbol{B} \quad \boldsymbol{AB} \quad \boldsymbol{A_{n-1}B}\ ] = n$ and $\Phi_k^i = L_f^{k-1}h_i(x)$ for $1 \leq k \leq r_i$, $1 \leq i \leq m$. Hence, the linearized system is

$$\dot{\boldsymbol{z}} = \boldsymbol{A}\boldsymbol{z} + \boldsymbol{B}\boldsymbol{v} \tag{4.48}$$

The new control vector $\boldsymbol{v}$ can be chosen as follows

$$\boldsymbol{v} = -\boldsymbol{K}\boldsymbol{z} \tag{4.49}$$

where $\boldsymbol{K} \in \mathbb{R}^{2m\times 2m}$ is a gain matrix of feedback state. The functions $\boldsymbol{\alpha}(\boldsymbol{x})$ and $\boldsymbol{\beta}(\boldsymbol{x})$ are found as

$$\boldsymbol{\alpha}(\boldsymbol{x}) = -\boldsymbol{A}^{-1}(\boldsymbol{x})\bar{\boldsymbol{b}}(\boldsymbol{x}) \tag{4.50}$$

$$\boldsymbol{\beta}(\boldsymbol{x}) = -\boldsymbol{A}^{-1}(\boldsymbol{x}) \tag{4.51}$$

where the matrices $\boldsymbol{A}(\boldsymbol{x}) \in \mathbb{R}^{m\times m}$ and $\bar{\boldsymbol{b}}(\boldsymbol{x}) \in \mathbb{R}^{m}$ are found as

$$\boldsymbol{A}(\boldsymbol{x}) = \begin{bmatrix} L_{g_1}L_f^{r_1-1}h_1(x) & ... & L_{g_m}L_f^{r_1-1}h_1(x) \\ L_{g_1}L_f^{r_2-1}h_2(x) & ... & L_{g_m}L_f^{r_2-1}h_1(x) \\ ... & ... & ... \\ L_{g_1}L_f^{r_m-1}h_1(x) & ... & L_{g_m}L_f^{r_m-1}h_1(x) \end{bmatrix} \tag{4.52}$$

$$\bar{\boldsymbol{b}}(\boldsymbol{x}) = \begin{bmatrix} L_f^{r_1}h_1(x) \\ L_f^{r_2}h_2(x) \\ ... \\ L_f^{r_m}h_m(x) \end{bmatrix} \tag{4.53}$$

where $r_i \in \mathbb{Z}$ with $i = 1, ..., m$ is the relative degree. The relative degree is defined as

Definition 5.1 (ISIDORI, 1995): A multivariable nonlinear system of the form (4.39) and (4.40) has a (vector) relative degree $\{ \ r_1 \quad ... \quad r_m \ \}$ at a point x° if

(i) $L_{g_j} L_f^k h_i(x) = 0$, for all $1 \leq j \leq m$, for all $k < r_i - 1$, for all $i \leq i \leq m$ and for all x in a neighborhood of x°,

(ii) The matrix $\boldsymbol{A}(\boldsymbol{x})$ is nonsingular at $\boldsymbol{x} = \boldsymbol{x}^\circ$.

The transformation existence conditions and the exact linearization follow belllow.

Theorem 4.1 (ISIDORI, 1995): Suppose the matrix $\boldsymbol{g}(\boldsymbol{x}^\circ)$ has rank m. The state space exact linearization problem is solvable if an only if

(i) for each $0 \leq i \leq n-1$, the distribution Δ_i has constant dimension near $\boldsymbol{x}^\circ$;

(ii) the distribution Δ_{n-1} has dimension n;

(iii) for each $0 \leq i \leq n-2$, the distribution Δ_i is involutive

The distribution is defined $\Delta_i = span\{ad_f^k g_j : 0 \leq k \leq i, 1 \leq j \leq m\}$. See definition of $ad_f^k g_j$ and Δ_i in section 4.3.1.1.

Proposition 5.1 (ISIDORI, 1995) Suppose a system that has a (vector) relative degree $\{ \ r_1 \quad ... \quad r_m \ \}$ at a point x°. Then

$$r_1 + ... + r_m \leq n$$

Set, for $1 \leq i \leq m$ with $\Phi_{r_i}^i(\boldsymbol{x}) = L_f^{r_i - 1} h_i(x)$

If $r = r_1 + ... + r_m$ is strictly less than n, it is always possible to find $n - r$ more functions $\Phi_{r+1}(x), ..., \Phi_n(x)$ such that mapping (see mapping in section 4.3.1.1)

$$\boldsymbol{\Phi}(x) = [\Phi_1^1(x), ..., \Phi_{r_1}^1(x), ..., \Phi_1^m(x), ..., \Phi_{r_m}^m(x), \Phi_{r+1}(x), ..., \Phi_n(x)]^T$$

has a Jacobian matrix which is nonsingular at $\boldsymbol{x}^\circ$ and therefore qualifies as a local coordinates transformation in a neighborhood of $\boldsymbol{x}^\circ$.

4.3.2 Lagrange Multiplier-based Controller

The Lagrange Multiplier to control crafts or vessels in formation is proposed by Ihle, Jouffry and Fossen (2005), Ihle (2006), Ihle, Jouffry and Fossen (2006) and Moratelli Jr et al. (2013). The idea is to use the constraint force determined by the Lagrange $-\lambda$ method (MEIROVITCH, 1970; LANCZOS, 1986) as the control law. In the context of the Classical Mechanics, the constraint forces are reactive forces at joints between rigid bodies. Here, this force is understood as control force that satisfies the constraint equals to zero.

To introduce the proposed control law, let $T_i(\dot{\boldsymbol{\eta}})$ be the kinetic energy of the vessels $i = 1, 2$ and $\mathscr{C}(\boldsymbol{\eta}) \in \mathbb{R}^p$ be the constraint function vector where p is the number of constraints, respectively. The total energy of the system is

$$\mathscr{L}(\boldsymbol{\eta}, \dot{\boldsymbol{\eta}}) = \sum_{i=1}^{2} T_i - \boldsymbol{\lambda}^T \mathscr{C}(\boldsymbol{\eta}) \tag{4.54}$$

where $\boldsymbol{\lambda} \in \mathbb{R}^p$ is the Lagrange Multiplier and $\mathscr{L}(\boldsymbol{\eta}, \dot{\boldsymbol{\eta}})$ is the Lagrangian (MEIROVITCH, 1970; LANCZOS, 1986). For DPS application, the potential energy is neglected and it can be deducted from 4.54. The energy $T_i(\dot{\boldsymbol{\eta}})$ is written as

$$T_i(\dot{\boldsymbol{\eta}}) = \frac{1}{2} \dot{\boldsymbol{\eta}}^T \boldsymbol{M_i} \dot{\boldsymbol{\eta}} \tag{4.55}$$

Let $\boldsymbol{b}$ be the only external forces and moment vector of the system. Applying the Euler-Lagrange differential equations (MEIROVITCH, 1970; LANCZOS, 1986), the vessel dynamics can be written as

$$\boldsymbol{M}_\eta \ddot{\boldsymbol{\eta}} + (\boldsymbol{D}_{\boldsymbol{\eta}} - \boldsymbol{J}(\psi_1, \psi_2) \boldsymbol{M} \boldsymbol{J}(\psi_1, \psi_2)^T \dot{\boldsymbol{J}}(\psi_1, \psi_2) \boldsymbol{J}(\psi_1, \psi_2)^T) \dot{\boldsymbol{\eta}} = \boldsymbol{b} - \boldsymbol{W}(\boldsymbol{\eta})^T \boldsymbol{\lambda} \tag{4.56}$$

where $\boldsymbol{W}(\boldsymbol{\eta}) \in \mathbb{R}^{m \times m}$ is the Jacobian matrix of the constraint $\mathscr{C}(\boldsymbol{\eta})$ with respect to $\boldsymbol{\eta}$. The matrix $\boldsymbol{M}_\eta = \boldsymbol{J}(\psi_1, \psi_2) \boldsymbol{M} \boldsymbol{J}(\psi_1, \psi_2)^T \in \mathbb{R}^{6 \times 6}$ and the matrix $\boldsymbol{D}_\eta = \boldsymbol{J}(\psi_1, \psi_2) \boldsymbol{D} \boldsymbol{J}(\psi_1, \psi_2)^T \in \mathbb{R}^{6 \times 6}$ are the matrices of inertia and Centripetal and Coriolis effects with respect to global coordinates. The matrix $\boldsymbol{D}$ is found using the same assumptions of section 2.2 to determine the

control model. (see the Appendix A). The control vector can be found as

$$\boldsymbol{u}_\lambda = -\boldsymbol{W}(\boldsymbol{\eta})^T \boldsymbol{\lambda} \tag{4.57}$$

where $\boldsymbol{u}_\lambda \in \mathbb{R}^6$ is the control vector. Now, $\ddot{\mathscr{C}}(\boldsymbol{\eta})$ can be found differentiating the constraint twice with respect to time as follows

$$\dot{\mathscr{C}}(\boldsymbol{\eta}) = \boldsymbol{W}(\boldsymbol{\eta}, \boldsymbol{x}_r)\dot{\eta} = [\mathbf{0}] \tag{4.58}$$

The second time-derivative yields

$$\ddot{\mathscr{C}}(\boldsymbol{\eta}) = \dot{\boldsymbol{W}}(\boldsymbol{\eta})\dot{\eta} + \boldsymbol{W}(\boldsymbol{\eta})\ddot{\eta} = [\mathbf{0}] \tag{4.59}$$

The constraint function acceleration can be stabilized by a feedback function using the constraint and its first derivative as follows

$$\ddot{\mathscr{C}}(\boldsymbol{\eta}) = -\boldsymbol{K}_p.\mathscr{C}(\boldsymbol{\eta}) - \boldsymbol{K}_d.\dot{\mathscr{C}}(\boldsymbol{\eta}) = [\mathbf{0}] \tag{4.60}$$

where $\boldsymbol{K}_p$ and $\boldsymbol{K}_d \in \mathbb{R}^{6\times6}$ are gain matrices. Now, making (4.60) equals to (4.59) and isolating the term $\boldsymbol{W}(\boldsymbol{\eta})\ddot{\eta}$ yields

$$\boldsymbol{W}(\boldsymbol{\eta})\ddot{\eta} = -(\dot{\boldsymbol{W}}(\boldsymbol{\eta})\dot{\eta} + \boldsymbol{K}_p.\mathscr{C}(\boldsymbol{\eta}) + \boldsymbol{K}_d.\dot{\mathscr{C}}(\boldsymbol{\eta})) \tag{4.61}$$

Now, substituting $\ddot{\boldsymbol{\eta}}$ from (4.56) into (4.61), and isolating the constraint force term $\boldsymbol{W}^T\boldsymbol{\lambda}$, the Lagrangian control law $\boldsymbol{u}_\lambda = -\boldsymbol{W}^T\boldsymbol{\lambda}$ results

$$\boldsymbol{u}_\lambda = -\boldsymbol{b} + (\boldsymbol{D}_{\boldsymbol{\eta}} - \boldsymbol{J}\boldsymbol{M}\boldsymbol{J}\dot{\boldsymbol{J}}\boldsymbol{J}^T)\dot{\boldsymbol{\eta}} - \boldsymbol{M}_\eta\boldsymbol{W}^{-1}(\dot{\boldsymbol{W}}\dot{\eta} + \boldsymbol{K}_p.\mathscr{C} + \boldsymbol{K}_d.\dot{\mathscr{C}}) \tag{4.62}$$

4.3.3 Proportional-Derivative-like Controller

The PD-like control law written with respect to Earth-frame and calculated based on the estimated variables is presented as

$$\boldsymbol{u}_{PD} = \boldsymbol{K}_p\hat{\boldsymbol{e}} + \boldsymbol{K}_d\dot{\hat{\boldsymbol{e}}} - \hat{\boldsymbol{b}} \tag{4.63}$$

$$\boldsymbol{e} = \boldsymbol{\eta_r} - \hat{\boldsymbol{\eta}} \tag{4.64}$$

where $\boldsymbol{u}_{PD} \in \mathbb{R}^6$ is the control vector, $\boldsymbol{e} \in \mathbb{R}^6$ is the positioning error vector and $\boldsymbol{\eta_r} \in \mathbb{R}^6$ is the vessel reference vector. The matrices $\boldsymbol{K}_p$ and $\boldsymbol{K}_d \in \mathbb{R}^{6\times6}$ are the proportional and derivative control matrix. These matrices can be found from a pole allocation using the control model in (4.1). These matrices result as

$$\boldsymbol{K}_p = \boldsymbol{M}.diag\{\ \omega_{n_1}^2 \quad ... \quad \omega_{n_6}^2\ \} \tag{4.65}$$

$$\boldsymbol{K}_d = 2\boldsymbol{M}.diag\{\ \varsigma_{c_{n_1}}\omega_{n_1} \quad ... \quad \varsigma_{c_{n_6}}\omega_{n_6}\ \} - \boldsymbol{D} \tag{4.66}$$

where $\varsigma_{c_{n_i}}$ and ω_{n_i} with $i = 1, ..., 6$ are control parameters.

4.4 Dynamic Positioning Controllers

Three different control laws are presented in order to control the DP vessels carrying out the offloading operation. The Geometric controller is developed through Input-to-Output (I/O) exact linearization for Multiple-Input- Multiple-Output (MIMO) system theory. This law integrates both DP vessel controllers (FPWSO and shuttle tanker). The Lagrange Multiplier-based controller proposed by Ihle (2006) is applied using a constraint function. The equivalence between Lagrange Multiplier-based controller and geometric controller is presented. PD-like controller is studied and this law does not control the vessels in the integrated way, i.e., no information is exchanged between the vessels. Taking low speed of the vessel and constant reference, the similar performance between geometric and PD-like controllers is demonstrated.

4.4.1 Relative Positioning

During the offloading operation, the relative positioning between the vessels needs to be maintained in order to avoid dangerous proximity or excessive hawser tension. To describe this relative positioning, consider Figure 4.5 that illustrates the positioning between vessels based on their

set-points. The vessels' positioning is imposed by the relative distance between the $FPWSO$ stern and the ST bow. The bow of the shuttle tanker is aligned with FPWSO longitudinal axis.

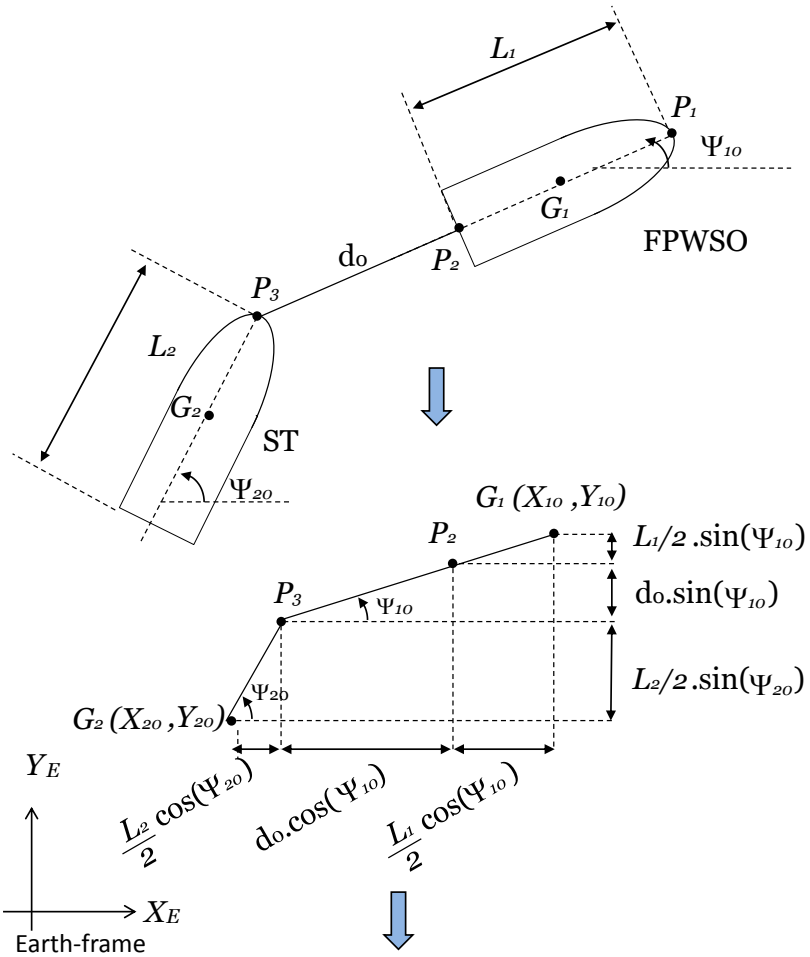

Figure 4.5: Relative positioning between vessels

So, this relative positioning can be described as follows

$$X_{10} - X_{20} = (\frac{L1}{2} + d_0)cos(\psi_{10}) + \frac{L_2}{2}cos(\psi_{20}) \tag{4.67}$$

$$Y_{10} - Y_{20} = (\frac{L1}{2} + d_0)sin(\psi_{10}) + \frac{L_2}{2}sin(\psi_{20}) \tag{4.68}$$

where L_1 and L_2 are the length of the FPWSO and ST, respectively. The variables X_{10}, Y_{10}, ψ_{10}, X_{20}, Y_{20} and ψ_{20} are the vessels' set-points and d_0 is the reference distance. Once FPWSO set-point is defined, the relative distance d_0 can be used to determine the shuttle tanker set-point. So, vessels' set-point vector can be written as

$$\boldsymbol{\eta}_0 = \begin{bmatrix} X_{10} \\ Y_{10} \\ \psi_{10} \\ X_{20} \\ Y_{20} \\ \psi_{20} \end{bmatrix} = \begin{bmatrix} X_{10} \\ Y_{10} \\ \psi_{10} \\ X_{10} - (d_0 + L_1/2)cos(\psi_{10}) - (L_2/2)cos(\psi_{20}) \\ Y_{10} - (d_0 + L_1/2)sin(\psi_{10}) - (L_2/2)sin(\psi_{20}) \\ \psi_{20} \end{bmatrix} \tag{4.69}$$

where $\boldsymbol{\eta}_0 \in \mathbb{R}^6$ is the set-point vector. In order to avoid abrupt input into the closed-loop control system due to the set-point change, a linear dynamical system to change the set-point values is implemented. Let the linear reference model be as follows

$$\dot{\boldsymbol{z}}_{1r} = \boldsymbol{z}_{2r} \tag{4.70}$$

$$\dot{\boldsymbol{z}}_{2r} = \boldsymbol{A_1 z}_{1r} + \boldsymbol{A_2 z}_{2r} + \boldsymbol{A_3 z}_0 \tag{4.71}$$

The variables $\boldsymbol{z}_{1r}$ and $\boldsymbol{z}_{2r} \in \mathbb{R}^5$ are internal variables of the reference model. The relative set-point vector is $\boldsymbol{z}_0 = [\ X_{10} \quad Y_{10} \quad \psi_{10} \quad d_0 \quad \psi_{20}\ ]^T$. The matrices $\boldsymbol{A_1}$, $\boldsymbol{A_2}$ and $\boldsymbol{A_3}$ are defined as

$$\boldsymbol{A_1} = -\boldsymbol{A_3} = -diag\{\ \omega_{r_1}^2 \quad ... \quad \omega_{r_5}^2\ \} \tag{4.72}$$

$$\boldsymbol{A_2} = -2.diag\{\ \varsigma_{r_1}\omega_{r_1} \quad ... \quad \varsigma_{r_5}\omega_{r_5}\ \} \tag{4.73}$$

The variables $\omega_{r_{nr}}$ and ς_{n_r} with $n_r = 1...5$ are parameters of the linear reference model. The reference model (4.70) and (4.71) can be rewritten as

$$\dot{\boldsymbol{z}}_r = \boldsymbol{A}_r\boldsymbol{z}_r + \boldsymbol{B}_r\bar{\boldsymbol{z}}_0 \tag{4.74}$$

$$\boldsymbol{y}_r = \boldsymbol{z}_r \tag{4.75}$$

where $\boldsymbol{z}_r = [\ \boldsymbol{z}_{1r}^T \quad \boldsymbol{z}_{2r}^T\ ]^T \in \mathbb{R}^{10}$ is the state-space vector of the reference model and $\boldsymbol{y}_r \in \mathbb{R}^{10}$ is

the output vector. The vector $\bar{\boldsymbol{z}}_0 = [\ \mathbf{0}_{5x1}^T \quad \boldsymbol{z}_0^T\ ]^T \in \mathbb{R}^{10}$ is the system input. The matrices $\boldsymbol{A}_r \in \mathbb{R}^{10\times10}$ and $\boldsymbol{B}_r \in \mathbb{R}^{10\times5}$ are defined as

$$\boldsymbol{A}_r = \begin{bmatrix} \mathbf{0}_{5x5} & \boldsymbol{I}_{5x5} \\ \boldsymbol{A_1} & \boldsymbol{A_2} \end{bmatrix} \tag{4.76}$$

$$\boldsymbol{B}_r = \begin{bmatrix} \mathbf{0}_{5x5} \\ \boldsymbol{A_3} \end{bmatrix} \tag{4.77}$$

The reference vector $\boldsymbol{\eta}_r \in \mathbb{R}^6$ can be written using the $\boldsymbol{z}_{1_r} = [\ X_{1r} \quad Y_{1r} \quad \psi_{1r} \quad d_r \quad \psi_{2r}\ ]^T$ vector as follows

$$\boldsymbol{\eta}_r = \begin{bmatrix} X_{1r} \\ Y_{1r} \\ \psi_r \\ X_{2r} \\ Y_{2r} \\ \psi_{2r} \end{bmatrix} = \begin{bmatrix} X_{1r} \\ Y_{1r} \\ \psi_{1r} \\ X_{1r} - (d_r + L_1/2)cos(\psi_{1r}) - (L_2/2)cos(\psi_{2r}) \\ Y_{1r} - (d_r + L_1/2)sin(\psi_{1r}) - (L_2/2)sin(\psi_{2r}) \\ \psi_{2r} \end{bmatrix} \tag{4.78}$$

Now, take the error vector $\boldsymbol{e} \in \mathbb{R}^6$ for dynamic positioning systems written as

$$\boldsymbol{e} = \boldsymbol{\eta}_r - \boldsymbol{\eta} \tag{4.79}$$

Using the error vector (4.79), if the FPWSO moves out from its set-point, the shuttle tanker maintains its positions and heading. However, a constraint can be written to maintain the relative distance moving both vessels. This constraint is defined as

$$\mathscr{C}(\boldsymbol{\eta}, \boldsymbol{z}_{1_r}) = \begin{bmatrix} X_1 - X_{1r} \\ Y_1 - Y_{1r} \\ \psi_1 - \psi_{1r} \\ X_2 - X_1 + (d + L_1/2)cos(\psi_1) + (L_2/2)cos(\psi_2) \\ Y_2 - Y_1 + (d + L_1/2)sin(\psi_1) + (L_2/2)sin(\psi_2) \\ \psi_2 - \psi_{2r} \end{bmatrix} = \mathbf{0} \tag{4.80}$$

where the constraint $\mathscr{C}(\boldsymbol{\eta}, \boldsymbol{z}_{1_r}) \in \mathbb{R}^6$. This constraint imposes that FPWSO error vector is calculated with its set-point and the ST reference depends on the actual FPWSO positions and heading. Hence, if FPWSO leaves its set-point, the shuttle tanker controller acts in order to maintain the distance between vessels. The opposite does not occur because the FPWSO can not leave its set-point due to riser connection. The new control strategy proposal is to integrate the control law action using the constraint vector.

4.4.2 Geometric control for Dynamic Positioning Vessels

In the Geometric Mechanics context (section 4.3.1.1), the constraint force used to create a control law (section 4.3.2) is a vector into the cotangent space of the system configuration (see section 4.3.1.1). In order to obtain this force, the linearizaton of the output $\boldsymbol{y}$ (4.42) is used to create the control force $\boldsymbol{u_G}$ (4.44) in the same cotangent space. Now, taking the vessel dynamics (4.56), the reference model (4.74) and the constraint (4.80), a system can be written concisely as

$$\dot{\boldsymbol{x}} = \boldsymbol{f}(\boldsymbol{x}) + \boldsymbol{g}(\boldsymbol{x})\boldsymbol{u} \tag{4.81}$$

$$\boldsymbol{y} = \boldsymbol{h}(\boldsymbol{\eta}, \boldsymbol{z_{1r}}) = \mathscr{C}(\boldsymbol{\eta}, \boldsymbol{z}_{1r}) \tag{4.82}$$

where $\boldsymbol{x} = [\ \boldsymbol{\eta}^T \quad \boldsymbol{z_{1r}}^T \quad \dot{\boldsymbol{\eta}}^T \quad \boldsymbol{z_{2r}}^T\ ]^T \in \mathbb{R}^{22}$. The output $\boldsymbol{y}$ is equal to the constraint function. The functions $\boldsymbol{f}(\boldsymbol{x})$ and $\boldsymbol{g}(\boldsymbol{x})$ are written as

$$\boldsymbol{f}(\boldsymbol{x}) = \begin{bmatrix} f_1(\boldsymbol{x}) \\ f_2(\boldsymbol{x}) \\ f_3(\boldsymbol{x}) \\ f_4(\boldsymbol{x}) \end{bmatrix} = \begin{bmatrix} \dot{\boldsymbol{\eta}} \\ \boldsymbol{z_{1r}} \\ \boldsymbol{M}_\eta^{-1}\left[(-\boldsymbol{D}_\eta + \boldsymbol{J}\boldsymbol{M}\boldsymbol{J}^T\dot{\boldsymbol{J}}\boldsymbol{J}^T)\dot{\boldsymbol{\eta}} + \boldsymbol{b}\right] \\ \boldsymbol{A_1 z_{1r}} + \boldsymbol{A_2 z_{2r}} + \boldsymbol{A_3 z_0} \end{bmatrix} \tag{4.83}$$

$$\boldsymbol{g}(\boldsymbol{x}) = \begin{bmatrix} \boldsymbol{0_{6x1}} \\ \boldsymbol{0_{5x1}} \\ \boldsymbol{M}_\eta^{-1} \\ \boldsymbol{0_{5x1}} \end{bmatrix} \tag{4.84}$$

The order of the system (4.81) is $n = 22$ because it is composed of the vessel dynamics (6DOF of order 2) and a linear reference model of order 10. If the second time-derivative of the output (4.82) is done, it can be seen that the relative degree of the system is $r = 12$. Hence, the exact linearization is not possible since $r < n$. The reason is the inclusion of the linear reference model into the system model. Despite the fact that $r < n$, the Proposition 5.1 states that it is possible to find a coordination transformation. A simple way to prove it is to assure the non-singularity of $\boldsymbol{A(x)}$ matrix. This matrix can be calculated as

$$\boldsymbol{A(x)} = L_{\boldsymbol{g}} L_{\boldsymbol{f}} \boldsymbol{h}(\boldsymbol{x}) = \nabla L_{\boldsymbol{f}} \boldsymbol{h}(x)\boldsymbol{g} = \nabla(\nabla \boldsymbol{h}.\boldsymbol{f})\boldsymbol{g} \tag{4.85}$$

where ∇ is the gradient operator. Hence, $\nabla \boldsymbol{h}$ is

$$\nabla \boldsymbol{h} = \left[\begin{array}{cccccccccc|c} 1 & 0 & 0 & 0 & 0 & 0 & 0 & -1 & 0 & 0 & 0 & \\ 0 & 1 & 0 & 0 & 0 & 0 & 0 & -1 & 0 & 0 & 0 & \\ 0 & 0 & 1 & 0 & 0 & 0 & 0 & 0 & -1 & 0 & 0 & \\ -1 & 0 & -(d+\frac{L_1}{2})s\psi_1 & 1 & 0 & -\frac{L_2}{2}s\psi_2 & 0 & 0 & 0 & c\psi_1 & 0 & \mathbf{0}_{6\times 11} \\ 0 & -1 & (d+\frac{L_1}{2})c\psi_1 & 0 & 1 & \frac{L_2}{2}c\psi_2 & 0 & 0 & 0 & s\psi_1 & 0 & \\ 0 & 0 & 0 & 0 & 0 & 1 & 0 & 0 & 0 & 0 & -1 & \end{array}\right] \tag{4.86}$$

The term $L_{\boldsymbol{f}}\boldsymbol{h}(\boldsymbol{x})$ is

$$L_{\boldsymbol{f}}\boldsymbol{h}(\boldsymbol{x}) = \nabla \boldsymbol{h}.\boldsymbol{f} = \dot{\boldsymbol{y}} = \left[\begin{array}{c} \dot{X}_1 - \dot{X}_{1r} \\ \dot{Y}_1 - \dot{Y}_{1r} \\ \dot{\psi}_1 - \dot{\psi}_{1r} \\ \dot{X}_2 - \dot{X}_1 - (d+L_1/2)s\psi_1\dot{\psi}_1 + c\psi_1\dot{d} - L_2/2s\psi_2\dot{\psi}_2 \\ \dot{Y}_2 - \dot{Y}_1 + (d+L_1/2)c\psi_1\dot{\psi}_1 + s\psi_1\dot{d} + L_2/2c\psi_2\dot{\psi}_2 \\ \dot{\psi}_2 - \dot{\psi}_{2r} \end{array}\right] = \tag{4.87}$$

$$= [\ \boldsymbol{W} \quad \boldsymbol{W}_r \quad \mathbf{0}_{6\times 6} \quad \mathbf{0}_{6\times 5}\ ]$$

where $\boldsymbol{W} \in \mathbb{R}^{6\times 6}$ is the Jacobian matrix of the $\boldsymbol{y}$ with respect to $\boldsymbol{\eta}$ and $\boldsymbol{W}_r \in \mathbb{R}^{6\times 5}$ is the Jacobian matrix of the constraint $\boldsymbol{y}$ with respect to $\boldsymbol{z}_{1_r}$. Now, the term $L_{\boldsymbol{g}}L_{\boldsymbol{f}}\boldsymbol{h}(\boldsymbol{x}) = \nabla L_{\boldsymbol{f}}\boldsymbol{h}(x)\boldsymbol{g}$ is required. To facilitate the reading, $\nabla L_{\boldsymbol{f}}\boldsymbol{h}(x)$ is divided into four parts related to each variable in $\boldsymbol{x}$ as

$$\nabla L_f h(x) = [\ \nabla L_f h(x)_{\boldsymbol{\eta}} \quad \nabla L_f h(x)_{\boldsymbol{z_{1r}}} \quad \nabla L_f h(x)_{\dot{\boldsymbol{\eta}}} \quad \nabla L_f h(x)_{\boldsymbol{z_{2r}}}\ ] \tag{4.88}$$

Hence,

$$\boldsymbol{\nabla} L_{\boldsymbol{f}}\boldsymbol{h}(x)_{\boldsymbol{\eta}} = \dot{\boldsymbol{W}} = \left[\begin{array}{ccccccc} & & & \mathbf{0}_{3x3} & & & \\ 0 & 0 & -(L_1/2+d)c(\psi_1)\dot{\psi}_1 - \dot{d}s(\psi_1) & 0 & 0 & -(L_2/2)c(\psi_2)\dot{\psi}_2 \\ 0 & 0 & -(L_1/2+d)s(\psi_1)\dot{\psi}_1 + \dot{d}c(\psi_1) & 0 & 0 & -(L_2/2)s(\psi_2)\dot{\psi}_2 \\ 0 & 0 & 0 & 0 & 0 & 0 \end{array}\right] \tag{4.89}$$

$$\boldsymbol{\nabla} L_{\boldsymbol{f}}\boldsymbol{h}(\boldsymbol{x})_{\boldsymbol{z_{1r}}} = \dot{\boldsymbol{W}}_{\boldsymbol{r}} = \left[\begin{array}{cc} \mathbf{0}_{3x3} & \mathbf{0}_{3x2} \\ & -s(\psi_1)\dot{\psi}_1 \quad 0 \\ \mathbf{0}_{3x3} & c(\psi_1)\dot{\psi}_1 \quad 0 \\ & 0 \quad 0 \end{array}\right] \tag{4.90}$$

$$\boldsymbol{\nabla} L_{\boldsymbol{f}} \boldsymbol{h}(\boldsymbol{x})_{\dot{\boldsymbol{\eta}}} = \boldsymbol{W} = \begin{bmatrix} & \boldsymbol{I}_{3x3} & & & \boldsymbol{0}_{3x3} & \\ -1 & 0 & -(L_1/2+d)s(\psi_1) & 1 & 0 & -(L_2/2)s(\psi_2) \\ 0 & -1 & (L_1/2+d)c(\psi_1) & 0 & 1 & (L_2/2)c(\psi_2) \\ 0 & 0 & 0 & 0 & 0 & 1 \end{bmatrix} \tag{4.91}$$

$$\boldsymbol{\nabla} L_{\boldsymbol{f}} \boldsymbol{h}(\boldsymbol{x})_{\boldsymbol{z}_{2r}} = \boldsymbol{W}_{\boldsymbol{r}} = \begin{bmatrix} -\boldsymbol{I}_{3x3} & \boldsymbol{0}_{3x2} & \\ & c(\psi_1) & 0 \\ \boldsymbol{0}_{3x3} & s(\psi_1) & 0 \\ & 0 & -1 \end{bmatrix} \tag{4.92}$$

Substituting (4.89) to (4.92) into (4.88) yields

$$\boldsymbol{\nabla} L_{\boldsymbol{f}} \boldsymbol{h}(\boldsymbol{x}) = [\ \dot{\boldsymbol{W}} \quad \dot{\boldsymbol{W}}_{\boldsymbol{r}} \quad \boldsymbol{W} \quad \boldsymbol{W}_{\boldsymbol{r}}\ ] \tag{4.93}$$

Hence, calculating $\boldsymbol{A(x)}$ using (4.84) yields

$$\boldsymbol{A(x)} = \nabla L_f h(x) \boldsymbol{g} = [\ \dot{\boldsymbol{W}} \quad \dot{\boldsymbol{W}}_{\boldsymbol{r}} \quad \boldsymbol{W} \quad \boldsymbol{W}_{\boldsymbol{r}}\ ] \begin{bmatrix} \boldsymbol{0_{6x1}} \\ \boldsymbol{0_{5x1}} \\ \boldsymbol{M}_{\eta}^{-1} \\ \boldsymbol{0_{5x1}} \end{bmatrix} = \boldsymbol{W} \boldsymbol{M}_{\eta}^{-1} \tag{4.94}$$

The matrix $\boldsymbol{M}_{\eta} = \boldsymbol{J}\boldsymbol{M}\boldsymbol{J}^T$ is non-singular because the rotation matrix has $|\boldsymbol{J}| = 1$ and the inertia matrix is positive-definitive. The term $\boldsymbol{W}$ in (4.91) is also nonsingular. The non-singularity of $\boldsymbol{A(x)}$ for all $x^{\circ} \in \mathbb{R}^{22}$ is proved because the term $\boldsymbol{W}\boldsymbol{M}_{\eta}^{-1}$ is non-singular (product of two non-singular matrices) for all $\boldsymbol{x}^{\circ} \in \mathbb{R}^{22}$. Hence, the system has a coordinate transformation. To find the control law, the term $\bar{\boldsymbol{b}}\boldsymbol{(x)} = L_{\boldsymbol{f}}^2 \boldsymbol{h}(x) = \nabla L_{\boldsymbol{f}} \boldsymbol{h}.\boldsymbol{f}$ (4.53) results

$$\bar{\boldsymbol{b}}\boldsymbol{(x)} = L_{\boldsymbol{f}}^2 \boldsymbol{h}(x) = \dot{\boldsymbol{W}}(\boldsymbol{\eta}, \boldsymbol{z}_{1r})\dot{\boldsymbol{\eta}} + \boldsymbol{W}(\boldsymbol{\eta}, \boldsymbol{z}_{1r})\boldsymbol{f}_3(\boldsymbol{x}) + \dot{\boldsymbol{W}}_r(\boldsymbol{\eta}, \boldsymbol{z}_{1r})\dot{\boldsymbol{z}}_{1r} + \boldsymbol{W}_r(\boldsymbol{\eta}, \boldsymbol{z}_{1r})\ddot{\boldsymbol{z}}_{1r} \tag{4.95}$$

Substituting $\boldsymbol{f}_3(\boldsymbol{x})$ into (4.95) and calculating $\boldsymbol{u}_G$ in (4.44) yields

$$\boldsymbol{u}_G = -\boldsymbol{b} + (\boldsymbol{D}_{\boldsymbol{\eta}} - \boldsymbol{J}\boldsymbol{M}\boldsymbol{J}\dot{\boldsymbol{J}}\boldsymbol{J}^T)\dot{\boldsymbol{\eta}} - \boldsymbol{M}_{\eta}\boldsymbol{W}^{-1}(\dot{\boldsymbol{W}}\dot{\eta} + \dot{\boldsymbol{W}}_r\dot{z}_{1r} + \boldsymbol{W}_r\ddot{z}_{1r} + \boldsymbol{v}) \tag{4.96}$$

where $\boldsymbol{v}$ is the new control vector. The new control vector is set as

$$\boldsymbol{v} = \boldsymbol{K}_p.\mathscr{C}(\boldsymbol{\eta}, \boldsymbol{z}_{1_r}) + \boldsymbol{K}_d.\dot{\mathscr{C}}(\boldsymbol{\eta}, \boldsymbol{z}_{1_r}) \tag{4.97}$$

where $\boldsymbol{K}_p$ and $\boldsymbol{K}_d \in \mathbb{R}^{6\times6}$ are gain matrices.

4.4.3 Lagrange Multiplier-based Controller for Dynamic Positioning

Lagrangian control law is obtained using a constraint function $\mathscr{C}(\boldsymbol{\eta})$, as discussed in Section 4.3.2. The constraint proposed in Section 4.4.1 depends on vectors $\boldsymbol{\eta}$ and also $\boldsymbol{z_{1r}}$. To find the $\boldsymbol{u}_\lambda$ using the $\mathscr{C}(\boldsymbol{\eta}, \boldsymbol{z}_{1r})$, this constraint is differentiated twice with respect to time as follows

$$\dot{\mathscr{C}}(\boldsymbol{\eta}, \boldsymbol{z}_{1r}) = \boldsymbol{W}(\boldsymbol{\eta}, \boldsymbol{z}_{1r})\dot{\eta} + \boldsymbol{W}_r(\boldsymbol{\eta}, \boldsymbol{z}_{1r})\dot{z}_{1r} = [\boldsymbol{0}_{6\times1}] \tag{4.98}$$

$$\ddot{\mathscr{C}}(\boldsymbol{\eta}, \boldsymbol{z}_{1r}) = \dot{\boldsymbol{W}}(\boldsymbol{\eta}, \boldsymbol{z}_{1r})\dot{\eta} + \boldsymbol{W}(\boldsymbol{\eta}, \boldsymbol{z}_{1r})\ddot{\eta} + \dot{\boldsymbol{W}}_r(\boldsymbol{\eta}, \boldsymbol{z}_{1r})\dot{z}_{1r} + \boldsymbol{W}_r(\boldsymbol{\eta}, \boldsymbol{z}_{1r})\ddot{z}_{1r} = [\boldsymbol{0}_{6\times1}] \tag{4.99}$$

The constraint function acceleration $\ddot{\mathscr{C}}(\boldsymbol{\eta}, \boldsymbol{z}_{1r})$ is stabilized by a feedback function as

$$\ddot{\mathscr{C}}(\boldsymbol{\eta}, \boldsymbol{z}_{1r}) = -\boldsymbol{K}_p.\mathscr{C}(\boldsymbol{\eta}, \boldsymbol{z}_{1r}) - \boldsymbol{K}_d.\dot{\mathscr{C}}(\boldsymbol{\eta}, \boldsymbol{z}_{1r}) = [\boldsymbol{0}_{6\times1}] \tag{4.100}$$

where $\boldsymbol{K}_p$ and $\boldsymbol{K}_d \in \mathbb{R}^{6\times6}$ are gain matrices. Doing (4.100) equals to (4.99), and isolating the term $\boldsymbol{W}(\boldsymbol{\eta}, \boldsymbol{z}_{1r})\ddot{\eta}$ yields

$$\boldsymbol{W}(\boldsymbol{\eta}, \boldsymbol{z}_{1r})\ddot{\eta} = -(\dot{\boldsymbol{W}}(\boldsymbol{\eta}, \boldsymbol{z}_{1r})\dot{\eta} + \dot{\boldsymbol{W}}_r(\boldsymbol{\eta}, \boldsymbol{z}_{1r})\dot{z}_{1r} + \boldsymbol{W}_r(\boldsymbol{\eta}, \boldsymbol{z}_{1r})\ddot{z}_{1r} + \boldsymbol{K}_p.\mathscr{C}(\boldsymbol{\eta}, \boldsymbol{z}_{1r}) + \boldsymbol{K}_d.\dot{\mathscr{C}}(\boldsymbol{\eta}, \boldsymbol{z}_{1r})) \tag{4.101}$$

The reference and its derivatives are assumed to be known and that the matrix $\boldsymbol{W}(\boldsymbol{\eta}, \boldsymbol{z}_{1r})^{-1}$ exists. Now, substituting $\ddot{\boldsymbol{\eta}}$ from (4.56) into (4.101), and isolating the constraint force term $\boldsymbol{W}^T\boldsymbol{\lambda}$, the control law $\boldsymbol{u}_\lambda = -\boldsymbol{W}^T\boldsymbol{\lambda}$ results

$$\boldsymbol{u}_\lambda = -\boldsymbol{b} + (\boldsymbol{D}_{\boldsymbol{\eta}} - \boldsymbol{J}\boldsymbol{M}\boldsymbol{J}\dot{\boldsymbol{J}}\boldsymbol{J}^T)\dot{\boldsymbol{\eta}} - \boldsymbol{M}_\eta\boldsymbol{W}^{-1}(\dot{\boldsymbol{W}}\dot{\eta} + \dot{\boldsymbol{W}}_r\dot{z}_{1r} + \boldsymbol{W}_r\ddot{z}_{1r} + \boldsymbol{K}_p.\mathscr{C} + \boldsymbol{K}_d.\dot{\mathscr{C}}) \tag{4.102}$$

Using $\mathscr{C}(\boldsymbol{\eta}, \boldsymbol{z}_{1r})$, the Jacobian matrices $\boldsymbol{W}$, $\boldsymbol{W_r}$ and their time derivatives result

$$\boldsymbol{W} = \begin{bmatrix} & \boldsymbol{I}_{3x3} & & & \boldsymbol{0}_{3x3} & \\ -1 & 0 & -(L_1/2+d)s(\psi_1) & 1 & 0 & -(L_2/2)s(\psi_2) \\ 0 & -1 & (L_1/2+d)c(\psi_1) & 0 & 1 & (L_2/2)c(\psi_2) \\ 0 & 0 & 0 & 0 & 0 & 1 \end{bmatrix} \tag{4.103}$$

$$\dot{\boldsymbol{W}} = \begin{bmatrix} & \mathbf{0}_{3x3} & & & \mathbf{0}_{3x3} & \\ 0 & 0 & -(L_1/2+d)c(\psi_1)\dot{\psi}_1 - \dot{d}s(\psi_1) & 0 & 0 & -(L_2/2)c(\psi_2)\dot{\psi}_2 \\ 0 & 0 & -(L_1/2+d)s(\psi_1)\dot{\psi}_1 + \dot{d}c(\psi_1) & 0 & 0 & -(L_2/2)s(\psi_2)\dot{\psi}_2 \\ 0 & 0 & 0 & 0 & 0 & 0 \end{bmatrix} \tag{4.104}$$

$$\boldsymbol{W_r} = \begin{bmatrix} -\boldsymbol{I}_{3x3} & \mathbf{0}_{3x2} \\ & c(\psi_1) \quad 0 \\ \mathbf{0}_{3x3} & s(\psi_1) \quad 0 \\ & 0 \quad -1 \end{bmatrix} \tag{4.105}$$

$$\dot{\boldsymbol{W}}_{\boldsymbol{r}} = \begin{bmatrix} \mathbf{0}_{3x3} & \mathbf{0}_{3x2} \\ & -s(\psi_1)\dot{\psi}_1 \quad 0 \\ \mathbf{0}_{3x3} & c(\psi_1)\dot{\psi}_1 \quad 0 \\ & 0 \quad 0 \end{bmatrix} \tag{4.106}$$

Comparing this control law to the geometric control law $\boldsymbol{u}_G$, the constraint force from Lagrangian multiplier-based controller is the same geometric control law since the matrices $\boldsymbol{K}_p$ and $\boldsymbol{K}_d$ are equal to the matrices of the geometric control (for control vector $\boldsymbol{v}$). Hence, if the constraint of the Lagrangian Multiplier-based controller depends on the position and reference and the geometric control law is obtained from a output equals to the constraint of the Lagrangian Multiplier-based controller, these controllers are equivalent, i.e., $\boldsymbol{u}_G \equiv \boldsymbol{u}_\lambda$. To prove that, the second-time derivative of the output is

$$\begin{gathered} \ddot{\boldsymbol{y}} = L_f^2 \boldsymbol{h}(\boldsymbol{x}) + L_g L_f \boldsymbol{h}(\boldsymbol{x})\boldsymbol{u} = \\ = \dot{\boldsymbol{W}}(\boldsymbol{\eta}, \boldsymbol{x}_{1r})\dot{\boldsymbol{\eta}} + \boldsymbol{W}(\boldsymbol{\eta}, \boldsymbol{x}_{1r})\ddot{\boldsymbol{\eta}} + \dot{\boldsymbol{W}}_r(\boldsymbol{\eta}, \boldsymbol{x}_{1r})\dot{\boldsymbol{x}}_r + \boldsymbol{W}_r(\boldsymbol{\eta}, \boldsymbol{x}_r)\ddot{\boldsymbol{x}}_r \end{gathered} \tag{4.107}$$

Hence, both control laws are an Input-to-Output linearization for the MIMO system presented. In the LM-approach, the distance between the vessels is understood as a constraint that is obeyed. As a result of feedback linearization, some nonlinear terms are canceled and the control needs to meet the demanded forces and moment in order to satisfy the constraint. In terms of Geometric Mechanics, the control law inserts a constraint force that maintains the system configuration restricted into a submanifold. This result reflects the Frobenius integrability theorem. Both control laws are identical, so the simulations in Chapter 6 present results with geometric and PD-like controllers only.

4.4.4 Conventional Error as Constraint

If the constraint function (system output) is equal to the error vector (4.108), geometric controller will have the error dynamics stabilized by a feedback of this error vector and its derivative. To show this result, take the error vector and the control model (2.18) with respect to Earth-frame as

$$\boldsymbol{e} = \boldsymbol{\eta_r} - \boldsymbol{\eta} \tag{4.108}$$

$$\boldsymbol{M}_\eta \ddot{\boldsymbol{\eta}} + (\boldsymbol{D_\eta} - \boldsymbol{J}(\psi_1, \psi_2)\boldsymbol{M}\boldsymbol{J}(\psi_1, \psi_2)^T \dot{\boldsymbol{J}}(\psi_1, \psi_2)\boldsymbol{J}(\psi_1, \psi_2)^T)\dot{\boldsymbol{\eta}} = \boldsymbol{b} + \boldsymbol{u} \tag{4.109}$$

The Jacobian matrices of the error vector $\boldsymbol{e} = \dot{\mathscr{C}}(\boldsymbol{\eta}, \boldsymbol{x}_r)$ can be found as

$$\boldsymbol{W}(\boldsymbol{\eta}, \boldsymbol{\eta_r}) = -\boldsymbol{I}_{6\times 6} \tag{4.110}$$

$$\boldsymbol{W_r}(\boldsymbol{\eta}, \boldsymbol{\eta_r}) = \boldsymbol{I}_{6\times 6} \tag{4.111}$$

where $\boldsymbol{W(\eta, \eta_r)} \in \mathbb{R}^{6\times 6}$ is the Jacobian matrix of the error vector with respect to $\boldsymbol{\eta}$ and $\boldsymbol{W}_r(\boldsymbol{\eta}, \boldsymbol{\eta}_r) \in \mathbb{R}^{6\times 6}$ is the Jacobian matrix of the error vector with respect to $\boldsymbol{\eta}_r$. The Jacobian matrix derivatives are $\dot{\boldsymbol{W}} = \dot{\boldsymbol{W}}_r = \boldsymbol{0}_{6\times 6}$.

Now, using the output linearization procedure (section 4.4.2) and calculating the geometric control law in (4.96), it is possible to find the following control law

$$\boldsymbol{u}_G = \boldsymbol{u}_\lambda = -\boldsymbol{b} + (\boldsymbol{D_\eta} - \boldsymbol{J}\boldsymbol{M}\boldsymbol{J}\dot{\boldsymbol{J}}\boldsymbol{J}^T)\dot{\boldsymbol{\eta}} - \boldsymbol{M}_\eta \boldsymbol{W}^{-1}(\dot{\boldsymbol{W}}\dot{\eta} + \dot{\boldsymbol{W}}_r\dot{\eta}_r + \boldsymbol{W}_r\ddot{\eta}_r + \boldsymbol{v}) \tag{4.112}$$

Substituting the Jacobian matrices into (4.112) yields

$$\boldsymbol{u}_G = \boldsymbol{u}_\lambda = -\boldsymbol{b} + \boldsymbol{M}_\eta(\boldsymbol{D_\eta} - \boldsymbol{J}\boldsymbol{M}\boldsymbol{J}\dot{\boldsymbol{J}}\boldsymbol{J}^T)\dot{\boldsymbol{\eta}} + \boldsymbol{M}_\eta(\ddot{\eta}_r + \boldsymbol{v}) \tag{4.113}$$

Hence, substituting the control law in (4.113) into (4.109) results

$$\ddot{\boldsymbol{e}} = -\boldsymbol{v} = -\boldsymbol{K}_p\boldsymbol{e} - \boldsymbol{K}_d\dot{\boldsymbol{e}} \tag{4.114}$$

where $\boldsymbol{v} \in \mathbb{R}^6$ is the new control vector, $\boldsymbol{K}_p$ and $\boldsymbol{K}_d \in \mathbb{R}^{6\times 6}$ are diagonal matrices. This

procedure linearizes the error dynamics using a static feedback linearization. Now, using the transformation $\boldsymbol{\tau}_c = \boldsymbol{J}(\psi)^T \boldsymbol{u}$, take (4.109) rewritten in body-frames coordinates as follows

$$\boldsymbol{M}\dot{\boldsymbol{\nu}} + \boldsymbol{D}\nu = \boldsymbol{J}(\psi_1, \psi_2)^T)(\boldsymbol{b} + \boldsymbol{u}) \tag{4.115}$$

A PD-like controller is proposed as

$$\boldsymbol{u}_{PD} = \boldsymbol{K}_p \boldsymbol{e} + \boldsymbol{K}_d \dot{\boldsymbol{e}} - \boldsymbol{b} \tag{4.116}$$

$$\boldsymbol{K}_p = \boldsymbol{M}\boldsymbol{J}(\psi_1, \psi_2)^T \overline{\boldsymbol{K}}_p \tag{4.117}$$

$$\boldsymbol{K}_d = \boldsymbol{M}\boldsymbol{J}(\psi_1, \psi_2)^T \overline{\boldsymbol{K}}_d - \boldsymbol{D}\boldsymbol{J}(\psi_1, \psi_2)^T \tag{4.118}$$

where $\overline{\boldsymbol{K}}_p$ and $\overline{\boldsymbol{K}}_d \in \mathbb{R}^{6\times 6}$ are diagonal matrices. Calculating the second time-derivative of the error vector and using (2.1) results

$$\dot{\boldsymbol{e}} = \dot{\boldsymbol{\eta}}_{\boldsymbol{r}} - \dot{\boldsymbol{\eta}} = \dot{\boldsymbol{\eta}}_{\boldsymbol{r}} - \boldsymbol{J}(\psi_1, \psi_2)\boldsymbol{\nu} \tag{4.119}$$

$$\ddot{\boldsymbol{e}} = \ddot{\boldsymbol{\eta}}_{\boldsymbol{r}} - \dot{\boldsymbol{J}}(\psi_1, \psi_2)\boldsymbol{\nu} - \boldsymbol{J}(\psi_1, \psi_2)\dot{\boldsymbol{\nu}} \tag{4.120}$$

Substituting the control vector (4.116) into (4.115), collecting the term $\dot{\boldsymbol{\nu}}$, and inserting it into (4.120) yields

$$\ddot{\boldsymbol{e}} = \ddot{\boldsymbol{\eta}}_{\boldsymbol{r}} - \dot{\boldsymbol{J}}(\psi_1, \psi_2)\boldsymbol{\nu} - \boldsymbol{J}(\psi_1, \psi_2)\boldsymbol{M}^{-1}\boldsymbol{D}\boldsymbol{J}(\psi_1, \psi_2)^T \dot{\boldsymbol{\eta}}_{\boldsymbol{r}} - \overline{\boldsymbol{K}}_p \boldsymbol{e} - \overline{\boldsymbol{K}}_d \dot{\boldsymbol{e}} \tag{4.121}$$

Assuming constant reference, its time-derivative is null. The yaw velocity is assumed slow and the term $\dot{\boldsymbol{J}}(\psi_1, \psi_2)\boldsymbol{\nu}$ is considered null. Hence, the error dynamics in (4.121) can be approximate as

$$\ddot{\boldsymbol{e}} \approx -\overline{\boldsymbol{K}}_p \boldsymbol{e} - \overline{\boldsymbol{K}}_d \dot{\boldsymbol{e}} \tag{4.122}$$

The resulting error dynamics in (4.122) from a nonlinear PD-like controller is similar to the linearized error dynamics in (4.114) from a feedback linearization procedure. Hence, it would be expected similar behavior between the geometric and PD-like controller if the error vector $\boldsymbol{e}$

were used by both controllers.

4.5 Thrust Allocation

The control law $\boldsymbol{u}$ described in local coordinates can be obtained as

$$\boldsymbol{\tau}_c = \boldsymbol{J}(\psi)^T \boldsymbol{u} \tag{4.123}$$

The local control vector $\boldsymbol{\tau}_c \in \mathbb{R}^6$ is divided into two vectors $\boldsymbol{\tau}_{c_i} \in \mathbb{R}^3$ for each vessel i. Once the local control law $\boldsymbol{\tau}_{c_i}$ is calculated by the controller, it is necessary to determine the thrust control vector $\overline{\boldsymbol{\tau}}_{p_i} \in \mathbb{R}^{n_i}$ to distribute the thrusts among the n_i actuators. The relationship between these vector is

$$\boldsymbol{\tau}_{c_i} = \overline{\boldsymbol{B}}_i . \overline{\tau}_{p_i} \tag{4.124}$$

In general, the vessels with DPS installed are overactuated and their actuators can be main propellers, azimuth and tunnel thrusters. Then, the actuator configuration matrix $\overline{\boldsymbol{B}}_i$ is

$$\overline{\boldsymbol{B}}_i = \begin{bmatrix} c(\alpha_1) & \dots & c(\alpha_j) \\ s(\alpha_1) & \ddots & s(\alpha_j) \\ -c(\alpha_1) * y_1 + s(\alpha_1) * x_1 & \dots & -c(\alpha_j) * y_j + s(\alpha_j) * x_j \end{bmatrix} \tag{4.125}$$

where α_{n_i} is the thruster angle, x_{n_i} and y_{n_i} are the longitudinal and transverse positions of the actuators. For tunnel thrusters, $\alpha = 90^\circ$ and for main propellers $\alpha = 0^\circ$. See details about actuator configuration matrix in Tannuri (2002)). The thrust control vector can be determined as

$$\overline{\boldsymbol{\tau}}_{p_i} = \overline{\boldsymbol{A}}_i \boldsymbol{\tau}_{c_i} \tag{4.126}$$

$$\overline{\boldsymbol{A}}_i = \overline{\boldsymbol{W}}_i^{-1} \overline{\boldsymbol{B}}_i^T (\overline{\boldsymbol{B}}_i \overline{\boldsymbol{W}}_i^{-1} \overline{\boldsymbol{B}}_i^T)^{-1} \tag{4.127}$$

where $\overline{\boldsymbol{A}}_i \in \mathbb{R}^{3 \times n_i}$ is the generalized inverse matrix, $\overline{\boldsymbol{W}}_i \in \mathbb{R}^{n_i \times n_i}$ is the weighting diagonal

matrix. The elements of the weighting diagonal matrix $\overline{\boldsymbol{W}}_i$ can be obtained from (GRANJA, 2009) as

$$w_{n_i \times n_i} = 5.77 \frac{Pmax_{n_i}}{Tmax_{n_i}^2} \tag{4.128}$$

where $w_{n_i \times n_i}$ is the element of the weighting thruster matrix, $Pmax_{n_i}$ is the maximum power and $Tmax_{n_i}$ is the maximum thrust. The saturation of the actuators is considered as

$$\boldsymbol{\tau}_d = \frac{1}{2} \left(\boldsymbol{\tau}_{max} + \boldsymbol{\tau}_{min} - |\boldsymbol{\tau}_{max} - \overline{\boldsymbol{\tau}}_p| + |\overline{\boldsymbol{\tau}}_p - \boldsymbol{\tau}_{min}| \right) \tag{4.129}$$

where $\boldsymbol{\tau}_d = [\ \boldsymbol{\tau}_{d_1}^T \quad \boldsymbol{\tau}_{d_2}^T\ ]^T \in \mathbb{R}^{n_1+n_2}$ is the demanded thrust vector. The complete thrust control force is $\overline{\boldsymbol{\tau}}_p = [\ \overline{\boldsymbol{\tau}}_{p_1}^T \quad \overline{\boldsymbol{\tau}}_{p_2}^T\ ]^T \in \mathbb{R}^{n_1+n_2}$. The vector of maximum thrust is $\boldsymbol{\tau}_{max} = [\ \boldsymbol{\tau}_{max_1}^T \quad \boldsymbol{\tau}_{max_2}^T\ ]^T \in \mathbb{R}^{n_1+n_2}$. The vector of minimum thrust is $\boldsymbol{\tau}_{min} = [\ \boldsymbol{\tau}_{min_1}^T \quad \boldsymbol{\tau}_{min_2}^T\ ]^T \in \mathbb{R}^{n_1+n_2}$.

Once one of the actuators is saturated and there are actuators with available thrust to be allocated, the saturated actuator is removed from the thruster configuration and the weighting matrices, and the allocation logic is redone. This process continues until the demanded force and moment are met or the rank of the thruster configuration be less than 3.

In practice, there is some time lag between the demanded control force $\boldsymbol{\tau}_d$ and the real thrust $\boldsymbol{\tau}_p$ of the actuators. This lag is considered through the actuator dynamics as (FOSSEN, 1994)

$$\dot{\boldsymbol{\tau}}_p = \boldsymbol{T}_d(\boldsymbol{\tau}_p - \boldsymbol{\tau}_d) \tag{4.130}$$

where matrix $\boldsymbol{T}_d \in \mathbb{R}^{3\times(n_1+n_2)}$ is a diagonal matrix of time constants. Figure 4.6 presents a block diagram that illustrates the thrust allocation with the actuator dynamics.

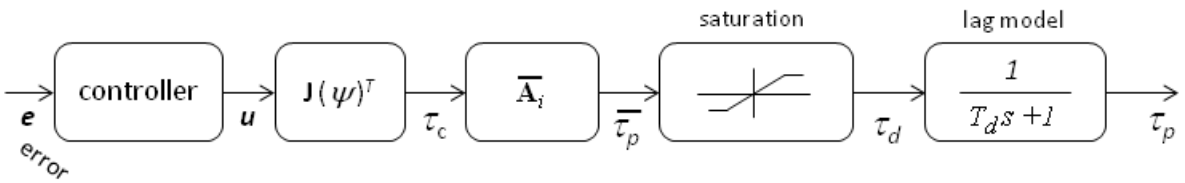

Figure 4.6: Block diagram for thrust allocation

Chapter 5

Hybrid Concept applied to Offloading Operation

5.1 Switching Controller based on Draft and Sea State

The switching control application requires the assessment of significant parameter range on the system dynamics. In the case of DPS vessels involved in the offloading operations, the parameters are the vessels' draft and the peak-frequency of the wave-frequency vessel motions. The former affects directly the vessels' dynamics by changing their inertia matrices, and the latter is one of the parameters for the definition of the cut-off frequency of the filter (estimator). Dong (2005) proposed a hybrid concept for DP vessels and suggested the cut-off frequencies for four operational ranges. A cross spectrum analysis is performed here in order to determine peak-frequency ranges. In this analysis, vessel drafts, sea state and the angle of incidence of the waves are all evaluated on the system, and the response spectra calculated, using the RAOs. See Appendix C for details. The main conclusions from these analyses are:

1. Draft does not affect motion peak-frequency for a given sea state and wave angle of incidence

2. The angle of incidence does not change the peak-frequency for a given draft and sea state

3. For filtering purposes, the peak-frequency motions can be split into four ranges. These ranges are very similar to those proposed by Dong (2005)

Draft alters the vessels' inertia matrix. This matrix is used for tuning control parameters. Therefore, draft variation impacts upon controller performance.

Assuming a maximum positioning error of 10% in the perturbation model, three draft ranges are obtained (see Appendix B). Due to the fact that motion peak-frequency does not alter with draft variation, those three draft ranges are associated with those four sea state ranges. So, we define $\mathscr{M} := \bigcup_{p \in \mathscr{P}} \mathscr{M}_p$ with $p = 1, ..., 12$ and $\mathscr{C} := \bigcup_{q \in \mathscr{Q}} \mathscr{C}_q$ with $q = 1, ..., 12$ (three draft ranges times the four sea state ranges). Once the number of estimators has been determined, the hybrid concept applied to the offloading operation is presented as in Figure 5.1. Tables 5.1 and 5.2 present the sea state ranges and the draft ranges of each vessel, respectively.

Table 5.1: Reference sea states (DONG, 2005)

Sea State Reference s	Sea State Condition	ω_p [rad/s]	Observer
1	Calm Seas	> 0.79	Nonlinear observer with notch filter
2	Moderate Seas	0.79 - 0.67	Nonlinear observer with notch filter
3	High Seas	0.67-0.45	Nonlinear observer with notch filter
4	Extreme Seas	< 0.45	Nonlinear observer for extreme seas

Table 5.2: Reference drafts for control model

Reference Draft k	Shuttle tanker h [m]	FPWSO h [m]
1	8.00	21.00
2	12.48	18.21
3	17.50	15.42

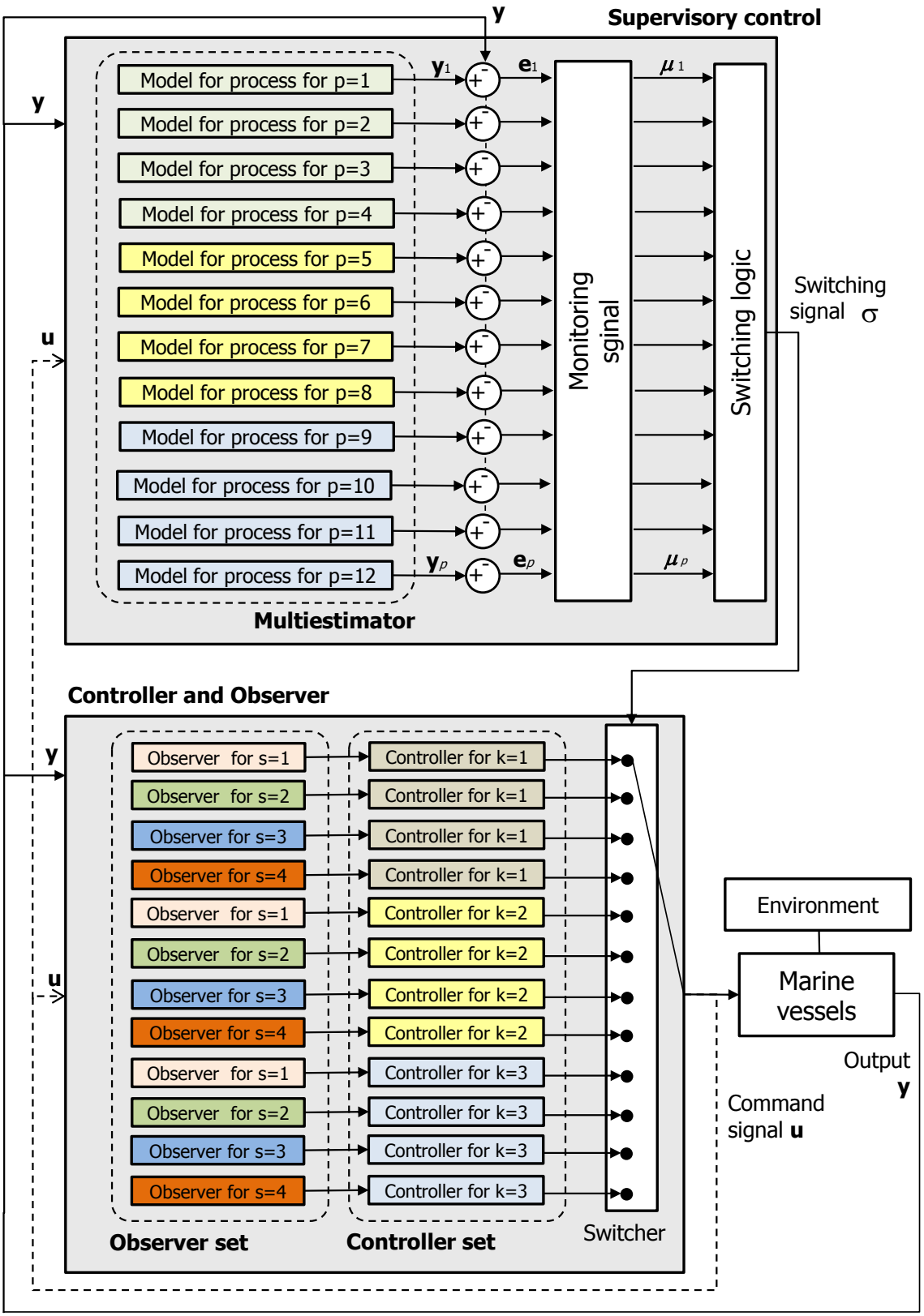

Figure 5.1: Hybrid concept applied to offloading operation

As presented in Chapter 3, the mapping is $\sigma = \rho$ and, as a consequence, $\mathscr{P} \equiv \mathscr{Q}$. Table 5.3 presents a mapping between the multi-estimator, the draft ranges and sea states for reference purposes. To simplify the reference, the multi-estimator is denoted by p, the sea states ranges are denoted by $s = 1, ..., 4$ as defined in Table 5.1, and draft ranges are denoted by $k = 1, ..., 3$ as defined in Table 5.2. To monitor sea state, the motion peak-frequency is assumed to be slow-varying, i.e., $\dot{\omega}_p = 0$ (DONG, 2005), and its estimate is calculated as presented in Section 5.4. The offloading operation between DP vessels takes around 24h. Then, their drafts are assumed to be slow-varying, i.e., $\dot{\boldsymbol{h}} \approx \mathbf{0}$, where $\boldsymbol{h} = [\ h_1 \quad h_2\ ]^T$ are the drafts for FPWSO and the shuttle tanker, respectively.

Table 5.3: Mapping between supervisor and controller set

Multi-estimator $p = q$	Sea state ranges s	Draft ranges k
1	1	1
2	2	1
3	3	1
4	4	1
5	1	2
6	2	2
7	3	2
8	4	2
9	1	3
10	2	3
11	3	3
12	4	3

The switching controller possesses a controller set based on the geometric control law and the nonlinear observer. PD-like controller is also studied using the same observer. The switching control model for the offloading operation is presented in the following sections. The multi-estimator and the controller and observer sets that comprise the switching control are presented. Finally, the peak-frequency tracker, draft survey calculation and supervisory tuning are all discussed.

5.2 Nonlinear Observer Set and Multi-estimator

The observer set and multi-estimator for the hybrid control presented here are based on the indices in Table 5.3.

5.2.1 Multi-estimator with Wave-Frequency Model

The nonlinear observer with wave-frequency motion model was proposed in Section 4.2.1. This observer is applied to three of the four sea state ranges of the switching controller ($s = 1, ..., 3$). So, nine estimators of the supervisory control are based on the nonlinear observer model ($p = \{1, ..., 12\} - \{4, 8, 12\}$). Considering Section 4.2.1, an extended system model is written as

$$\dot{\boldsymbol{\xi}} = \boldsymbol{\Omega}\boldsymbol{\xi} + \boldsymbol{\Sigma}\boldsymbol{w} \tag{5.1}$$

$$\dot{\boldsymbol{\eta}} = \boldsymbol{J}(\psi_1, \psi_2)\boldsymbol{\nu} \tag{5.2}$$

$$\dot{\boldsymbol{b}} = -T^{-1}\boldsymbol{b} + \boldsymbol{\Psi}\boldsymbol{n} \tag{5.3}$$

$$\boldsymbol{M}_k\dot{\boldsymbol{\nu}} + \boldsymbol{D}_k\boldsymbol{\nu} = \boldsymbol{J}^T(\psi_1, \psi_2)\boldsymbol{b} + \boldsymbol{\tau}_c \tag{5.4}$$

$$\dot{\boldsymbol{h}} = \mathbf{0}_{2\times 1} \tag{5.5}$$

$$\dot{\boldsymbol{\omega_p}} = \mathbf{0} \tag{5.6}$$

$$\mathbf{y} = \begin{bmatrix} (\boldsymbol{\eta} + \boldsymbol{\Gamma}\boldsymbol{\xi})^T & \boldsymbol{h}^T & \boldsymbol{\omega_p} \end{bmatrix}^T \tag{5.7}$$

where $\boldsymbol{M}_k$ and $\boldsymbol{D}_k$ denote the matrices calculated in draft range k. This model is similar to the system model presented by Dong (2005) except for the inclusion of (5.5). Dong (2005) took the peak-frequency to be slow-varying, i.e., $\dot{\boldsymbol{\omega_p}} = \mathbf{0}$. Here, the drafts are also assumed to be slow-varying, i.e., $\dot{\boldsymbol{h}} = \mathbf{0}$. Thus, the output vector is $\mathbf{y} \in \mathbb{R}^9$ with the extended system model

having draft vector $\boldsymbol{h}$. A system can be expressed concisely using (5.1) to (5.7) as

$$\dot{\mathbf{x}}_p = A_p \mathbf{x}_p + \boldsymbol{B}_q \boldsymbol{\tau}_q + \boldsymbol{E}_p \overline{\boldsymbol{w}} \tag{5.8}$$

$$\mathbf{y} = \boldsymbol{C}_p \mathbf{x}_p \tag{5.9}$$

where the state vector is $\mathbf{x}_p = [\ \boldsymbol{\xi}^T \quad \boldsymbol{\eta}^T \quad \boldsymbol{b}^T \quad \boldsymbol{\nu}^T \quad \boldsymbol{h}^T \quad \boldsymbol{\omega}_p\ ]^T \in \mathbb{R}^{33}$ and the disturbance vector is $\overline{\boldsymbol{w}} = [\ \boldsymbol{w}^T \quad \boldsymbol{n}^T\ ]^T \in \mathbb{R}^{12}$. The control vector is $\boldsymbol{\tau}_q \in \mathbb{R}^6$. The matrices $\boldsymbol{A}_p \in \mathbb{R}^{33\times33}$, $\boldsymbol{B}_q \in \mathbb{R}^{33\times6}$, $\boldsymbol{E}_p \in \mathbb{R}^{33\times12}$ and $\boldsymbol{C}_p \in \mathbb{R}^{9\times33}$ are written as

$$\boldsymbol{A}_p = \begin{bmatrix} \boldsymbol{\Omega} & \mathbf{0}_{12\times21} \\ \mathbf{0}_{21\times12} & \boldsymbol{A}_{LF} \end{bmatrix} \tag{5.10}$$

$$\boldsymbol{B}_q = \begin{bmatrix} \mathbf{0}_{12\times6} \\ \boldsymbol{B}_{LF} \end{bmatrix} \tag{5.11}$$

$$\boldsymbol{E}_p = \begin{bmatrix} \boldsymbol{\Sigma}_{12\times6} & \mathbf{0}_{12\times6} \\ \mathbf{0}_{21\times6} & \boldsymbol{E}_{LF} \end{bmatrix} \tag{5.12}$$

$$\boldsymbol{C}_p = \begin{bmatrix} \boldsymbol{\Gamma} & \boldsymbol{I}_{6\times6} & \mathbf{0}_{6\times6} & \mathbf{0}_{6\times6} & \mathbf{0}_{6\times2} & \mathbf{0}_{6\times1} \\ \mathbf{0}_{2\times6} & \mathbf{0}_{2\times6} & \mathbf{0}_{2\times6} & \mathbf{0}_{2\times6} & \boldsymbol{I}_{2\times2} & \mathbf{0}_{2\times1} \\ \mathbf{0}_{1\times6} & \mathbf{0}_{1\times6} & \mathbf{0}_{1\times6} & \mathbf{0}_{1\times6} & \mathbf{0}_{1\times2} & 1 \end{bmatrix} \tag{5.13}$$

The matrices $\boldsymbol{A}_{LF} \in \mathbb{R}^{21\times21}$, $\boldsymbol{B}_{LF} \in \mathbb{R}_{q_i}^{21\times6}$, $\boldsymbol{E}_{LF} \in \mathbb{R}_{q}^{21\times6}$ are written as

$$\boldsymbol{A}_{LF} = \begin{bmatrix} \mathbf{0}_{6\times6} & \mathbf{0}_{6\times6} & \boldsymbol{J}(\psi_1, \psi_2) & \mathbf{0}_{6\times2} & \mathbf{0}_{6\times1} \\ \mathbf{0}_{6\times6} & -\boldsymbol{T}^{-1} & \mathbf{0}_{6\times6} & \mathbf{0}_{6\times2} & \mathbf{0}_{6\times1} \\ \mathbf{0}_{6\times6} & \mathbf{0}_{6\times6} & -\boldsymbol{M}_{\boldsymbol{k}}^{-1}\boldsymbol{D}_k & \mathbf{0}_{6\times2} & \mathbf{0}_{6\times1} \\ \mathbf{0}_{2\times6} & \mathbf{0}_{2\times6} & \mathbf{0}_{2\times6} & \boldsymbol{I}_{2\times2} & \mathbf{0}_{2\times1} \\ \mathbf{0}_{1\times6} & \mathbf{0}_{1\times6} & \mathbf{0}_{1\times6} & \mathbf{0}_{1\times2} & 1 \end{bmatrix} \tag{5.14}$$

$$\boldsymbol{B}_{LF} = \begin{bmatrix} \mathbf{0}_{6\times6} \\ \mathbf{0}_{6\times6} \\ \boldsymbol{M}_{\boldsymbol{k}}^{-1} \\ \mathbf{0}_{2\times6} \\ \mathbf{0}_{1\times6} \end{bmatrix} \tag{5.15}$$

$$\boldsymbol{E}_{LF} = \begin{bmatrix} \mathbf{0}_{6\times6} \\ \boldsymbol{\Psi} \\ \mathbf{0}_{6\times6} \\ \mathbf{0}_{2\times6} \\ \mathbf{0}_{1\times6} \end{bmatrix} \tag{5.16}$$

This system model is used as the estimator model for the wave-frequency motion of the switching control. So, the estimator is constructed similarly to the state observer as presented in Section 4.2.1. Considering (5.1) to (5.6), the state observer vector $\hat{\mathbf{x}}_p$ can be written as

$$\dot{\hat{\mathbf{x}}}_p = \boldsymbol{A_p}\hat{\mathbf{x}}_p + \boldsymbol{B}_q\boldsymbol{\tau}_q + \boldsymbol{K}_{p_s}(\mathbf{y} - \mathbf{y}_p) \tag{5.17}$$

$$\mathbf{y}_p = \boldsymbol{C}_p\hat{\mathbf{x}}_p \tag{5.18}$$

where the state observer vector is $\hat{\mathbf{x}}_p = \begin{bmatrix} \hat{\boldsymbol{\xi}}^T & \hat{\boldsymbol{\eta}}^T & \hat{\boldsymbol{b}}^T & \hat{\boldsymbol{\nu}}^T & \hat{\boldsymbol{h}}^T & \hat{\boldsymbol{\omega}}_{\boldsymbol{p}} \end{bmatrix}^T \in \mathbb{R}^{33}$. The vector $\mathbf{y}_p \in \mathbb{R}^9$ is the output of the state observer of the process p (see Figure 5.1). The frequency $\hat{\omega}_p$ is the peak-frequency spectrum obtained from the spectra analysis (see Section 5.4) and the estimated draft vector $\hat{\boldsymbol{h}}$ is obtained from the draft survey calculation (see Section 5.5). Matrix $\boldsymbol{K}_{p_s} \in \mathbb{R}^{33\times 9}$ is written as

$$\boldsymbol{K}_{p_s} = \begin{bmatrix} \boldsymbol{K}_{1_s} & \mathbf{0}_{12\times 2} & \mathbf{0}_{12\times 1} \\ \boldsymbol{K}_{LF_s} & \mathbf{0}_{21\times 2} & \mathbf{0}_{21\times 1} \end{bmatrix} \tag{5.19}$$

where $\boldsymbol{K}_{1_s} \in \mathbb{R}^{12\times 6}$ and $\boldsymbol{K}_{LF_s} \in \mathbb{R}^{21\times 6}$. Matrix $\boldsymbol{K}_{LF_s} \in \mathbb{R}^{21\times 6}$ is written as

$$\boldsymbol{K}_{LF_s} = \begin{bmatrix} \boldsymbol{K}_{2_s} \\ \boldsymbol{K}_{3_s} \\ \boldsymbol{K}_{4_s} \\ \mathbf{0}_{2\times 6} \\ \mathbf{0}_{1\times 6} \end{bmatrix} \tag{5.20}$$

with the matrices $\boldsymbol{K}_{2_s}$, $\boldsymbol{K}_{3_s}$ and $\boldsymbol{K}_{4_s} \in \mathbb{R}^{6\times 6}$ being presented in Section 4.2 and calculated as presented by Fossen and Strand (1999). Each matrix with index s is calculated for sea state range s.

5.2.2 Multi-estimator for Extreme Seas

The nonlinear observer for extreme seas was presented in Section 4.2.2. This model is applied to one of the four sea state ranges of the switching control when $s = 4$. So, three estimators of the supervisory control use this nonlinear observer model ($p = \{4, 8, 12\}$). Consider the following

system model for extreme seas

$$\dot{\boldsymbol{\eta}}_T = \boldsymbol{J}(\psi_1, \psi_2)\hat{\boldsymbol{\nu}}_T \tag{5.21}$$

$$\dot{\boldsymbol{b}}_T = -T^{-1}\boldsymbol{b}_T + \boldsymbol{\Psi}\boldsymbol{n} \tag{5.22}$$

$$\boldsymbol{M}_k\dot{\nu}_T + \boldsymbol{D}_k\nu_T = \boldsymbol{J}^T(\psi_1, \psi_2)\boldsymbol{b}_T + \boldsymbol{\tau}_c \tag{5.23}$$

$$\dot{\boldsymbol{h}} = \mathbf{0}_{2\times 1} \tag{5.24}$$

$$\dot{\boldsymbol{\omega_p}} = \mathbf{0} \tag{5.25}$$

The output vector $\boldsymbol{y} \in \mathbb{R}^9$ is written as

$$\mathbf{y} = \begin{bmatrix} \boldsymbol{\eta}_T^T & \boldsymbol{h}^T & \boldsymbol{\omega_p} \end{bmatrix}^T \tag{5.26}$$

Similarly to the previous section, the model is concisely written as

$$\dot{\mathbf{x}}_p = \boldsymbol{A_p}\mathbf{x}_p + \boldsymbol{B}_q\boldsymbol{\tau}_q + \boldsymbol{E}_p\overline{\boldsymbol{w}} \tag{5.27}$$

where the vector $\mathbf{x}_p = \begin{bmatrix} \boldsymbol{\eta}_T^T & \boldsymbol{b}_T^T & \boldsymbol{\nu}_T^T & \boldsymbol{h}^T & \boldsymbol{\omega}_p \end{bmatrix}^T \in \mathbb{R}^{21}$, $\boldsymbol{A_p} = \boldsymbol{A_{LF}} \in \mathbb{R}^{21\times 21}$, $\boldsymbol{B_p} = \boldsymbol{B_{LF}} \in \mathbb{R}^{21\times 21}$ in (5.15) and $\boldsymbol{E_p} = \boldsymbol{E_{LF}} \in \mathbb{R}^{21\times 21}$. The disturbance vector is $\overline{\boldsymbol{w}} = \boldsymbol{n} \in \mathbb{R}^6$. The system model presented is the switching control estimator model for extreme seas. The switching control estimator is constructed similarly to the state observer as presented in Section 4.2.2. Based on (5.21) to (5.25), the state observer vector $\hat{\mathbf{x}}_p$ can be written as

$$\dot{\hat{\mathbf{x}}}_p = \boldsymbol{A_p}\hat{\mathbf{x}}_p + \boldsymbol{B}_q\boldsymbol{\tau}_q + \boldsymbol{K}_{p_s}(\mathbf{y} - \mathbf{y}_p) \tag{5.28}$$

$$\mathbf{y}_p = \boldsymbol{C}_p\hat{\mathbf{x}}_p \tag{5.29}$$

where $\hat{\mathbf{x}}_p = \begin{bmatrix} \hat{\boldsymbol{\eta}}_T^T & \hat{\boldsymbol{b}}_T^T & \hat{\boldsymbol{\nu}}_T^T & \hat{\boldsymbol{h}}^T & \hat{\boldsymbol{\omega}}_{\boldsymbol{p}} \end{bmatrix}^T \in \mathbb{R}^{21}$. The matrix $\boldsymbol{C_p} \in \mathbb{R}^{9\times 21}$ is written as

$$\boldsymbol{C}_p = \begin{bmatrix} \boldsymbol{I}_{6\times 6} & \mathbf{0}_{6\times 6} & \mathbf{0}_{6\times 6} & \mathbf{0}_{6\times 2} & \mathbf{0}_{6\times 1} \\ \mathbf{0}_{2\times 6} & \mathbf{0}_{2\times 6} & \mathbf{0}_{2\times 6} & \boldsymbol{I}_{2\times 2} & \mathbf{0}_{2\times 1} \\ \mathbf{0}_{1\times 6} & \mathbf{0}_{1\times 6} & \mathbf{0}_{1\times 6} & \mathbf{0}_{1\times 2} & 1 \end{bmatrix} \tag{5.30}$$

The matrices $\boldsymbol{K_{2_{Ts}}}$, $\boldsymbol{K_{3_{Ts}}}$ and $\boldsymbol{K_{4_{Ts}}} \in \mathbb{R}^{6\times6}$ that compose $\boldsymbol{K_{p_s}}$ are similar to the estimator model for wave-frequency motion.

5.3 Controller Set

The geometric control law is used into the supervisory switching controller set. For the sake of comparison, the PD-like control law is also studied. Both geometric and PD-like controllers are determined for the vessels' dynamic positioning systems in offloading operations, as presented in Sections 4.4.2 and 4.4.4, respectively.

The current section describes both control laws employed when selecting the switching controller. The control laws take into account the estimated values of positions and headings, and velocities and external forces. For each controller, two state observers are considered, i.e., with and without wave-frequency vessel motions.

5.3.1 Geometric Controller Set

In order to present the geometric control law for the nonlinear observer with the wave-frequency model, the control law is indexed from (4.96) and yields

$$\boldsymbol{u}_{G_p} = -\hat{\boldsymbol{b}} + (\boldsymbol{D}_{\hat{\eta}} - \boldsymbol{J}\boldsymbol{M}_k\boldsymbol{J}\dot{\boldsymbol{J}}\boldsymbol{J}^T)\dot{\hat{\boldsymbol{\eta}}} - \boldsymbol{M}_{\hat{\eta}}\boldsymbol{W}^{-1}(\dot{\boldsymbol{W}}\dot{\hat{\eta}} + \dot{\boldsymbol{W}}_r\dot{x}_r + \boldsymbol{W}_r\ddot{x}_r + \boldsymbol{v}_p) \tag{5.31}$$

where $\boldsymbol{u}_{G_p} \in \mathbb{R}^6$ is the control vector for $p = \{1, ..., 12\} - \{4, 8, 12\}$.

$$\begin{aligned}\boldsymbol{\tau}_{q_i} = \boldsymbol{J}(\boldsymbol{y})^T\boldsymbol{u}_{G_i} = -\boldsymbol{J}(\boldsymbol{y})^T\hat{\boldsymbol{b}} + (\boldsymbol{D}_k - \boldsymbol{M}_k\boldsymbol{J}(\boldsymbol{y})\dot{\boldsymbol{J}}(\boldsymbol{y}))\hat{\boldsymbol{\nu}} - \\ -\boldsymbol{M}_k\boldsymbol{J}(\boldsymbol{y})^{-1}\boldsymbol{W}^{-1}(\dot{\boldsymbol{W}}\boldsymbol{J}(\boldsymbol{y})\boldsymbol{\nu} + \dot{\boldsymbol{W}}_r\dot{x}_r + \boldsymbol{W}_r\ddot{x}_r + \boldsymbol{v}_i)\end{aligned} \tag{5.32}$$

$$\boldsymbol{v}_i = \boldsymbol{K}_{p_k}.\mathscr{C}(\hat{\boldsymbol{\eta}}, \boldsymbol{x}_r) + \boldsymbol{K}_{d_k}.\dot{\mathscr{C}}(\hat{\boldsymbol{\eta}}, \boldsymbol{x}_r) \tag{5.33}$$

The matrices $\boldsymbol{D}_{\hat{\eta}}$ and $\boldsymbol{M}_{\hat{\eta}}$ are defined in Section 4.3.2. The matrices $\boldsymbol{W}$, $\dot{\boldsymbol{W}}$, $\boldsymbol{W}_r$ and $\dot{\boldsymbol{W}}_r$ are defined in Section 4.3.2. The new control vector is $\boldsymbol{v}_i \in \mathbb{R}^6$. The positioning constraint is $\mathscr{C}(\hat{\boldsymbol{\eta}}, \boldsymbol{x}_r)$ and is presented in (4.80).

The gain matrices $\boldsymbol{K}_p \in$ and $\boldsymbol{K}_d \in \mathbb{R}^{6\times6}$ are defined as

$$\boldsymbol{K}_{p_k} = diag\{\ \omega_{n_1}^2 \quad ... \quad \omega_{n_6}^2\ \} \tag{5.34}$$

$$\boldsymbol{K}_{d_k} = 2.diag\{\ \varsigma_{c_{n_1}}\omega_{n_1} \quad ... \quad \varsigma_{c_{n_6}}\omega_{n_6}\ \} \tag{5.35}$$

where $\varsigma_{c_{n_i}}$ and ω_{n_i} are control parameters. For control laws with $p = \{4, 8, 12\}$, the geometric law is presented as follows

$$\begin{aligned}\boldsymbol{\tau}_{q_i} = &-\boldsymbol{J}(\boldsymbol{y})^T\hat{\boldsymbol{b}}_{\boldsymbol{T}} + (\boldsymbol{D}_k - \boldsymbol{M}_k\boldsymbol{J}(\boldsymbol{y})\dot{\boldsymbol{J}}(\boldsymbol{y}))\hat{\boldsymbol{\nu}}_T - \\ &-\boldsymbol{M}_k\boldsymbol{J}(\boldsymbol{y})^{-1}\boldsymbol{W}^{-1}(\dot{\boldsymbol{W}}\boldsymbol{J}(\boldsymbol{y})\boldsymbol{\nu}_T + \dot{\boldsymbol{W}}_r\dot{x}_r + \boldsymbol{W}_r\ddot{x}_r + \boldsymbol{v}_{\boldsymbol{T}i})\end{aligned} \tag{5.36}$$

$$\boldsymbol{v}_{\boldsymbol{T}i} = \boldsymbol{K}_{p_k}.\mathscr{C}(\hat{\boldsymbol{\eta}}_{\boldsymbol{T}}, \boldsymbol{x}_r) + \boldsymbol{K}_{d_k}.\dot{\mathscr{C}}(\hat{\boldsymbol{\eta}}_{\boldsymbol{T}}, \boldsymbol{x}_r) \tag{5.37}$$

where the gain matrices $\boldsymbol{K}_p$ and $\boldsymbol{K}_d$ are the same as in (5.34) and (5.35), respectively. Other matrices and the constraint in (5.36) and (5.37) are calculated for $\boldsymbol{x}_{p_i}$ for $i = \{4, 8, 12\}$.

5.3.2 The Proportional and Derivative Controller Set

The proportional and derivative controller with $p = \{1, ..., 12\} - \{4, 8, 12\}$ is presented as follows

$$\boldsymbol{u}_{PD_i} = \boldsymbol{K}_{p_k}\hat{\boldsymbol{e}} + \boldsymbol{K}_{d_k}\dot{\hat{\boldsymbol{e}}} - \hat{\boldsymbol{b}} \tag{5.38}$$

$$\boldsymbol{\tau}_{q_i} = \boldsymbol{J}(\boldsymbol{y})^T\boldsymbol{u}_{PD_i} \tag{5.39}$$

where $\boldsymbol{u}_{PD_i} \in \mathbb{R}^6$ is the control vector. The matrix $\boldsymbol{K}_{p_k} \in \mathbb{R}^{6\times6}$ is the proportional control gain matrix and $\boldsymbol{K}_{d_k} \in \mathbb{R}^{6\times6}$ is the derivative control gain matrix defined as

$$\boldsymbol{K}_{p_k} = \boldsymbol{M}_k.diag\{\ \omega_{n_1}^2 \quad ... \quad \omega_{n_6}^2\ \} \tag{5.40}$$

$$\boldsymbol{K}_{d_k} = 2.\boldsymbol{M}_k.diag\{\ \varsigma_{c_{n_1}}\omega_{n_1} \quad ... \quad \varsigma_{c_{n_6}}\omega_{n_6}\ \} - \boldsymbol{D}_k \tag{5.41}$$

where $\varsigma_{c_{n_i}}$ and ω_{n_i} are control parameters. The error vector and its time-derivative are written

as

$$\hat{\boldsymbol{e}} = [\hat{\boldsymbol{\eta}} - \boldsymbol{\eta}_r] \tag{5.42}$$

$$\dot{\hat{\boldsymbol{e}}} = [\boldsymbol{J}(\boldsymbol{y})\hat{\boldsymbol{\nu}} - \dot{\boldsymbol{\eta}}_r] \tag{5.43}$$

where $\hat{\boldsymbol{e}}$ and $\dot{\hat{\boldsymbol{e}}} \in \mathbb{R}^6$. For the control laws for $i = \{4, 8, 12\}$, the PD-like control law is presented as follows

$$\boldsymbol{u}_{PD_i} = \boldsymbol{K}_{p_k}\hat{\boldsymbol{e}}_T + \boldsymbol{K}_{d_k}\dot{\hat{\boldsymbol{e}}}_T - \hat{\boldsymbol{b}}_T \tag{5.44}$$

where the gain matrices $\boldsymbol{K}_p$ and $\boldsymbol{K}_d$ are the same as in (5.40) and (5.41), respectively. The error vector and its time-derivative are written using the estimates from the nonlinear observer for extreme seas as follows

$$\hat{\boldsymbol{e}} = [\hat{\boldsymbol{\eta}}_T - \boldsymbol{\eta}_r] \tag{5.45}$$

$$\dot{\hat{\boldsymbol{e}}} = [\boldsymbol{J}(\boldsymbol{y})\hat{\boldsymbol{\nu}}_T - \dot{\boldsymbol{\eta}}_r] \tag{5.46}$$

5.4 Peak-Frequency Tracker

Vessel motion peak-frequency of the vessel motions is used to estimate the wave-frequency motion in the measurement signal. This peak-frequency motion does not necessarily correspond to sea spectrum peaks. However, the differences in values are negligible and can be ignored. This is evaluated in Appendix C.

In order to estimate motion peak-frequency ω_p, a spectrum estimate of the vessel motion is made during the simulations. A fixed data (window of the motion is recorded and the motion spectra of surge, sway and yaw of the vessels is evaluated. To improve spectrum analysis, a cascaded high-pass frequency filter is applied to the motion measurement. This filter is given by

$$\psi_{hf}(s) = \prod^{n_f} \frac{T_f.s}{1 + T_f.s} \tag{5.47}$$

where $\psi_{hf}(s)$ is the transfer function of the high-pass frequency filter, T_f is the cut-off high-frequency and n_f is the number of the filters in cascade. A more detailed analysis can be found in Fossen (1994). Figure 5.47 presents the spectra of ST surge motion comparing cascaded high-pass frequency filters with different orders.

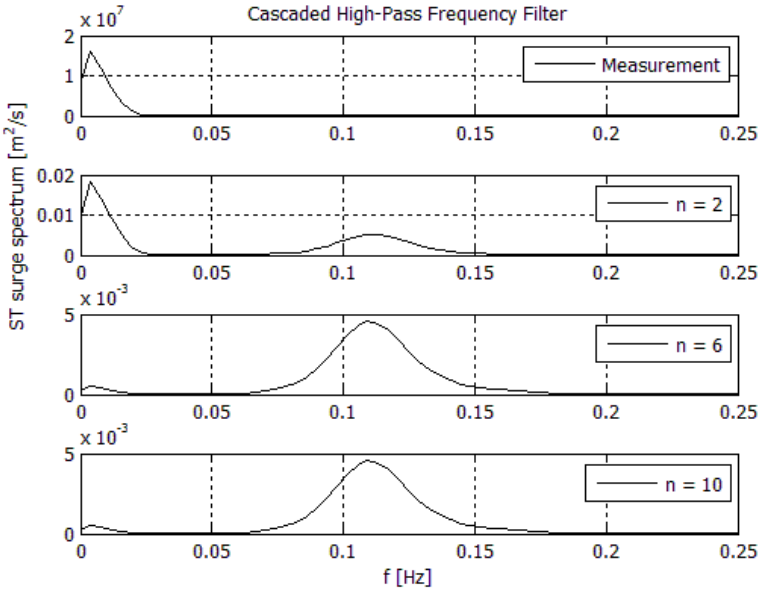

Figure 5.2: Spectrum analysis of the Cascaded High-Pass Frequency Filter

Figure 5.47 shows that the higher the filter order, the lower the low-frequency peak which greatly facilitates high frequency peak detection. During simulations, filter order is $n = 10$. The peak-frequency is obtained from the average surge and sway peaks of both vessels. Yaw motion is not included because, even applying the cascaded filter, the estimate of the frequency ω_p is not accurate enough.

5.5 Draft Survey Monitoring

Draft variation during offloading is taken into account by the supervisory control. The multi-estimator uses vessel drafts to estimate the error vector e_{p_i} of the process i. Vessel draft can be calculated by a draft survey calculation since oil transfer flow between vessels is known. Hence, if the draft is known during the offloading operation, the inertia properties can be estimated. Here, the trim and heel are assumed to be null. See Appendix A for more details about inertia

properties.

5.6 Supervisory Control Tuning

The chattering that can occur during the change of control law and state observer is avoided by means of the switching logic hysteresis. The hysteresis parameter h needs to be chosen correctly in order to neither freeze switching if the value h is too high, nor cause chattering if the value h is too low. Böling, Seborg and Hespanha (2005) appropriately choose the forgetting factor λ so as to avoid impulsive or slow behavior of μ_p. Previous simulations evinced positive results for the scale-independent hysteresis switching logic $\mu_p = 1/10$, hysteresis $h = 20\%$ and a data window of 500s interval to generate motion spectra.

Chapter 6

Simulation Results

6.1 General

Hybrid concept performance as applied to an offloading operation is evaluated through simulation of some scenarios from Brazilian waters. A typical environmental scenario is presented in Figure 6.1. The current flows south (S) and its velocity range is 0.1-0.7m/s. This velocity range and incidence angle represent 99% and 33% of the occurrence, respectively. The wind and waves (local sea) come from the northeast direction (NE). This direction represents a little more than 30% of the direction occurrence.

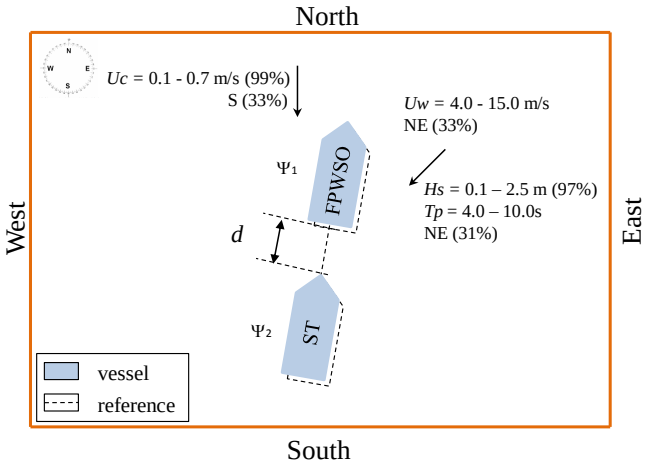

Figure 6.1: Typical environmental conditions for Brazilian basin

Figure 6.1 also presents the significant wave height, wave-frequency peak and wind velocity ranges. Due to the difference between the incidence angles of the wind/wave and current, a convenient reference for the heading of the vessels is between 0° and 45°. To analyze controller performance under different environmental scenarios and references, five simulation cases are considered as follows:

- Case 1: Analyze controller performance due to a change in the position reference;
- Case 2: Evaluate the positioning of the vessels due to the changes in their relative distance;
- Case 3: Evaluate the consequence, in terms of relative positioning, when an extra force acts on the FPWSO only;
- Case 4: Test switching control in transitions from calm environmental scenarios to gradually harshening;
- Case 5: Test switching control in transitions from harsh environmental scenarios to gradually becoming calm;
- Case 6: Assess controller performance during a day-long operation when the environmental scenario is harshening.

Both geometric controller and PD-like controller are considered. For the cases 1 to 5, the controllers' parameters are tuned to three different drafts (reference drafts from perturbation model - see Figure 6.2). To evaluate the performance of these controllers, simulations are carried out using constant drafts set for these reference drafts. The observers' parameters are selected by the supervisory control. The case 6 is a realistic scenario where the drafts vary and the observer/controller parameters are automatically selected by the supervisory control.

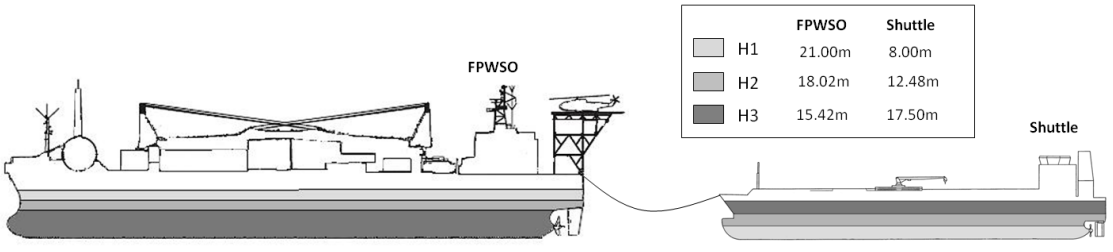

Figure 6.2: Reference Draft for the vessels

Table 6.1 and Table 6.2 present the references for the vessels and the parameters of the environmental scenarios, respectively.

Table 6.1: Reference for simulations

		Position and Heading					
		FPWSO			Shuttle tanker		Draft condition
Simulation	Time	X1r [m]	Y1r [m]	Ψ1r [°]	Ψ2r [°]	d [m]	
Case1: Reference	3.600s	10.0	10.0	80° - 90°	80° - 90°	150.0	H1, H2, H3 (constant)
Case2: Distance	3.600s	10.0	10.0	80°	80°	150.0 - 200.0	H1, H2, H3 (constant)
Case3: Extra Force	4.000s	10.0	10.0	80°	80°	150.0	H1, H2, H3 (constant)
Case4: Harshening	4.000s	10.0	10.0	80°	80°	150.0	H1, H2, H3 (constant)
Case5: Becoming calm	4.000s	10.0	10.0	80°	80°	150.0	H1, H2, H3 (constant)
Case6: Day-long	1 day	0.0	0.0	80°	80°	150.0	varying

Table 6.2: Scenarios for simulations

	Environment conditions						
	Current		Wind		Wave		
Simulation	Uc [m/s]	α [°]	Uw [m/s]	α [°]	Hs [m]	Tp [s]	α [°]
Case 1: Reference	0.7	180°	10.0	225°	1.5	4.8	225°
Case 2: Distance	0.7	180°	10.0	225°	2.0	17.0	225°
Case 3: Extra Force	0.7	180°	10.0	225°	2.0	8.0	225°
Case 4: Harshening	0.7	180°	10.0	195°	2.0	4.5 - 15.0	195°
Case 5: Becoming calm	0.7	180°	10.0	195°	2.0	15.0 - 4.5	195°
Case 6: Day-long	0.7	180°	4.0 - 15.0	225°	1.0 - 2.5	4.0 - 14.0	225°

6.2 Case 1: Reference Change

This section presents simulation results that tests controller performance when the reference is changed. The environmental scenario for these simulations is presented in Figure 6.3. The sea state condition is kept constant and the observer parameters are selected by the supervisory control and they are equal to the first range of the peak frequency motion (calm sea). The heading references for FPWSO and the shuttle tanker are modified from 10° to 0°. To maintain the alignment with the FPWSO, the shuttle tanker has its reference changed.

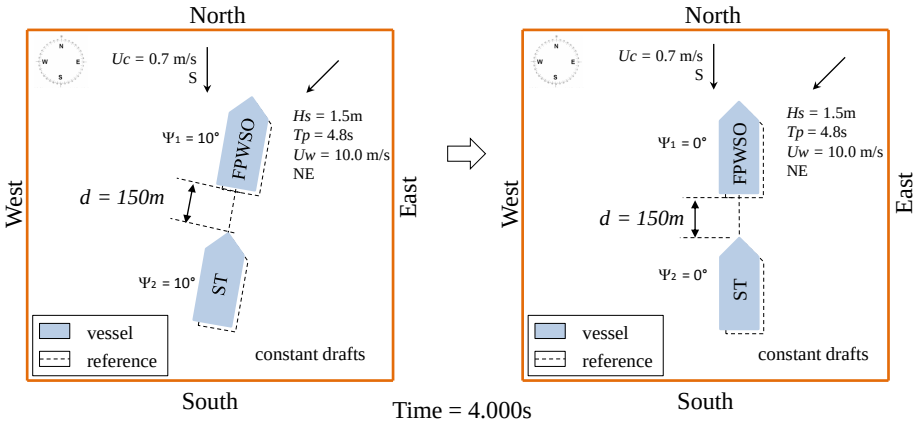

Figure 6.3: Environmental conditions and first maneuver

Geometric controller achieves the reference and maintains the vessels in their correct positions and headings as presented in Figures 6.4. The relative distance is also maintained by the controllers for each draft as seen in Figure 6.6. PD-like controller also achieves the reference and maintains the vessels' positioning and relative distance as presented in Figure 6.5.

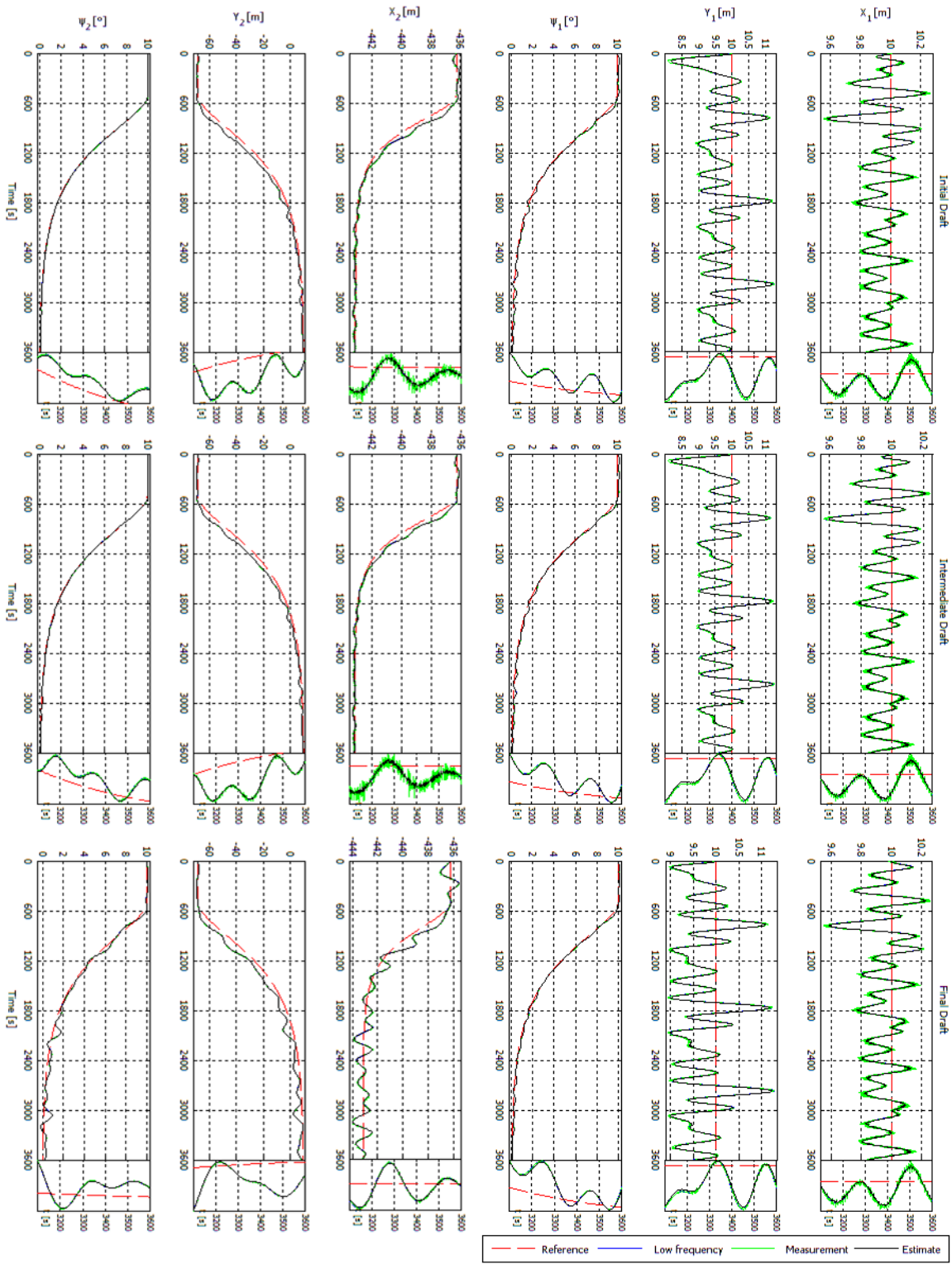

Figure 6.4: Positioning using Geometric Controller

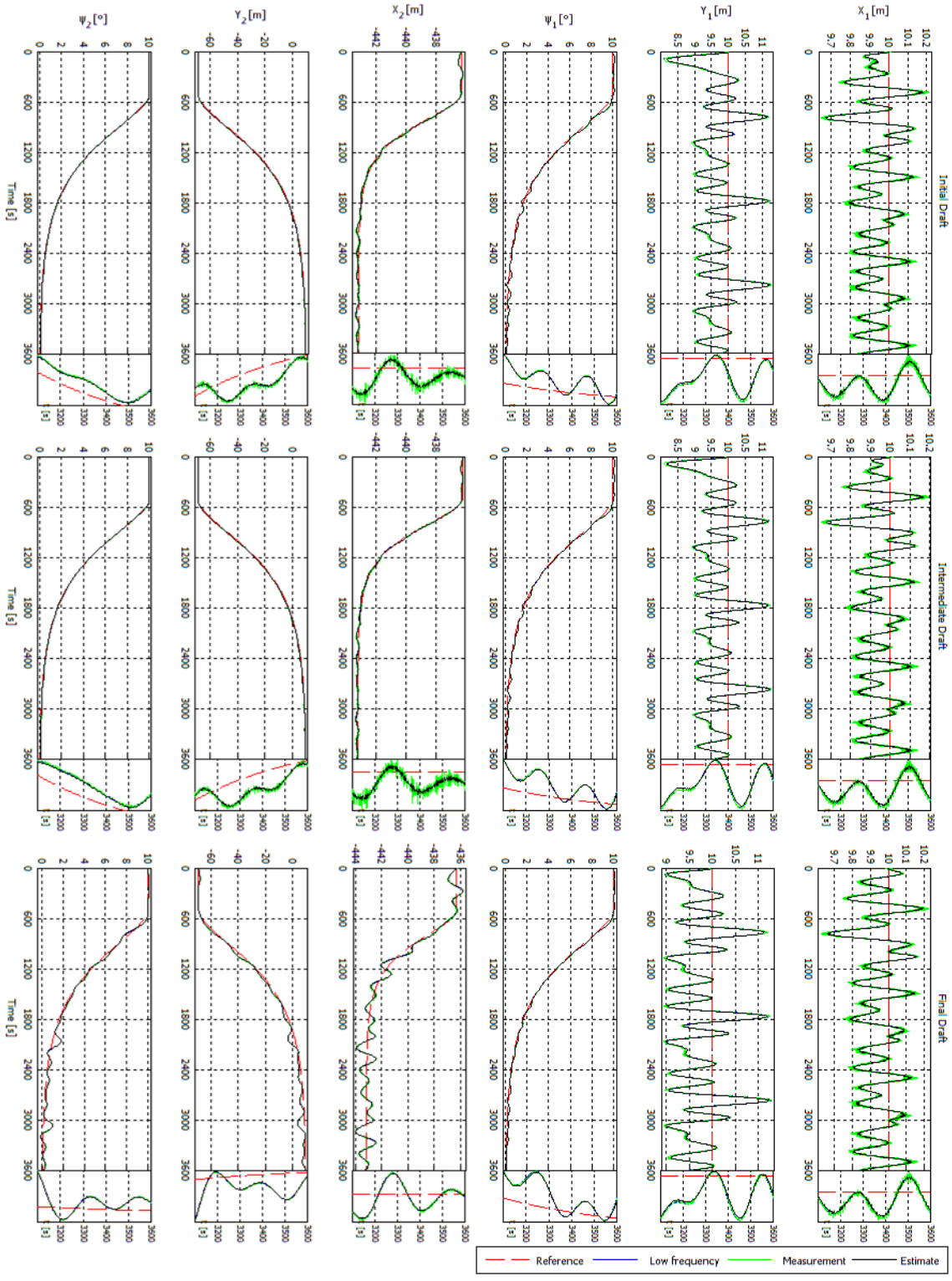

Figure 6.5: Positioning using PD-like Controller

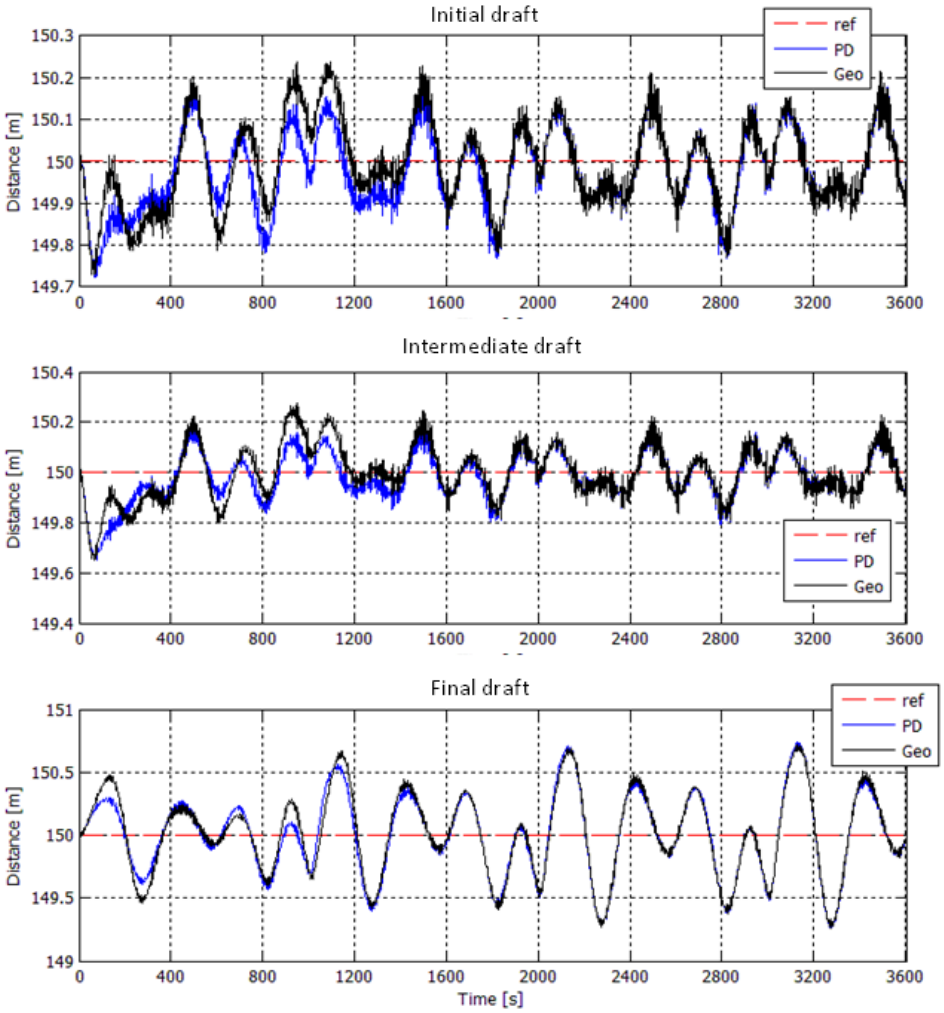

Figure 6.6: Distance between vessels

Estimates velocities are well-estimated by the nonlinear observer with wave-frequency model because they converge to real values, with the exception of the estimated surge velocity of the shuttle tanker as presented in Figures 6.7 and 6.8. As discussed in Appendix C, the surge motion of the shuttle tanker can exhibit a bimodal spectrum response. The cut-off frequency of the nonlinear observer is always tuned for the highest peak-frequency of the spectrum. So, the second peak with the lowest energy amplitude could not be filtered properly. Consequently, some wave-frequency motion appears in the surge control force of the shuttle tanker. The observer filters the wave-frequency motion when final draft is set better than other drafts. Despite the fact that the surge motion presents some wave-frequency influence, overall positioning is carried out correctly.

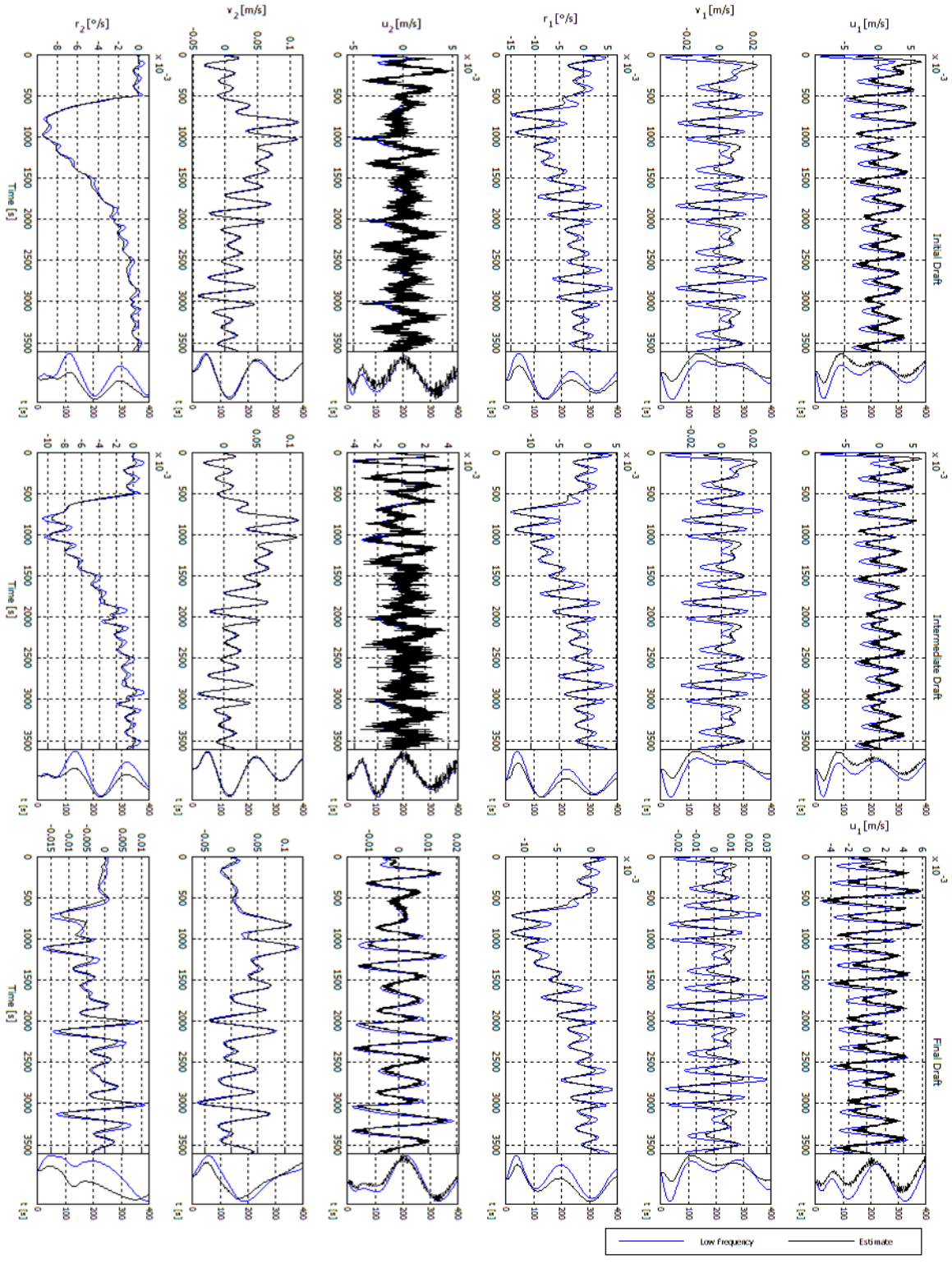

Figure 6.7: Vessel velocities using Geometric Controller

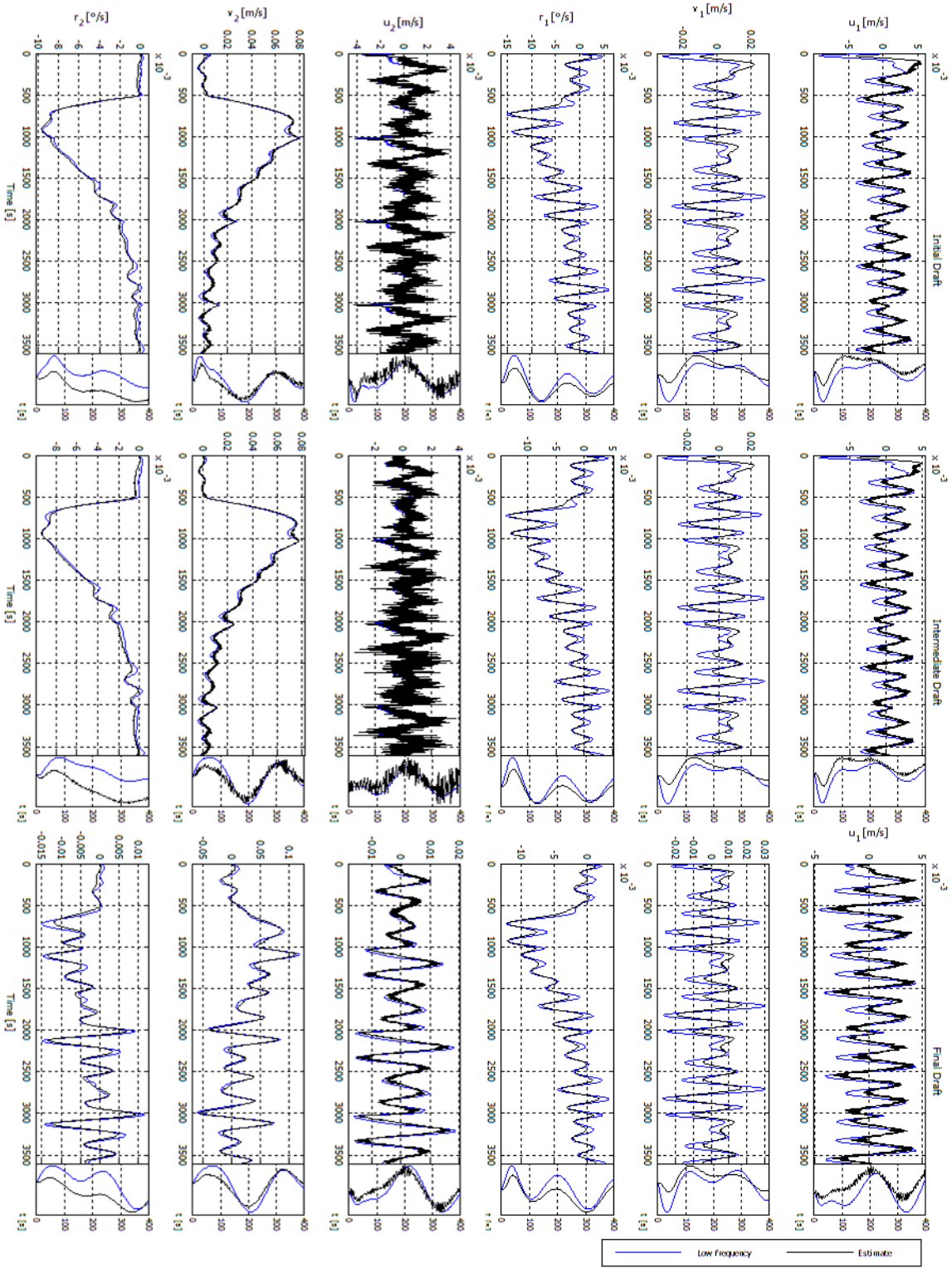

Figure 6.8: Vessel velocities using PD-like Controller

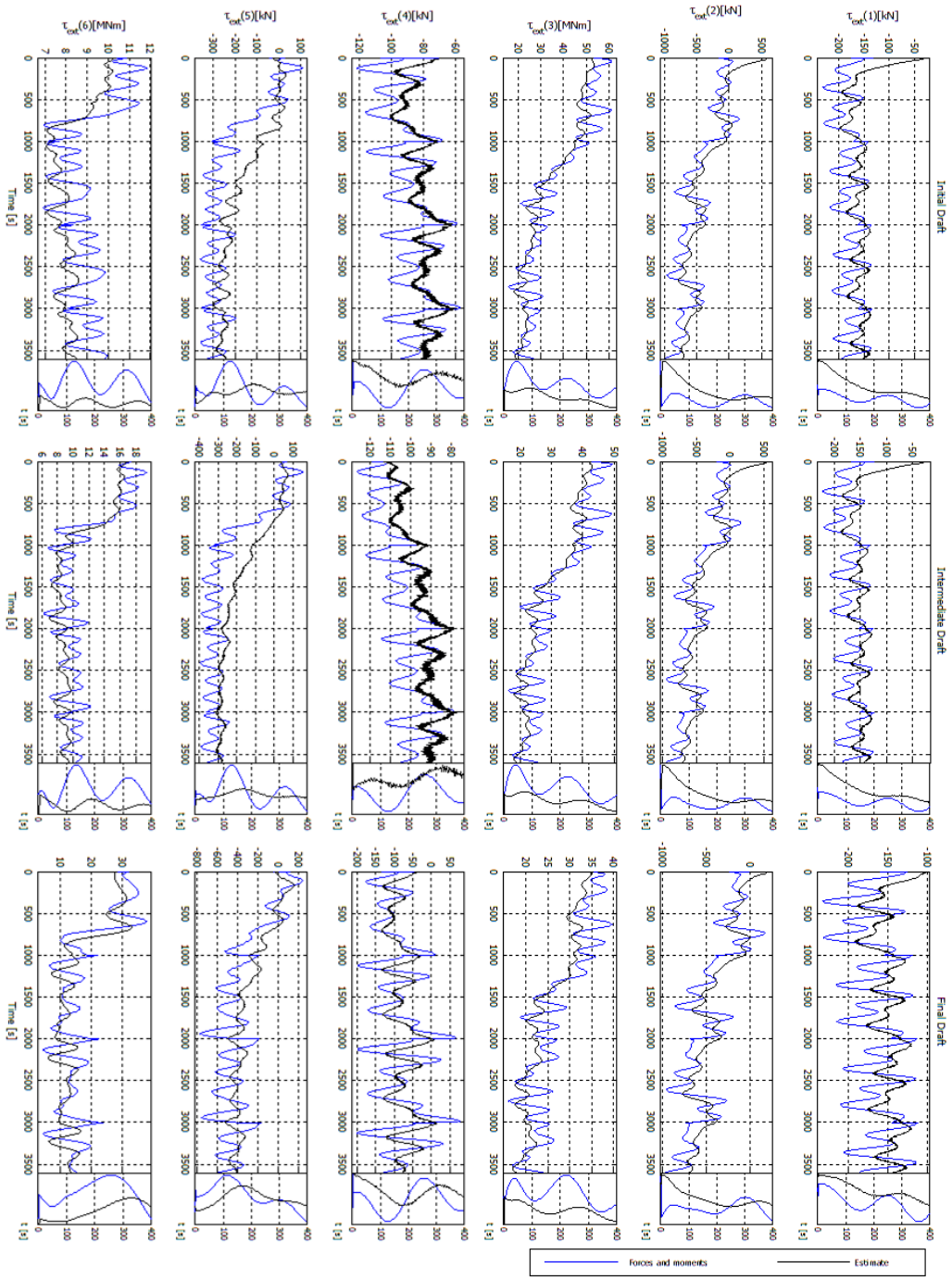

Figure 6.9: External forces using Geometric Controller

External forces estimates from Markov process converge to values approximating to the real external forces in terms of magnitude and frequency as shown in Figures 6.9 and 6.10.

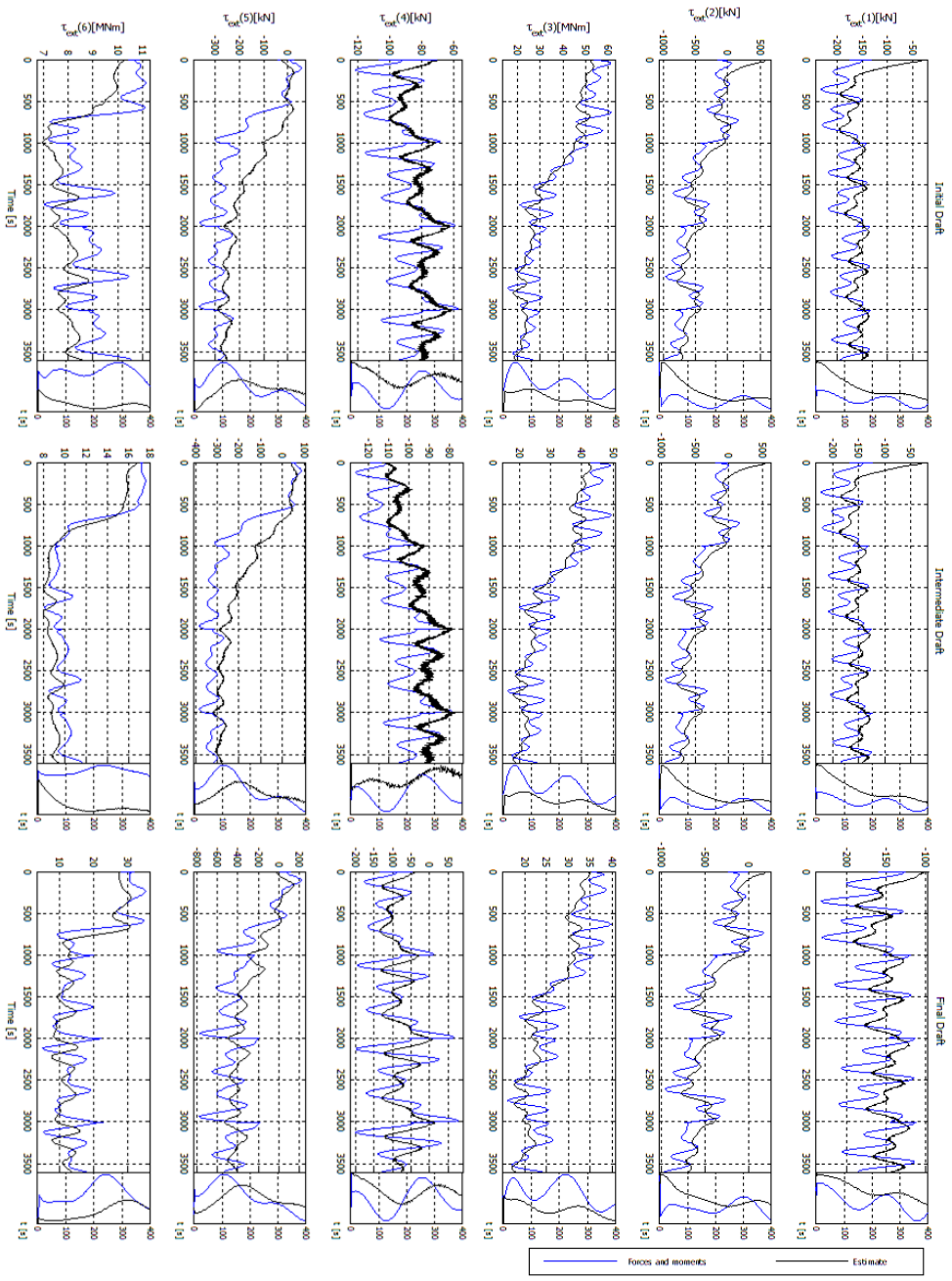

Figure 6.10: External forces using PD-like Controller

The geometric control law is presented in Figure 6.11. PD-like control law (Figure 6.12) is similar to this control law. Wave-frequency motion appears on surge control law of the shuttle tanker as position estimate was not filtered properly. The performance of the controllers is good because the matrices $\boldsymbol{M}$ and $\boldsymbol{D}$ are set for the draft simulated. When offloading is taking place, the performance tends to deteriorate until the hybrid control switches the controller parameters.

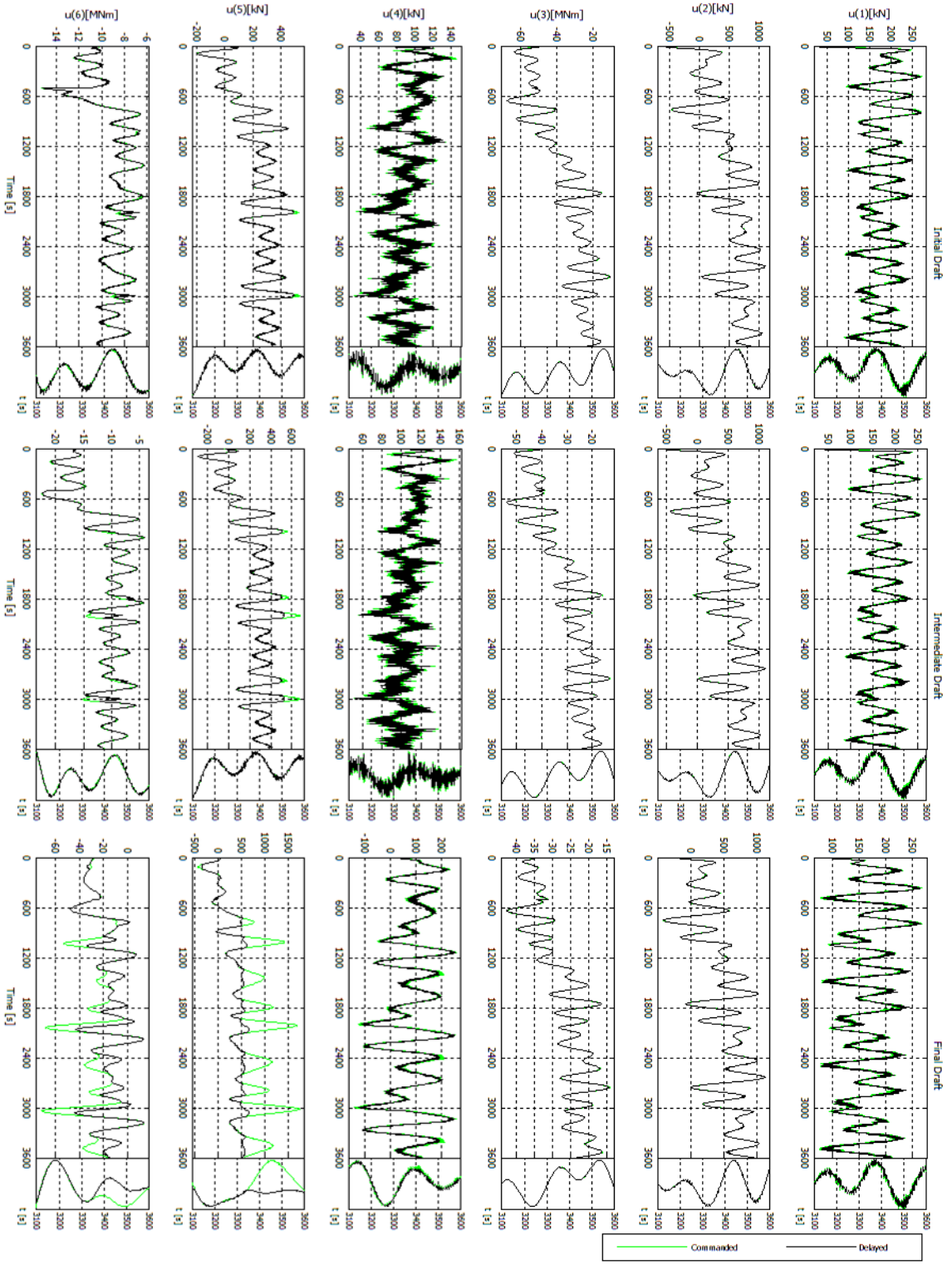

Figure 6.11: Control forces using Geometric Controller

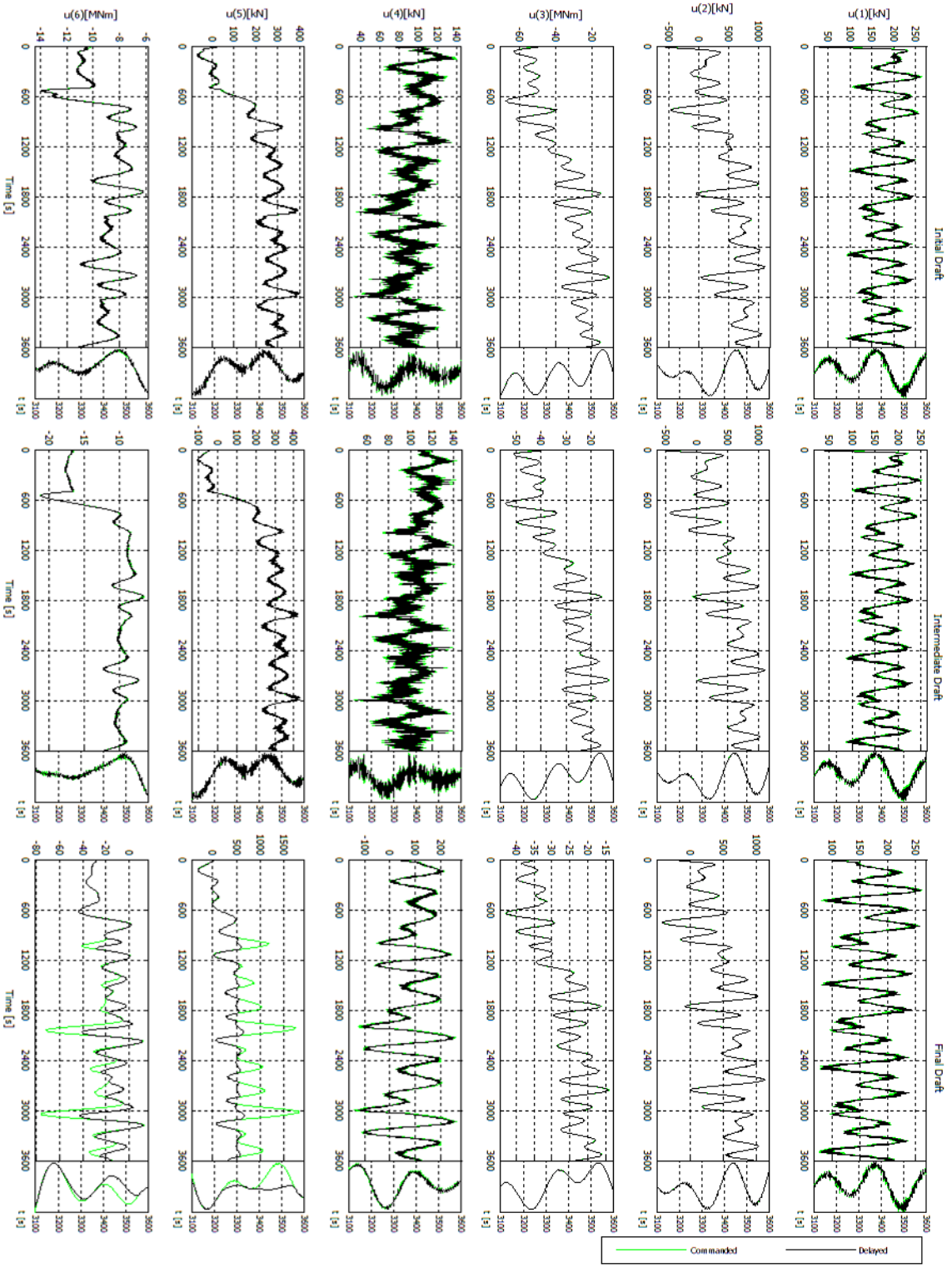

Figure 6.12: Control forces using PD-like Controller

6.3 Case 2: Distance Change

The simulation results that tests controller performance when the distance between vessels is changed are presented. The environmental scenario for these simulations is presented in Figure 6.13. Sea state condition is constant and the observer parameters are selected by the supervisory control and they are equal to the fourth range of the peak frequency motion (extreme sea). Distance between the vessels is altered from 150.0m to 200.0m.

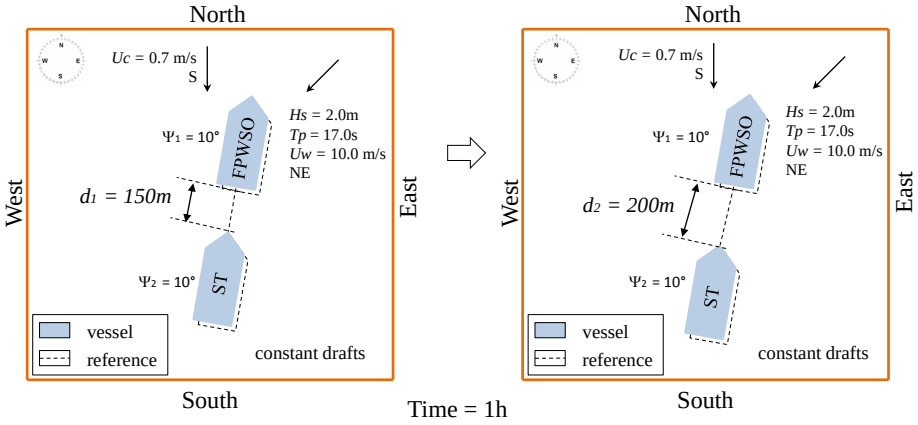

Figure 6.13: Environmental conditions and second maneuver

The geometric control law is presented in Figure 6.14. PD-like control law is similar to this control law and it is presented in Figure 6.15. The relative distance is also maintained by the controllers for each draft as seen in Figure 6.16. The shuttle tanker heading presents with a different value from the heading set-point. This error occurs because the external forces and moment on the vessel are close to maximum thruster capability.

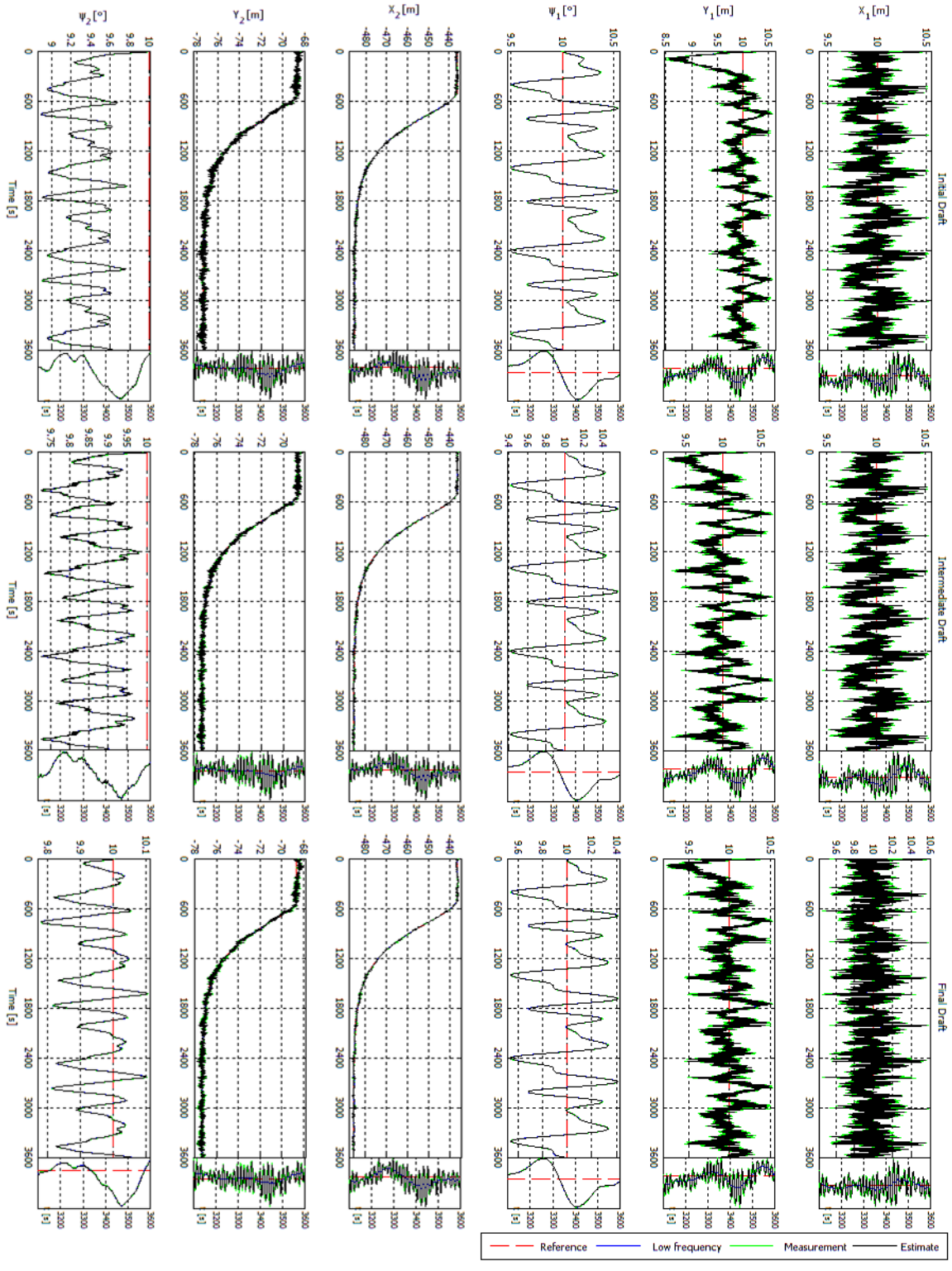

Figure 6.14: Positioning using Geometric Controller

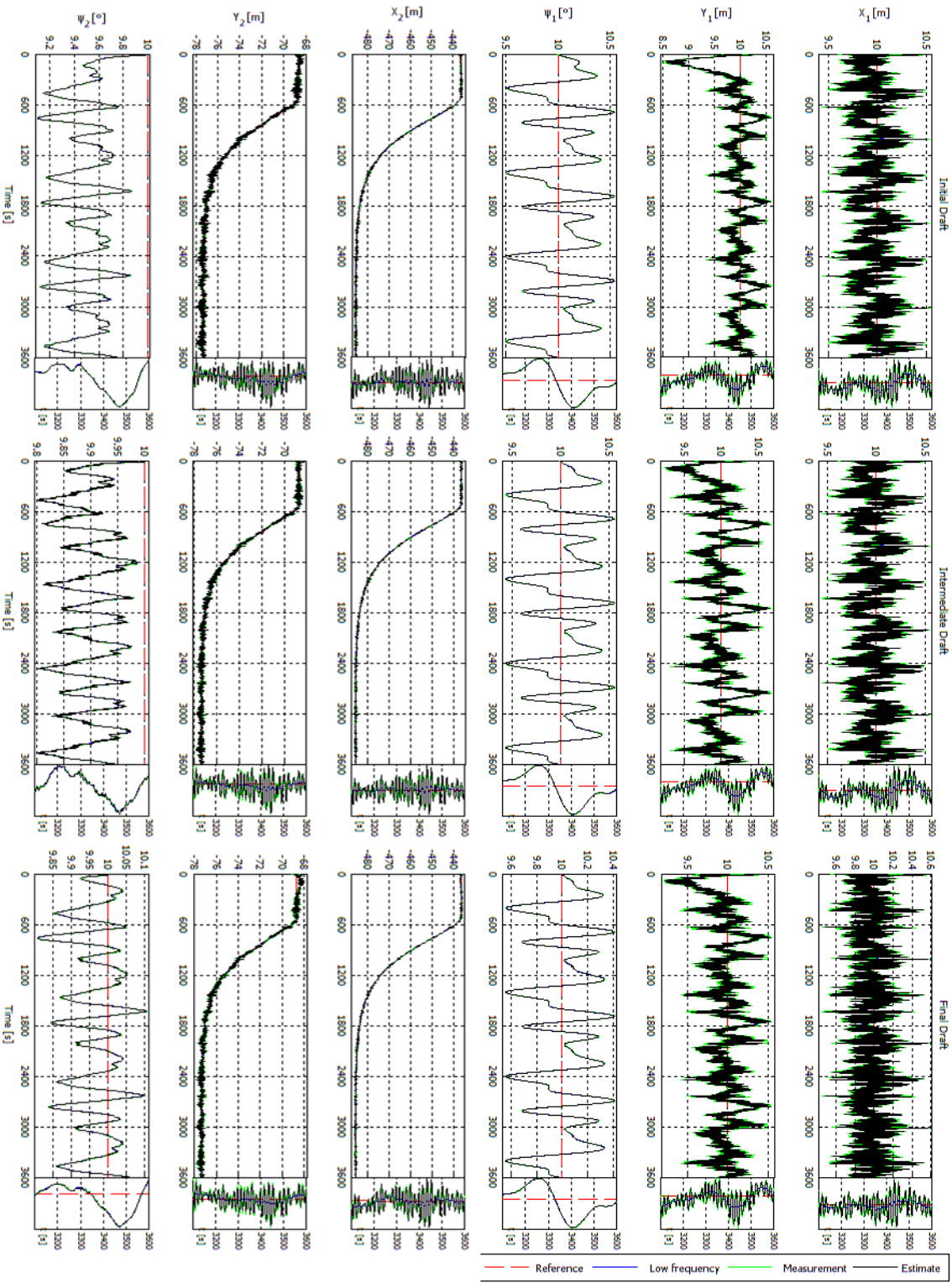

Figure 6.15: Positioning using PD-like Controller

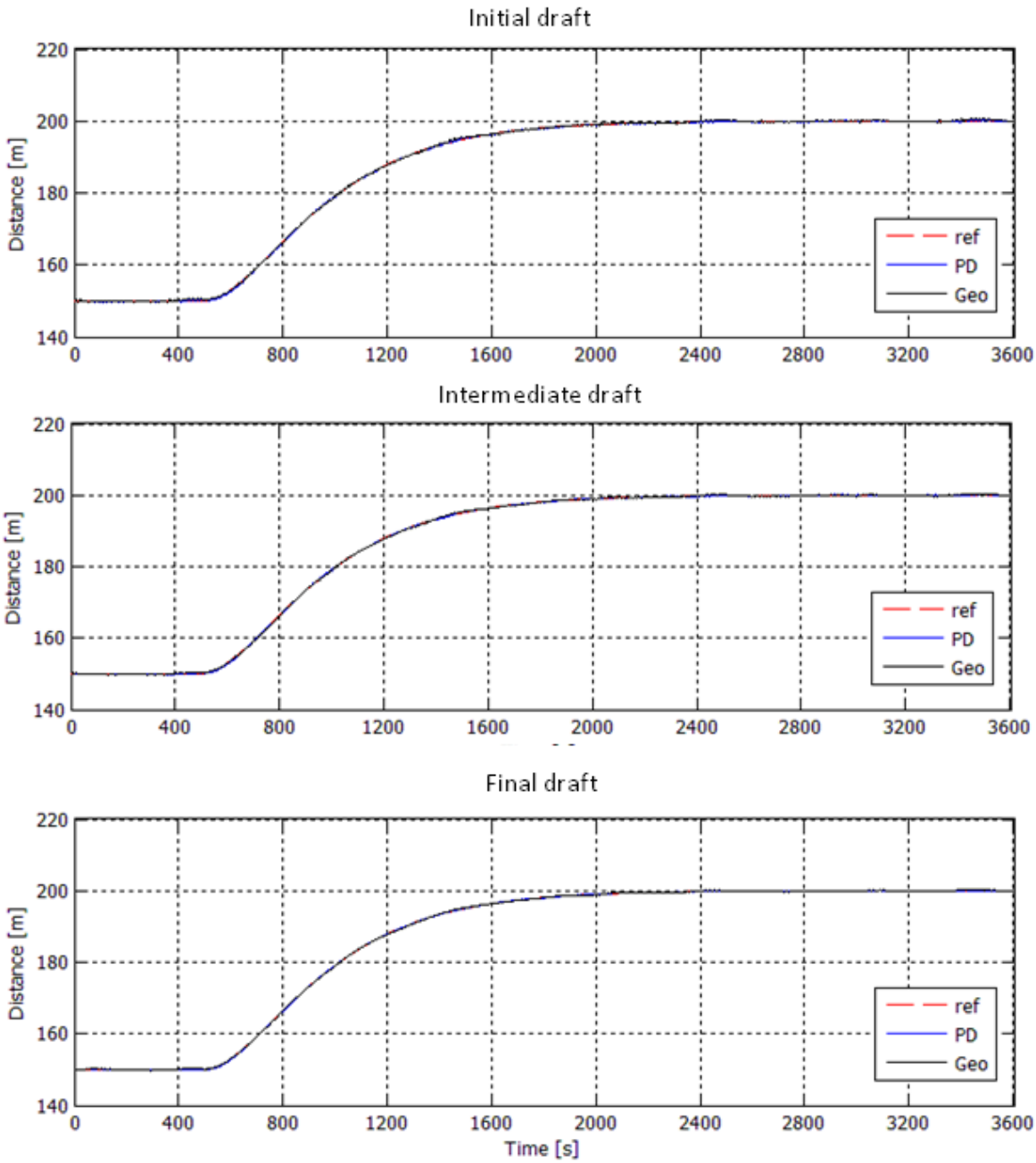

Figure 6.16: Distance between vessels

Vessel motions present the wave-frequency motion influence (Figures 6.14 and 6.15) as well as the velocity estimates do it (Figures 6.17 and 6.18). However, the yaw velocities and headings for both vessels do not to evince this frequency influence on yaw motion due to their high yaw inertia mainly in the final draft case.

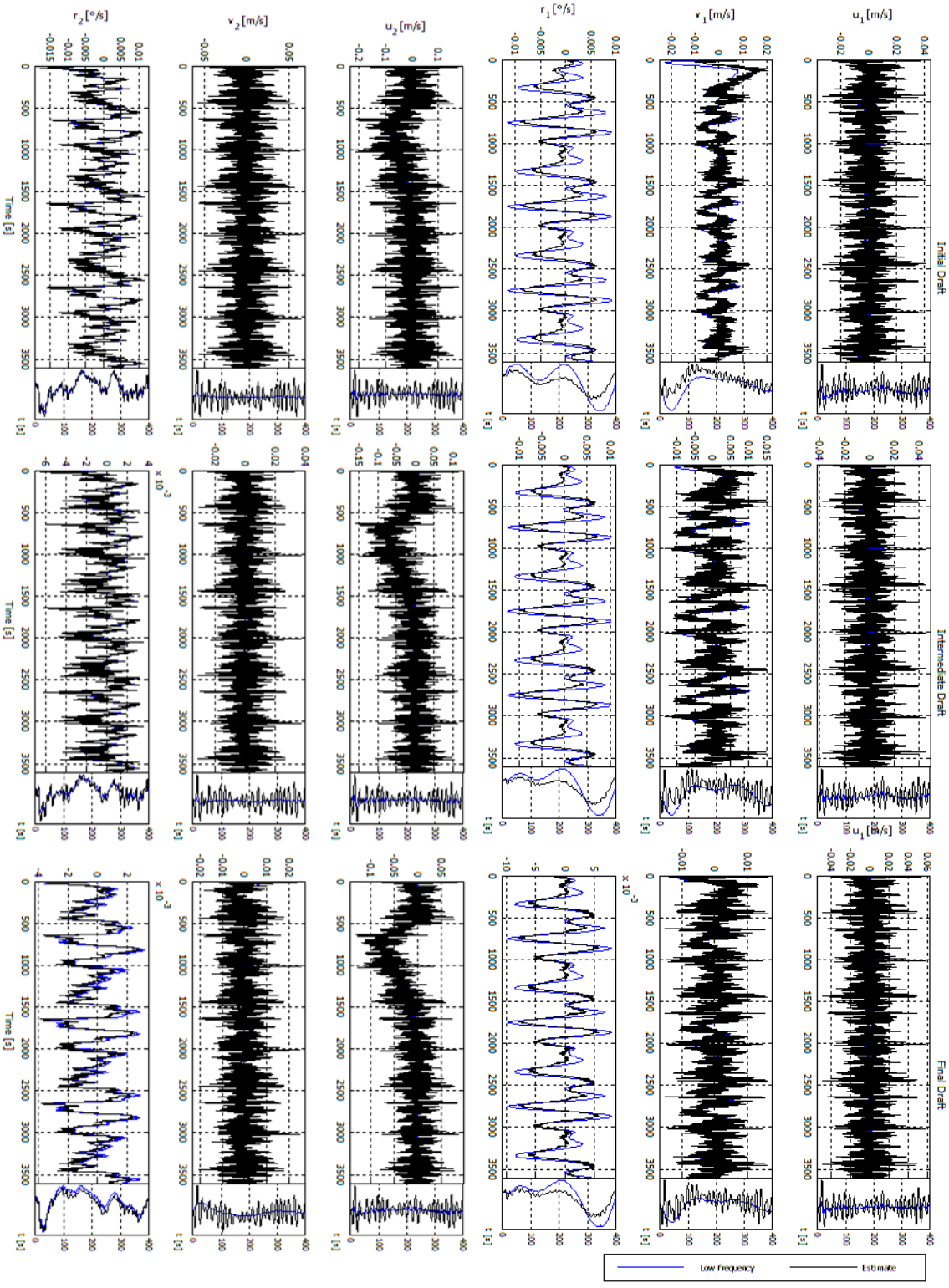

Figure 6.17: Vessel velocities using Geometric Controller

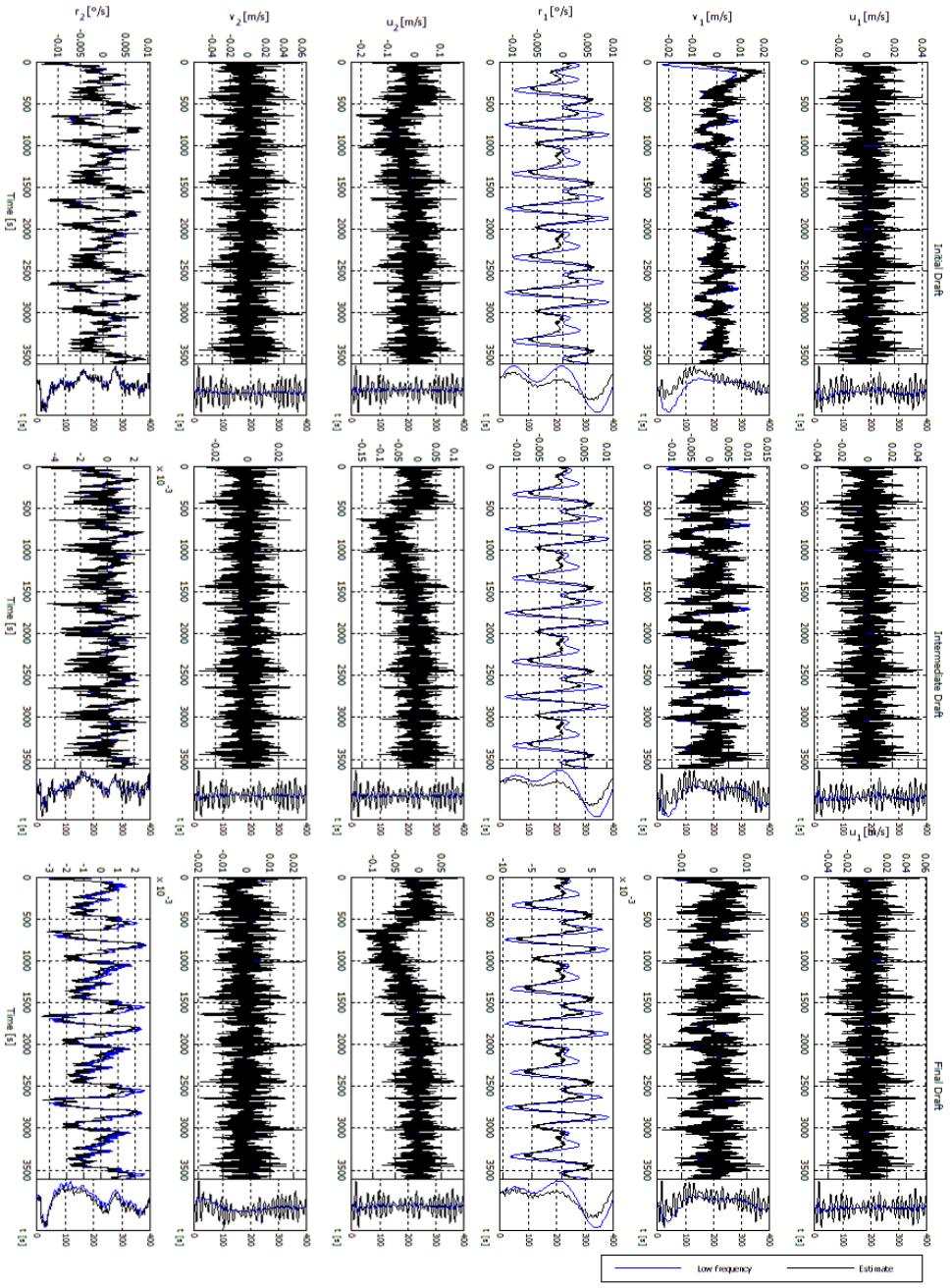

Figure 6.18: Vessel velocities using PD-like Controller

Both estimated external forces and moments (see Figures 6.19 and 6.20) and control laws (see Figures 6.21 and 6.22) undergo wave-frequency influence. In spite of this wave-frequency motion influence and some control saturation, both geometric and PD-like controllers are able to maintain positioning and the relative distance for each draft simulated.

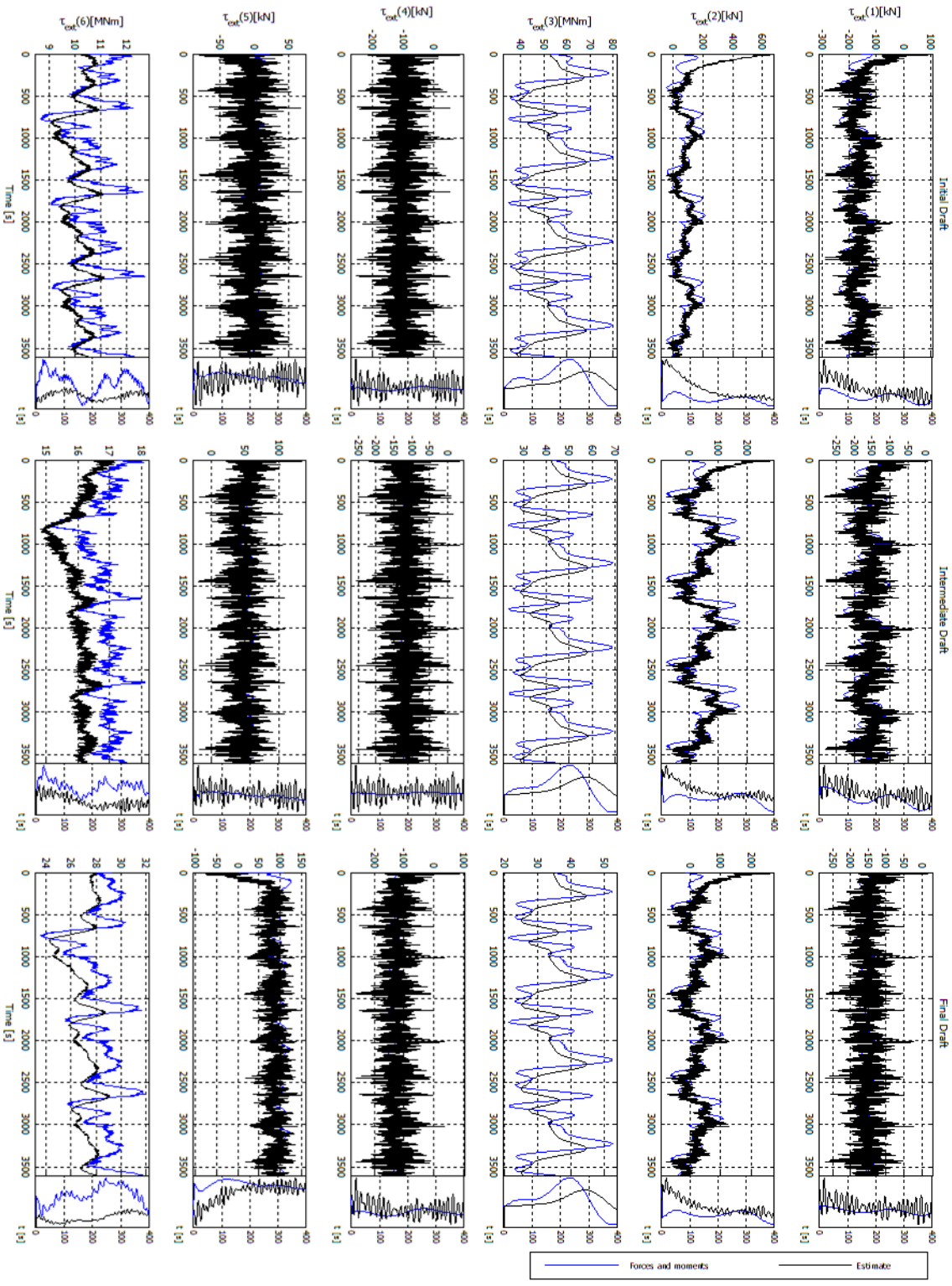

Figure 6.19: External forces using Geometric Controller

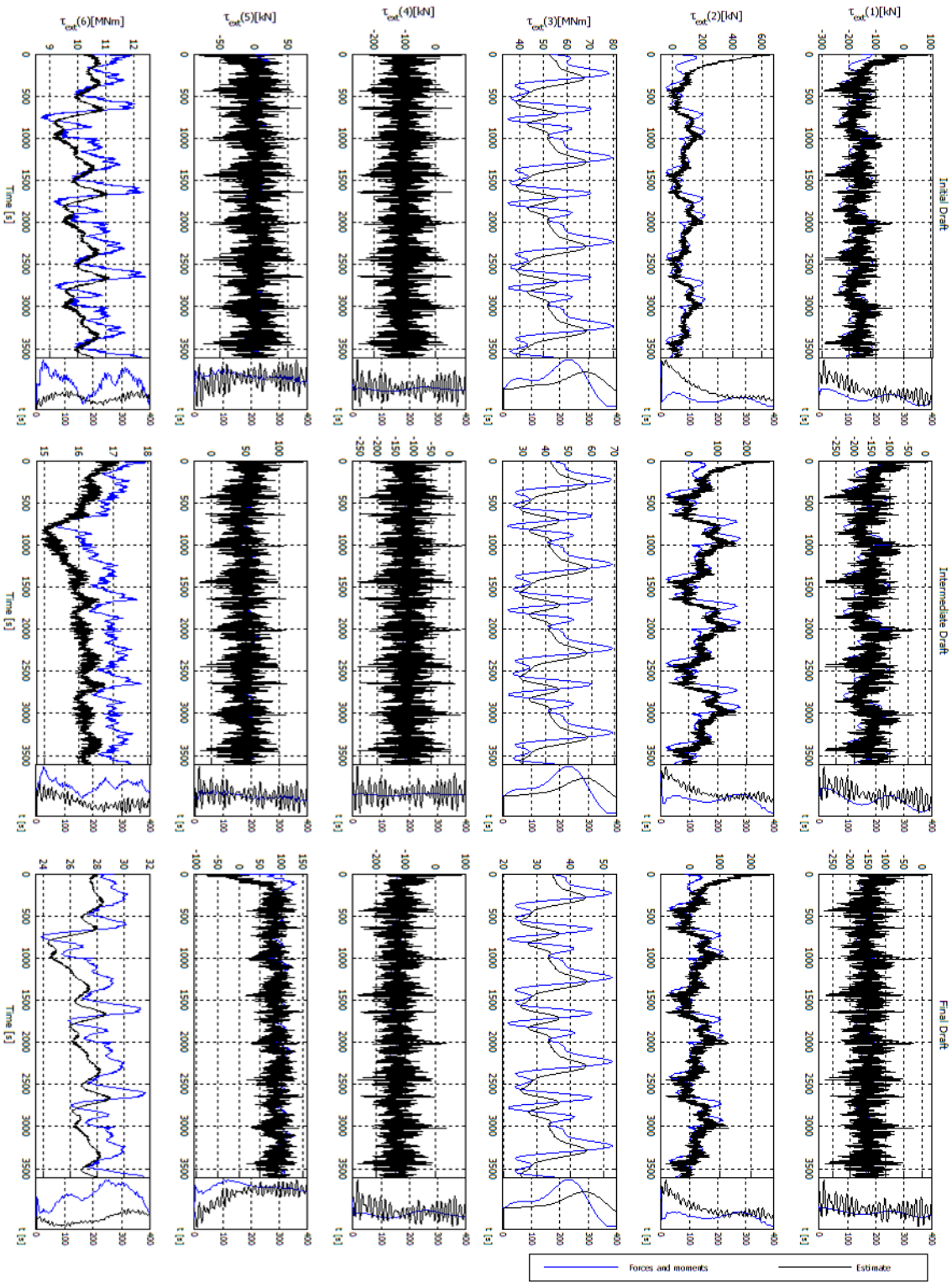

Figure 6.20: External forces using PD-like Controller

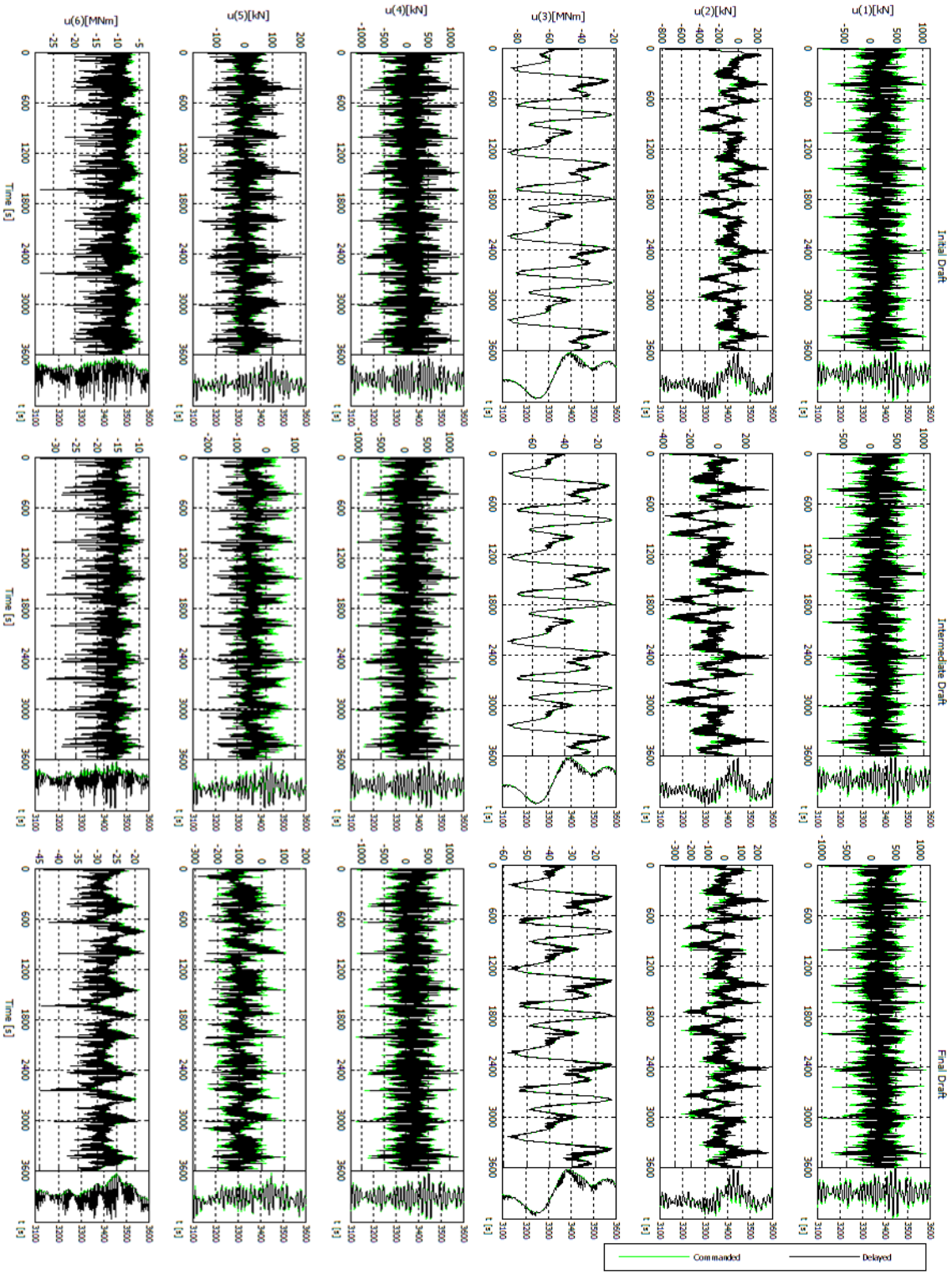

Figure 6.21: Control forces using Geometric Controller

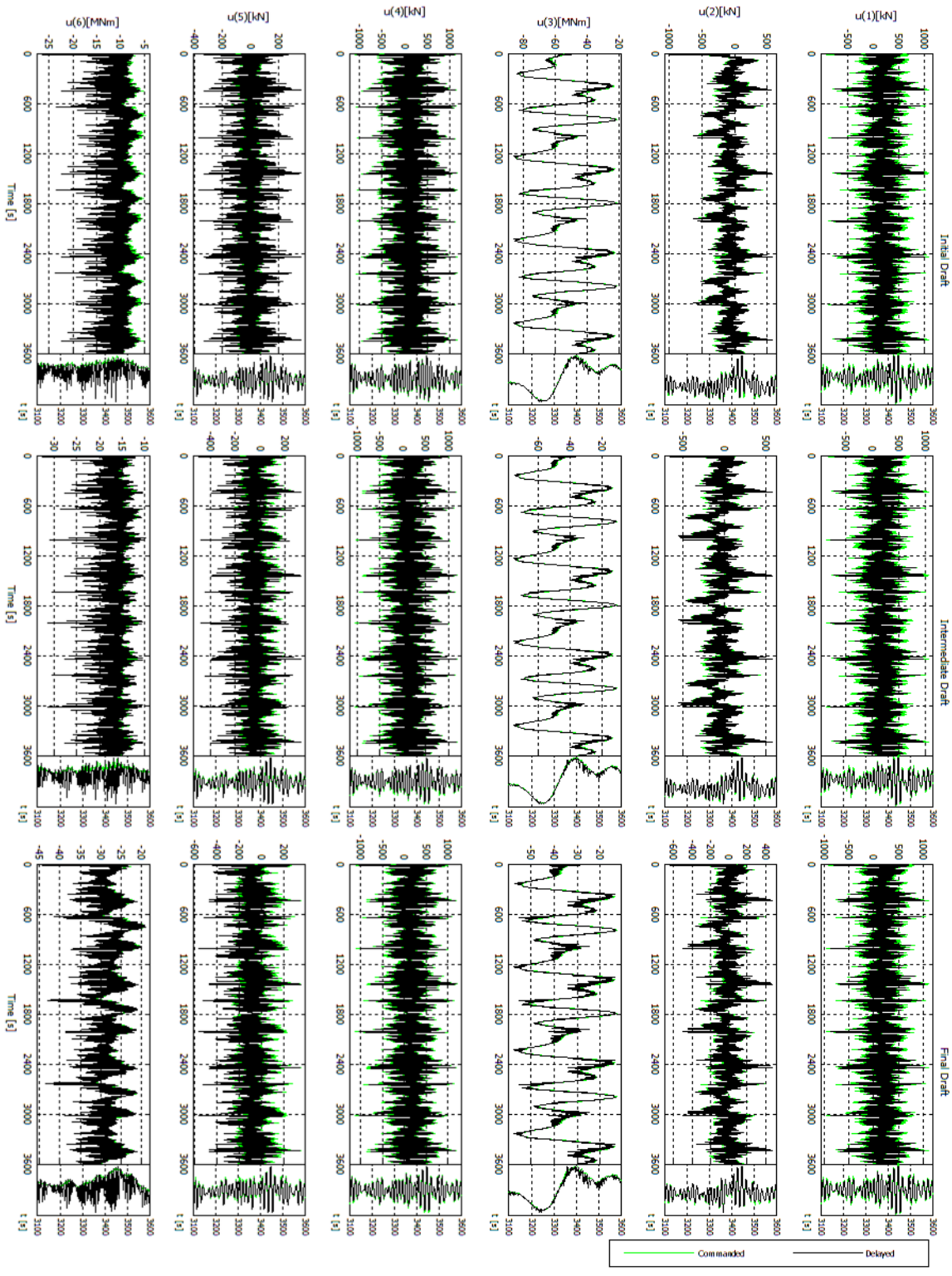

Figure 6.22: Control forces using PD-like Controller

6.4 Case 3: Occurrence of an Extra Force

Although controllers' performance has been very similar so far, when some event happens to the FPWSO and does not occur with the shuttle tanker, a small difference can be found. For instance, if a strong wind blast reaches the FPWSO and does not affect the shuttle tanker, some movement of the FPWSO is to be expected. This can happen because the height of the FPWSO and its exposed area to wind, with respect to water level, are both greater than those of shuttle tanker. As discussed in Chapter 4, if the PD-like controller is applied with the error $\boldsymbol{e}$, the set-point of the shuttle tanker is not altered even if the FPWSO moves from its set-point. The geometric controller is applied using the constraint as output and if the FPWSO moves from her set-point, the ST also moves.

To evaluate this behavior, simulations with an additional force to the FPWSO are performed. The environmental scenario for this simulation is presented in Figure 6.23. The sea state condition is kept constant and the observer parameters are selected by the supervisory control and they are equal to the first range of the peak frequency motion (calm sea). The extra force is inserted in the interval of 1.500s to 2.500s.

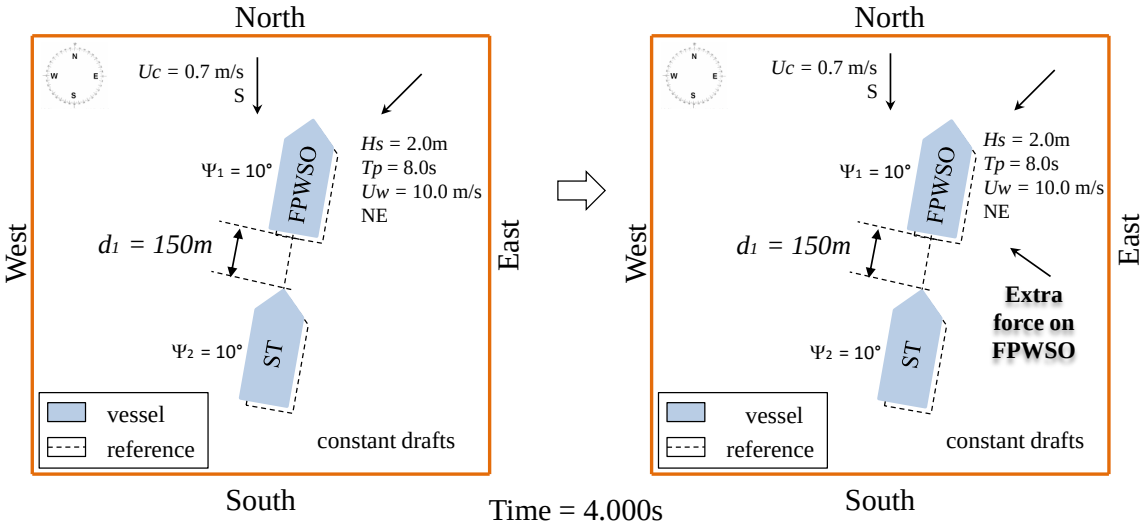

Figure 6.23: Environmental conditions and third maneuver

Vessels' positioning are maintained for both controllers even after the extra force occurrence appears or ceases as presented in Figures 6.24 and 6.25. The difference between the controllers

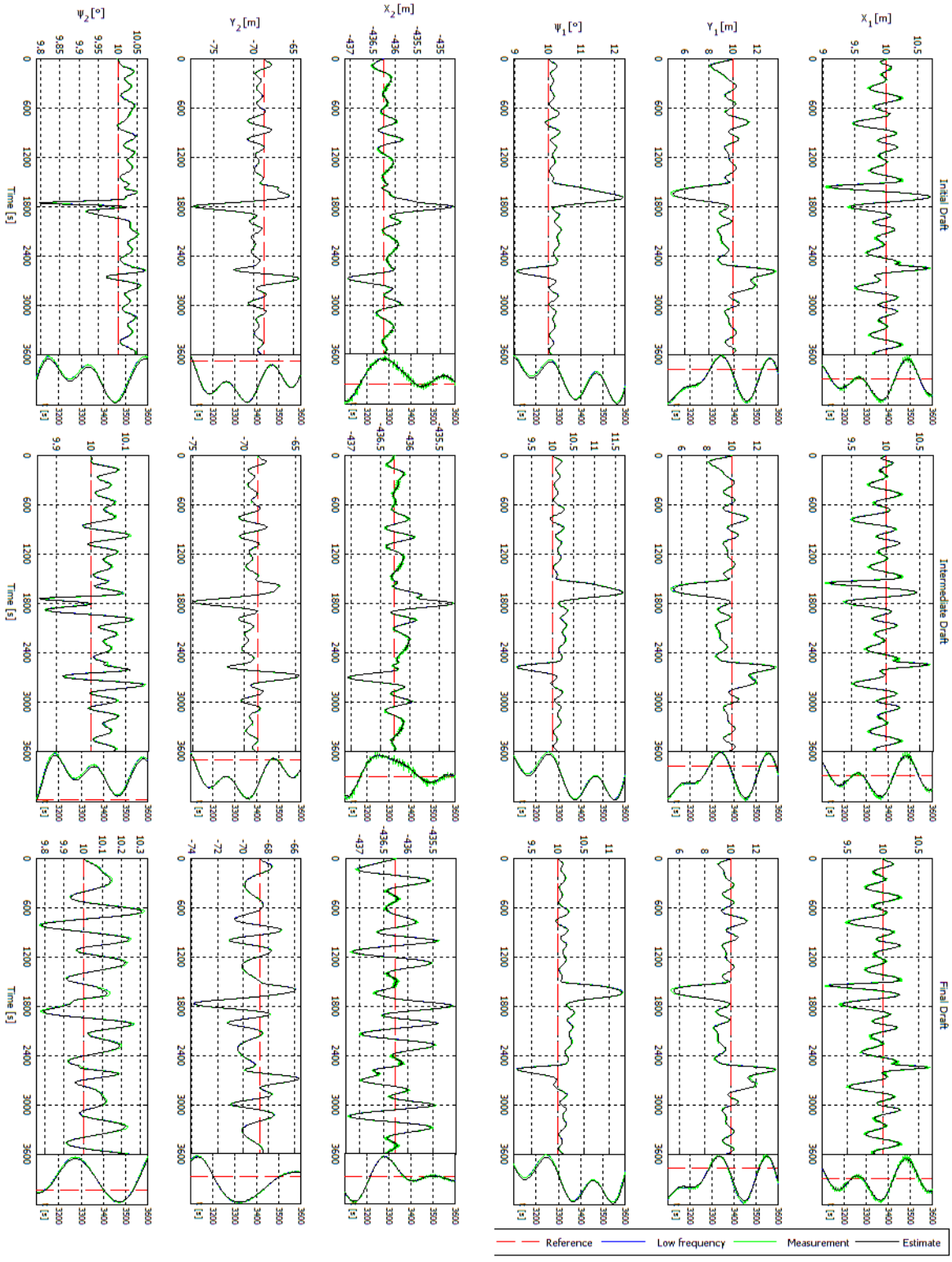

Figure 6.24: Positioning using Geometric Controller

is the shuttle tanker positioning. As discussed, the geometric controllers acts upon the shuttle tanker to maintain the relative distance and the PD-like controller does not act upon it.

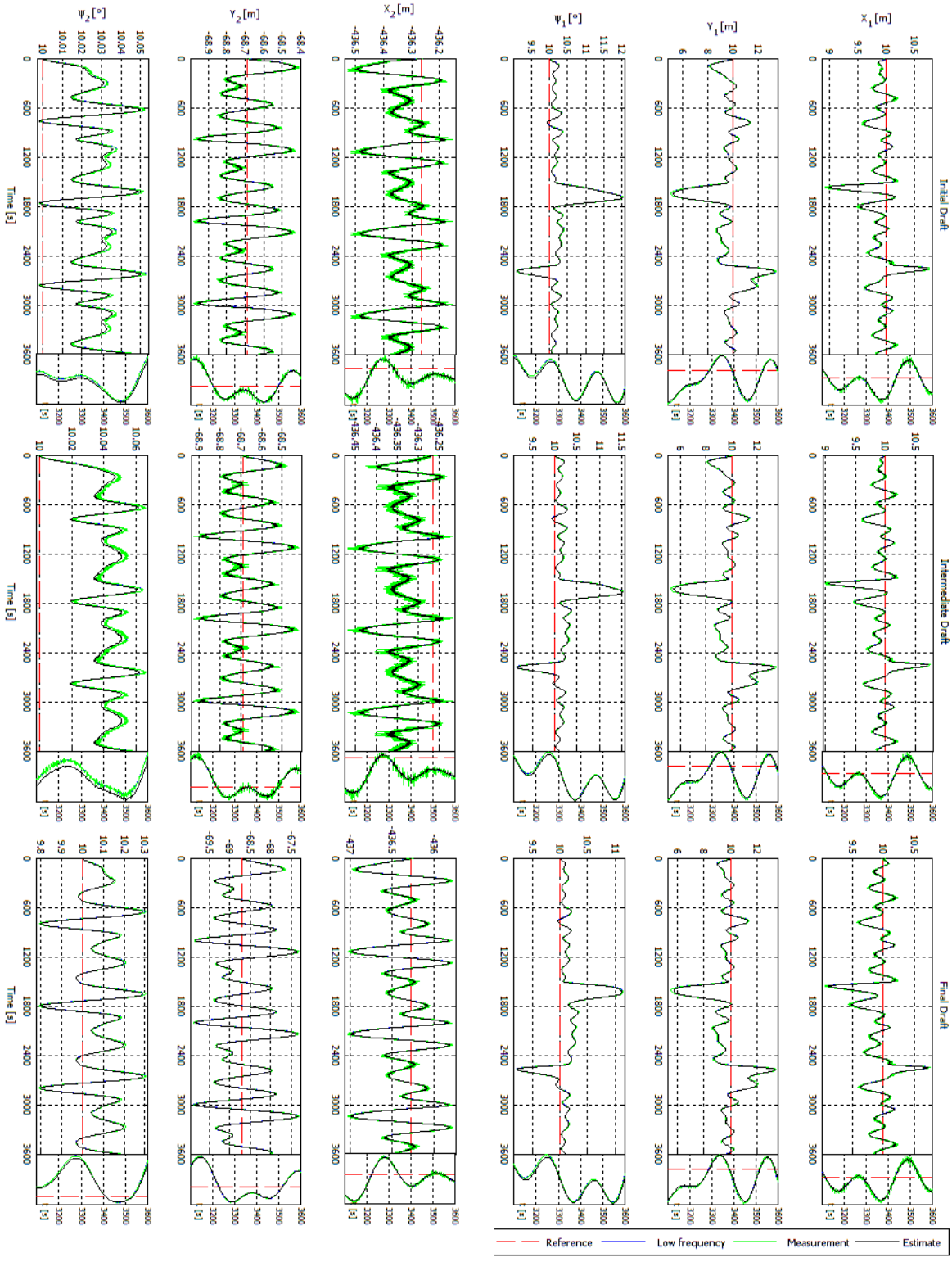

Figure 6.25: Positioning using PD-like Controller

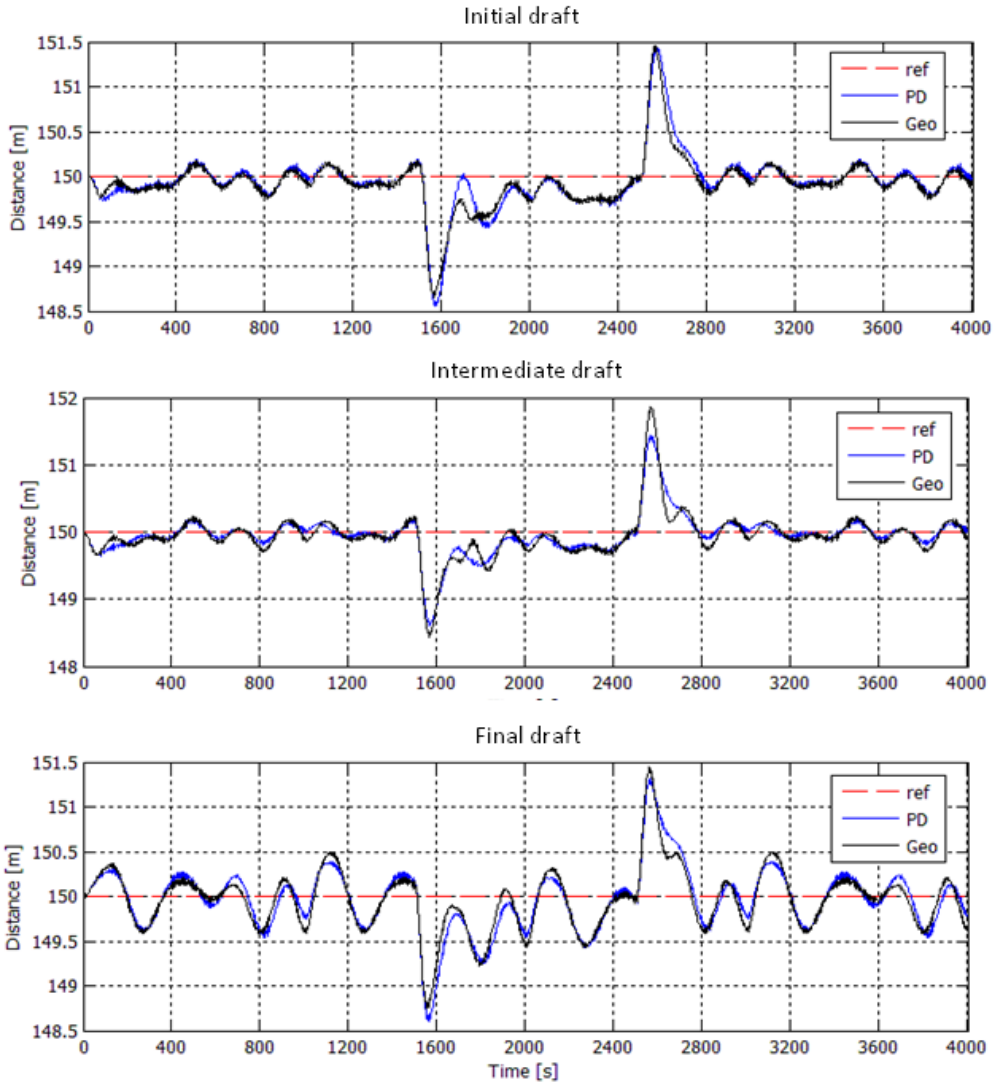

Figure 6.26: Distance between vessels

The simulations show that the distance error is small between both controllers' results when the extra force is inserted into it (peak after 1.500s) and the force ceases (peak around 2.500s). In spite of this small error difference, the error amplitude is negligible and the controllers can be consider similar.

Velocities are well-estimated by the nonlinear observer with wave-frequency model, with the exception of the estimated surge velocity of the shuttle tanker as presented in Figures 6.27 and 6.28. This behavior is the same one discussed in Section 6.2. The nonlinear observers estimates using the geometric controller present some estimated velocity peaks due to change in shuttle tanker reference.

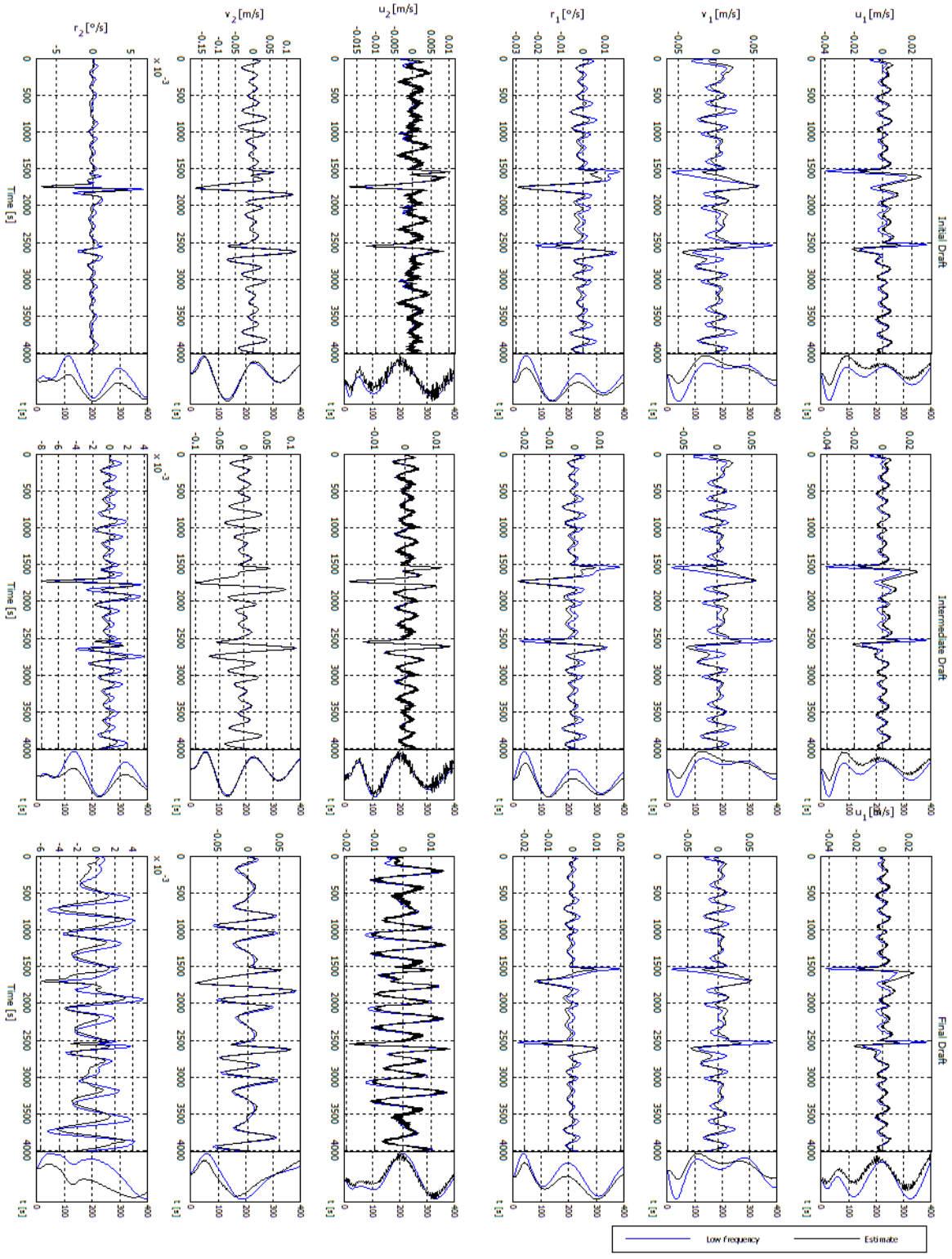

Figure 6.27: Vessel velocities using Geometric Controller

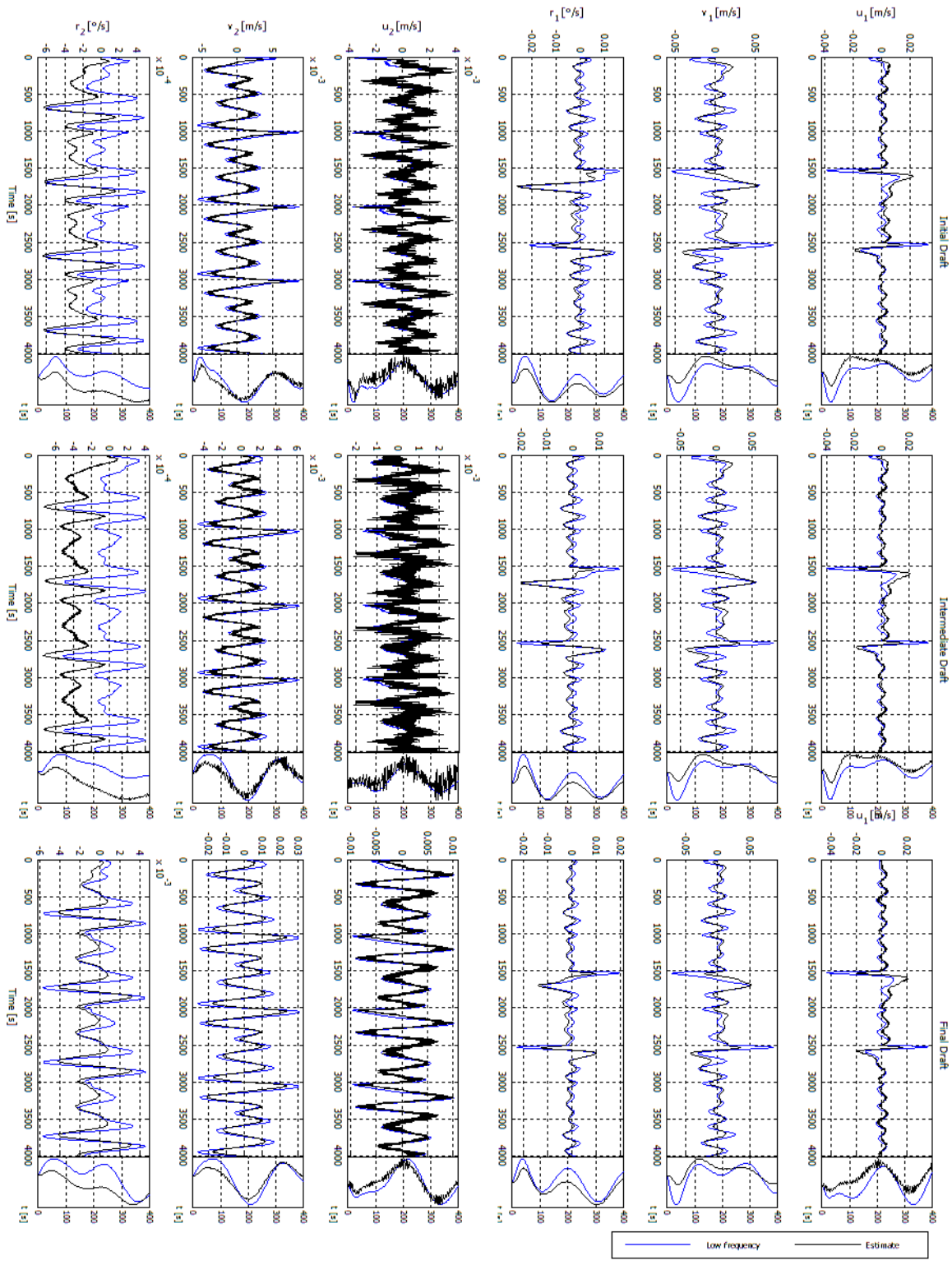

Figure 6.28: Vessel velocities using PD-like Controller

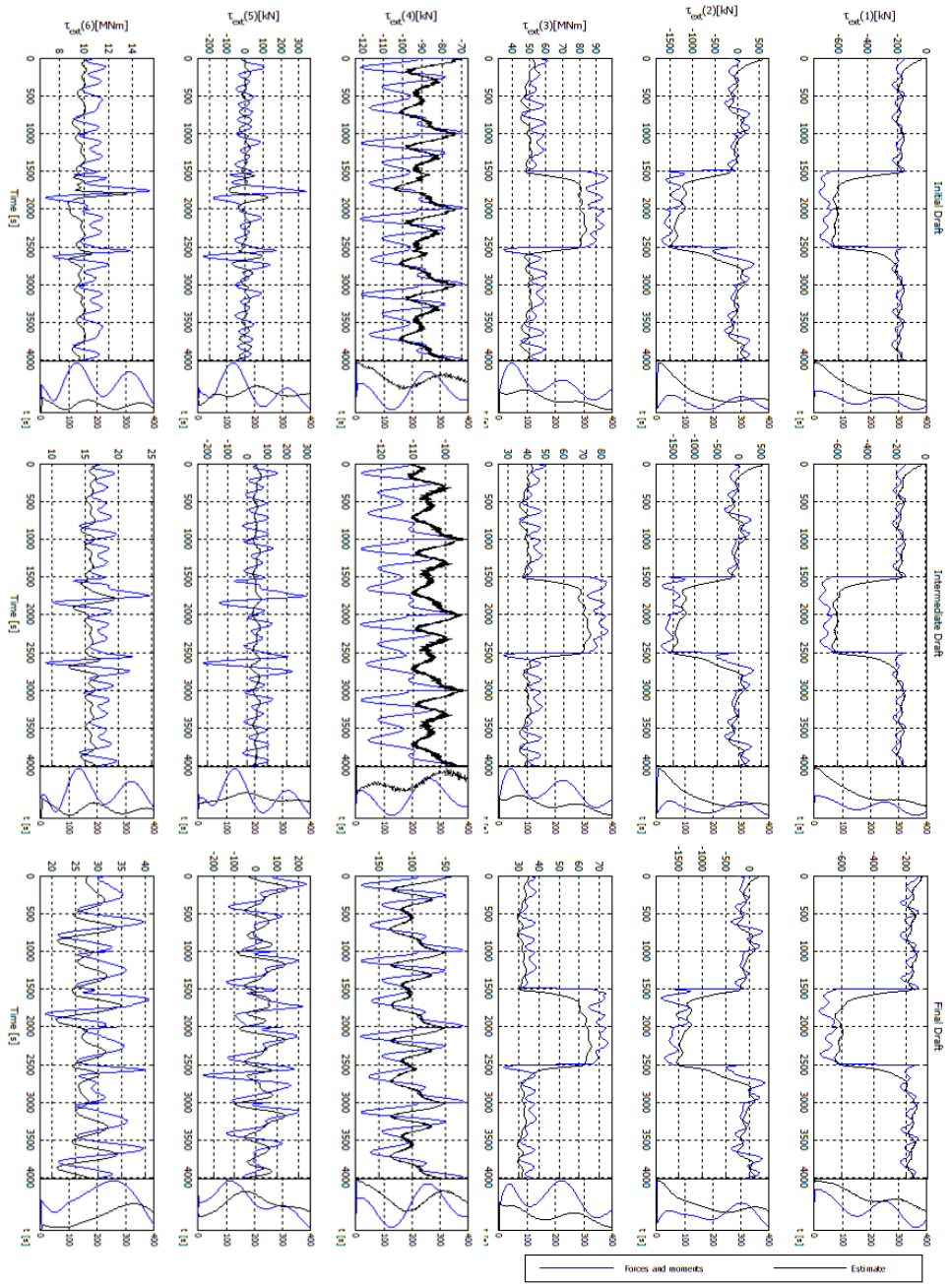

Figure 6.29: External forces using Geometric Controller

Estimation of the external forces and moment depend on the control law considered. This dependence is due to the shuttle tanker reference that is changed only in the case of PD-like controller. So, an external force and moment difference can be found between the controllers as presented in Figures 6.29 and 6.30.

Obviously, both controller have different actions that make the shuttle tanker moves in the case

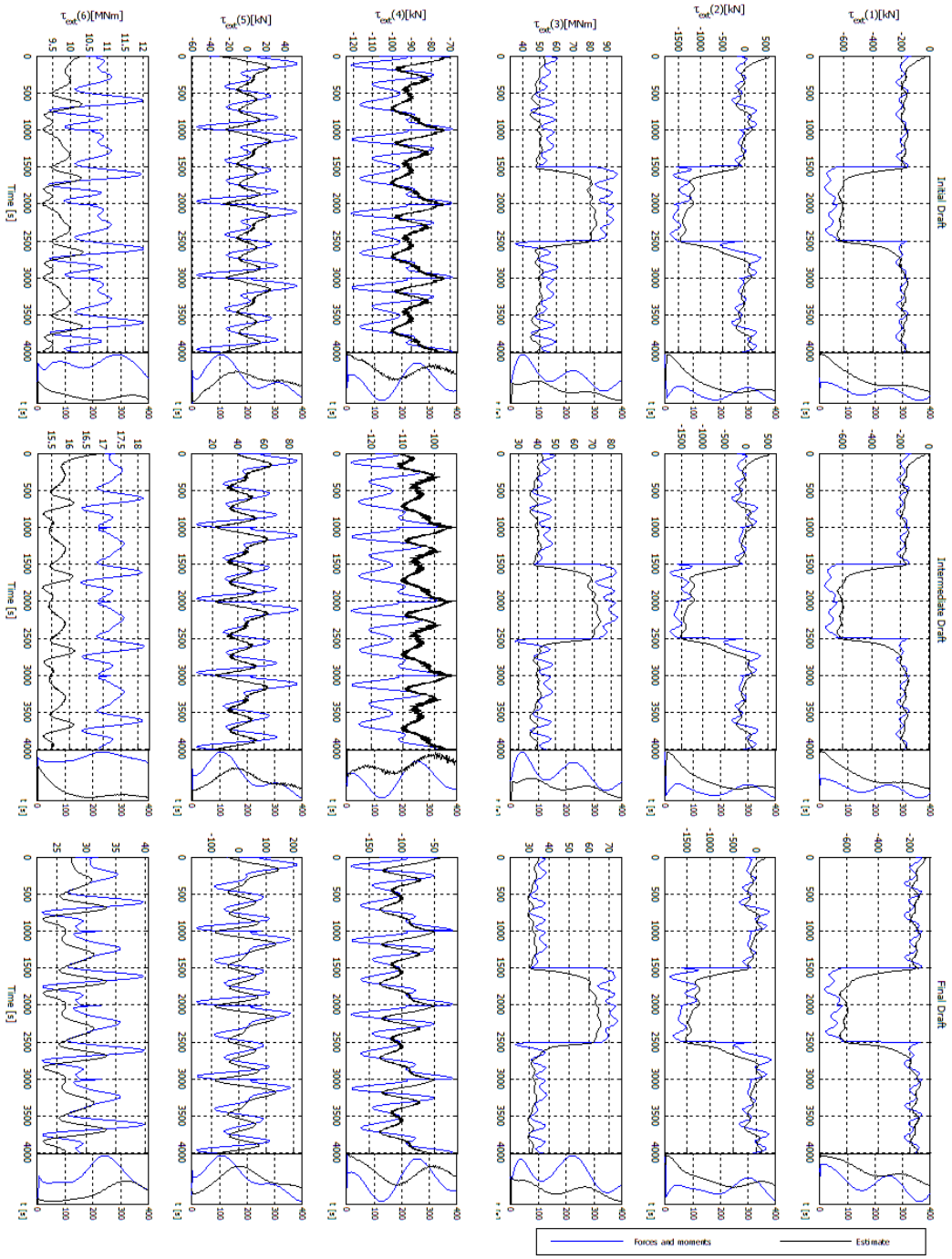

Figure 6.30: External forces using PD-like Controller

of geometric controller and do not move it in the case of the PD-like controller. Control forces peaks appear in the ST geometric control forces as in Figure 6.31 that does not appear in the ST PD-like control forces as presented in Figure 6.32. This occurs due to difference between the geometric controller constraint and PD-like error.

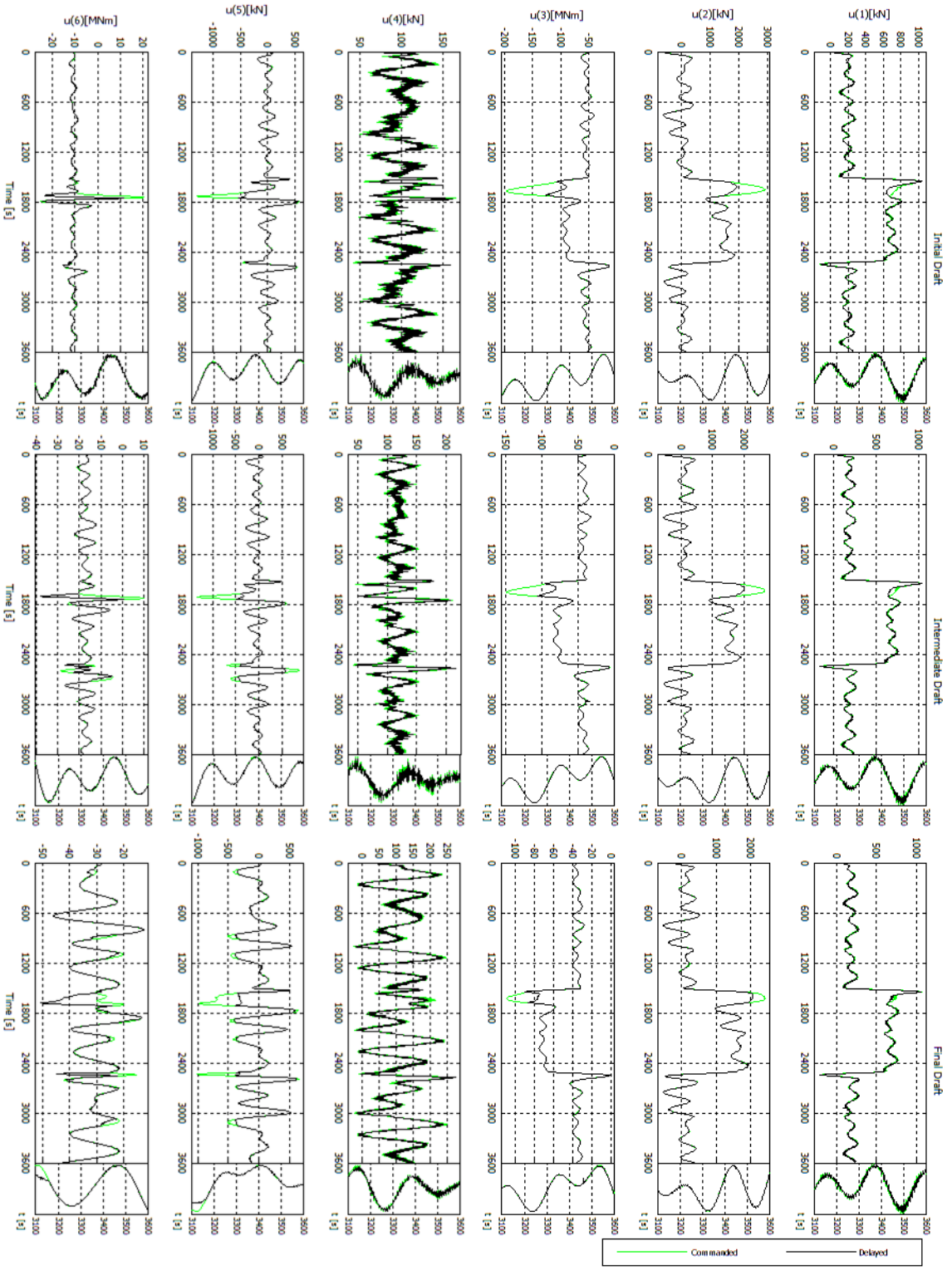

Figure 6.31: Control forces using Geometric Controller

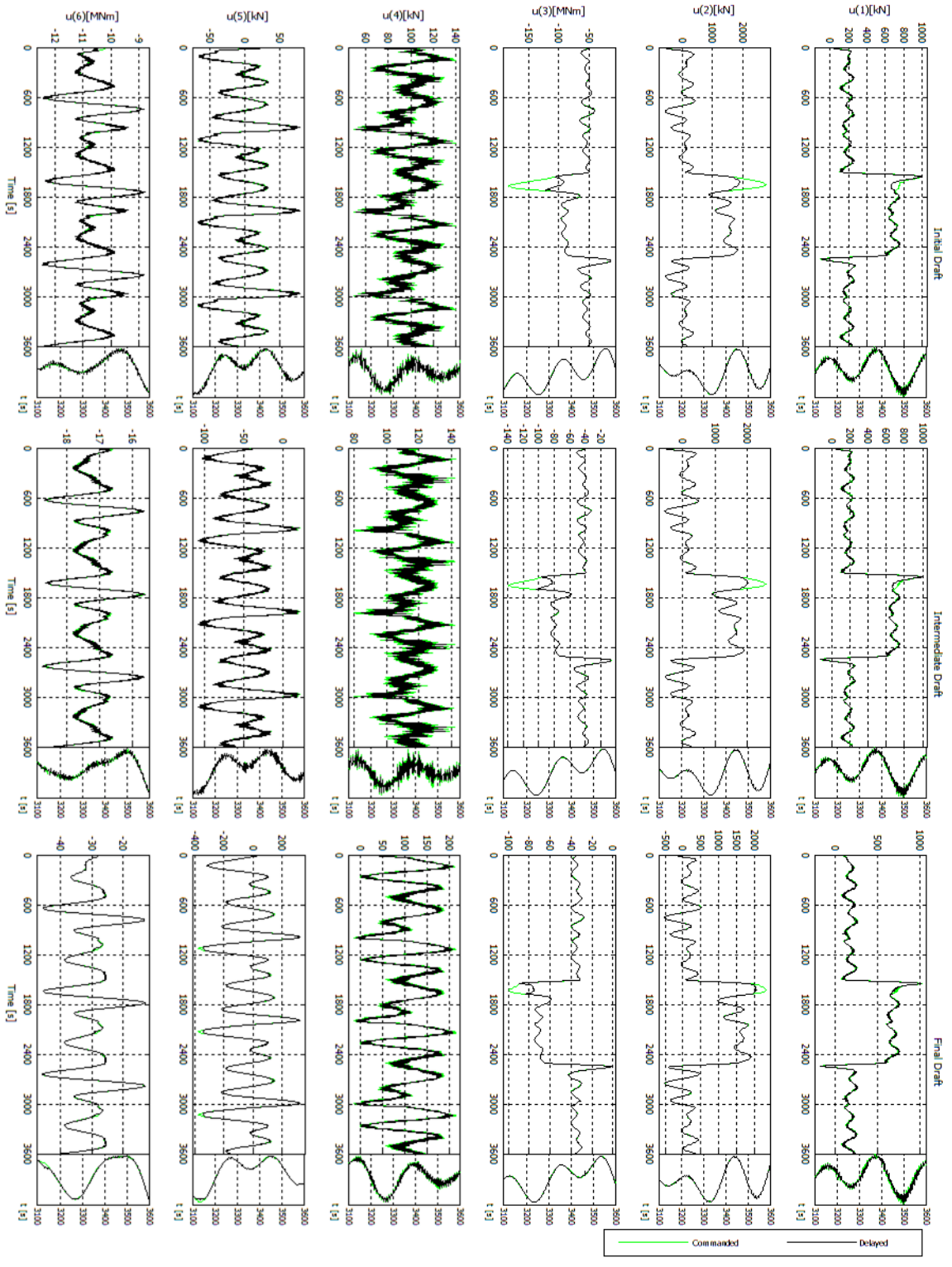

Figure 6.32: Control forces using PD-like Controller

6.5 Case 4: Harshening Sea State

Simulations are carried out to evaluate the switching control when the sea state is harshening. The environmental scenario for these simulations is presented in Figure 6.33. The direction of the current and wind are kept constant. The direction of the waves and the significant wave height Hs are also kept constant excepting the value of the peak period Tp. The peak period of the waves varies from 4.5s to 15.0s. The switching signal σ and the estimated peak frequency $\hat{\omega}_p$ are now calculated.

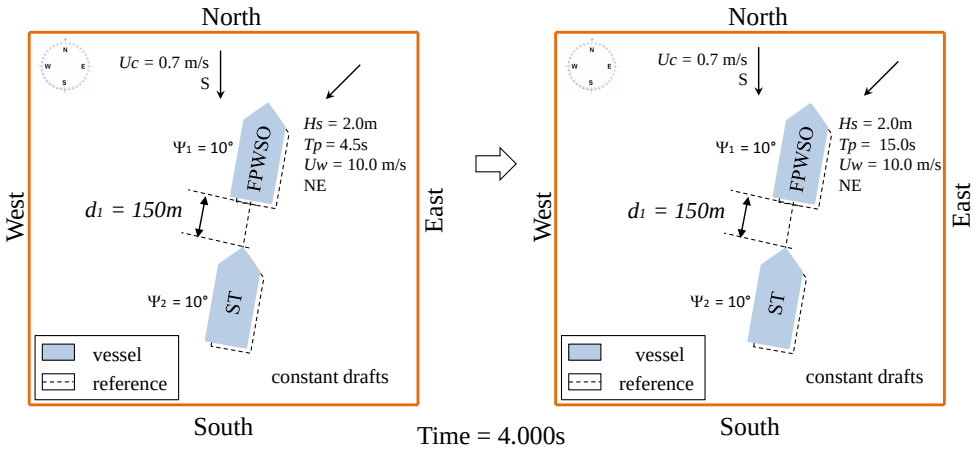

Figure 6.33: Environmental conditions and forth maneuver

Vessels' positioning and the relative distance are maintained for both controllers during the simulation with the sea condition variation as presented in Figures 6.34, 6.35 and 6.36. Wave-frequency motion influence on the position and heading estimates was expected due to the nonlinear observer parameter changes.

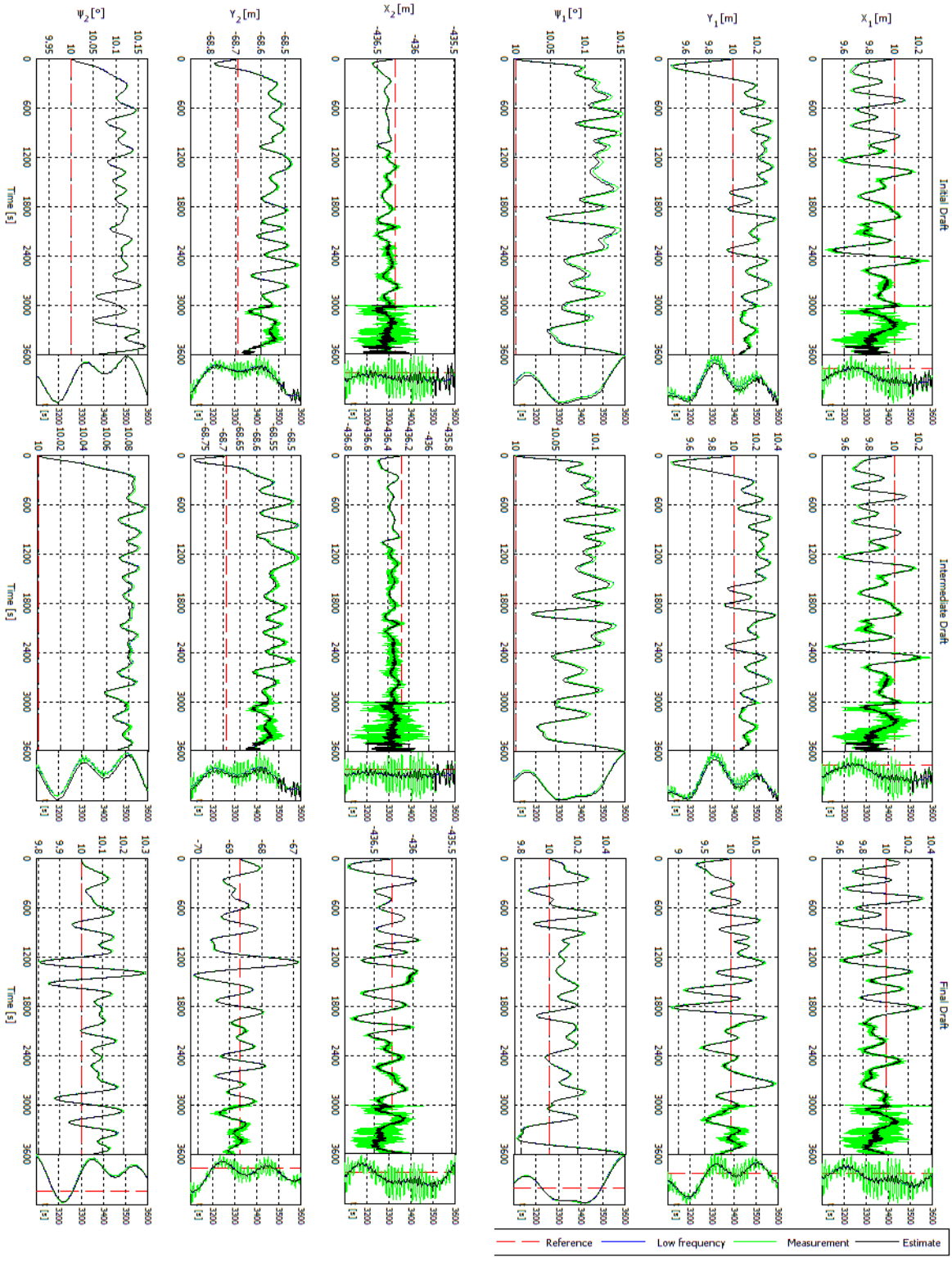

Figure 6.34: Positioning using Geometric Controller

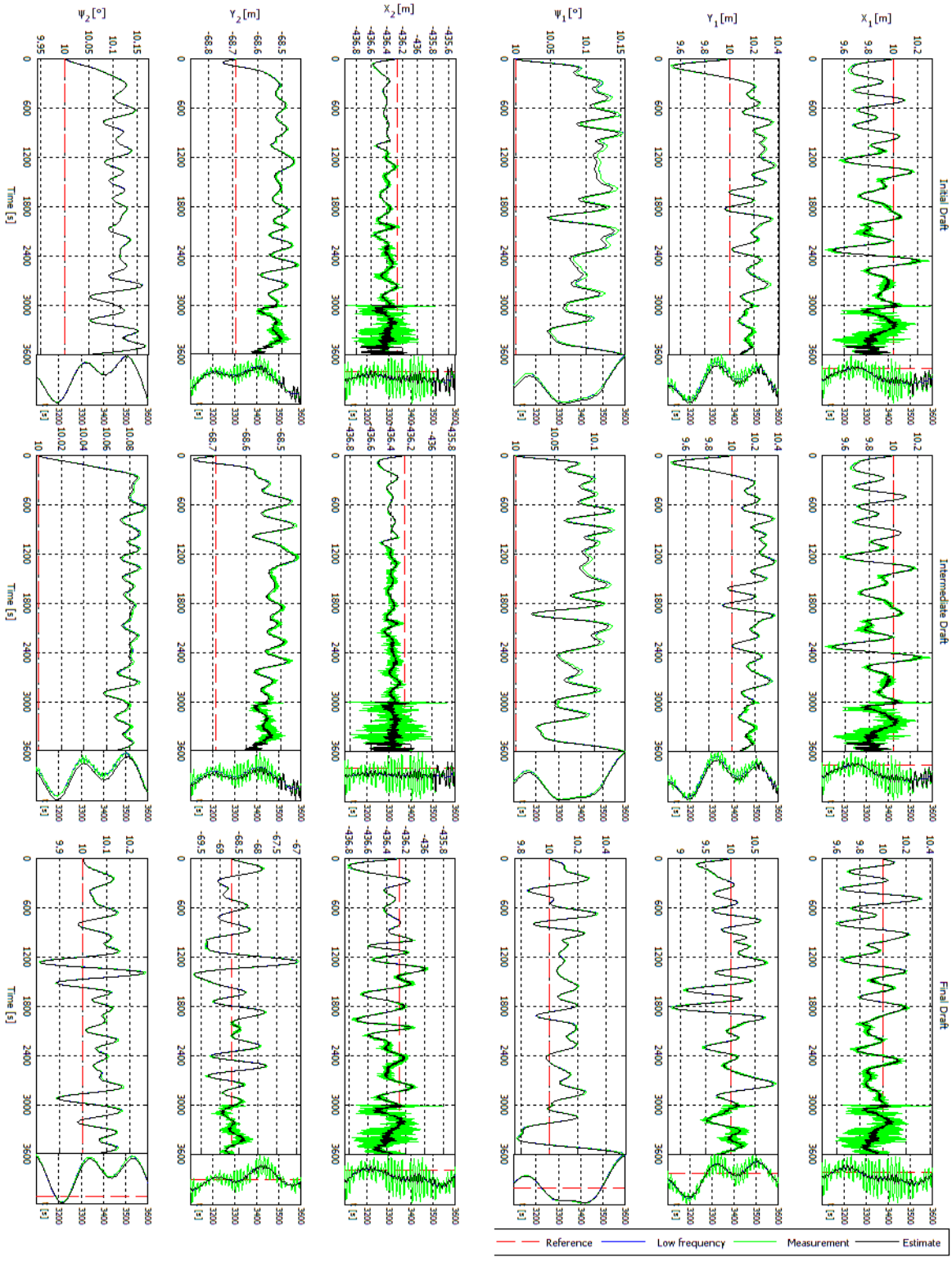

Figure 6.35: Positioning using PD-like Controller

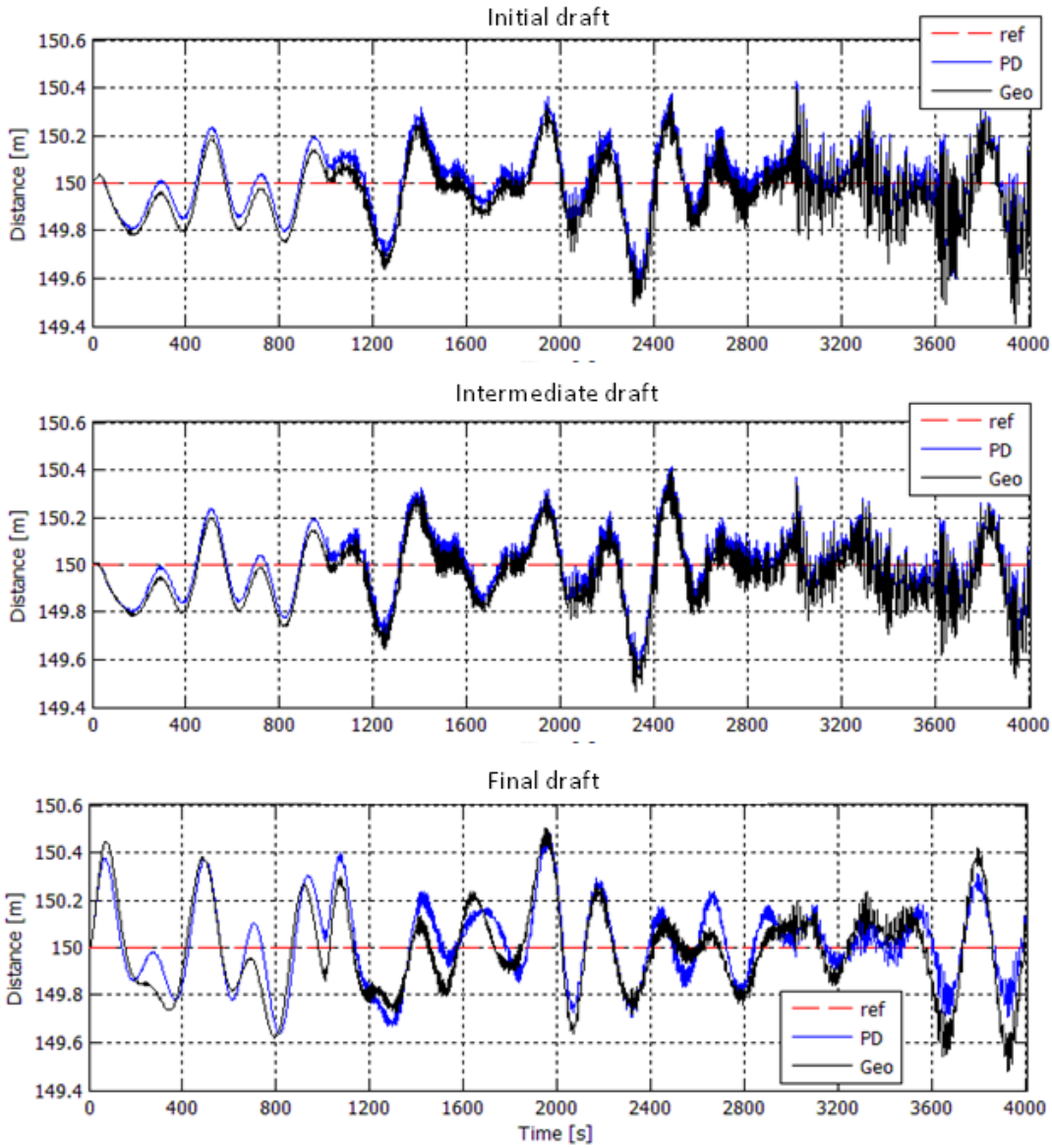

Figure 6.36: Distance between vessels

The velocity estimates made by the nonlinear observers are good because they converge to real values as presented in Figures 6.37 and 6.38, even if its parameters are changed by the switching controller. The wave-influence motion influence is filtered from the estimated velocities as presented in those figures excepting for $t > 3.500s$.

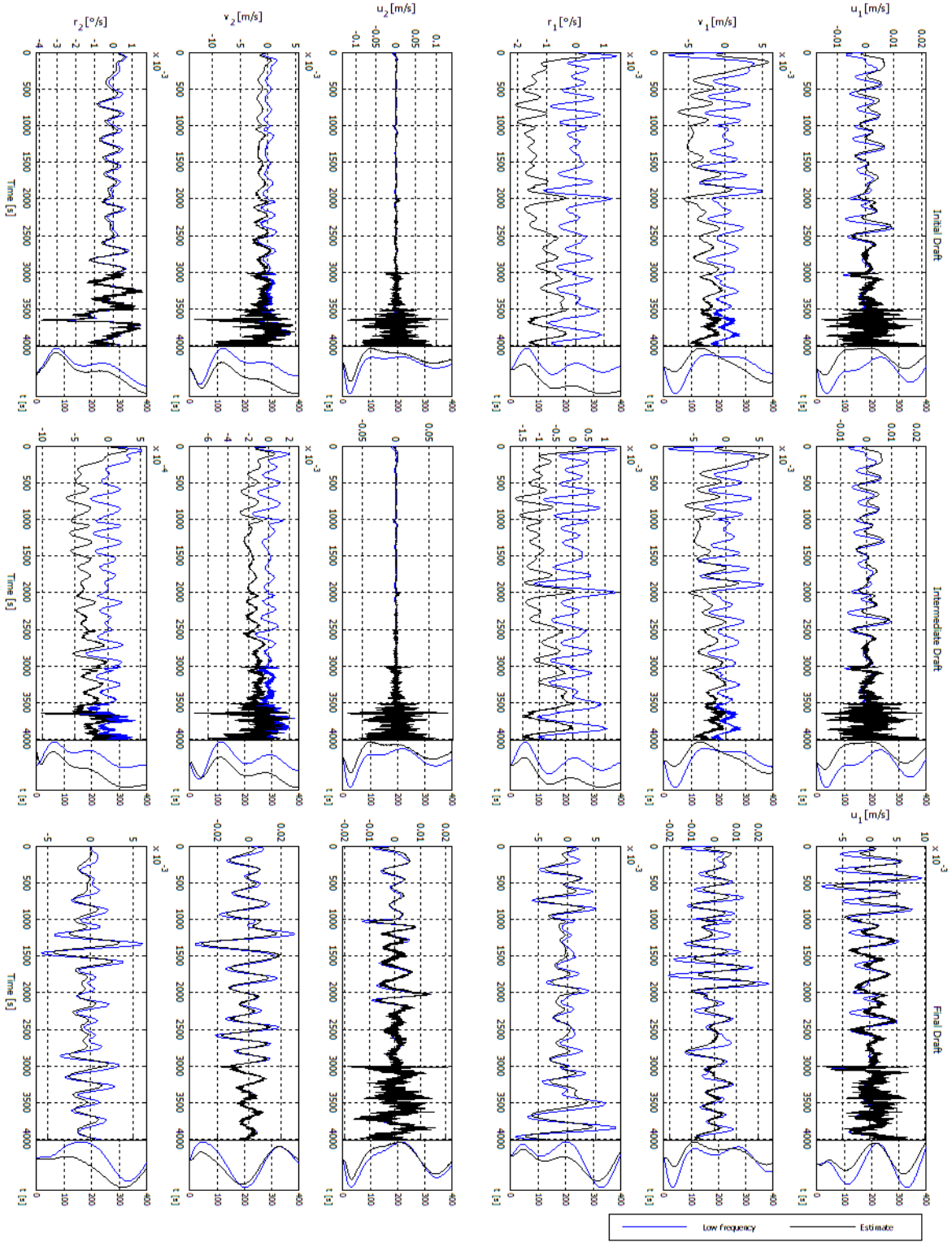

Figure 6.37: Vessel velocities using Geometric Controller

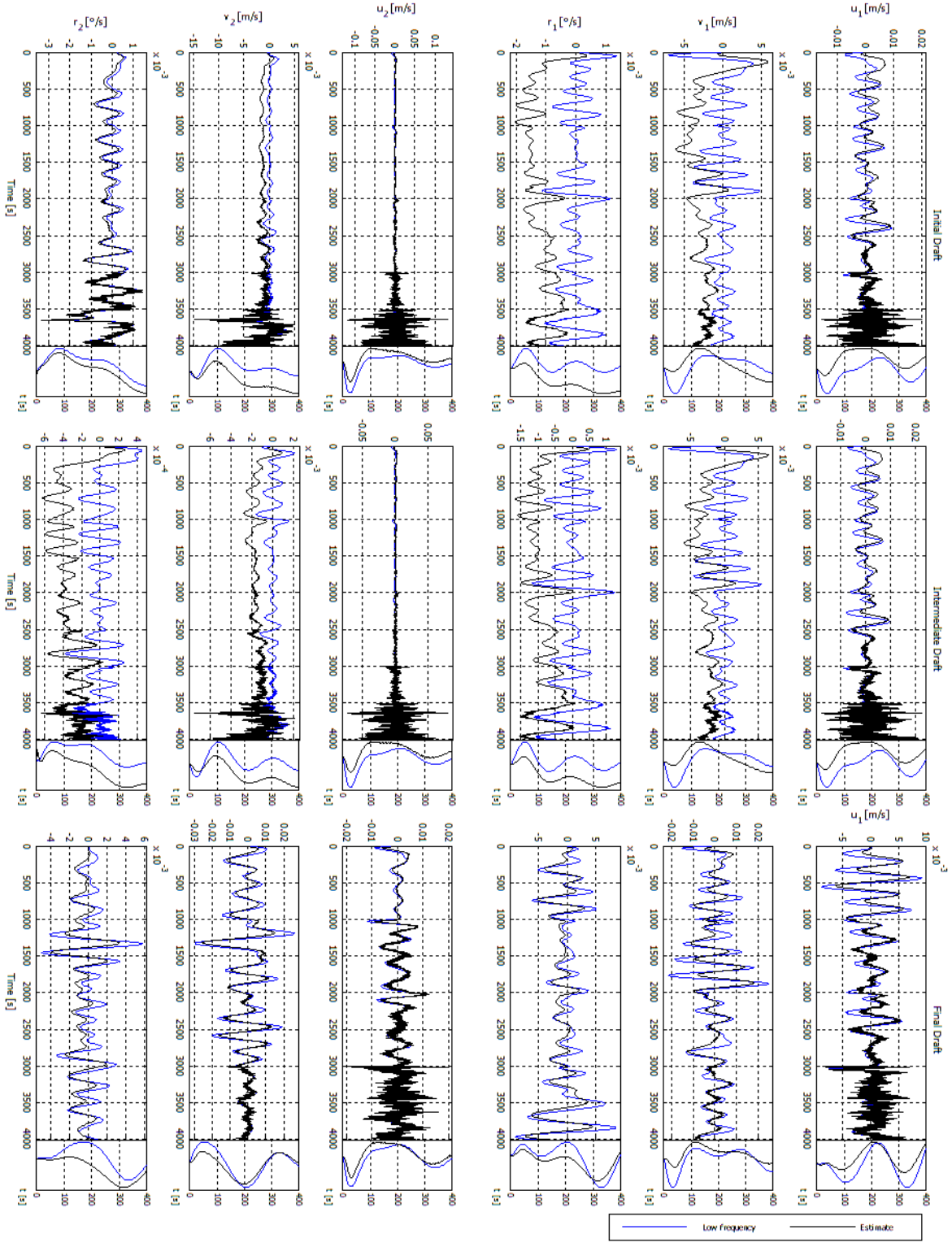

Figure 6.38: Vessel velocities using PD-like Controller

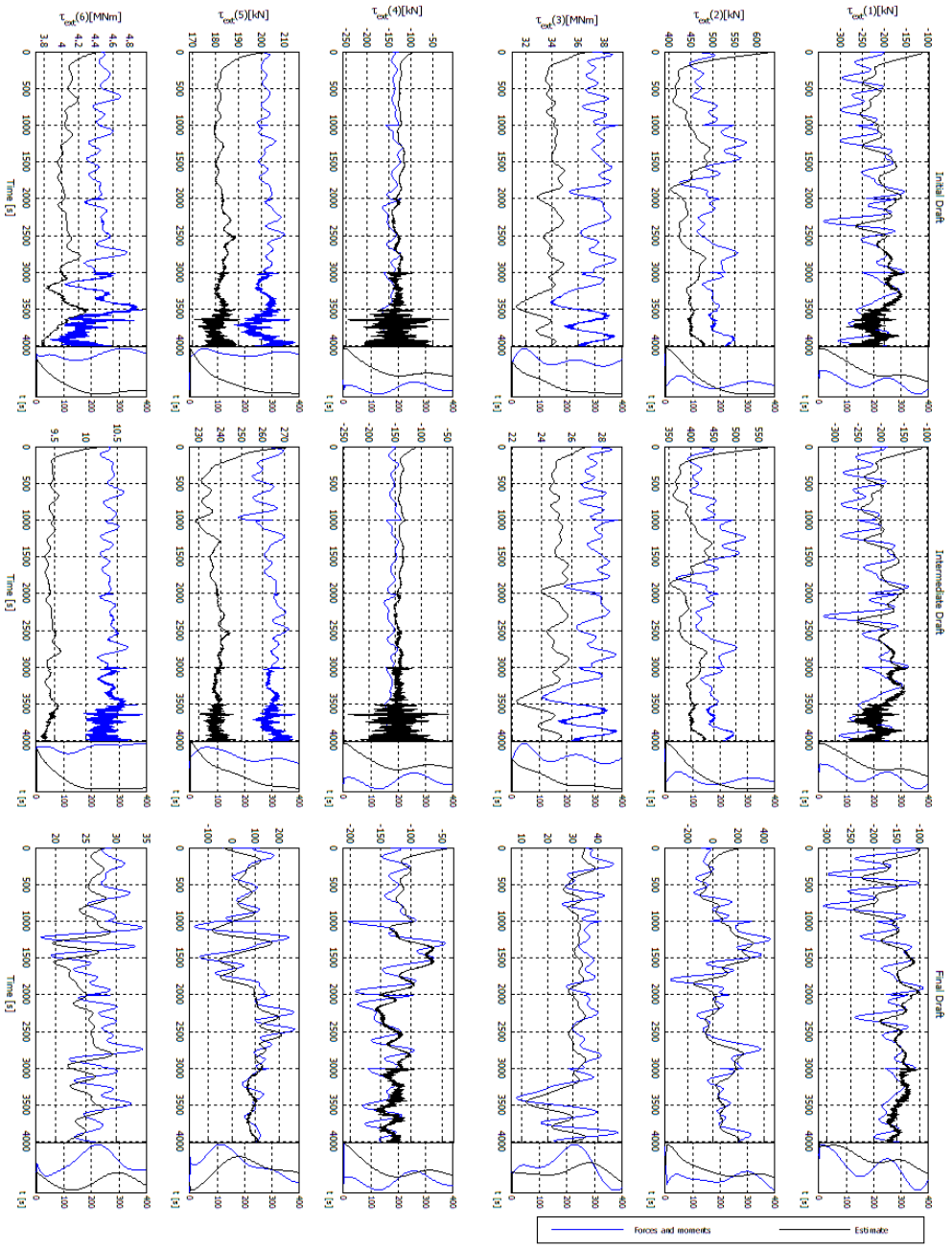

Figure 6.39: External forces using Geometric Controller

The external force estimates made by the nonlinear observer are also good as presented in Figures 6.39 and 6.40 in spite of some magnitude errors. The effect of the nonlinear observer for extreme seas on the external force estimates can be seen in those figures for $t > 3.500s$.

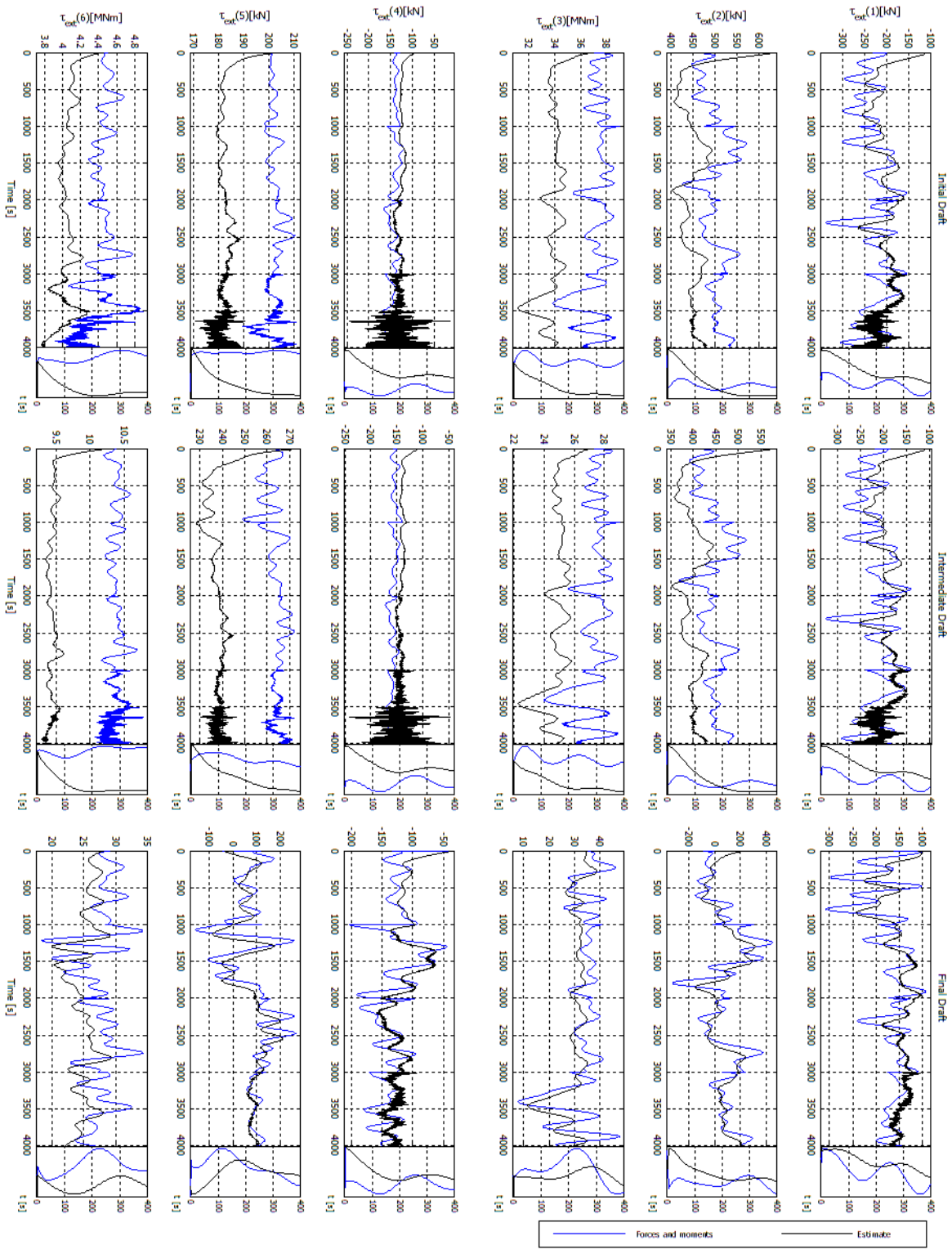

Figure 6.40: External forces using PD-like Controller

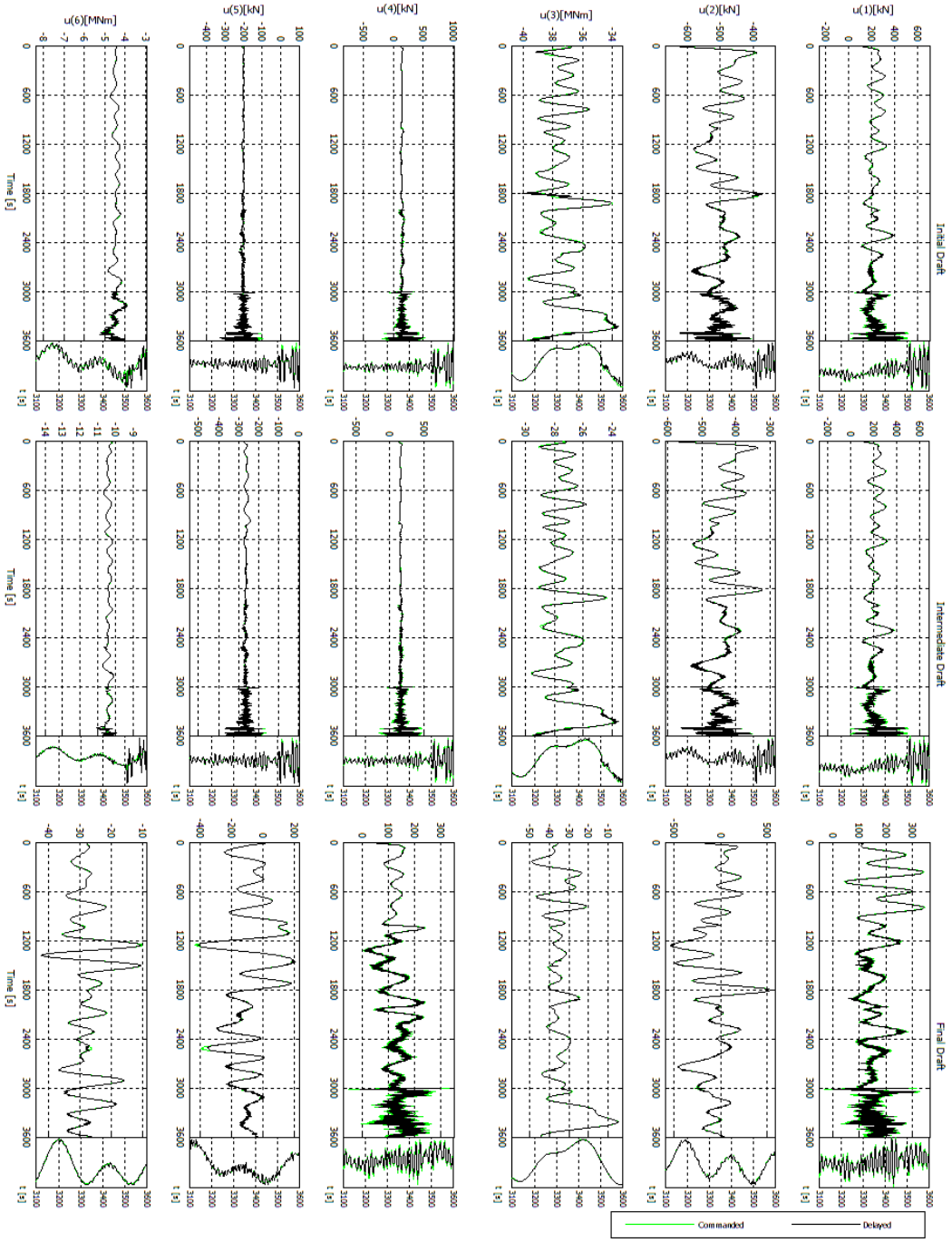

Figure 6.41: Control forces using Geometric Controller

Geometric control law is very similar to PD-like control forces as presented in Figures 6.41 and 6.42.

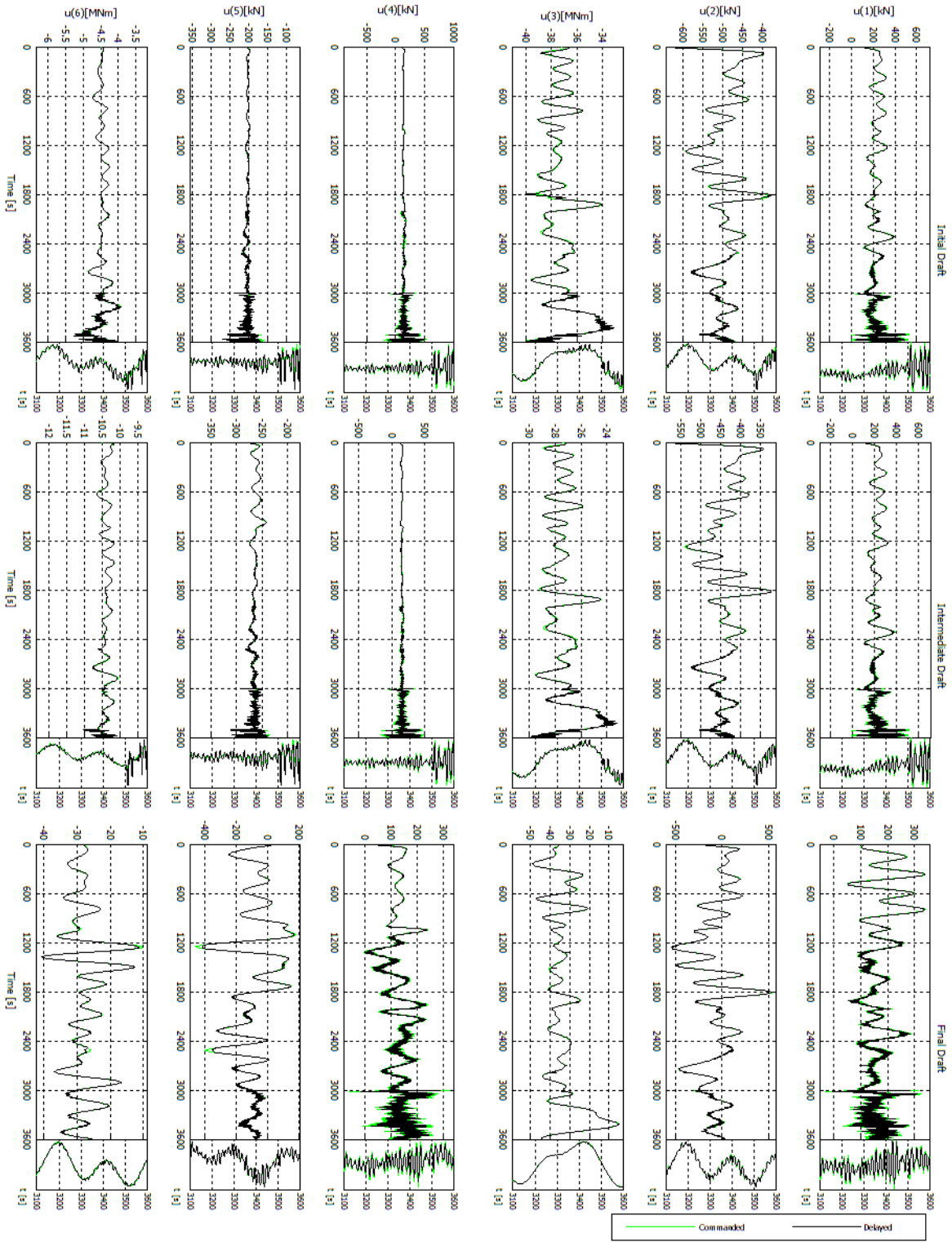

Figure 6.42: Control forces using PD-like Controller

During these simulations, the estimated peak frequency of the motion spectrum is lose to real values as presented in Figure 6.43. Hence, the switching control generates the switching signal σ, correctly selecting the nonlinear observer associated with estimated peak frequency as presented in Figure 6.43. Therefore, the estimates of the positions and headings for both vessels has filtered the wave-frequency motion influence. Obviously, this filtering process does not happen when the the nonlinear observer for extreme seas is selected ($t > 3.500s$).

The switching control takes 500s to change the nonlinear observer. This interval is the time difference between the change of the peak period Tp and the change in the switching signal σ. It is the maximum time in which the signal σ is updated because it is the length of the data window for generating the motion spectrum of the vessels. Despite the delay in switching the observer, the switching control changes the observer parameters correctly. Vessels' positioning are maintained in their set-points for both geometric and PD-like controllers, and for each draft simulated.

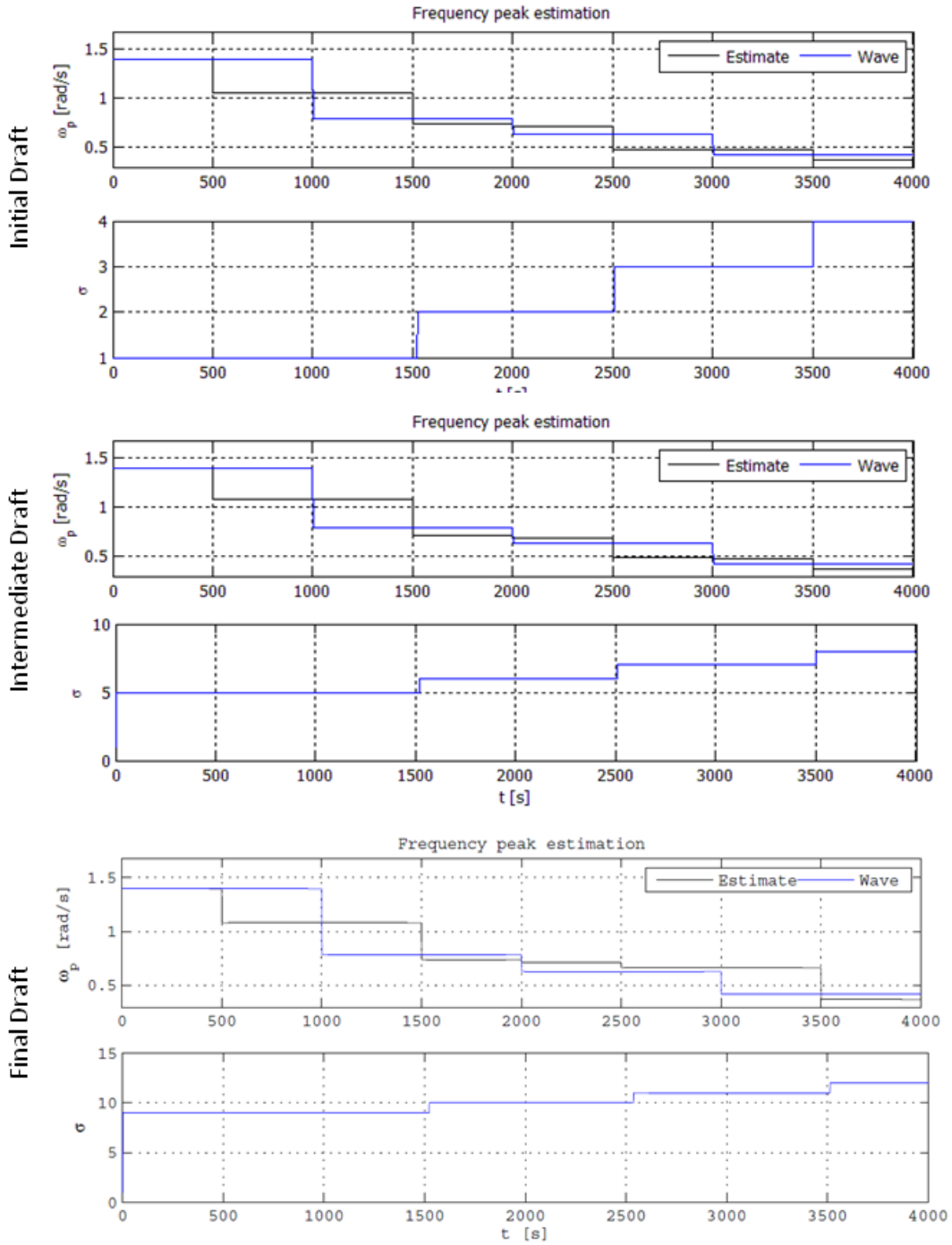

Figure 6.43: Peak Estimation and σ

6.6 Case 5: Sea State Becoming Calm

The simulations are carried out to evaluate the switching control when the sea state is getting calm are presented. The environmental scenario for these simulations is presented in Figure 6.44. The direction of the current and wind are kept constant. The direction of the waves and the significant wave height Hs are also kept constant excepting the value of the peak period Tp. The peak period of the waves varies from 15s to 4.5s. The switching signal σ and the estimated peak frequency $\hat{\omega}_p$ are now calculated.

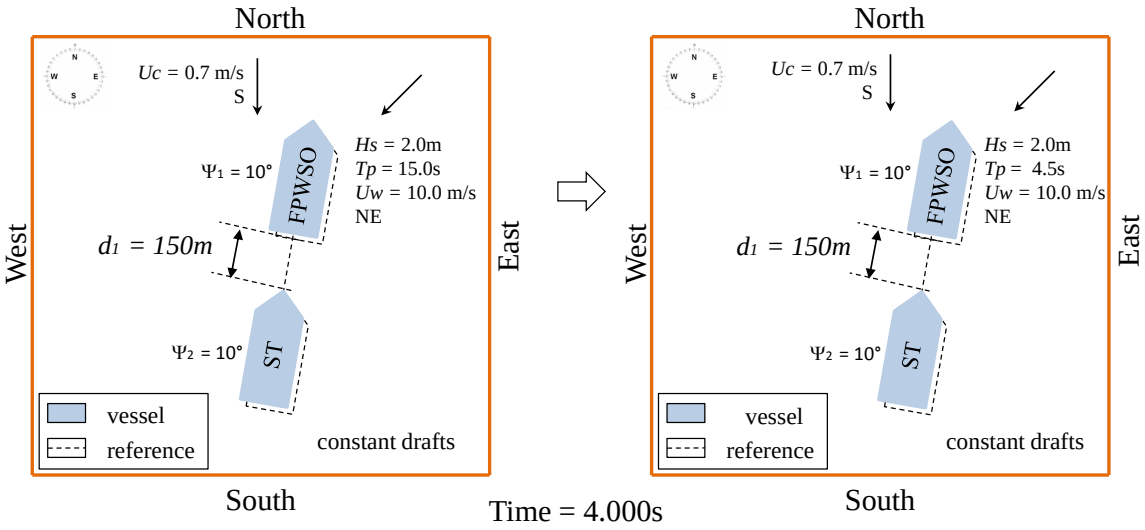

Figure 6.44: Environmental condition and fifth maneuver

Vessels' positioning and the relative distance are maintained for both controllers during the simulation with the sea condition variation as presented in Figures 6.45, 6.46 and 6.47. As the previous section, some wave-frequency motion influence was expected on the position and heading estimates.

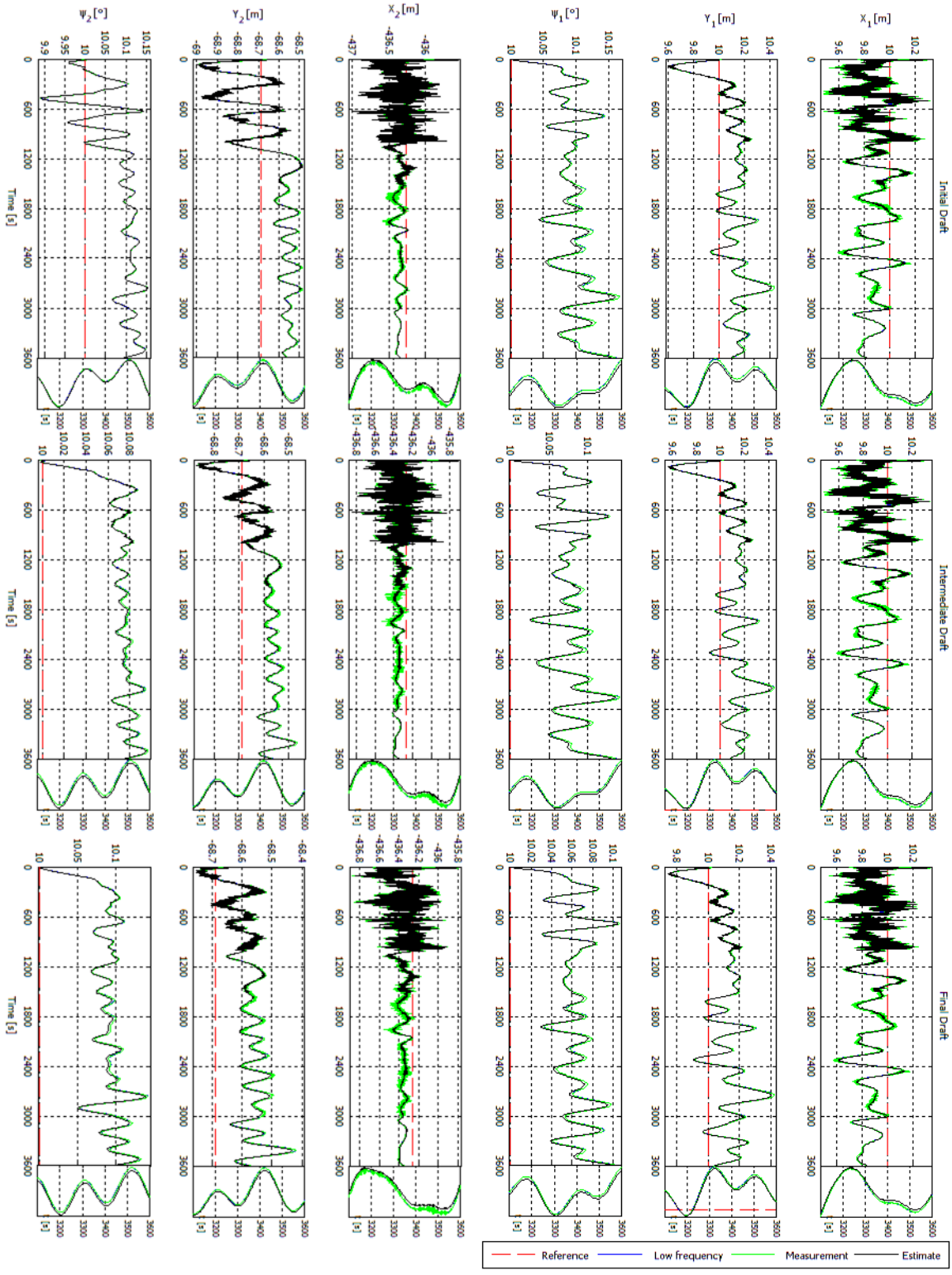

Figure 6.45: Positioning using Geometric Controller

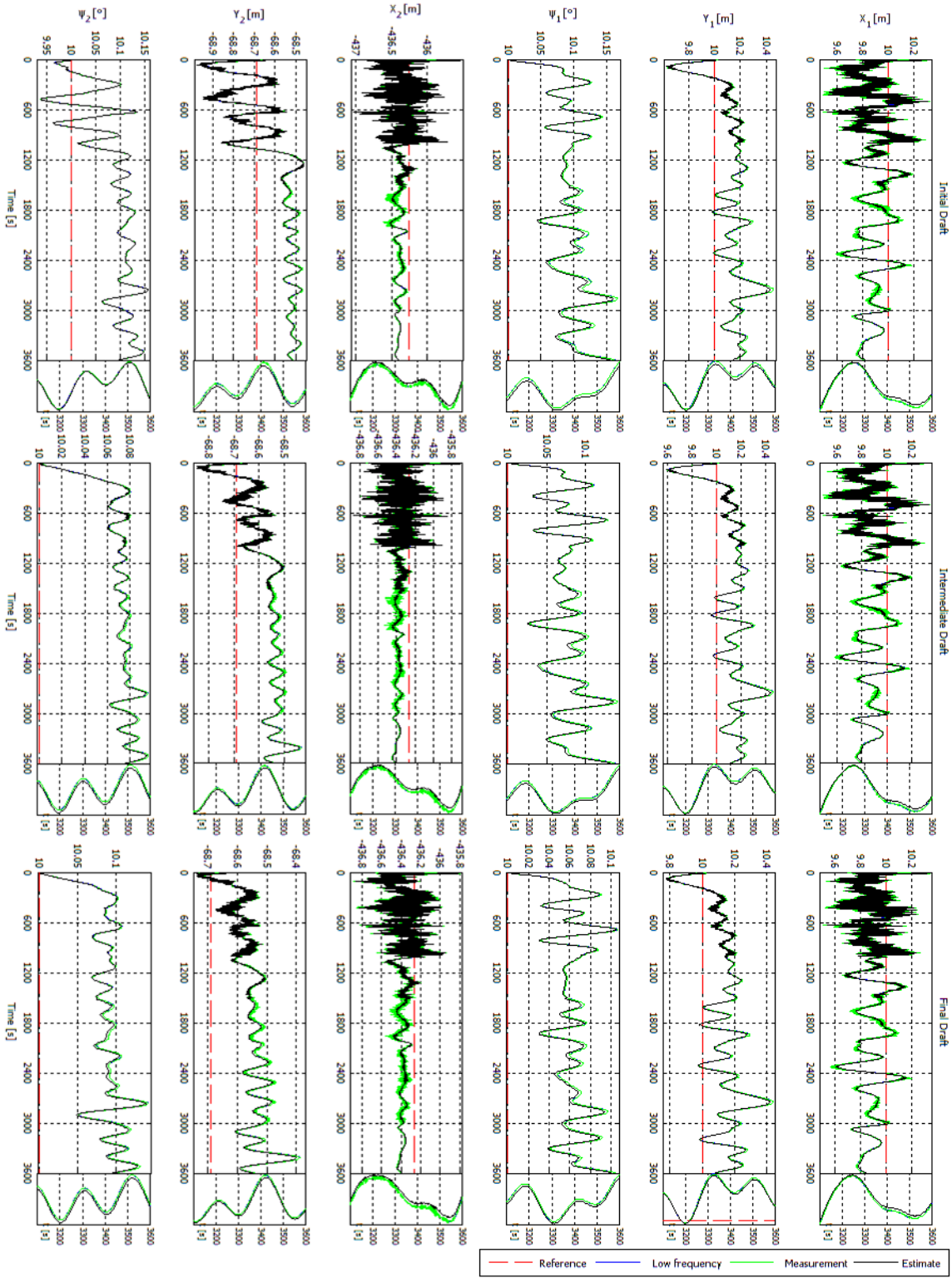

Figure 6.46: Positioning using PD-like Controller

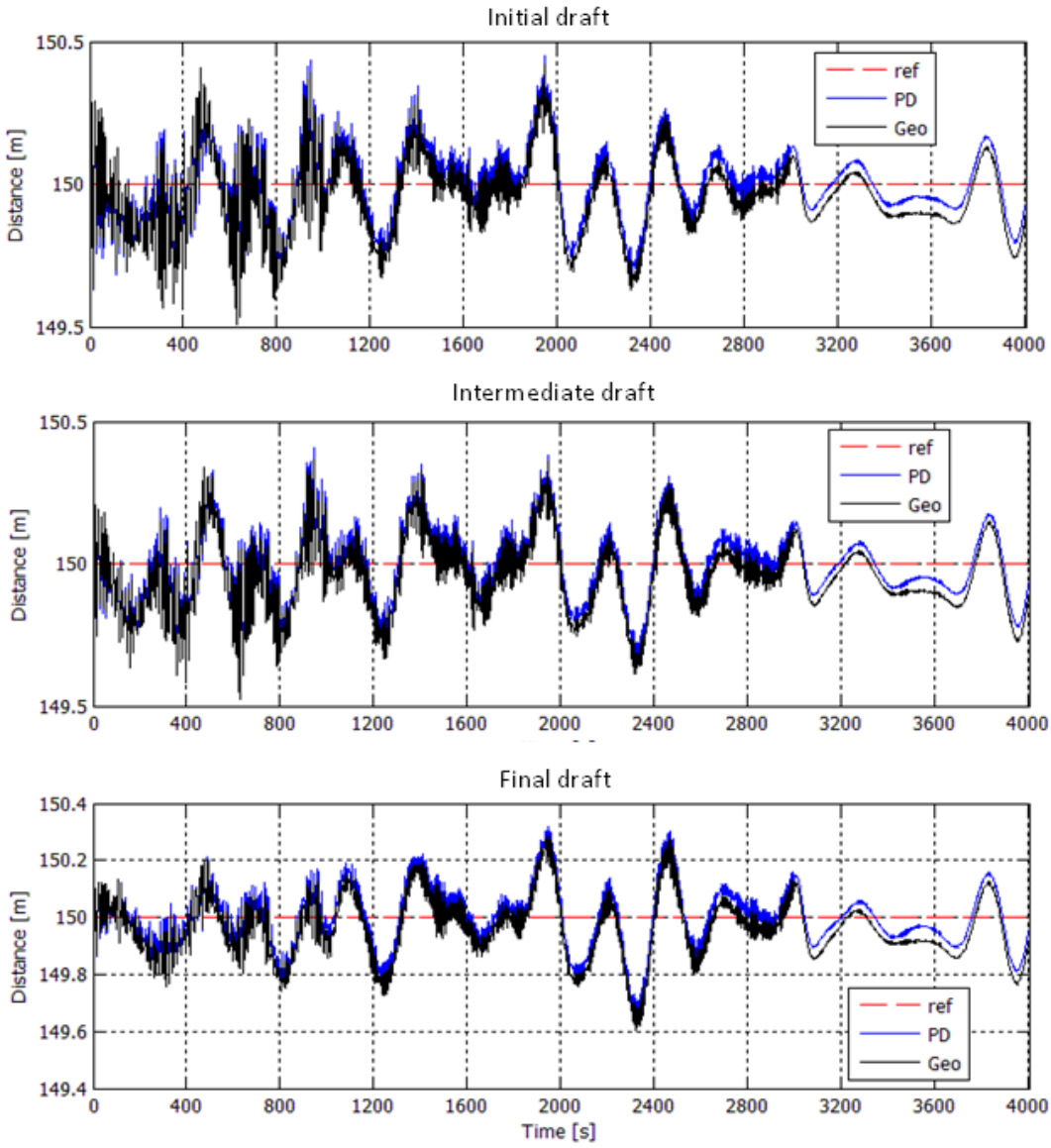

Figure 6.47: Distance between vessels

The estimates made by the nonlinear observer are good as presented in Figures 6.48 and 6.49, even if its parameters are changed by the switching controller. The wave-influence motion filtering on the can be seen in those figures excepting for $t < 500s$.

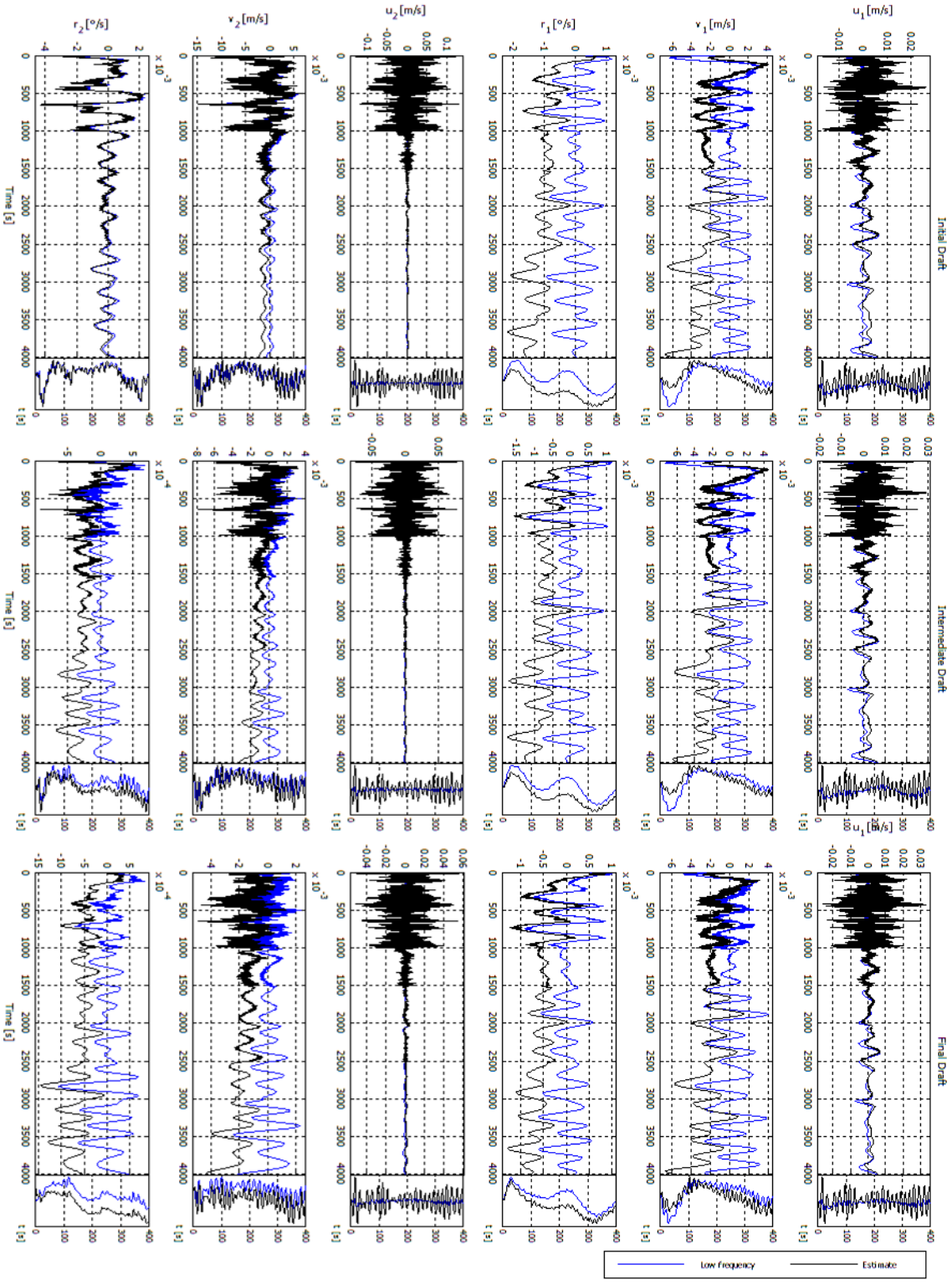

Figure 6.48: Vessel velocities using Geometric Controller

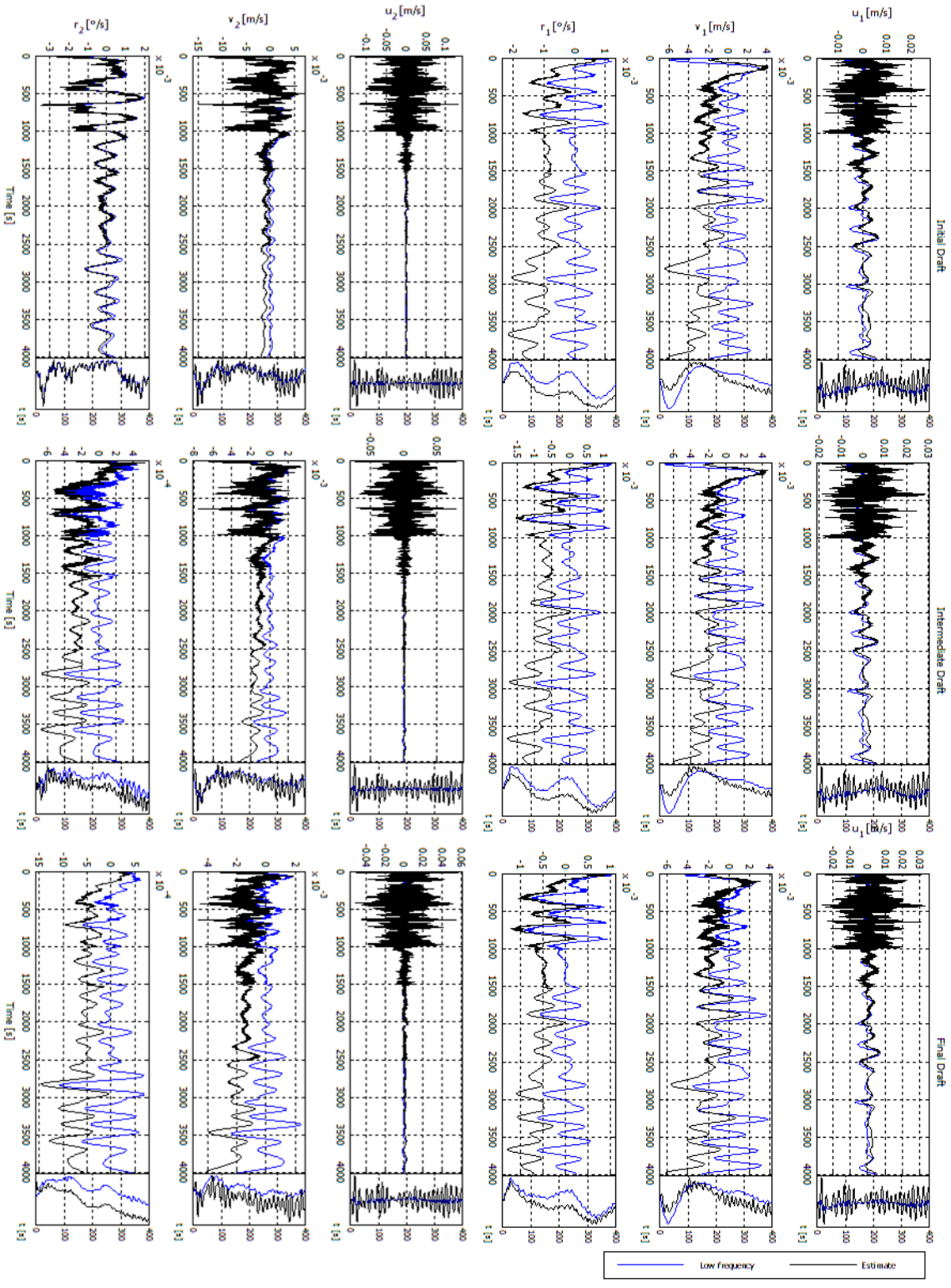

Figure 6.49: Vessel velocities using PD-like Controller

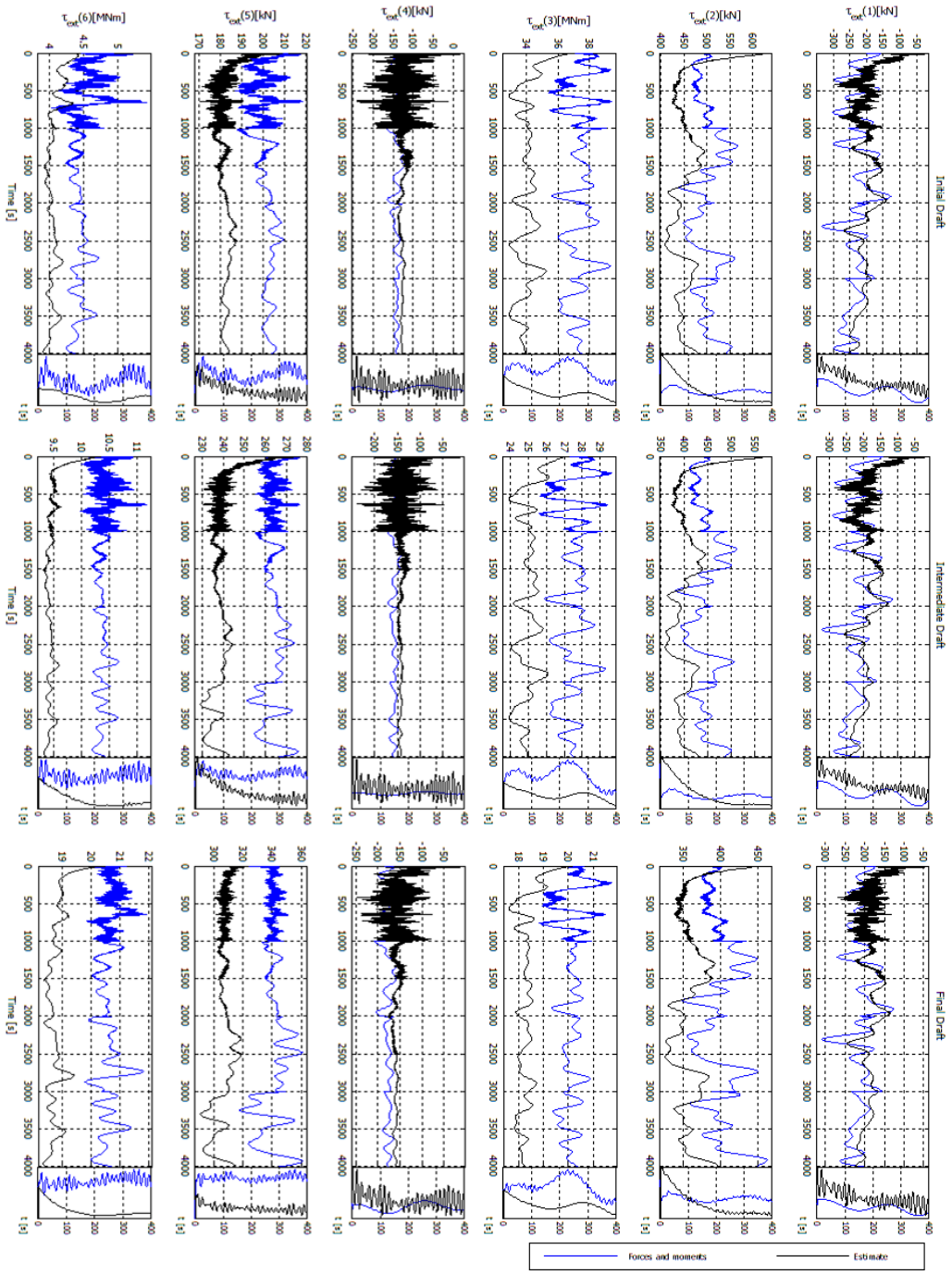

Figure 6.50: External forces using Geometric Controller

The external force estimates made by the nonlinear observer are also good as presented in Figures 6.50 and 6.51. The effect of the nonlinear observer for extreme seas on the external force estimates can be seen in those figures for $t < 500s$.

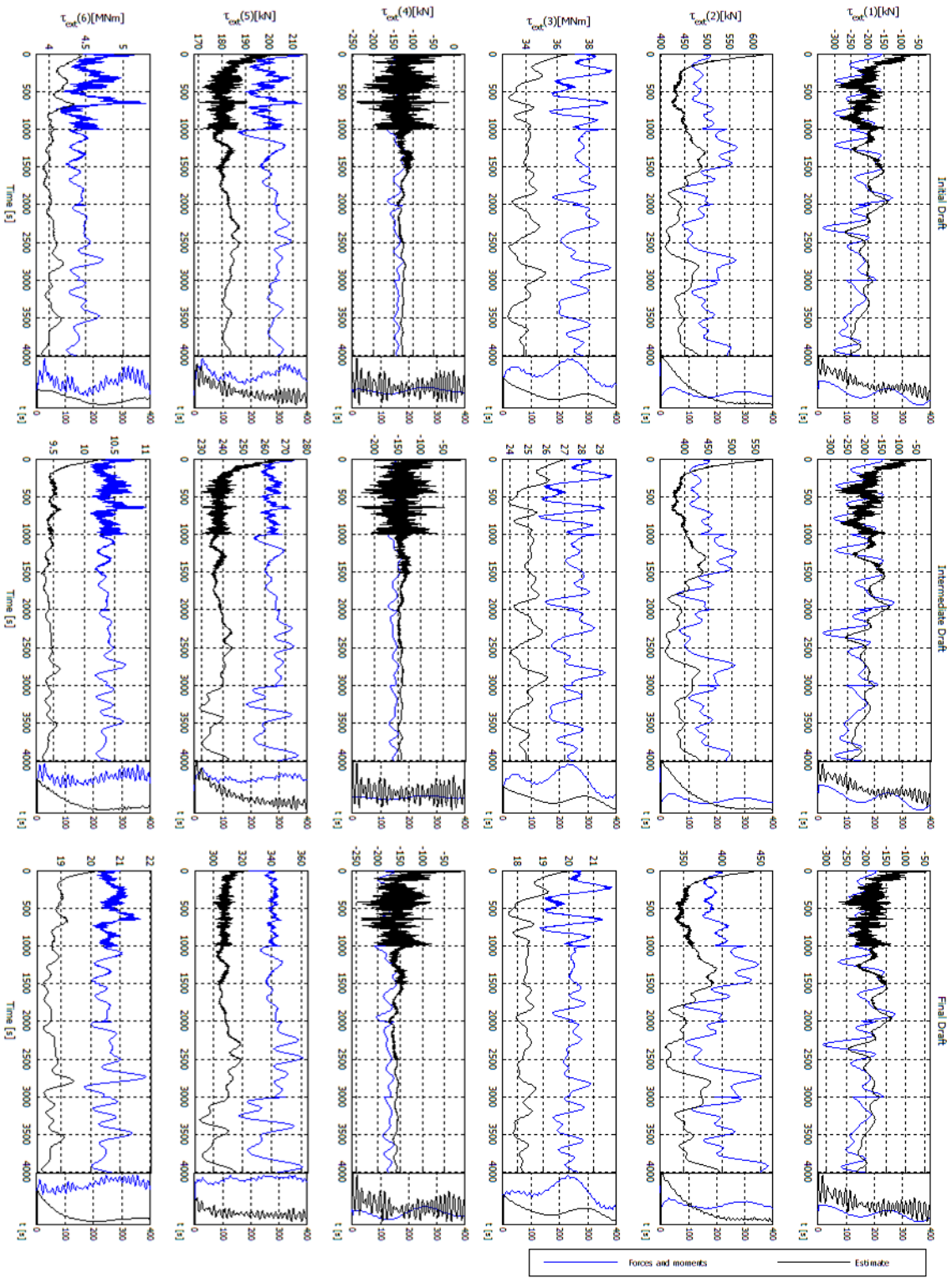

Figure 6.51: External forces using PD-like Controller

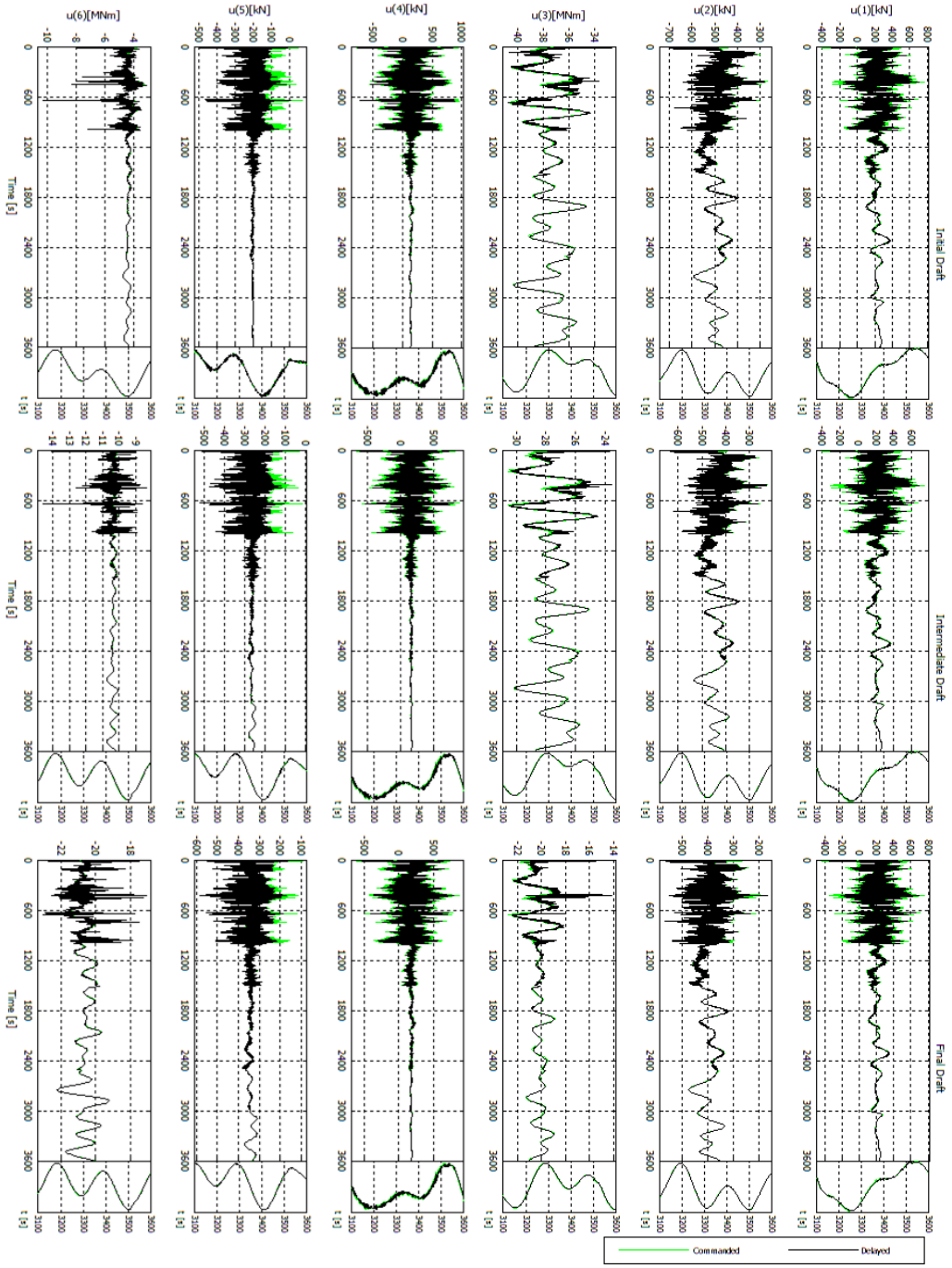

Figure 6.52: Control forces using Geometric Controller

Geometric control law is very similar to PD-like control law as presented in Figures 6.41 and 6.42.

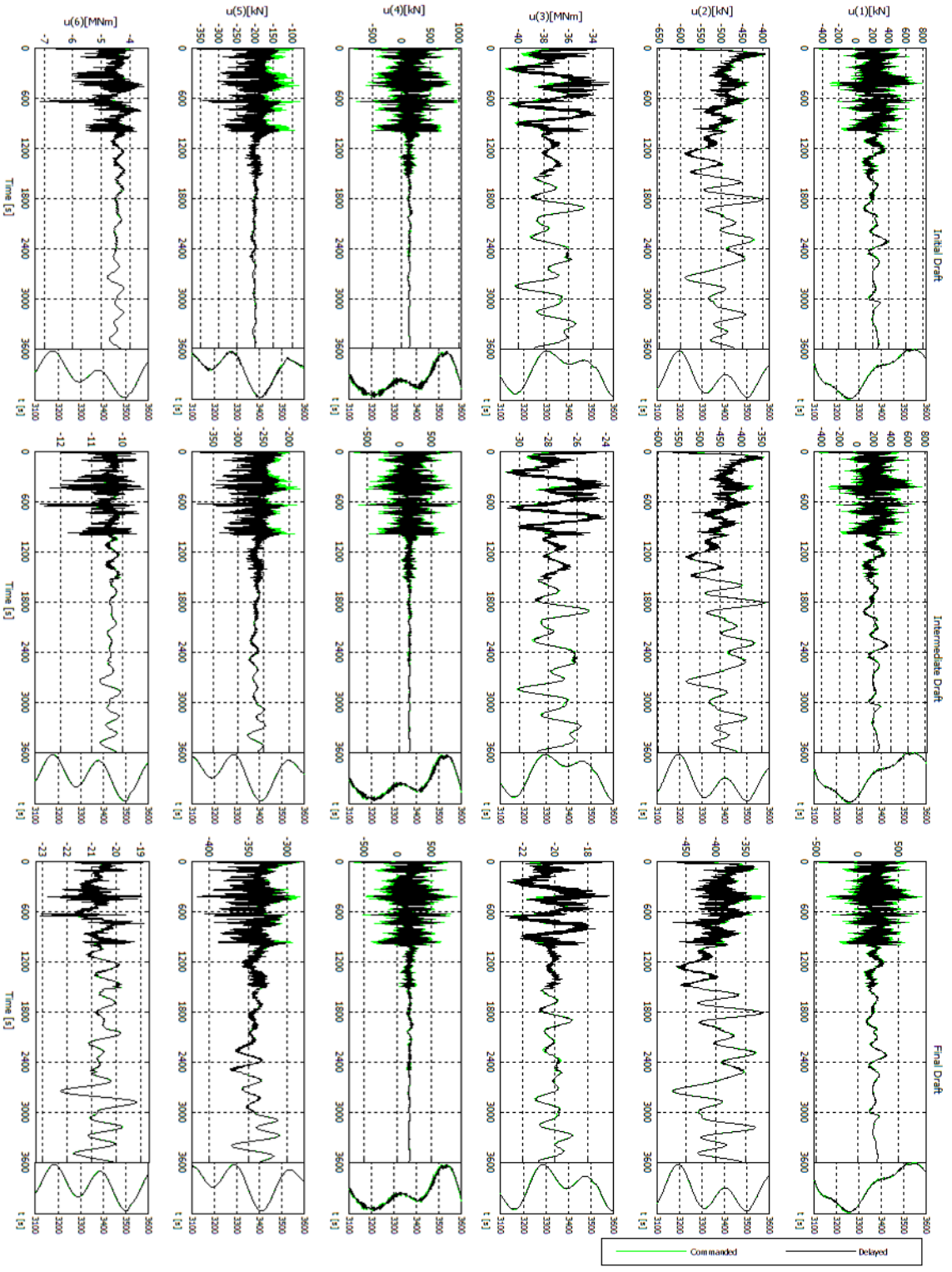

Figure 6.53: Control forces using PD-like Controller

During these simulations, the peak frequency of the motion spectrum is close to real values as presented in Figure 6.54. Hence, the switching control generates the switching signal σ, correctly selecting the nonlinear observer associated with estimated peak frequency as presented in Figure 6.54. Therefore, the estimates of the positions and headings for both vessels has filtered the wave-frequency influence. Obviously, this filtering process does not happen when the the nonlinear observer for extreme seas is selected ($t > 3.500s$).

As discussed in the previous section, the switching control takes 500s to change the nonlinear observer. The switching control changes the observer parameters correctly. Vessels' positioning are maintained in their set-points for both geometric and PD-like controllers, and for each draft simulated.

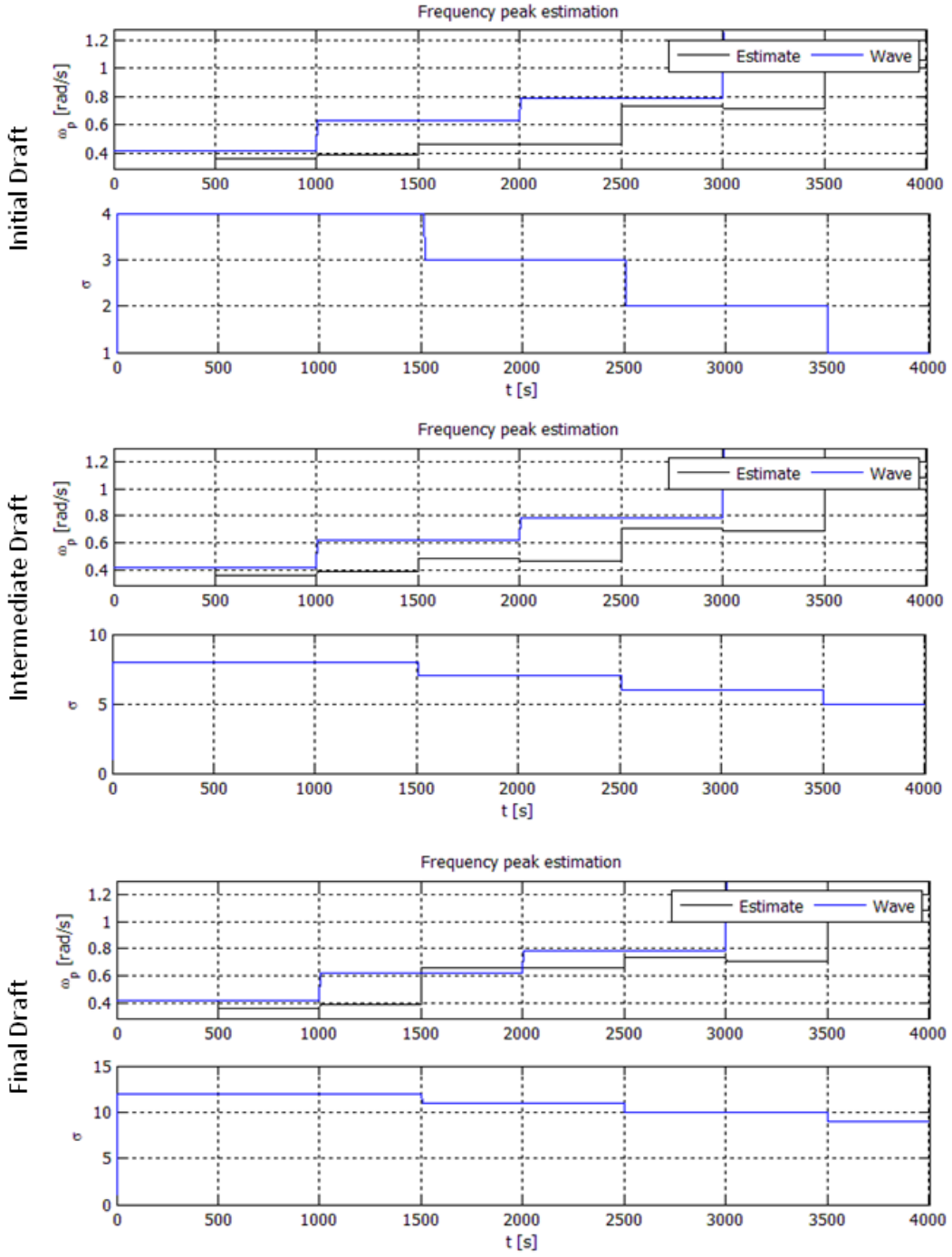

Figure 6.54: Peak Estimation and σ

6.7 Case 6: Day-long Operation Simulation

A day-long simulation is carried out to evaluate the switching control for a complete offloading operation. At simulation outset, the FPWSO has full draft and the shuttle tanker has ballast draft. The environmental scenario is presented in Figure 6.55. Sea state is associated with the wind similar to that to be found in Brazilian waters. In this simulation, sea state is harshening as such waves and wind parameters are changing. Current velocity and direction are kept constant.

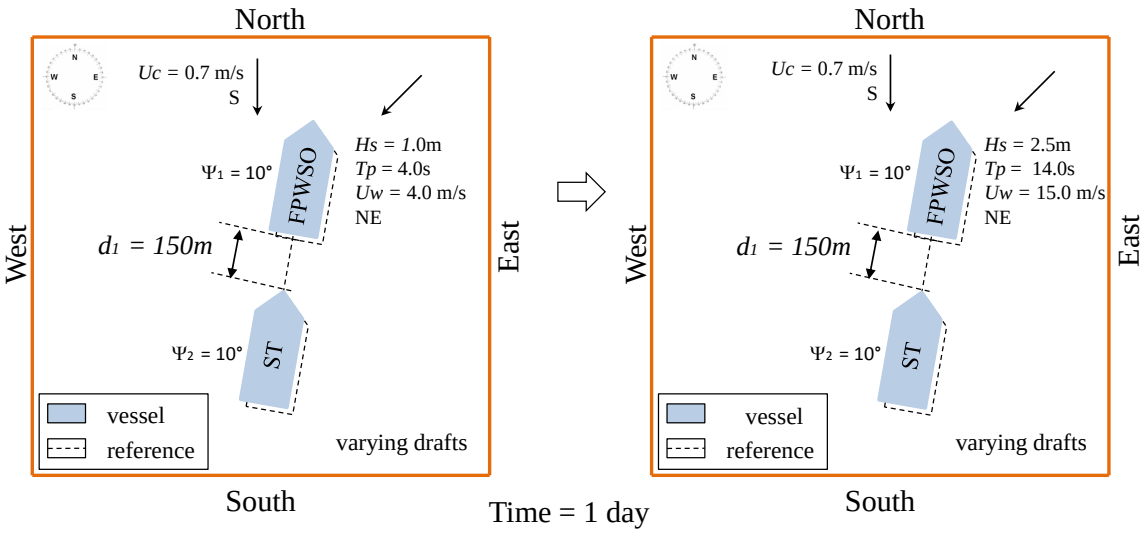

Figure 6.55: Environmental conditions and sixth maneuver

The positioning of the vessels are maintained as desired by both controllers as presented in Figures 6.56 and 6.57 (geometric controller) and Figures 6.58 and 6.59 (PD-like controller). The relative distance between vessels is also maintained around 150m as presented in Figure 6.60.

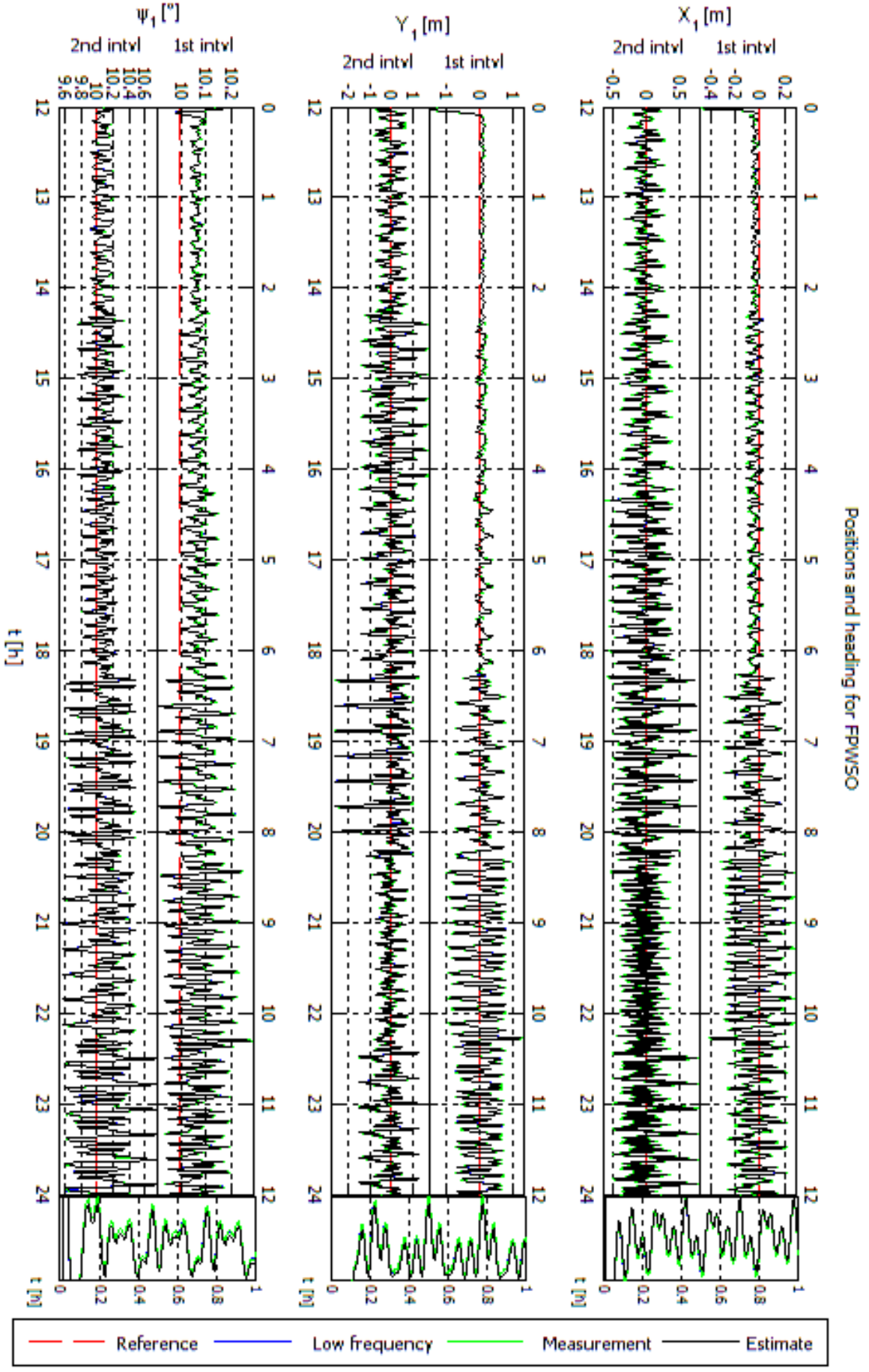

Figure 6.56: FPWSO positioning: geometric controller

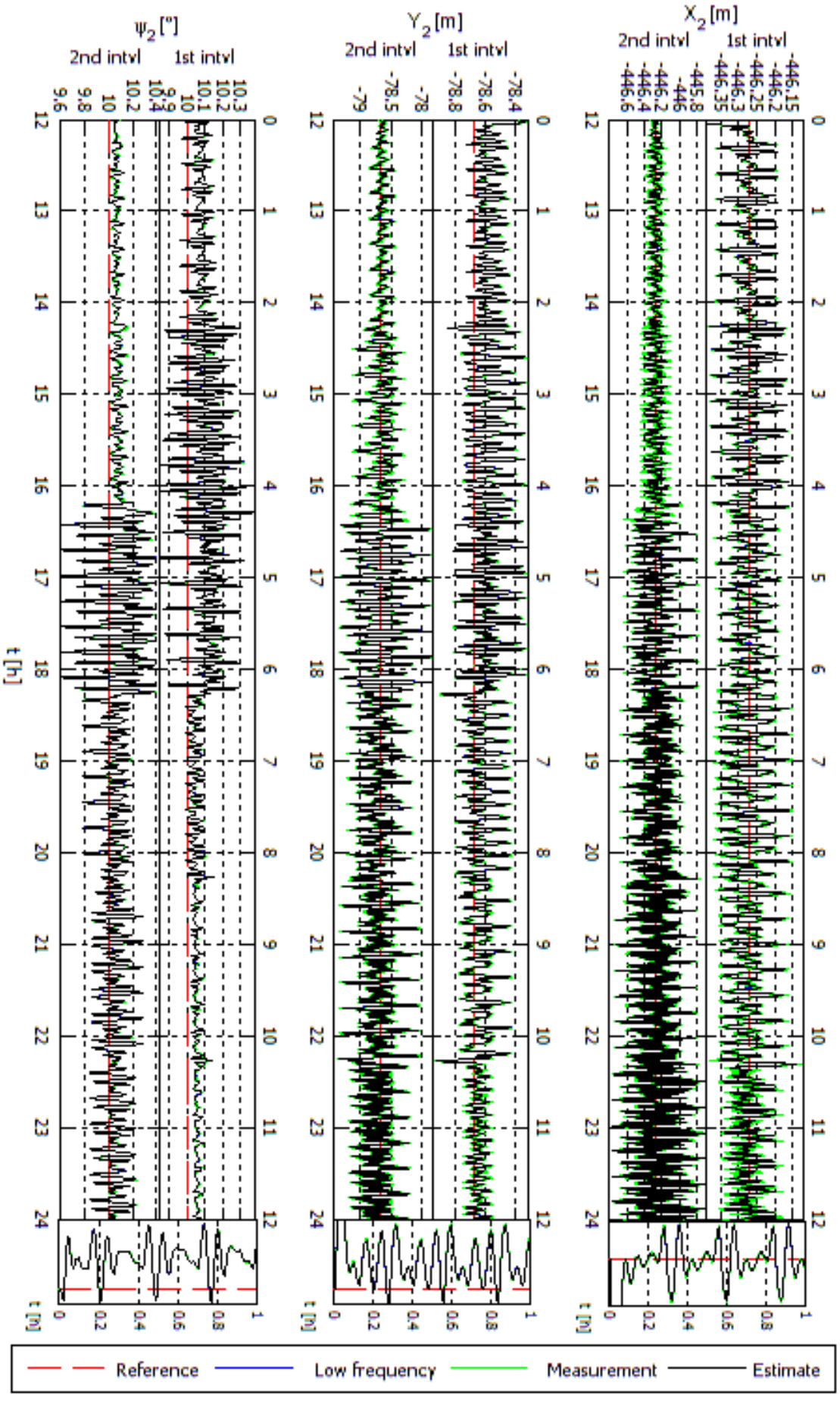

Figure 6.57: Shuttle tanker positioning: geometric controller

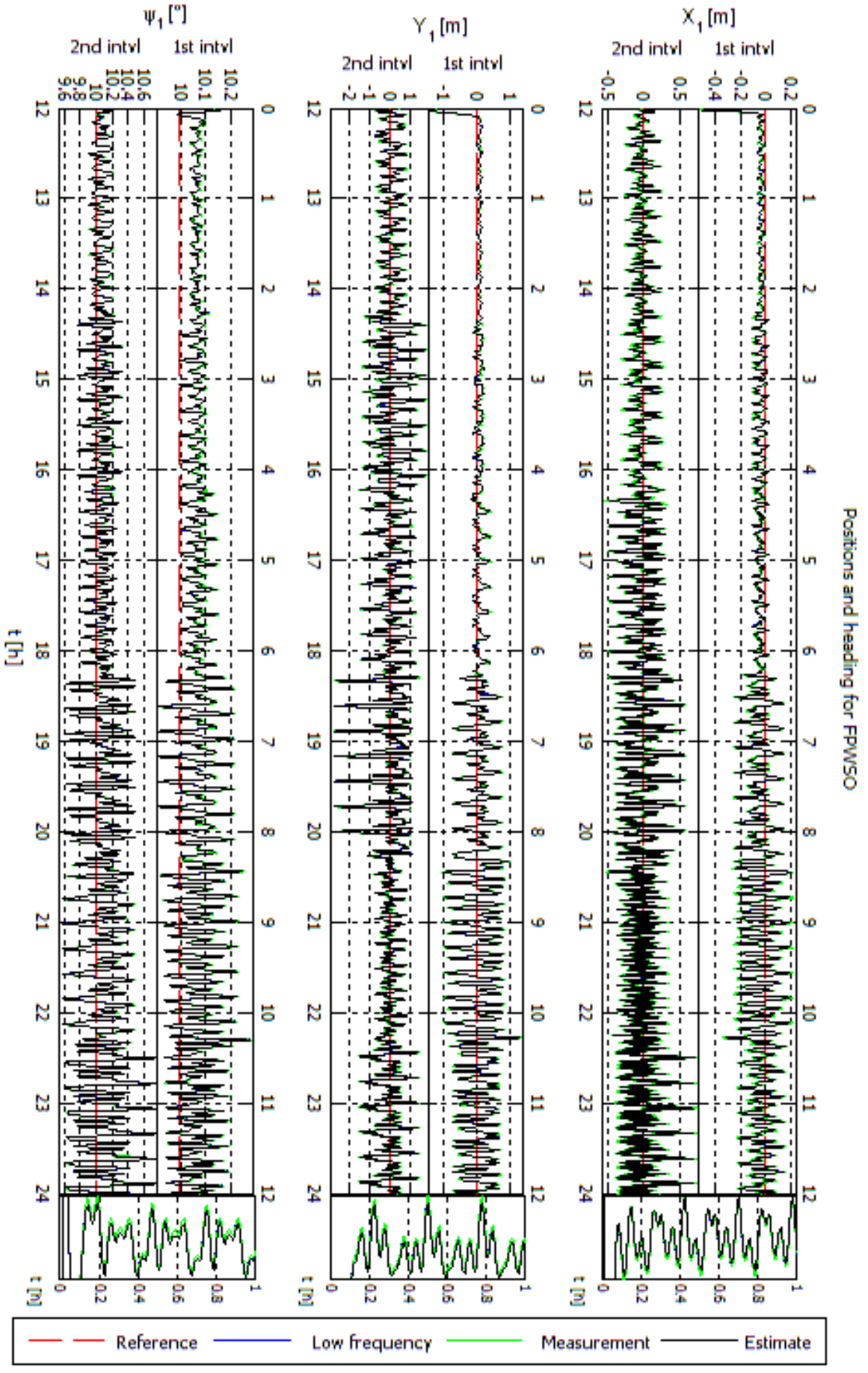

Figure 6.58: FPWSO positioning: PD-like controller

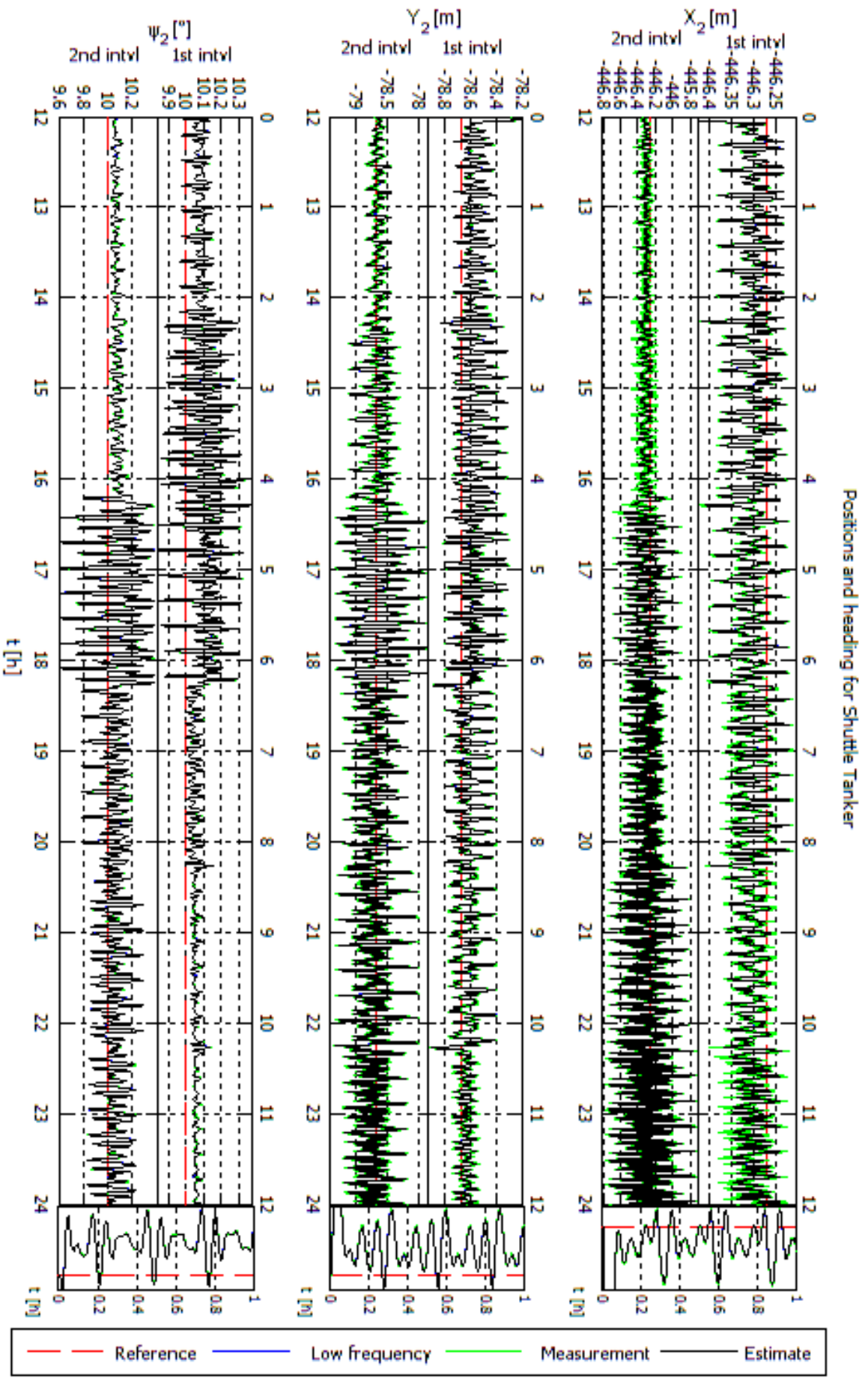

Figure 6.59: Shuttle tanker positioning: PD-like controller

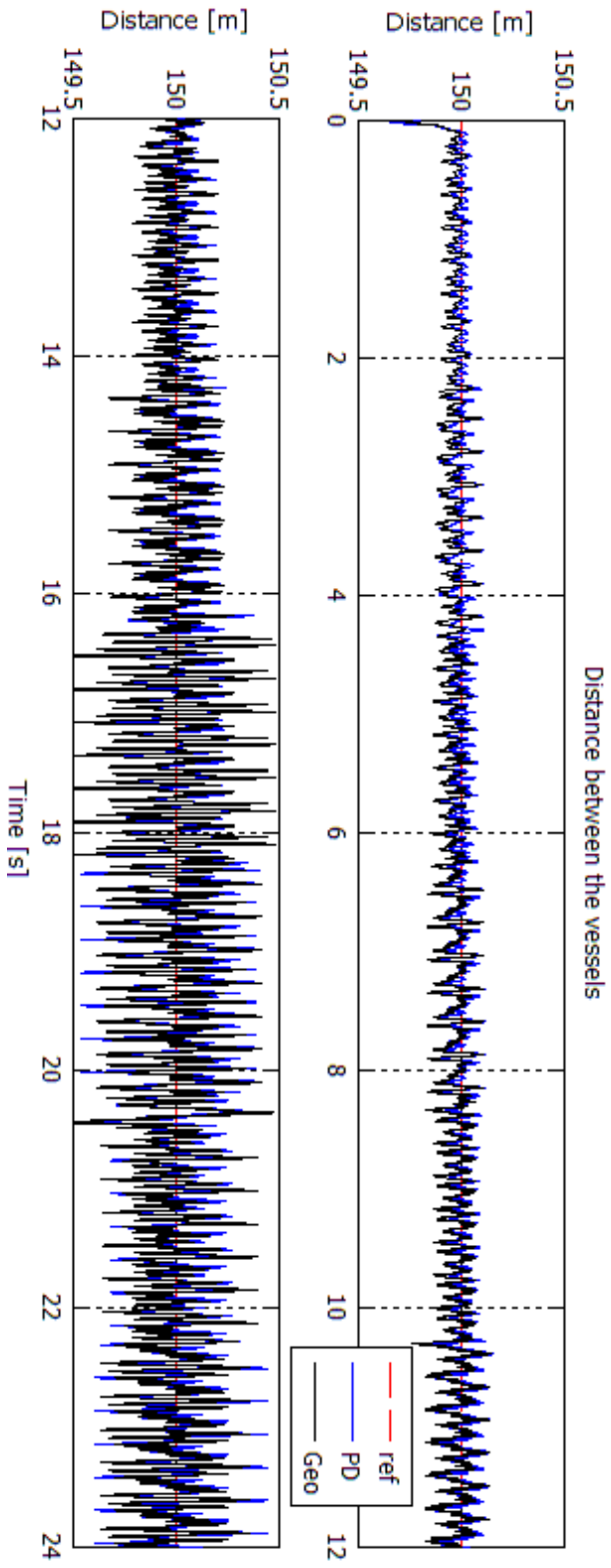

Figure 6.60: Distance between vessels

The nonlinear observer filters the wave-frequency motion from the positions and heading for both vessels (see Figure 6.57 to 6.60). The nonlinear observers for the wave-frequency model are selected from $t = 0h$ to $t = 16h$. The nonlinear observer for extreme seas is selected by the supervisory controller when $t > 16h$. The velocities estimates are close to the real velocities as presented in Figures 6.61 and fig:6.62 (geometric controller) and Figures 6.63 and 6.64 (PD-like controller).

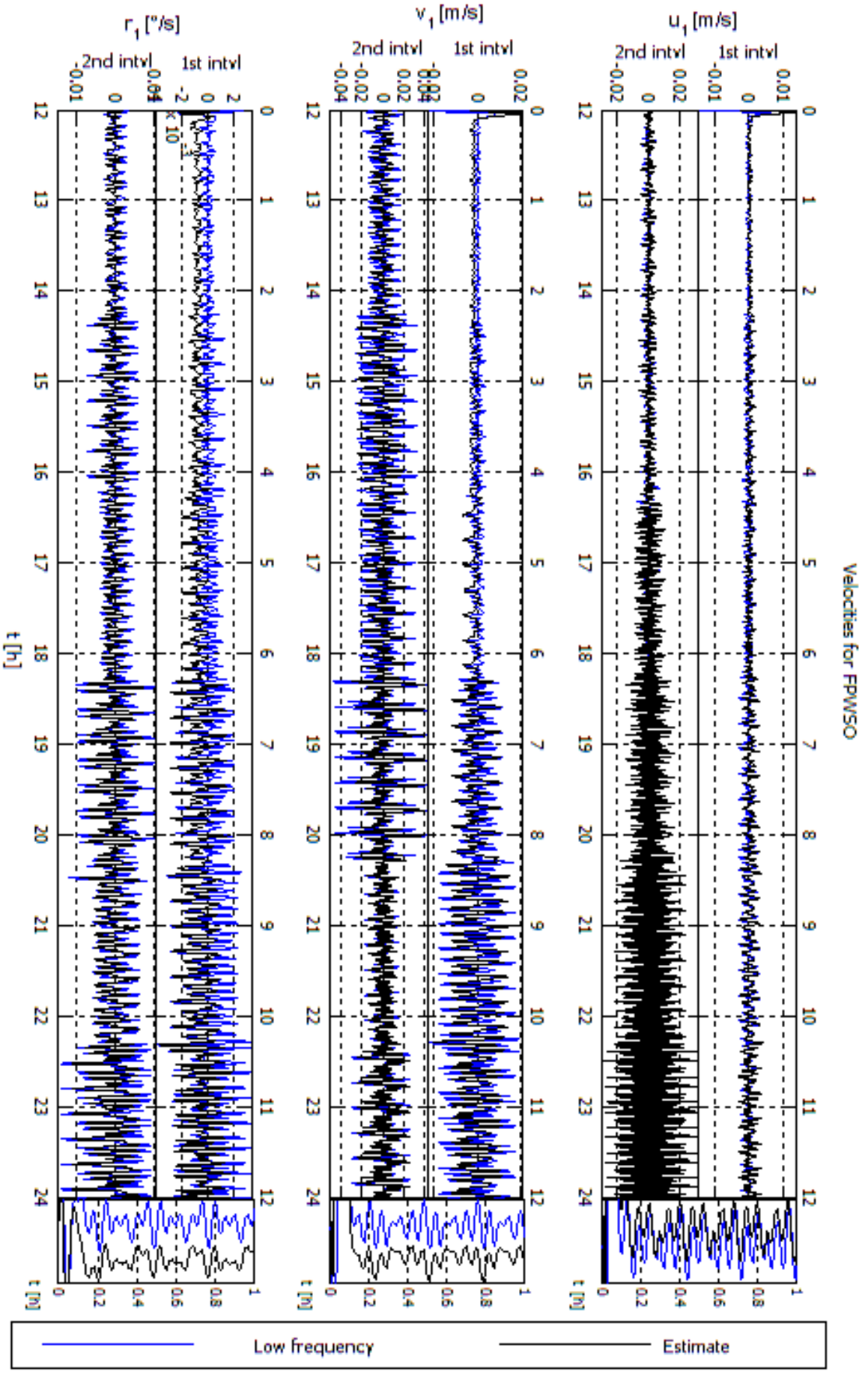

Figure 6.61: FPWSO velocities: geometric controller

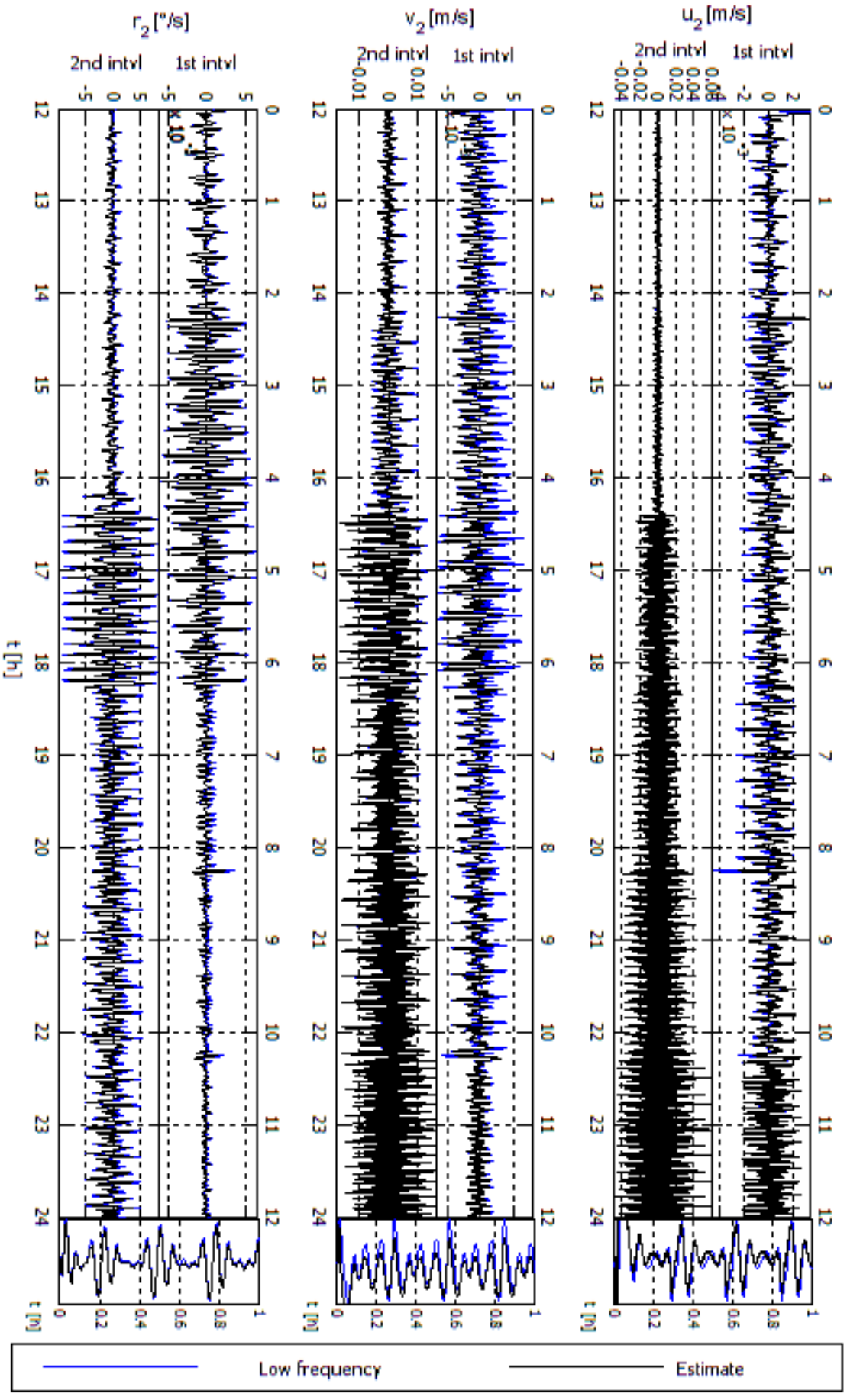

Figure 6.62: Shuttle tanker velocities: geometric controller

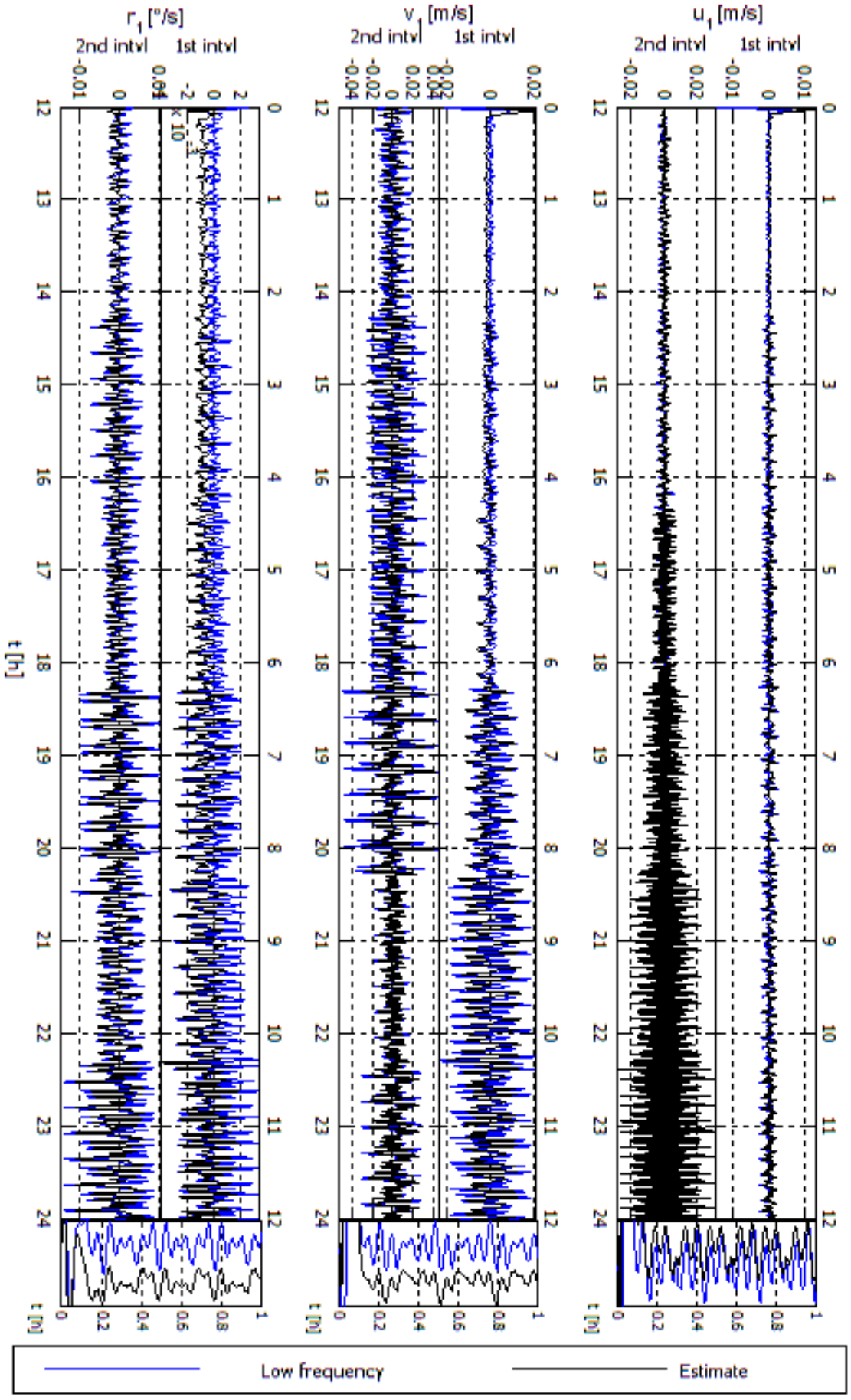

Figure 6.63: FPWSO velocities: PD-like controller

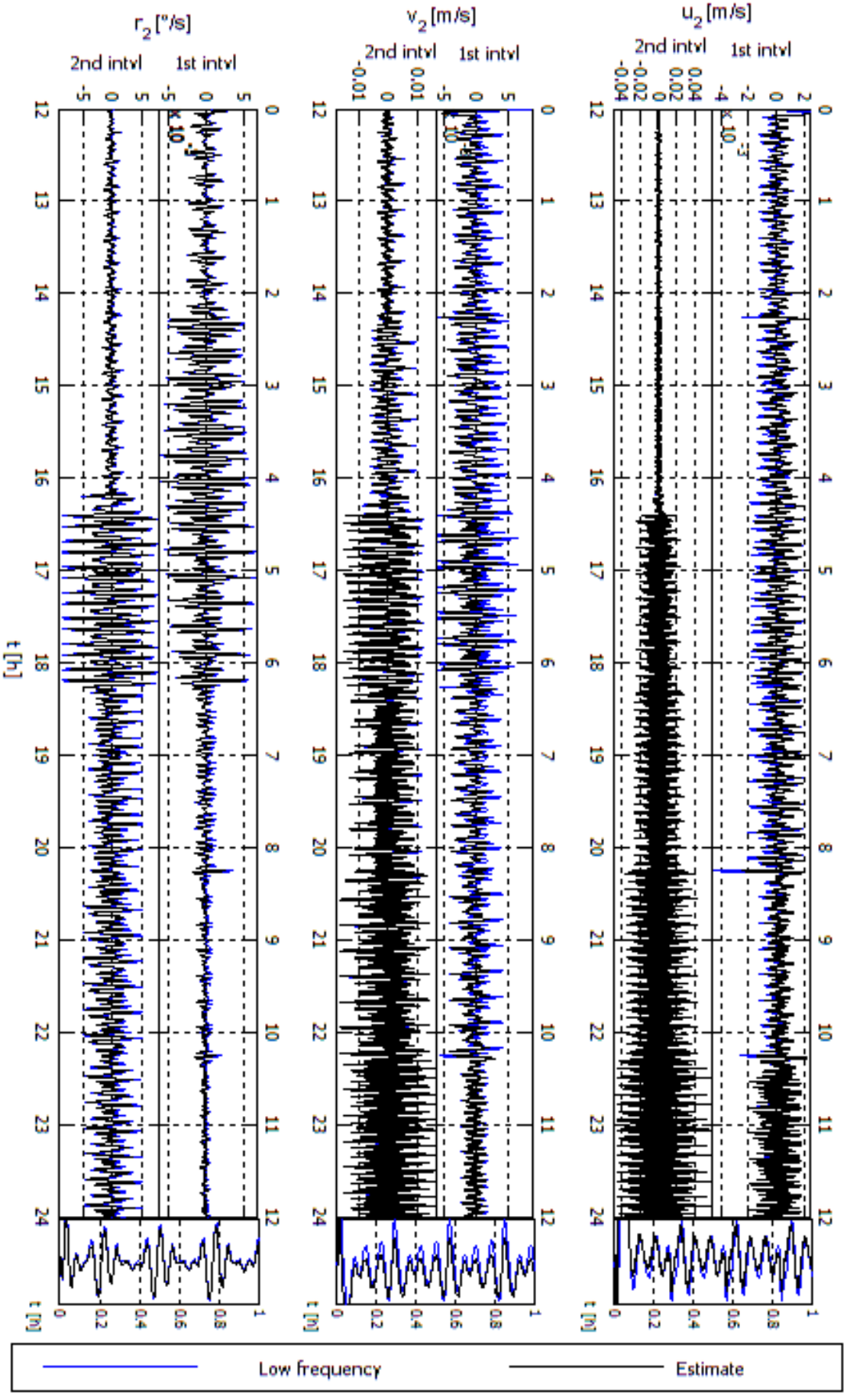

Figure 6.64: Shuttle tanker velocities: PD-like controller

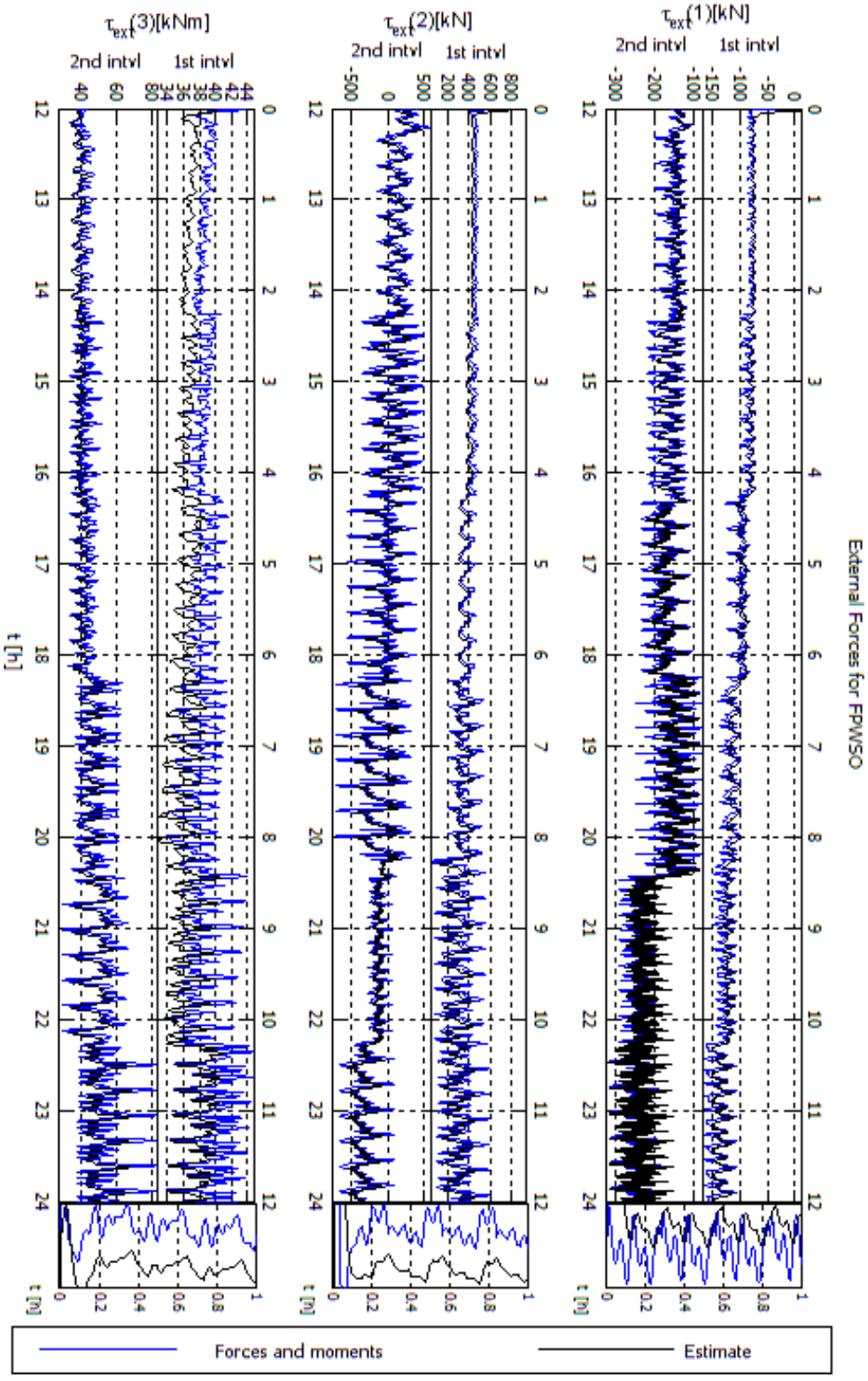

Figure 6.65: FPWSO external forces: geometric controller

External force estimates converge to the real values as presented in Figures 6.65 and fig:6.66 (geometric controller) and Figures 6.67 and 6.68 (PD-like controller).

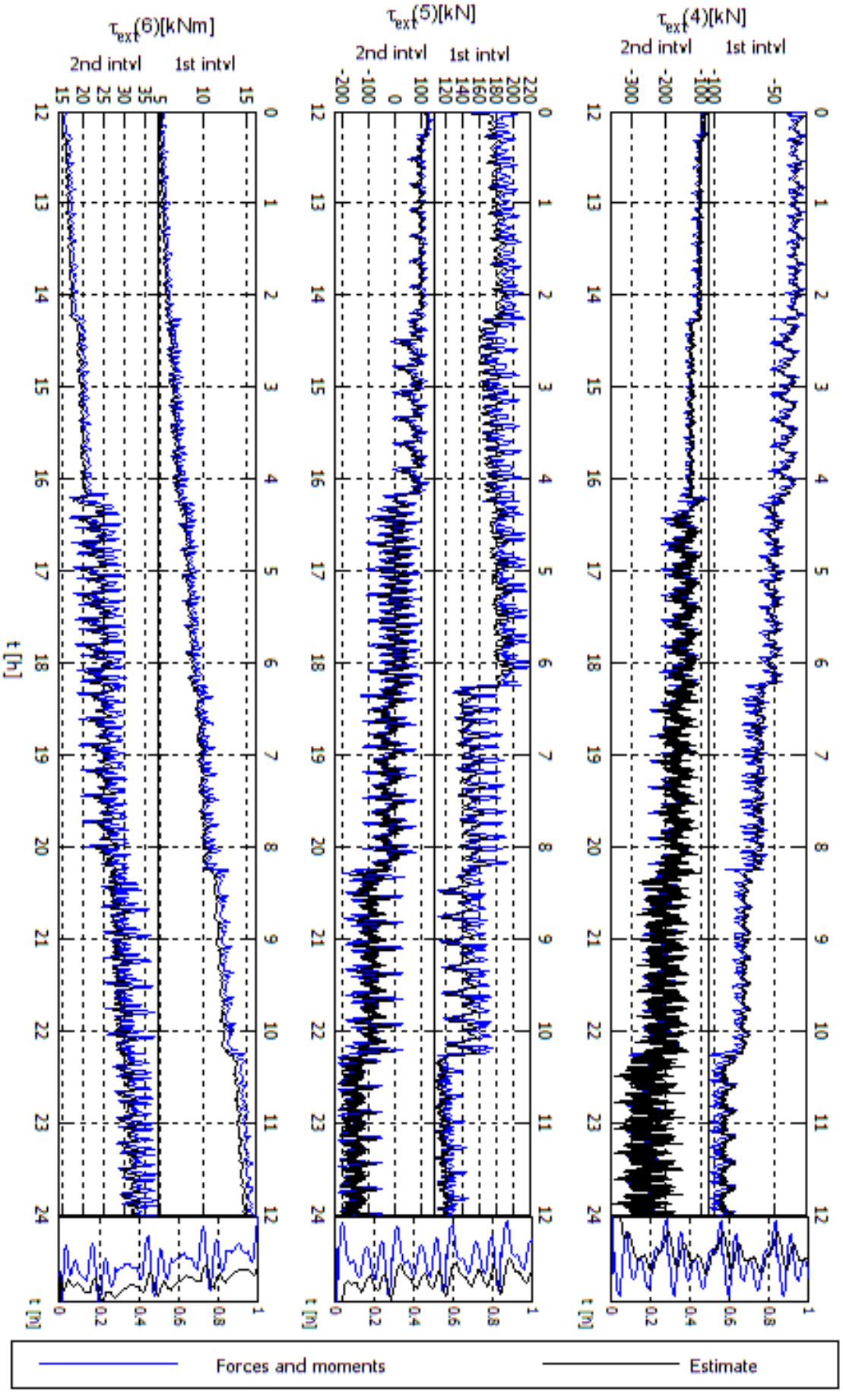

Figure 6.66: Shuttle tanker external forces: geometric controller

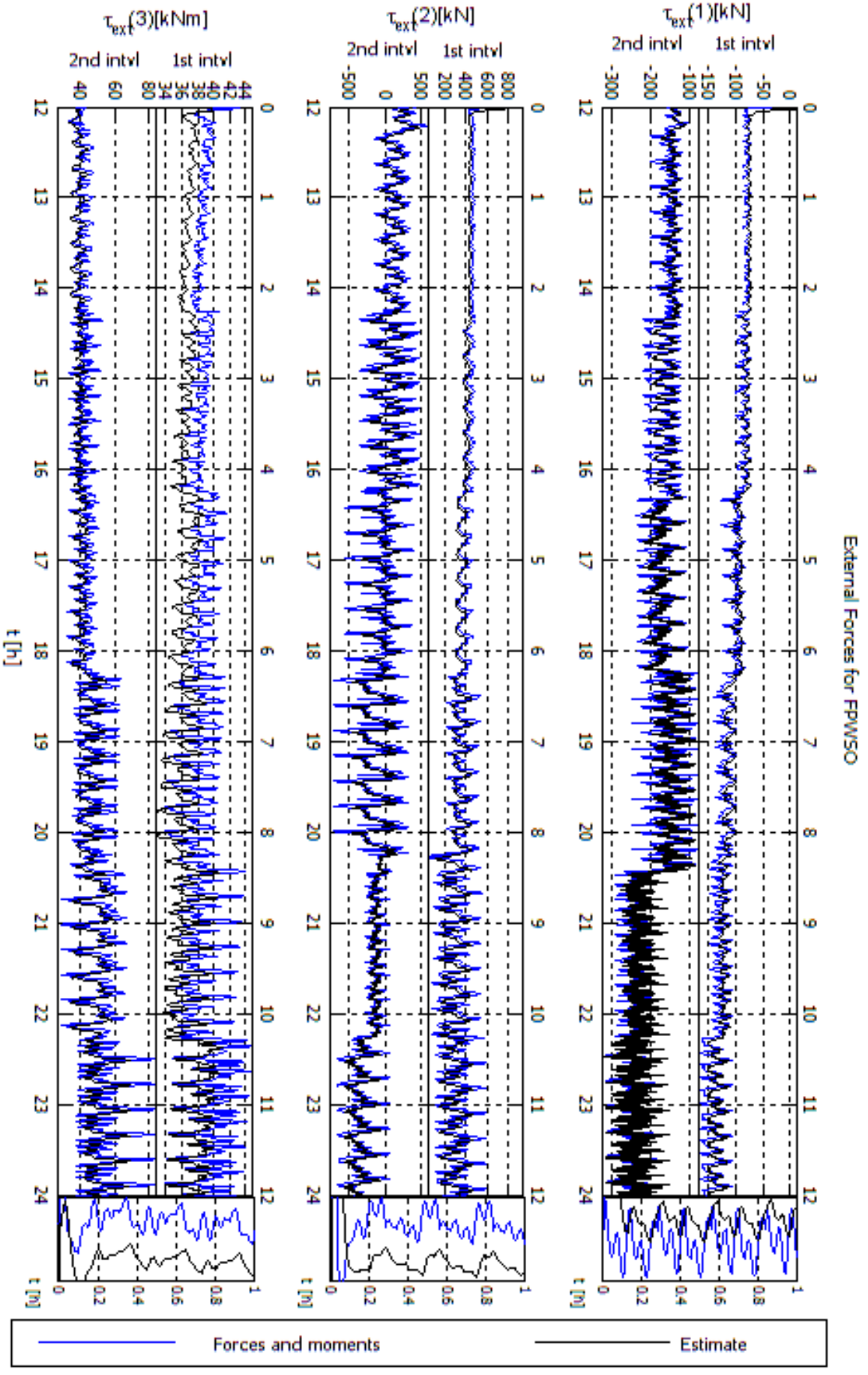

Figure 6.67: FPWSO external forces: PD-like controller

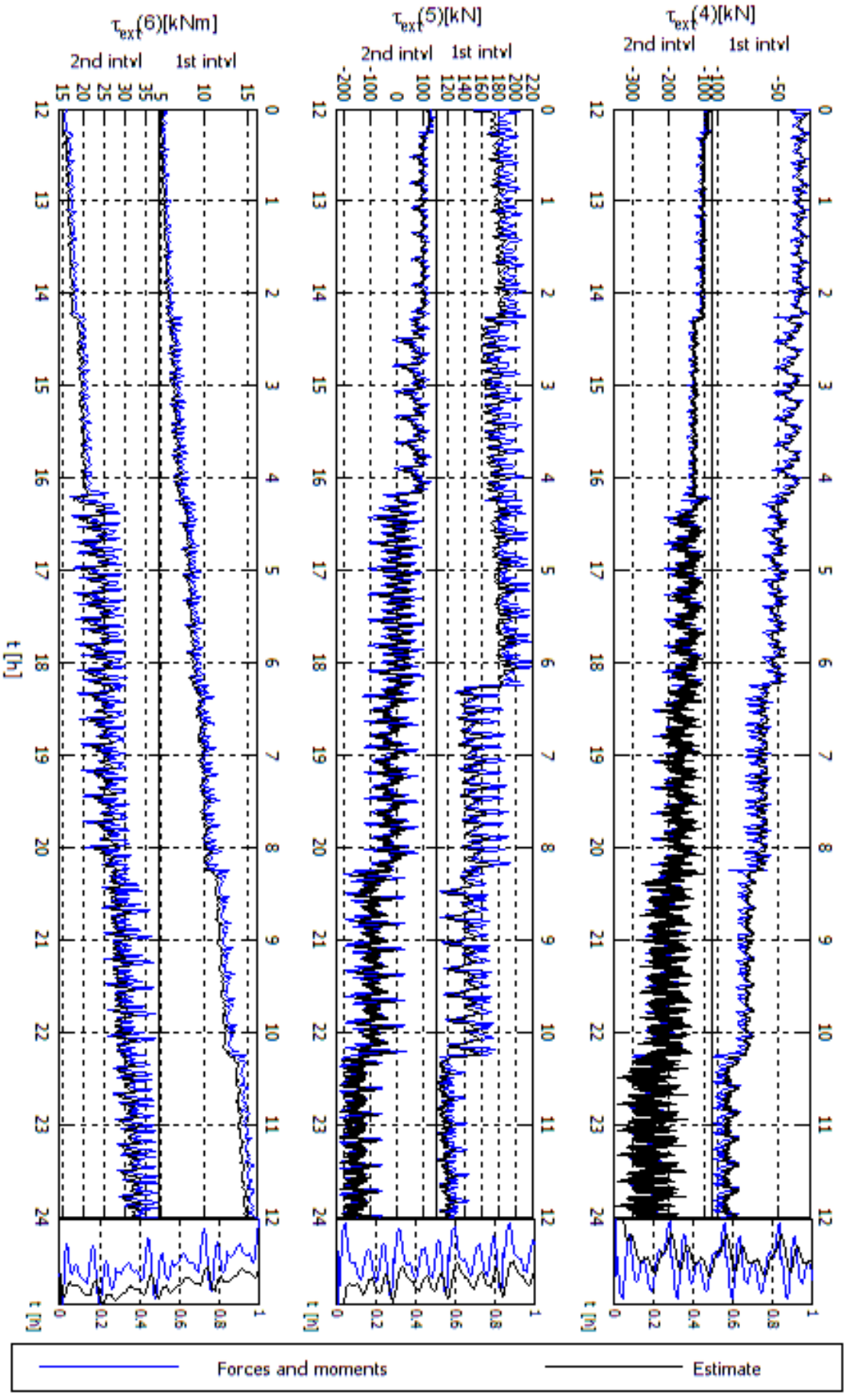

Figure 6.68: Shuttle tanker external forces: PD-like controller

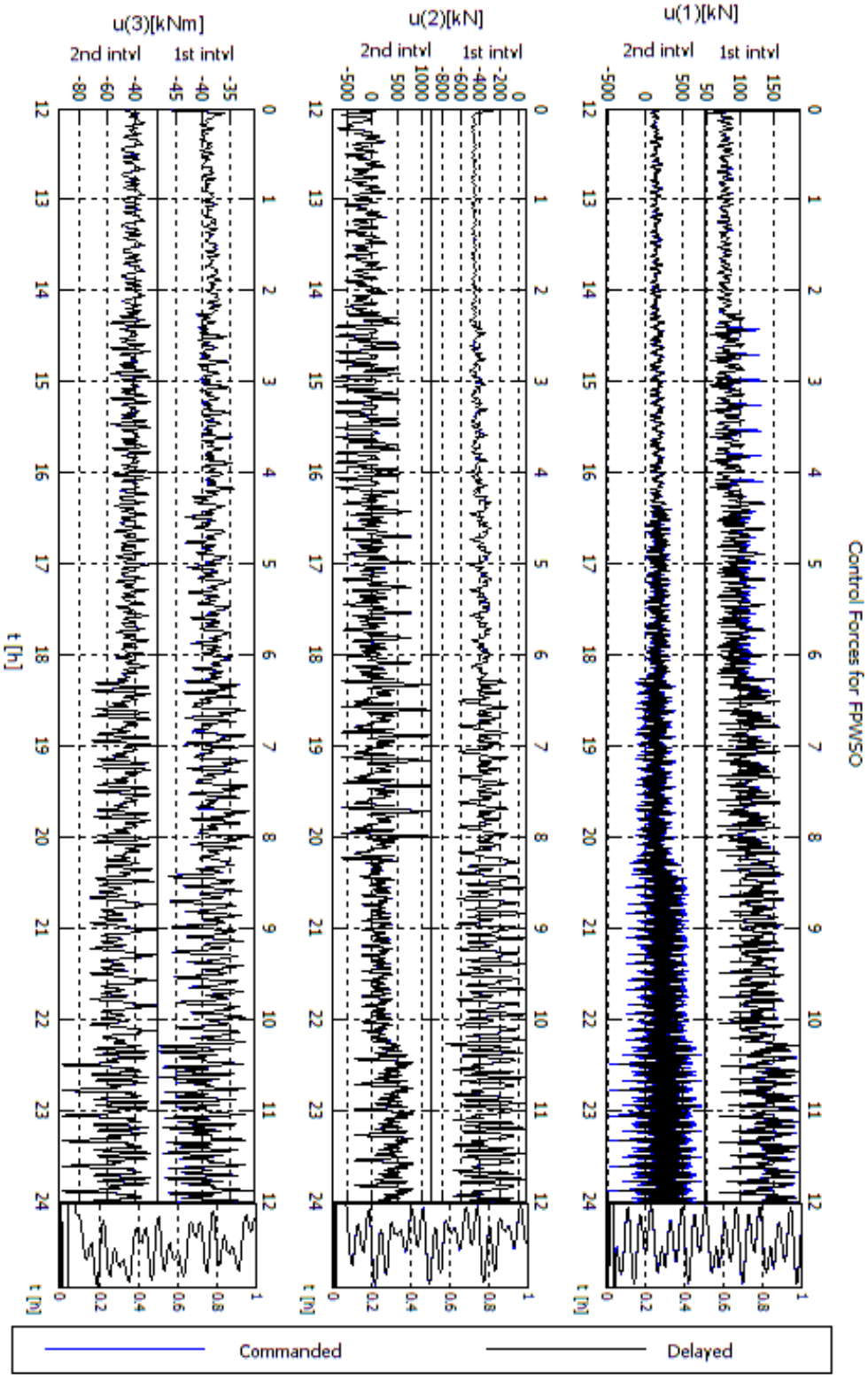

Figure 6.69: FPWSO control forces: geometric controller

Control laws calculated by both controllers are very similar to each other as presented in Figures 6.69 and fig:6.70 (geometric controller) and Figures 6.71 and 6.72 (PD-like controller).

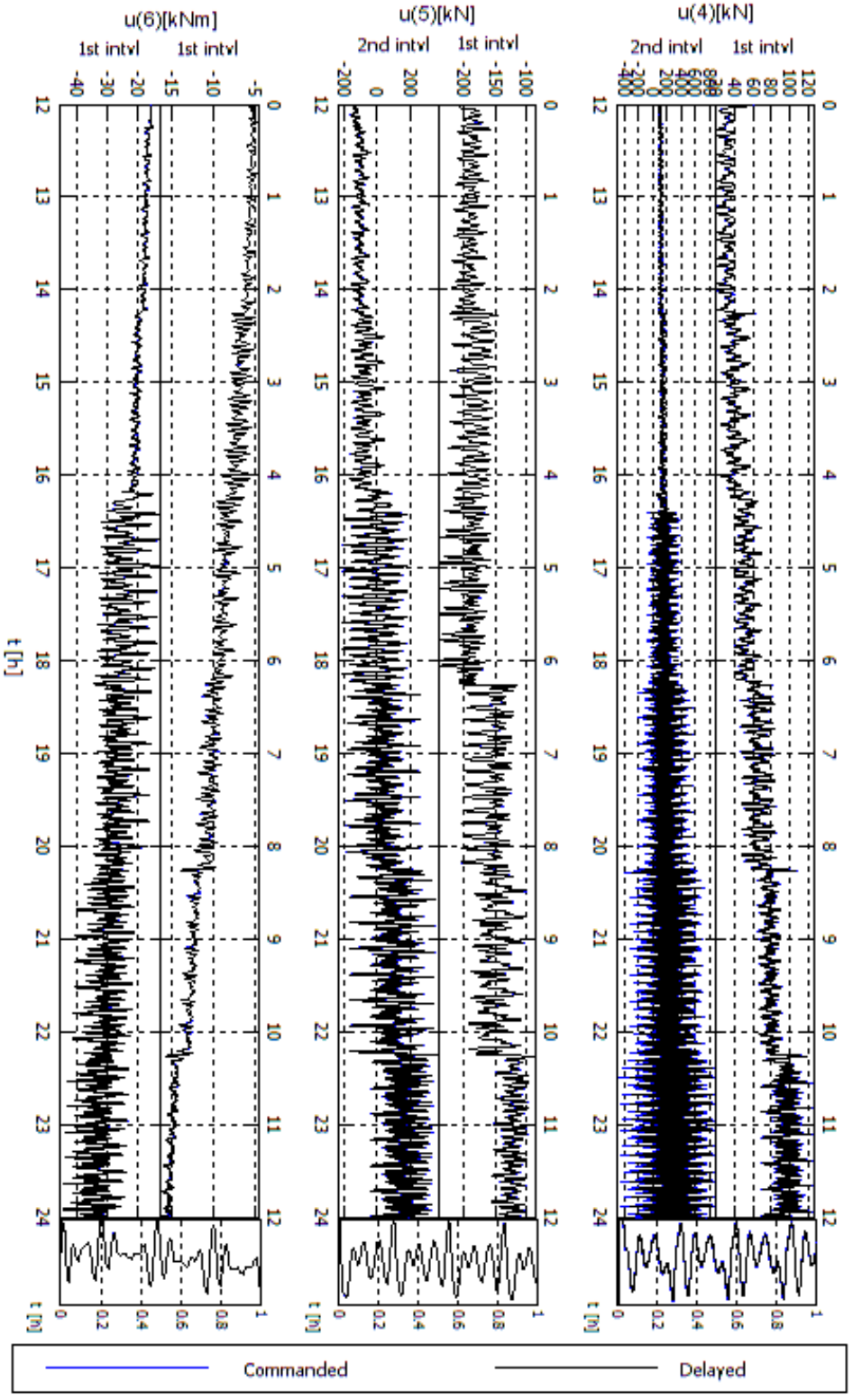

Figure 6.70: Shuttle tanker control forces: geometric controller

As discussed in Chapter 4, the controllers can be considered similar and as well as the switching controller.

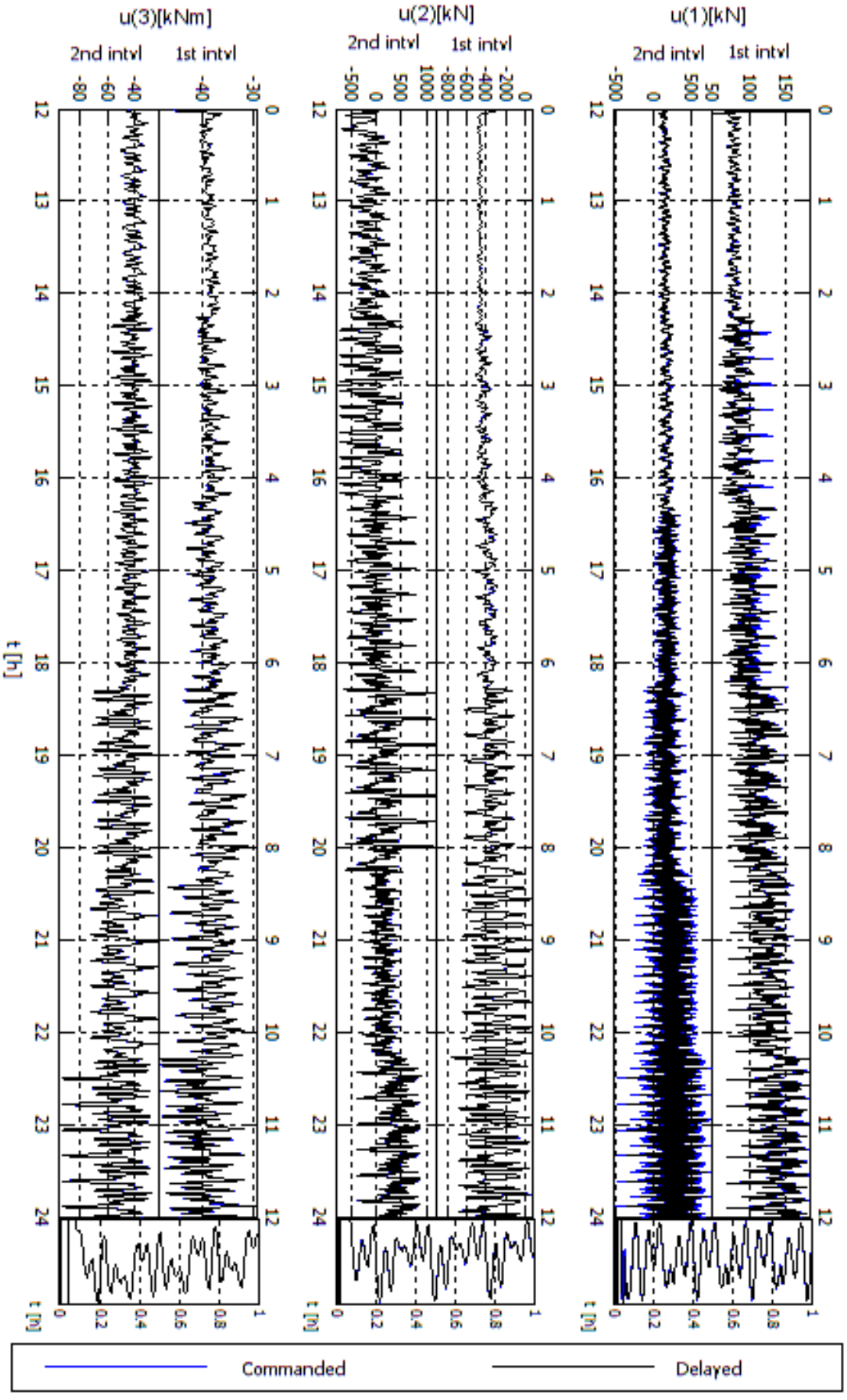

Figure 6.71: FPWSO control forces: PD-like controller

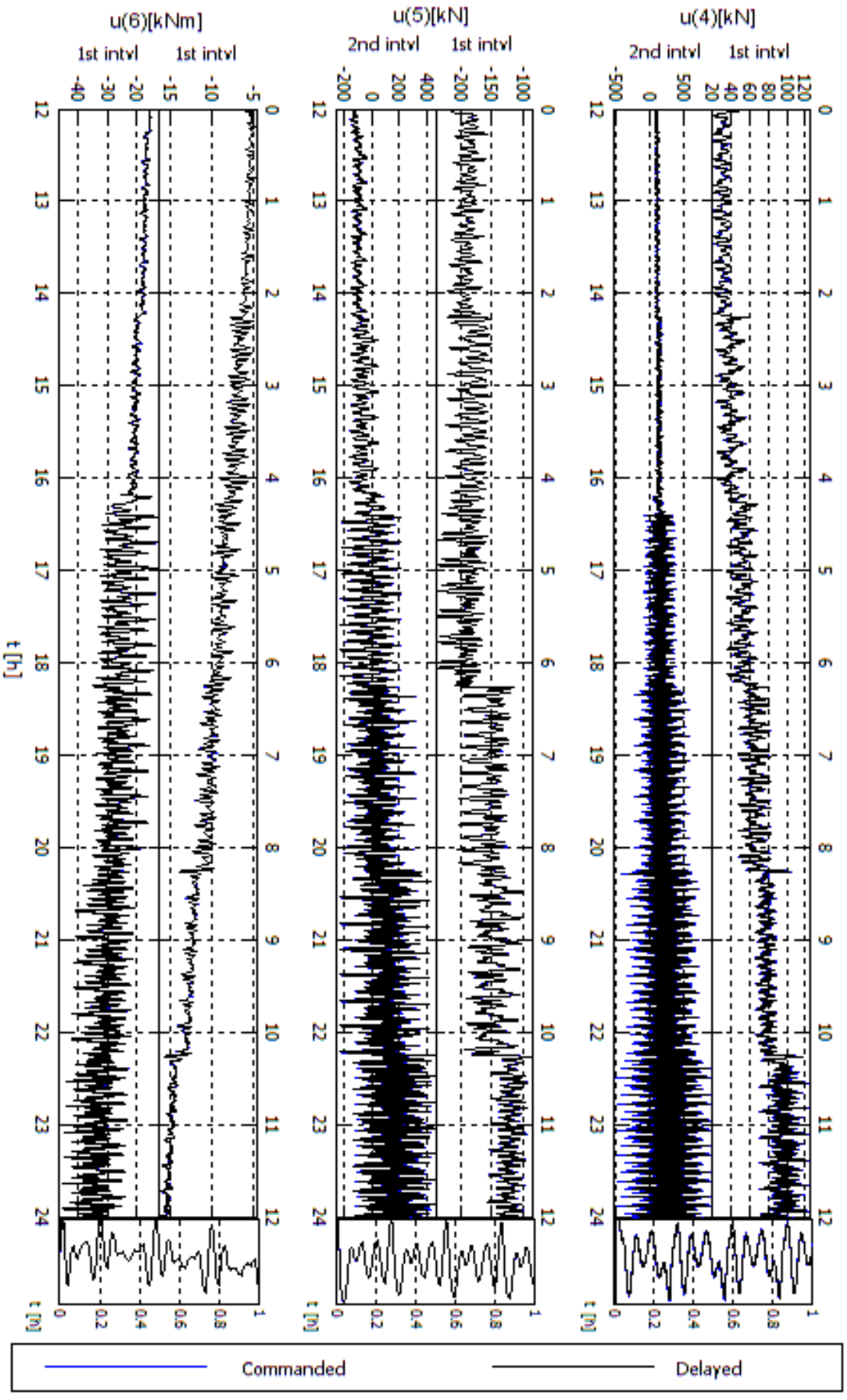

Figure 6.72: Shuttle tanker control forces: PD-like controller

The evolution of the sea state and the wind are presented in Figure 6.73. During the offloading operation, the switching controller is monitoring the peak frequency of the motion spectrum. The estimated peak frequency is close to the real peak frequency as presented in Figure 6.73. Drafts vary during the simulation and are assumed to be known (see Figure 6.73). So, the switching signal is switched to select the best observer/controller for the draft vector $\boldsymbol{h}$ and peak frequency ω_p pairing. The switching signal σ in Figure 6.73 is presented together with the arrows that indicate the intervals where the three reference drafts and the four sea state ranges can be found. Switching signal change is correct in accordance with Table 5.3. This means that the best observer/controller is selected for the draft vector and peak frequency pairing. So, the switching controller works as designed.

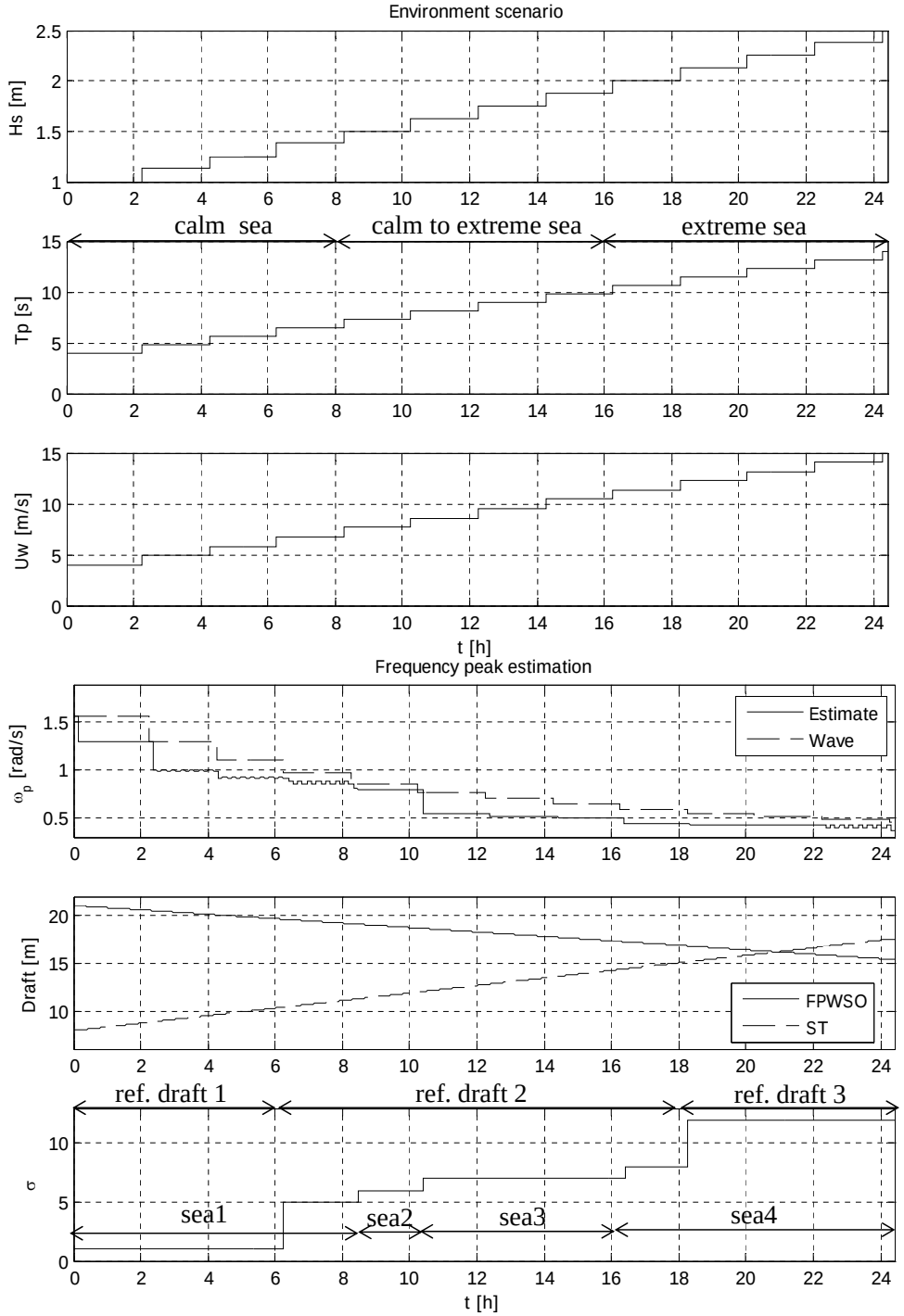

Figure 6.73: Environment, drafts, ω_p and σ

6.8 Discussion and Conclusions

In the case of reference and the distance simulations, the geometric controller is able to maintain vessel positions and headings with a similar degree of accuracy to that of the PD-like controller. As discussed in Section 4.4.4, geometric control and PD-like controller performance are very similar when the vessels move slowly and the reference is constant.

The main difference between the controllers is the inclusion of reference in the geometric control law. However, the control laws is very similar because of slow vessel velocities and constant reference.

A small difference in the performance of the controllers appears when some unexpected event occurs for the FPWSO. In this case, the geometric controller moves the shuttle tanker and the PD-like controller does not. This is so because the geometric control, with the linearized output equal to the constraint, alters shuttle tanker set-point when the FPWSO leaves its set-point. The PD-like controller has constant vessel set-point of the vessels constant and so does not control the relative distance between the vessels as the geometric control does. Despite this difference, the amplitude of that distance error is small and the controllers can be considered similar.

During simulations where sea conditions change constantly, the switching control chooses the correct nonlinear observer. Hence, the switching control operates correctly. The simulations present a maximum hanging lag of 500s. This delay is the data window formation spectrum generating and, as such, the maximum time for updating the parameters of the nonlinear observer. Data windows shorter than 500s are not enough to extract precise frequency motion estimate from the motion spectrum. This is the case because the vessels have a high inertia and their dynamics filter the wave-frequency motion to some extent.

Where the one day simulation is concerned, the switching control makes the correct nonlinear observer and controller choices based on estimated peak frequency motion and the vessel drafts. This switching meets maximum error criterion imposed by the perturbation model.

Nonlinear observer parameters are set for the highest peak frequency of the motion spectrum. Some response spectra analyzed in Appendix C present with a bimodal response. Consequently, for those periods of a day-long simulation when the bimodal response is present, the nonlinear

observer is not able to filter both peak frequencies. This occurs because the bandwidth of the filter does not include the second peak frequency and the observer does not suppress this frequency appropriately. This problem could be resolved by means of a fourth-order wave-frequency model whose bimodal response approximates the sea spectrum.

Chapter 7

Final Conclusions and Further Research

7.1 Final Conclusions

The main purpose of this work was to design a new integrated control strategy for the hybrid system to act upon a multibody system consisting of two dynamically positioned vessels. The vessels are the FPWSO and the shuttle tanker that carry out an offloading operation in tandem configuration. This control strategy ensures vessels remain within a relative distance of each other to avoid collision or excessive hawser tension. The hybrid controller takes into account variations in vessel draft and vessel motion peak-frequency as they may influence controller performance.

Integrated control making use of geometric theory for dynamically positioned vessels is feasible. Establishing relative positioning is an intuitive way to generate a output system for the control strategy. The geometric controller can be implemented by means of an output linearization procedure. The idea is simple in spite of the sophisticated mathematics involved in the differential geometry. The switching control structure takes into account variations in some system parameters. There is some difficulty to allow for in tuning switching logic parameters in order to guarantee correct switching as there is no procedure to tune them, and they have been derived

from previous numerical simulations.

When some major event, such as wind blast, impacts upon the FPWSO, it can lose its positioning and the shuttle tanker will follow the FPWSO because of their integrated control law. However, the same hybrid structure can take into account controllers with no integrated output which would be selected in the case of a major event. Another important factor to be considered is the availability of heading and position information. The integrated controller needs to have the vessels' position measurement and to send the command to the thrusters of both vessels in real-time which, in practical terms, is a technical limitation.

7.2 Further Research

Suggestions for further research would include:

- The hybrid control presented assumes an initial FPWSO draft as this vessel can begin her operation in different drafts. The hybrid control would be able to set a variety of initial FPWSO drafts. This would result in an increased estimator number.
- Thruster saturation can be interpreted as a hybrid dynamical system with three different dynamics: vessel dynamics in combination with thrust upper limit, intermediate (no saturation) and thrust lower limit. The switching control could take into account these new combined dynamics and, by means of the injected systems, system stability with thruster saturation could be proved;
- The nonlinear observer model could be extended to consider a fourth-order wave-frequency model in order to approximate a bimodal vessel motion spectrum;
- Side-by-side oil transfer could be controlled by hybrid and geometric means. Dynamics can account for the low speed of both vessels and their relative distance is maintained by the constraint geometric controller. Draft variation during oil transfer would be allowed for the hybrid control approach;
- The hybrid controller could incorporate observer models that estimate both peak-wave-frequency vessel motion and wave direction. Vessel set-point could be changed depending

on wave direction;

- Should DPS damage, such as drive-off, drift-off or black-out occur, the hybrid control would be able to take decoupled control laws into account;
- New constraints could be established to restrict maximum vessel deviation from set-point. For instance, a maximum FPWSO radius could be assumed and a constraint could be described by placing a logarithmic function into the geometric controller.

References

AARSET, M. F. et al. Nonlinear vectorial observer backstepping with integral action and wave filtering for ships. In: **Proceedings of the IFAC Conference on Control Applications in Marine Systems (CAMS1998)**. Fukuoka, Japan: [s.n.], p. 83–89, 1998.

ABRAHAM, R. A.; MARSDEN, J. E. **Foundations of Mechanics**. Massachusetts: Benjamin / Cumnings, 1978.

AGOSTINHO, A. C. **Controle por modos deslizantes aplicado a sistema de posicionamento dinâmico**. 2009. 110 p. Dissertation (Master) — Escola Politécnica da Universidade de São Paulo, São Paulo, 2009.

AGUIAR, L. et al. Ten autonomous mobile robots (and even more) in a route network like environment. In: **Proceedings of IEEE/RSJ International Conference on Intelligent Robots and Systems**. p. 260–267, 1995.

AIHARA, K.; SUZUKI, H. Theory of hybrid dynamical systems and its applications to biological and medical systems. **Philosophical Transactions of The Royal Society**, A (2010) 368, p. 4893–4914, 2000.

ANTONELLI, G.; CHIAVERINI, S. Fault tolerant kinematic control of platoons of autonomous robots. In: **Proceedings of the IEEE International Conference on Robotics & Automation**. New Orleans: [s.n.], p. 3313–3318, 2004.

ANTSAKLIS, P. J. Scanning the issue/technology. In: **Proceedings of the IEEE**. v. 88, n. 7, p. 879–887, July 2000.

ARANHA, J. A. P. Second-order horizontal steady forces and moment on a floating body with small forward speed. **Journal of Fluid Mechanics**, v. 303, p. 39–54, 1996.

ARANHA, J. A. P.; FERNANDES, A. C. On the second-order slow drift force spectrum. **Applied Ocean Research**, v. 17, n. 5, p. 311–313, 1995.

ARNOLD, V. I. **Mathematical methods of classical mechanics**. New York: Springer-Verlag, 1989.

BADGEROW, J. P.; HANSWORTH, F. R. Energy savings through formation flight? A re-examination of the vee formation. **Journal of Theoretical Biology**, v. 93, p. 41–52, 1981.

BAKKER, J. W. de et al. (Ed.). **Real-Time: Theory in Practice. Lecture Notes in Computer Science**. New York: Springer- Verlag, 1992.

BALAFOUTIS, C. A.; PATEL, R. V. **Dynamic analysis of robotic manipulators: a Cartesian tensor approach**. Boston: Klumer Academic Plublishers, 1991.

BALCHEN, J. G. et al. Dynamic positioning using kalman filtering and optimal control theory. In: **IFAC/IFIP Symposium on Automation in Offshore Oil Field Operation**. p. 183–186, 1976.

BALCHEN, J. G. et al. Dynamic positioning of floating vessels based on kalman filtering and optimal control. In: **Proceedings of the 19th IEEE Conference on Decision and Control**. USA: [s.n.], p. 852–864, 1980.

BEARD, R. W. et al. A coordination architecture for spacecraft formation control. **IEEE Transactions on Control Systems Technology**, v. 9, n. 6, p. 777–790, 2001.

BENDER, J. G. An overview of systems studies of automated highway systems. **IEEE Transactions of Vehicle Technology**, v. 40, p. 82–99, January 1991.

BENVENISTE, A.; BERRY, G. Special issue on the synchronous approach to reactive and real-time systems. In: **Proceedings of the IEEE**. v. 79, n. 9, 1991.

BöLING, J. M. et al. Multi-model control of a simulated ph neutralization process. In: **Proceedings of the 16th IFAC World Congress**. Czech Republic: [s.n.], v. 16, n. 1, p. 1671–1671, 2005.

BLOCH, A. M. et al. **Nonholonomic Mechanics and Control**. : Springer, 2003. 484 p.

BRANICKY, M. S. **Studies in hybrid systems: modeling, analysis, and control**. 1995. 198 p. Thesis (PhD) — Department of Electrical Engineering and Computer Science, Massachusetts Institute of Technology, Massachusetts, 1995.

BREIVIK, M. **Topics in Guided Motion Control of Marine Vehicles**. 2010. 225 p. Thesis (PhD) — Department of Engineering Cybernetics, Faculty of Information Technology, Mathe-

matics and Electrical Engineering, Norwegian University of Science and Technology (NTNU), Trondheim, 2010.

BøRHAUG, E. **Nonlinear Control and Synchronization of Mechanical Systems**. 2008. 298 p. Thesis (PhD) — Department of Engineering Cybernetics, Norwegian University of Science and Technology, Trondheim, 2008.

BROCK, D. L. et al. Coordination and control of multiple autonomous vehicles. In: **Proceedings of IEEE International Conference on Robotics & Automation**. p. 2725–2730, 1992.

BULLO, F.; LEWIS, A. D. **Geometric Control of Mechanical Systems**. New York: Springer, 2010. 726 p.

BUZOGANY, L. E. et al. Automated control of aircraft in formation flight. In: **Proceedings of AIAA Conf. Guidance, Navigation, and Control**. p. 1349–1370, 1993.

CASETTA, L. **Contribuições à mecânica dos sistema de massa variável**. 2008. 185 p. Thesis (PhD) — Polytechnic School, University of São Paulo, São Paulo, 2008.

DAVOREN, J. M.; NERODE, A. Logics for hybrid systems. In: **Proceedings of the IEEE**. v. 88, n. 7, p. 985–1010, July 2000.

DECARLO, R. A. et al. Perspectives and results on the stability and stabilizability of hybrid systems. In: **Proceedings of the IEEE**. v. 88, n. 7, p. 1069–1082, July 2000.

DONG, N. T. **Design of hybrid marine control systems for dynamic positioning**. 2005. 198 p. Thesis (PhD) — Department of Civil Engineering, National University of Singapore, São Paulo, 2005.

ENCARNAçãO, P.; PASCOAL, A. Combined trajectory tracking and path following: an application to the coordinated control of autonomous marine craft. In: **Proceedings of 40$^{\mathbf{th}}$ IEEE Conference on Decision & Control**. Orlando: [s.n.], p. 964–969, 2001.

FAX, J. A.; MURRAY, R. M. Information flow and cooperative control of vehicle formations. **IEEE Transactions on Automatic Control**, v. 49, n. 9, p. 1465–1476, 2004.

FEARTHRSTONE, R. **Robot dynamics algorithms**. Boston: Klumer Academic Plublishers, 1987.

FOSSEN, T. I. **Guidance and control of ocean vehicles**. New York: John Wiley and Sons Ltd., 1994.

FOSSEN, T. I.; STRAND, J. P. Passive nonlinear observer design for ships using lyapunov methods: full-scale experiments with a supply vessel. **Automatica**, v. 35, n. 1, p. 3–16, 1999.

GEMIGNANI, M. C. **Elementary topology**. New York: Dover Publications, 1972.

GHABCHELOO, R. **Coordinated Path Following of Multiple Autonomous Vehicles**. 2007. 205 p. Thesis (PhD) — Instituto Superior Técnico, Universidade Técnica de Lisboa, Lisboa, 2007.

GIRARD, A. R.; HEDRICK, J. K. Formation control of multiple vehicles using dynamic surface control and hybrid surface. **International Journal of Control**, v. 76, n. 9/10, p. 913–920, 2003.

GIULETTI, F. et al. Autonomous formation flight. **IEEE Control Systems Magazine**, v. 20, p. 34–44, 2000.

GOEBEL, R. et al. **Hybrical Dynamical Systems: Modeling, Stability adn Robustness**. Princeton: Princeton University Press, 2012. 212 p.

GRANJA, B. B. São Paulo: **Desenvolvimento de algoritmo de alocação de empuxo para sistema de posicionamento dinâmico utilizando leme**. Escola Politécnica - Universidade de São Paulo, 2009. 100 p.

GRIMBLE, M. J. et al. Use of kalman filtering techniques in dynamic ship-positioning systems. In: **IEEE Proceedings D (Control Theory and Applications)**. v. 127, n. 3, p. 93–102, May 1980.

HALBWACHS, N. **Synchronous Programming of Reactive Systems**. Boston: Klumer Academic Plublishers, 1993.

HESPANHA, J. P. **Logic-based switching algorithms in control**. 1998. 106 p. Thesis (PhD) — Yale University, New Haven, 1998.

HESPANHA, J. P. Tutorial on syupervisory control. In: **Lecture Notes for the Workshop Control Using Logic and Swicthing for 40th Conference on Decision and Control**. Florida: [s.n.], 2002.

HOERNER, S. F. **Fluid dynamic drag: practical information on aerodynamics drag and hydrodynamic resistance**. New Jersey: Hoerner Fluid Dynamics, 1958.

IHLE, I. A. F. **Coordinated Control of Marine Craft**. 2006. 169 p. Thesis (PhD) — Department of Engineering Cybernetics, Faculty of Information Technology, Mathematics and Electrical Engineering, Norwegian University of Science and Technology (NTNU), Trondheim, 2006.

IHLE, I.-A. F. et al. Formation control of marine surface craft using lagrange multipliers. In: **Proceedings of the 44th IEEE Conference on Decision and Control and the European Control Conference**. December 12-15 2005.

IHLE, I.-A. F. et al. Formation control of marine surface craft: a lagrangian approach. **IEEE Journal of Oceanic Engineering**, v. 31, n. 4, p. 922–934, October 2006.

IRSCHIK, H.; HOLL, H. J. Mechanics of variable-mass systems - part 1: Balance of mass and linear momoment. **Applied Mechanics Reviews**, v. 57, n. 02, p. 2, March 2004.

IRVINE, M. **Cable Structures**. : Dover Publications, 1981.

ISIDORI, A. **Nonlinear control systems**. 3rd. ed. London: Springer-Berlag, 1995. 549 p.

JAKUBCZYK, B. **Introduction to geometric nonlinear control; Controllability and Lie bracket**. Warsaw, Poland: Institute of Mathematics, Polish Academy of Sciences, 2001. 62 p. Lectures given at the Summer School on Mathematical Control Theory.

KAHN, M. E. **The near minimum time control of open loop articulated kinematic chains**. Massachusetts: Stanford AI Lab, 1969.

KATEBI, M. R. et al. $H^{\propto}$ robust control design for dynamic ship positioning. In: **IEEE Proceedings on Control Theory and Applications**. v. 144, n. 2, p. 11–120, March 1997.

KHALIL, H. K. **Nonlinear systems**. Upper Siddle River: Prentice-Hall, 2002.

KOUTSOUKOS, X. et al. Supervisory control of hybrid systems. In: **Proceedings of the IEEE**. v. 88, n. 7, p. 1026–1049, July 2000.

KUMAR, V. et al. **Lecture Notes in Control and Information Sciences - Cooperative control**. Berlin Heidelberg: Springer-Verlag, 2005.

LANCZOS, C. **The variational principles of mechanics**. 4^{th}. ed. New York: Dover Publications, 1986.

LAPIERRE, L. et al. Coordinated motion control of marine robot. In: **Proceedings of 6$^{\mathbf{th}}$ IFAC Conference on Maneuvering and Control of Marine Craft (MCMC'2003)**. Girona, Spain: [s.n.], 2003.

LAPIERRE, L. et al. Nonlinear path following control of autonomous underwater vehicles. In: **Proceedings of 1$^{\mathbf{st}}$ IFAC Conference on Guidance and Control of Underwater Vehicles (GCUV)**. Newport, South Wales, U.K: [s.n.], 2003.

LEITE, A. J. P. et al. Current forces in tankers and bifurcation of equilibrium of turret systems: hydrodynamic model and experiments. **Applied Ocean Research**, v. 20, p. 145–156, 1998.

LEWANDOWSKI, E. M. **The dynamics of marine craft**. : World Scientific, 2004.

LEWIS, E. V. **Principles of Naval Architecture:Volume III Motions in Waves and Controllability**. 2^{th}. Jersey City: Society of Naval Architects and Marine Engineers (SNAME), 1990. 429 p.

LIBERZON, D. **Switching in Systems and Control**. Boston: Birkhäuser, 2003. 233 p.

LIBERZON, D.; MORSE, A. S. Basic problems in stability and design of switched systems. **IEEE Control Systems**, v. 45, n. 7, p. 1279–1289, 1999.

LIMA, E. L. **Curso de Análise**. 11^{th}. ed. Rio de Janeiro: Instituto Nacional de Matemática Pura e Aplicada (IMPA), 2009.

LUH, J. Y. S.; ZHENG, Y. F. Constrained relations between two coordinated industrial robots for motion control. **International Journal of Robotics Research**, v. 6, n. 3, p. 60–70, 1987.

MARSDEN, J. E. **Lectures on Mechanics**. Cambridge: Cambridge University, 2004. Draft version.

MEIROVITCH, L. **Methods of analytical dynamics**. New York: Dover Publications, 1970.

MICHEL, A. N.; WANG, K. **Qualitative theory of dynamical systems: The role of stability preserving mappings**. New York: Marcel Dekker Inc., 1995.

MONFORTE, J. C. **Geometric, Control and Numerical Aspects of Nonholonomic Systems**. Berlin: Springer, 2002. 235 p.

MORATELLI JR, . L. et al. Observer-lagrangian-based controller applied to two dynamically controlled vessels. In: **The 9th IFAC Conference on Control Applications in Marine Systems (CAMS2013)**. Osaka: [s.n.], v. 9, n. 1, p. 274–279, September 2013.

NAKAMURA, M.; KAJIWARA, H. Control system design and model experiments on thruster assisted mooring system. In: **Proc. Seventh International Offshore and Polar Engineering Conference (ISOPE)**. p. 641–648, 1997.

NAYFEH, A. H. **Introduction to Perturbation Techniques**. Blacksburg: John Wiley and Sons, 1981.

NAYLOR, T. **Corporate strategy**. Amsterdam: North-Holland, 1982.

NIJMEIJER, H.; ANGELEZ, A. R. **Synchronization of Mechanical Systems (Nonlinear Science)**. London: World Scientific Pub Co Inc, 2003.

OCIMF. Prediction of wind and current loads on vlccs. **Oil Company International Marine Forum**, 1977.

OLIVA, W. M. **Geometric Mechanics**. New York: Springer, 2002. 272 p.

OR, Y.; AMES, A. D. Stability and completion of zeno equilibria in lagrangian hybrid systems. **IEEE Transactions on Automatic Control**, v. 56, n. 6, p. 1322–1336, June 2001.

PACHTER, M. et al. Automatic formation flight control. **Journal of Guidance, Control, and Dynamics**, v. 17, n. 6, p. 1380–1383, 1994.

PACHTER, M. et al. Tight formation control. **Journal of Guidance, Control, and Dynamics**, v. 24, n. 2, p. 246–254, 2001.

PESCE, C. P. The application of lagrange equations to mechanical systems with mass explicity dependent on position. **Journal of Applied Mechanics**, v. 70, p. 751–756, September 2013.

PESCE, C. P.; CASETTA, L. Variable mass systems dynamics in engineering mechanics education. In: **Proceedings of COBEM 2007 - 19$^{\mathbf{th}}$ International Congress of Mechanical Engineering**. November 5-9 2007.

PESCE, C. P. et al. The lagrange equations for systems with mass varying explicity with posiiton: Some applications to offshore engineering. **Journal of the Brazilian Society of Mechanical Sciences and Engineering**, XXXVIII, n. 4, p. 496–504, October-December 2006.

REN, W.; BEARD, R. W. Formation feedback control for multiple spacecraft via virtual structures. In: **IEEE Proceedings of Control Theory and Applications**. v. 151, n. 3, p. 357–368, 2004.

RESPONDEK, W. **Geometry of static and dynamic feedback**. Trieste, Italy and and Bedlewo-Warsaw, Poland: Laboratoire de Mathématiques, INSA de Rouen, 2002. 77 p. Lectures given at the Summer School on Mathematical Control Theory.

ROSENKRANZ, F. **An introduction to corporate modeling**. Califórnia: Duke University Press, 1970.

SANFELICE, R. G. et al. Invariance principles for hybrid systems with connections to detectability and asymptotic stability. **IEEE Transactions on Automatic Control**, v. 52, n. 12, p. 2282–2297, December 2007.

SASTRY, S. **Nonlinear Systems: Analysis, stability and control**. New York: Springer, 1999. 667 p.

SATTINGER, D. H.; WEAVER, O. L. **Lie groups and algebras with applications to physics, geometry, and mechanics**. New York: Springer-Verlag, 1986.

SCHAFT, V. der; SCHUMACHER, J. M. **An introduction to hybrid dynamical systems**. London: Springer-Verlag, 2000.

SHEIKHOLESLAM, S.; DESOER, C. A. Control of interconnected nonlinear dynamical systems: The platoon problem. **IEEE Transactions on Automatic Control**, v. 37, p. 806–810, 1992.

SIMOS, A. N. et al. A quasi-explicit hydrodynamic model for the dynamic analysis of a moored fpso under current action. **Journal of Ship Research**, v. 45, n. 4, p. 289–301, 2001.

SKJETNE, R. **The Maneuvering problem**. 2005. 259 p. Thesis (PhD) — Department of Engineering Cybernetics, Faculty of Information Technology, Mathematics and Electrical Engineering, Norwegian University of Science and Technology (NTNU), Trondheim, 2005.

SKJETNE, R. et al. Formation control by synchronizing multiple maneuvering systems. In: **Proceedings of 6th IFAC Conference on Manoeuvering and Control of Marine Craft (MCMC2003)**. Girona, Spain: [s.n.], 2003.

SKJETNE, R. et al. Nonlinear formation control of marine craft. In: **Proceedings of 41st IEEE Conf. on Decision and Control**. Las Vegas: [s.n.], p. 1699–1704, 2002.

SæLID, S. et al. Design and analysis of a dynamic positioning system based on kalman filtering and optimal control. **IEEE Transactions on Automatic Control**, v. 28, n. 3, p. 331–339, 1983.

SMOGELI, . N. et al. Design of a hybrid power/torque thruster controller with thrust loss estimation. In: **Proceedings of the IFAC Conference on Control Applications in Marine Systems (CAMS2004)**. Ancona, Italy: [s.n.], July 7-9 2004.

SONTAG, E. D. **Mathematical control Theory**. 2nd. ed. New York: Springer, 1998. 544 p.

SORENSEN, A. J. et al. Dynamic of ships and floaters in extreme seas. In: **Proceedings of OCEANS2002 MTS/IEEE**. p. 1849–1854, 2002.

SOUZA, E. C. de. **Modelagem e controle de uma classe de sistemas multi-corpos móveis**. 2008. 179 p. Thesis (PhD) — Polytechnic School, University of São Paulo, São Paulo, 2008.

SPARANO, J. V. **Relatório de Projeto**. : NYXKonwledge, 2011. (Confidential Techninal Report).

SPIVAK, M. **A comprehensive introduction to differential geometry**. 3rd. ed. New Jersey: Perish Publish, 1999.

SPRY, S.; HEDRICK, J. K. Formation control using generalized coordinates. In: **Proceedings of the 43th IEEE Conference on Decision and Control**. Paradise Island, The Bahamas: [s.n.], p. 2441–2446, 2004.

SøRENSEN, A. J. : **Marine Cybernetics: Modelling and Control. Lecture Notes.** 2005.

STEPANENKO, Y.; VUKOBRATOVIC, M. Dynamics of articulated open-chain active mechanisms. **Mathematical Biosciences**, v. 28, p. 137–170, 1976.

STILWELL, D. J.; BISHOP, B. E. Redundant manipulator techniques for a path planning and control of a platoon of autonomous vehicles. In: **Proceedings of 41th IEEE Conf. Decision & Control**. Las Vegas: [s.n.], p. 2093–2098, 2002.

SUN, Z.; GE, S. S. **Switched linear systems: control and design**. London: John Wiley and Sons, 1989.

SUSSMANN, H. J. A general theorem on local controllability. **SIAM Journal of Control and Optimization**, v. 25, n. 1, p. 159–194, 1987.

SVAKIN, A. V.; EVANS, R. J. **Hybrid dynamical systems: controller and sensor switching problems**. Boston: Birkhäuser, 2002.

TALMAN, R. **Geometric Mechanics**. Weinheim: Wiley-VCH, 2007. 606 p.

TANNURI, E. A. **Desenvolvimentonvolvimento de metodologia de projeto de sistema de posicionamento dinâmico apliado a operações em alto-mar**. 2002. Thesis (PhD) — Escola Politécnica da Universidade de São Paulo, São Paulo, 2002.

TANNURI, E. A. et al. Dynamic positioning systems: an experimental analysis of sliding mode control. **Control Engineering Practice**, v. 18, n. 10, p. 1121–1132, 2010.

TANNURI, E. A.; DONHA, D. C. H$^{\propto}$ controller design for dynamic positioning of a turret moored fpso. In: **Proceedings of 5th IFAC Conference on Manoeuvring and Control of Marine Crafts (MCMC2000)**. Denmark: [s.n.], p. 269–274, 2000.

TANNURI, E. A. et al. Dynamic positioning of a turred moored fpso using sliding mode control. **International Journal of Robust and Nonlinear Control**, v. 11, n. 13, 2001.

TANNURI, E. A. et al. Adaptative control strategy for the dynamic positioning of a shuttle tanker during offloading operations. **Journal of Offshore Mechanics ADN Artic Engineering**, v. 128, n. 3, p. 203–210, 2006.

TRELLEBORG. The Free Encyclopedia. Available from: <http://www.trelleborg.com/en/Marine-Systems>. Visited in: March, 2012.

VARAIYA, P. Smart cars on smart roads: problem of control. **IEEE Transactions on Automatic Control**, v. 38, n. 2, p. 195–207, 1993.

VICSEK, T. et al. Novel type of phase transition in a system of self-driven particles. **Physical Review Letters**, v. 75, n. 6, p. 1226–1229, 1995.

WANG, P. K. C.; HADAEGH, F. Y. Coordination and control of multiple microspacecraft moving in formation. **Journal of the Astronautical Sciences**, v. 44, n. 3, p. 315–355, 1996.

WEIMERSKIRCH, H. et al. Energy saving in flight formation. **Nature**, v. 413, p. 697–698, 2001.

WITSENHAUSEN, H. S. A class of hybrid-state continuous-time dynamic systems. **IEEE Transactions on Automatic Control**, v. 11, n. 2, p. 161–167, 1966.

WITTENBURG, J. **Dynamics of Systems of Rigid Bodies**. Stuttgart: B.G Teubner Stuttgart, 1977. 224 p.

YE, H. et al. A general model for the qualitative analysis of hybrid dynamical systems. In: **IEEE Conference on Decision and control**. New Orleans: [s.n.], v. 34, p. 1473–1477, 1995.

YE, H. et al. Stability theory for hybrid dynamical systems. **IEEE Transactions on Automatic Control**, v. 43, n. 4, p. 461–474, 1998.

ZAKARTCHOUK JR, . A.; MORISHITA, H. M. Backstepping controller for dynamic positioning of ships: Simulation and experimental results for a shuttle tanker model. In: **Proceedings of 8th IFAC Conference on Manoeuvering and Control of Marine Crafts (MCMC′2009)**. Guarujá, Brazil: [s.n.], 2009.

surge sway yaw heave pitch roll draft survey plant model control model dynamic positioning system multibody system geometric control hybrid system lobe RAO shuttle tanker FPWSO. beam draft

Glossary

Beam - Width of the hull.

Control model - Simplification with respect to the plant model in order to make easier the control design.

Draft - Depth of the hull submerged.

Draft survey - Calculation of the weight of cargo loaded or unloaded to or from a ship from measurements of changes in its displacement. The technique is based on Archimedes' principle.

Dynamic positioning system - Control system applied to vessels in order to keep position and heading under some reference by means of thruster and propellers exclusively.

FPWSO. - Floating, Production, Well intervation, Storage and Offloading unit is a vessel used by the offshore oil and gas industry for the production, processing of hydrocarbons and for storage of oil.

Geometric control - Control theory that applies differential geometry theory. Differential geometry is a mathematical discipline that uses the techniques of differential calculus, integral calculus, linear algebra and multilinear algebra to study problems in geometry.

Heave - Vertical translation motion of the vessel.

Hybrid system - Dynamical system that has discrete and continuous variables interacting between each other.

Lobe - Residue of the Fast Fourier Transform (FFT) that deteriorates the spectrum analysis.

Multibody system - System that consists of a collection of subsystems (bodies) connected by some kind of joint.

Pitch - Angular motion around transversal vessel direction.

Plant model - Dynamical model that tries to describe the system dynamics as close as possible the real system mechanics.

RAO - Response Amplitude Operator (RAO) is a transfer function used to determine the effect that a sea state will have upon the motion of a ship through the water.

Roll - Angular motion around longitudinal vessel direction.

Shuttle tanker - Vessel designed for oil transport from an offshore oil field as an alternative to constructing oil pipelines.

Surge - Longitudinal translation motion of the vessel.

Sway - Transversal translation motion of the vessel.

Yaw - Angular motion around normal direction of the vessel′s XY plane.

APPENDIX

Appendix A

Ship Properties

This appendix presents the main dimensional properties of the vessels studied. These properties are main dimensions, inertia, damping parameters, wet and wind areas and thruster configuration.

A.1 Ship Dimensions and Thruster Propellers

The main dimensions of the vessels are presented in Table A.1.

Table A.1: Vessel Dimensions

Vessel	L_{OA} [m]	L_{BP}[m]	B[m]	D[m]
FPWSO	337,3	320,0	54,5	27,0
Shuttle tanker	269,0	258,0	46,0	24,4

The dimension L_{OA} means the overall length of the vessel. The length between perpendiculars is L_{BP}. The beam is B. The variable D means the vessel depth. Both vessels have dynamic positioning systems that are used to maintain their positions and headings by means of thrusters. Their propulsive arrangements are presented in Figures A.1 and A.2 for the FPWSO and shuttle tanker, respectively. Tables A.2 and A.3 present vessel propulsion and its characteristic.

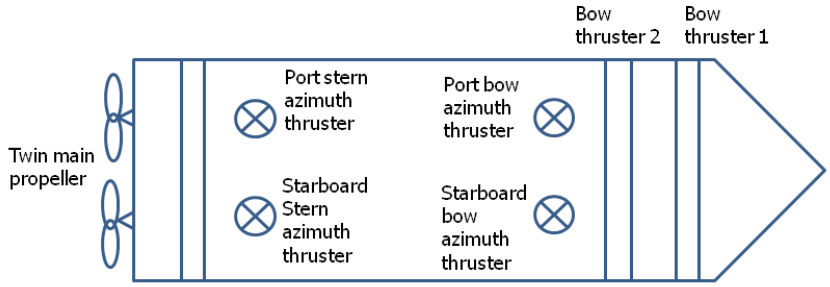

Figure A.1: FPWSO propulsive arrangement

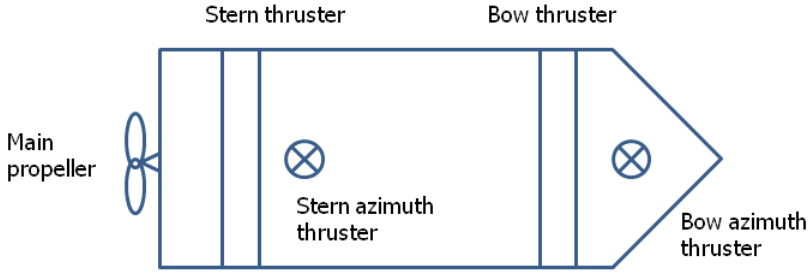

Figure A.2: Shuttle tanker propulsive arrangement

Table A.2: FPWSO thruster characteristics

Thruster	Power [kW]	Tmin [kN]	Tmax [kN]	Px [m]	Py [m]
Bow thruster	1030	-133	133	120	0
Bow thruster	1030	-133	133	110	0
Stern thruster	700	-89	89	100	0
Port bow azimuth	2420	0	400	90	15
Starboard bow azimuth	2420	0	400	90	-15
Port stern azimuth	3800	0	700	-90	15
Starboard stern azimuth	3800	0	700	-90	-15
Port twin propeller	6400	-730	1245	-166	0
Starboard twin propeller	6400	-730	1245	-166	0

The values T_{max}, T_{min}, P_x and P_y are the maximum and minimum thrust, the longitudinal position of the thruster related to the midship and the transverse position of the thruster related to the centerline, respectively.

Table A.3: ST thruster characteristics

Thruster	Power [kW]	Tmin [kN]	Tmax [kN]	Px [m]	Py [m]
Bow thruster	1910	-242	1910	120	0
Stern thruster	2380	-302	2380	-110	0
Bow azimuth thruster	2000	0	2000	110	0
Stern azimuth thruster	2000	0	2000	-85	0
Main propeller	18871	-832	188871	-120	0

A.2 Inertia and Damping Properties

The new strategy of control is proposed in order to study the offloading operation between the FPWSO and the shuttle tanker. The proposal takes into account the draft variation during the offloading. Hence, during the operation, the inertia properties vary and this variation needs to be considered by the ship dynamics. The parameters that are modified are presented in the following figures, except for the longitudinal center of gravity. This dimension does not change significantly and the midship is assumed to be the position of the gravity center. Figures A.3 to A.6 present some parameters used by ship dynamics model such as inertia of the rigid body and the added inertia, wet area of the hull and projected area to the wind. The values presented in these figures are approximations based on Sparano (2011) and the hull lines. It is assumed that the ship has the trim and hell angles null during the offloading. This is possible since a load plan be made for it.

The linear damping matrix D_i is estimated by trials with scale models in basin tanks. That matrix is found using

$$\boldsymbol{D_i} = \begin{bmatrix} Cd_{11} & 0 & 0 \\ 0 & Cd_{22} & Cd_{26} \\ 0 & Cd_{62} & Cd_{66} \end{bmatrix} Aw_i \tag{A.1}$$

where Aw_i is the hull wet area and the coefficients (for vessel i = *1,2*) are known and equal to $Cd_{11} = 2.079$, $Cd_{22} = 114.384$, $Cd_{26} = Cd_{62} = 5.199$ and $Cd_{66} = 535.52$.

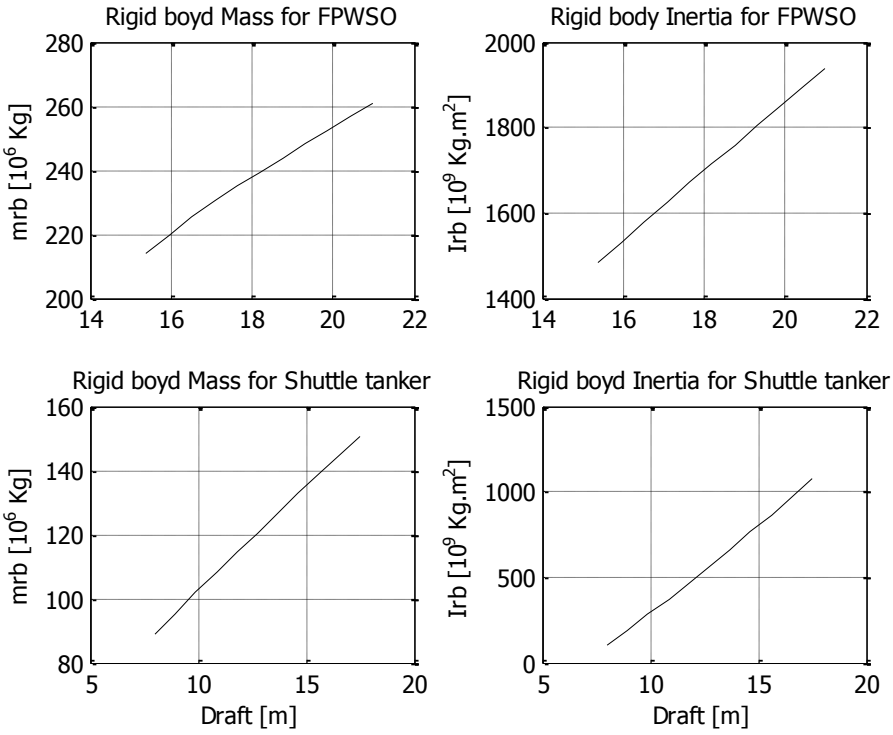

Figure A.3: Inertia of the rigid body of the vessels

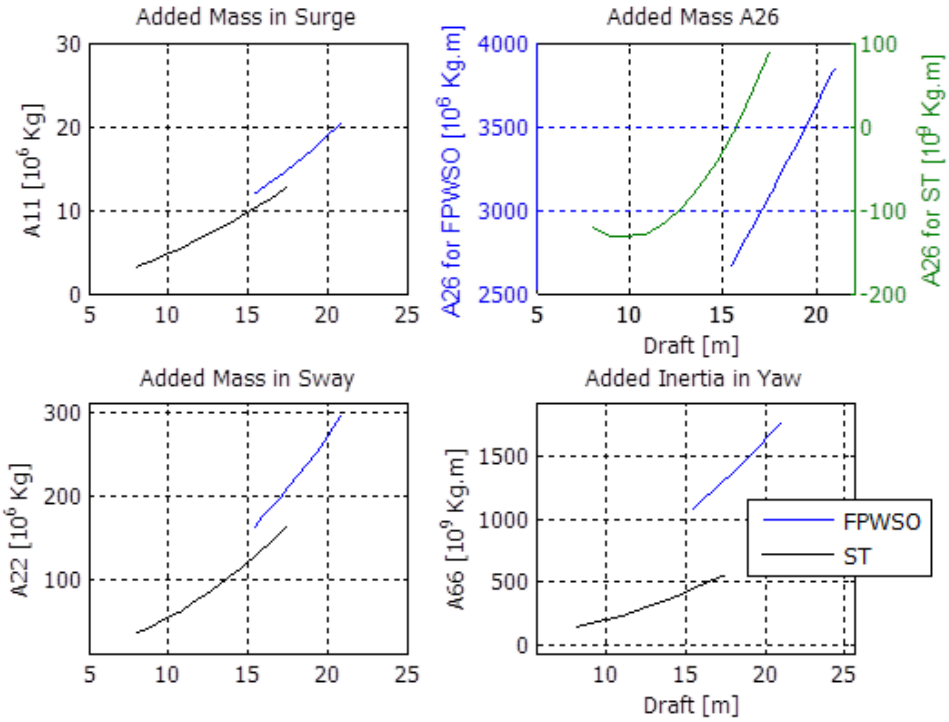

Figure A.4: Added inertia of the vessels

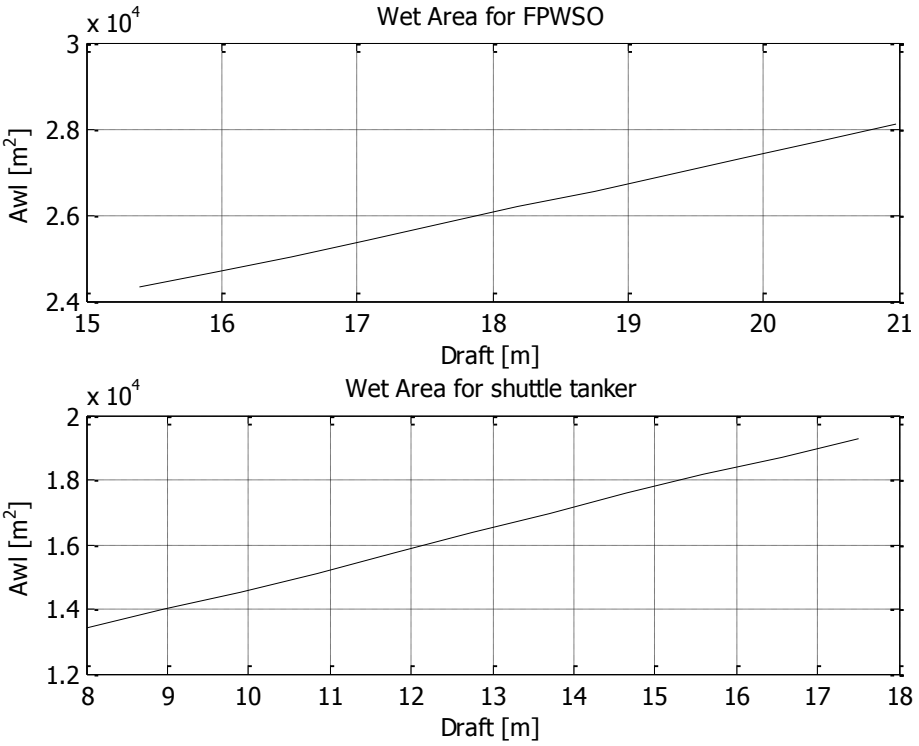

Figure A.5: wet area of the ship hulls

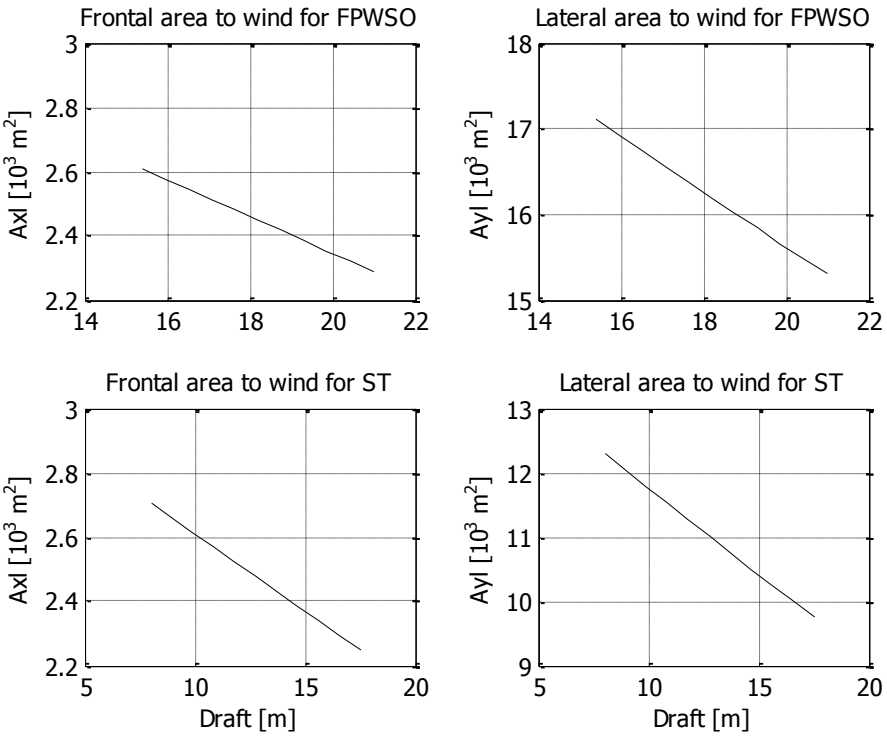

Figure A.6: Projected wind area for the vessels

Appendix B

Perturbation Model for Vessels

The positioning performance of a DP vessel depends on the tuning of the control parameters. The parameters of the controller are designed based on the inertia and damping properties of the vessel. The performance of the controller is affected since these parameters have suffered a high modification. The controller is well-known by its robustness and it is able to compensate possible non-modeled effects or small variations of the parameters of the vessels used to deseign the controller. However, when high variations of the design parameters occurs, the controller can not compensate these variations and its performance is deteriorated. This damage can be avoided if the parameter variation is known and the controller parameters could be changed without causing instability.

The DP vessels (FPSWO and shuttle tanker) carrying out an offloading operation have their draft modified due to the oil transfer. The controller is not able to compensate this variation in order to maintain the performance of the positioning for all variation of the draft. So, the proposal is to design a hybrid control that changes the parameters of the control when a significant change of the vessel draft is identified.

To determine which draft variation affects the performance of the positioning, a perturbation model for the closed-loop system (vessel and controller) is proposed. The idea is to evaluate the response of a simplified model of the vessel dynamics due to the variation of a small variation. This small variation ϵ is related is some extent with the variation of the draft. The modeling of

the vessel properties related to the small variation ϵ is presented. In the following sections, the perturbation method is presented and it is applied to the closed-loop system with the PD-like controller.

B.1 Perturbation Method

The behavior of a dynamical system with a variable small parameter can be described as function of that small parameter. In order to do analyze the influence of that parameter into the system response, the Perturbation Method can be applied. This method approximates the system response for a small perturbation ϵ with an error of the order $O(\epsilon)$. This theory is applied in order to approximate the vessel dynamics response as function of the small parameter ϵ related to the draft variation. This analysis will be helpful to evaluate the effect of the draft variation into the dynamic positioning of the vessels in offloading operation. Hence, the main concepts about Perturbation Method are presented.

Consider the system

$$\dot{x} = f(t, x, \epsilon) \tag{B.1}$$

where $t \in \mathbb{R}$ is the time on a interval $[t_0, t_1]$, $x\ D \in \mathbb{R}^n$ is a state vector on a domain , $\epsilon \in \mathbb{R}$ is a small parameter in the interval $[-\epsilon_0, \epsilon_0]$. It is desired the solution of the (B.1) for the following initial state

$$x(t_0) = \eta(\epsilon) \tag{B.2}$$

where η is a function that depends on ϵ. The objective of the Perturbation Method is to evaluate the "smallness" of perturbation parameter ϵ and to construct valid approximate solutions for sufficiently small $\|\epsilon\|$. The trivial solution of the (B.1) with initial condition (B.2) is given as

$$\dot{x} = f(t, x, 0), \qquad x(t_0) = \eta_0 \tag{B.3}$$

where $\eta_0 = \eta(0)$. It can be proved that (KHALIL, 2002)

$$\|x(t,\epsilon) - x_0(t)\| \leq k\,|\epsilon|\,, \forall\,|\epsilon| < |\epsilon_1|\,, \forall t \in [t_0, t_1] \tag{B.4}$$

The error is said to be of order $O(\epsilon)$ if (B.4) is satisfied. Let f and η be smooth functions with continuous partial derivatives with respect to x and ϵ up to order N. A higher approximation of $x(t,\epsilon)$ can be construct with a finite Taylor series as follows

$$x(t,\epsilon) = \sum_{k=0}^{N-1} x_k(t)\epsilon^k + \epsilon^N R_x(t,\epsilon) \tag{B.5}$$

where R_x is a remainder term. Using the Taylor's theorem, it can be proved the existence of a finite Taylor series

$$\eta(\epsilon) = \sum_{k=0}^{N-1} \eta_k(t)\epsilon^k + \epsilon^N R_\eta(\epsilon) \tag{B.6}$$

Hence,

$$x_k(t_0) = \eta_k, \qquad k = 0, 1, 2, ..., N-1 \tag{B.7}$$

Including (B.5) into (B.1) yields

$$\begin{aligned} \sum_{k=0}^{N-1} \dot{x}_k(t)\epsilon^k + \epsilon^N \dot{R}_x(t,\epsilon) &= f(t, x(t,\epsilon), \epsilon) \equiv h(t,\epsilon) \\ &= \sum_{k=0}^{N-1} h_k(t)\epsilon^k + \epsilon^N R_h(t,\epsilon) \end{aligned} \tag{B.8}$$

where $h(t,\epsilon)$ are functions of Taylor series coefficients of $x(t,\epsilon)$. The coefficients of the Taylor series $x_0, x_1, ..., x_{N-1}$ are found from the expressions

$$\dot{x}_0 = f(t, x_0, 0), \qquad x_0(t_0) = \eta_0 \tag{B.9}$$

$$\dot{x}_k = \mathbf{A}(t)x_k + g_k(t, x_0(t), ..., x_{k-1}(t)), \qquad x_k(t_0) = \eta_k \tag{B.10}$$

where $k = 1, ..., N-1$, $\mathbf{A}(t)$ is the Jacobian matrix of f and g_k is a polynomial with time-

dependent coefficients. Once found the terms $x_0, x_1, ..., x_{N-1}$, the approximation error e can be proved as follows (KHALIL, 2002)

$$e = x(t,\epsilon) - \sum_{k=0}^{N-1} x_k(t)\epsilon^k = O(\epsilon^N) \tag{B.11}$$

B.2 Applying Perturbation Model to Vessel Motion

The vessel properties such as inertia and damping are modified due to the draft variation. This variation is presented in Appendix A. To evaluate how this variation affects vessel dynamics, consider the vessel kinetics and simplified dynamics of one vessel as follows

$$\dot{\boldsymbol{\eta}} = \boldsymbol{J}(\psi)\boldsymbol{\nu} \tag{B.12}$$

$$\boldsymbol{M}\dot{\boldsymbol{\nu}} + \boldsymbol{D}\boldsymbol{\nu} = \boldsymbol{J}(\psi)^T(\boldsymbol{b} + \boldsymbol{u}) \tag{B.13}$$

where $\boldsymbol{M} \in \mathbb{R}^{3\times3}$ is the inertia matrix and $\boldsymbol{D} \in \mathbb{R}^{3\times3}$ is the damping matrix. The $\boldsymbol{J}(\psi) \in \mathbb{R}^{3\times3}$ is the rotation matrix. The $\boldsymbol{\eta} \in \mathbb{R}^3$ and the $\boldsymbol{\nu} \in \mathbb{R}^3$ are the vector of the position and velocity, respectively. The $\psi \in \mathbb{R}$ is the heading of the vessel. The $\boldsymbol{b} \in \mathbb{R}^3$ and $\boldsymbol{u} \in \mathbb{R}^3$ are the vectors of the external and the control forces and moment, respectively. Collecting $\dot{\boldsymbol{\nu}}$ yields

$$\dot{\boldsymbol{\nu}} = -\boldsymbol{M}^{-1}\boldsymbol{D}\boldsymbol{\nu} + \boldsymbol{M}^{-1}\boldsymbol{J}(\psi)^T(\boldsymbol{b} + \boldsymbol{u}) \tag{B.14}$$

The matrices $\boldsymbol{M}^{-1}\boldsymbol{D}$ and $\boldsymbol{M}^{-1}$ depend on the draft of the vessel. Hence, the elements of these matrices can be written as a function of draft, i.e, $\boldsymbol{M}^{-1}\boldsymbol{D}_{ij}(h)$ and $\boldsymbol{M}^{-1}_{ij}(h)$, where the indexes $i = 1, ..., 3$ and $j = 1, ..., 3 \in \mathbb{N}$ are the row and the column of the matrix and $h \in \mathbb{R}$ is the draft of the vessel. These functions are not linear with respect to the draft h. However, they can be linearized with respect to a small parameter defined as

$$\epsilon = log_{10}(\frac{h}{h_0}) \tag{B.15}$$

where $\epsilon \in \mathbb{R}$ and the $h_0 \in \mathbb{R}$ is the initial draft of the vessel when the offloading operation starts. The function (B.15) is called a gauge function (NAYFEH, 1981). Now, the elements of

the $\boldsymbol{M}^{-1}\boldsymbol{D}_{ij}$ and $\boldsymbol{M}_{ij}^{-1}$ can be written as

$$(\boldsymbol{M}^{-1}\boldsymbol{D})_{ij} = (\boldsymbol{M}_0^{-1}\boldsymbol{D}_0)_{ij} + \epsilon k_{1_{ij}} \tag{B.16}$$

$$\boldsymbol{M}_{ij}^{-1} = \boldsymbol{M}_{0_{ij}}^{-1} + \epsilon k_{2_{ij}} \tag{B.17}$$

where $\boldsymbol{M}_{0_{ij}}^{-1}$ and $(\boldsymbol{M}_0^{-1}\boldsymbol{D}_0)_{ij}$ are the values of these matrices for the initial draft and $k_{1_{ij}}$ and $k_{2_{ij}}$ are constants for $i = 1, ..., 3$ and $j = 1, ..., 3$. So, the matrices $\boldsymbol{M}^{-1}\boldsymbol{D}_{ij}$ and $\boldsymbol{M}_{ij}^{-1}$ can be written as follows

$$\boldsymbol{M}^{-1}\boldsymbol{D} = \boldsymbol{M}_0^{-1}\boldsymbol{D}_0 + \epsilon.\boldsymbol{K}_1 \tag{B.18}$$

$$\boldsymbol{M}^{-1} = \boldsymbol{M}_0^{-1} + \epsilon.\boldsymbol{K}_2 \tag{B.19}$$

where $\boldsymbol{K}_1$ and $\boldsymbol{K}_2 \in \mathbb{R}^{3\times3}$ are matrices of constant elements. Substituting (B.18) and (B.19) into (B.14) yields

$$\dot{\boldsymbol{\nu}} = (\boldsymbol{M}_0^{-1}\boldsymbol{D}_0 + \epsilon\boldsymbol{K}_1)\boldsymbol{\nu} + (\boldsymbol{M}_0^{-1} + \epsilon\boldsymbol{K}_2)\boldsymbol{J}(\psi)^T(\boldsymbol{b} + \boldsymbol{u}) \tag{B.20}$$

This perturbation model (B.20) is developed for one vessel, for instance, the FPWSO. The model for the shuttle tanker is found from the same procedure as presented above. However, the rate variation of the draft is different between the vessel, i.e., $\epsilon_1 \neq \epsilon_2$, where ϵ_1 and $\epsilon_2 \in \mathbb{R}$ are the small parameter for the FPWSO and the shuttle tanker, respectively. However, it is possible to write $\epsilon_2 = c.\epsilon_1$, where c is a constant, and the perturbation model for two vessels yields

$$\dot{\boldsymbol{\nu}} = (\boldsymbol{M}_0^{-1}\boldsymbol{D}_0 + \epsilon\boldsymbol{K}_1)\boldsymbol{\nu} + (\boldsymbol{M}_0^{-1} + \epsilon\boldsymbol{K}_2)\boldsymbol{J}(\psi_1, \psi_2)^T(\boldsymbol{b} + \boldsymbol{u}) \tag{B.21}$$

where $\boldsymbol{M_0} \in \mathbb{R}^{6\times6}$ is the inertia matrix and $\boldsymbol{D_0} \in \mathbb{R}^{6\times6}$ is the damping matrix in the initial draft. The small parameter is $\epsilon = \epsilon_1$. The $\boldsymbol{J}(\psi_1, \psi_2) \in \mathbb{R}^{6\times6}$ is the rotation matrix. The $\boldsymbol{\eta} \in \mathbb{R}^6$ and the $\boldsymbol{\nu} \in \mathbb{R}^6$ are the vector of the positions and velocities, respectively. The ψ_1 and $\psi_2 \in \mathbb{R}$ are the headings of the FPWSO and the shuttle tanker, respectively. The $\boldsymbol{b} \in \mathbb{R}^6$ and $\boldsymbol{u} \in \mathbb{R}^6$ are the vectors of the external and the control forces and moment, respectively.

To simplify the perturbation model, the vessel kinematics and dynamics are linearized around

the point $\boldsymbol{\eta}_0 = \mathbf{0}_{6\times 1}$. So, the complete model yields

$$\dot{\boldsymbol{\eta}} = \boldsymbol{\nu} \tag{B.22}$$

$$\dot{\boldsymbol{\nu}} = (\boldsymbol{M}_0^{-1}\boldsymbol{D}_0 + \epsilon\boldsymbol{K}_1)\boldsymbol{\nu} + (\boldsymbol{M}_0^{-1} + \epsilon\boldsymbol{K}_2)(\boldsymbol{b} + \boldsymbol{u}) \tag{B.23}$$

Once known the vectors $\boldsymbol{b}$ and $\boldsymbol{u}$, the perturbation model (B.23) presents the form $\dot{\boldsymbol{x}} = \boldsymbol{f}(t, \boldsymbol{x}, \epsilon)$ (B.1). So, it is possible to find an approximation of order N of $\boldsymbol{x}(t, \epsilon)$ using (B.5) with an error of the order $O(\epsilon^N)$.

Now, the idea is to compare the response of the approximation of the $\boldsymbol{x}(t, \epsilon)$ to the response of the $\boldsymbol{x}(t, 0)$ for a input as a step . An error E of comparison is defined as

$$E = max\|(\sum_{k=0}^{N-1} x_k(t)\epsilon^k + \epsilon^N R_x(t, \epsilon)) - \boldsymbol{x}(t, 0)\| \tag{B.24}$$

where $\boldsymbol{x}(t, \epsilon) = \sum_{k=0}^{N-1} x_k(t)\epsilon^k + \epsilon^N R_x(t, \epsilon)$ is the approximation (B.5). Once defined the maximum error $E_{max} \in \mathbb{R}$, the small variation ϵ is found and so the draft variation.

B.3 Perturbation Model with the Control Law

Consider the PD-like control law written as

$$\boldsymbol{u}_{PD} = \boldsymbol{K}_p(\boldsymbol{\eta}_r - \boldsymbol{\eta}) - \boldsymbol{K}_d\dot{\boldsymbol{\eta}} - \boldsymbol{b} \tag{B.25}$$

where $\boldsymbol{u}_{PD} \in \mathbb{R}^6$ is the control vector, $\boldsymbol{\eta}_r \in \mathbb{R}^6$ is a constant input vector and the $\boldsymbol{K}_p \in \mathbb{R}^{6\times 6}$ and $\boldsymbol{K}_d \in \mathbb{R}^{6\times 6}$ are the matrix gain. The vector $\boldsymbol{b}$ is assumed to be known.

Substituting (B.25) into (B.23) yields

$$\dot{\boldsymbol{\nu}} = (\boldsymbol{M}_0^{-1}\boldsymbol{D}_0 + \epsilon\boldsymbol{K}_1)\boldsymbol{\nu} + (\boldsymbol{M}_0^{-1} + \epsilon_1\boldsymbol{K}_2)(\boldsymbol{K}_p(\boldsymbol{\eta}_r - \boldsymbol{\eta}) - \boldsymbol{K}_d\dot{\boldsymbol{\eta}}) \tag{B.26}$$

The state vector is defined $\boldsymbol{x} = [\ \boldsymbol{\eta}^T \quad \boldsymbol{\nu}^T\ ]^T$. As presented in previous section, the coefficients of the Taylor series are found from substituting the approximation $\boldsymbol{x}(t, \epsilon)$ into (B.22) and (B.25).

Calcualting it with $N = 3$, the systems $\dot{\boldsymbol{x}}_k$ with $k = 0, ..., N-1$ yield

$\underline{K = 0}$

$$\dot{\boldsymbol{\eta}}_{10} = \dot{\boldsymbol{\nu}}_{10} \tag{B.27}$$

$$\dot{\boldsymbol{\nu}}_{10} = -\boldsymbol{M}_0^{-1}\boldsymbol{D}_0\boldsymbol{\nu}_{10} + \boldsymbol{M}_0^{-1}\left[\boldsymbol{K}_p(\boldsymbol{\eta}_r - \boldsymbol{\eta}_{10}) - \boldsymbol{K}_d\boldsymbol{\nu}_{10}\right] \tag{B.28}$$

$\underline{K = 1}$

$$\dot{\boldsymbol{\eta}}_{11} = \dot{\boldsymbol{\nu}}_{11} \tag{B.29}$$

$$\dot{\boldsymbol{\nu}}_{11} = -\boldsymbol{M}_0^{-1}\boldsymbol{D}_0\boldsymbol{\nu}_{11} - \boldsymbol{K}_1\boldsymbol{\nu}_{10} + \boldsymbol{M}_0^{-1}\left[-\boldsymbol{K}_p\boldsymbol{\eta}_{11} - \boldsymbol{K}_d\boldsymbol{\nu}_{11}\right] + \boldsymbol{K}_2\left[\boldsymbol{K}_p(\boldsymbol{\eta}_r - \boldsymbol{\eta}_{10}) - \boldsymbol{K}_d\boldsymbol{\nu}_{10}\right] \tag{B.30}$$

$\underline{K = 2}$

$$\dot{\boldsymbol{\eta}}_{12} = \dot{\boldsymbol{\nu}}_{12} \tag{B.31}$$

$$\dot{\boldsymbol{\nu}}_{12} = -\boldsymbol{M}_0^{-1}\boldsymbol{D}_0\boldsymbol{\nu}_{12} - \boldsymbol{K}_1\boldsymbol{\nu}_{11} + \boldsymbol{M}_0^{-1}\left[-\boldsymbol{K}_p\boldsymbol{\eta}_{12} - \boldsymbol{K}_d\boldsymbol{\nu}_{12}\right] + \boldsymbol{K}_2\left[-\boldsymbol{K}_p\boldsymbol{\eta}_{11} - \boldsymbol{K}_d\boldsymbol{\nu}_{11}\right] \tag{B.32}$$

So, integrating (B.27) to (B.32), the approximation of the $\boldsymbol{x}(t, \epsilon)$ with $N = 3$ is found and the small variation ϵ is determined once the E_{max} is defined.

B.4 Procedure for determining the Reference Drafts

The perturbation model for vessel dynamics is presented in the previous section. Now, the procedure to find the number of the reference drafts is discussed. The vessels start the offloading at the draft h_0. For these drafts, the matrices $\boldsymbol{K}_1$ and $\boldsymbol{K}_2$ are calculated as presented in section B.1. Also, the initial matrices $\boldsymbol{M}_0$ and $\boldsymbol{D}_0$ are found from h_0. The parameters of the control law are updated using these matrices of the inertia and damping.

Based on the perturbation model, consider the following procedure: integrate the approximations

$\dot{\boldsymbol{x}}_k$ for $k = 1, ..., N-1$. Find the small parameter ϵ for some error $E \leq E_{max}$. Calculate the new draft h_1 and check if this draft is the final draft. If it is true, stop the procedure. In the opposite, set h_0 equal to h_1 and redo the logic until the final draft. Figure B.1 summarizes this procedure.

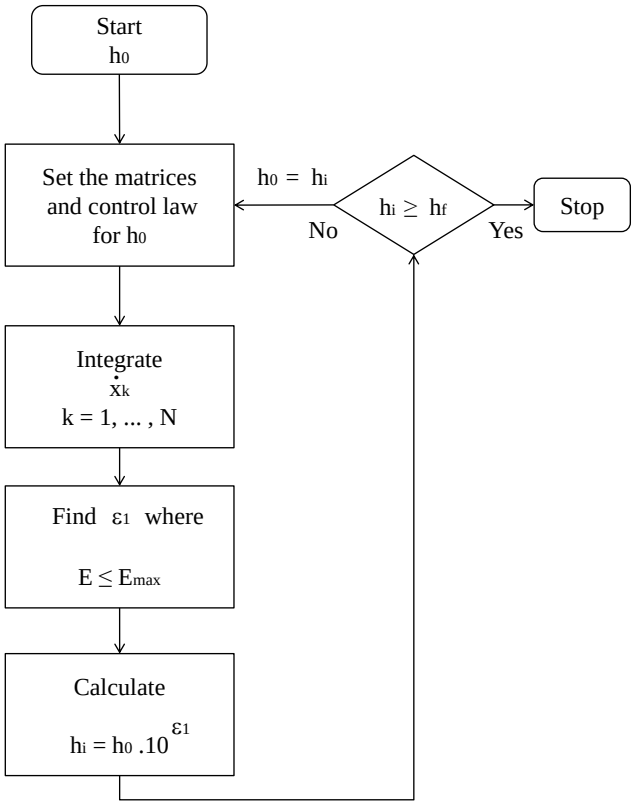

Figure B.1: Procedure for finding the reference drafts

B.5 Results and Discussion

The procedure of the previous section is applied with error E_{max} equal to 5% and 10%. The initial drafts of the vessels are 21.0m and 8.00 for the FPWSO and the shuttle tanker, respectively. The final drafts are 15.42m and 17.5m. The initial displacements of the vessels are 261.057m^3 and 88.848m^3, and the final displacement are 213.494m^3 and 150.720m^3 for the FPWSO and the shuttle tanker, respectively. The displacement of the vessels are different because during the offloading operation the FPWSO extracts crude oil and transfer processed oil to the shuttle tanker that just loads. The step input (maneuver) to evaluate the error is presented in Figure

B.2. The results of the perturbation models are presented in Tables B.1 B.2 for error of 5% and 10%, respectively. The ∇ symbol means the displacement of the vessel.

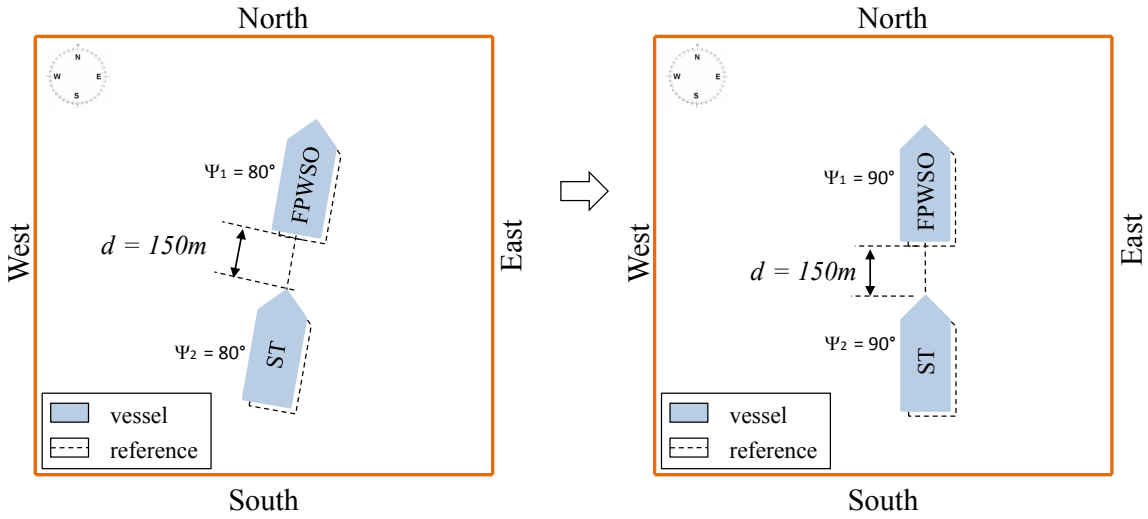

Figure B.2: Maneuver for perturbation model

As expected, a small error requires a high number of the reference drafts. The simulations present a displacement variation almost constant for each step. For an error of 5%, the variation is around 11.000m^3 for the FPWSO and 14.000m^3 for the shuttle tanker. The draft at the last step is almost close to the final draft of the vessels. For an error of 10%, the variation is around 20.000m^3 for the FPWSO and 26.000m^3 for the shuttle tanker. The draft at the last step is a little distant to the final draft of the vessels. However, the model is correct because if the next step occurred, the draft would exceed the final draft.

Table B.1: Maximum error of 5% for finding the reference drafts

	FPWSO			SHUTTLE		
step	H	∇ [m³]	var [m³]	H	∇ [m³]	var [m³]
0	21,0	261.057		8,0	88.848	
1	19,5	249.289	11.768	10,2	104.165	15.317
2	18,0	238.007	11.282	12,49	118.841	14.676
3	16,7	226.785	11.222	14,7	133.439	14.598
4	15,5	214.746	12.039	17,24	149.099	15.660

Table B.2: Maximum error of 10% for finding the reference drafts

	FPWSO			SHUTTLE		
step	H [m]	∇ [m³]	var [m³]	H	∇ [m³]	var [m³]
0	21,0	261.057		8,0	88.848	
1	18,38	240.904	20.153	11,9	115.073	26.225
2	16,05	220.546	20.358	16	141.555	26.482

Here, the error is assumed to be equal to 10% that is a reasonable variation for the positioning of the DP vessels. So, the number of three controllers are enough to guarantee that maximum error. However, the values of the reference drafts are a little modified. The reference drafts are set initial draft, final draft and the intermediate draft between those values. It is possible because the hybrid control switches the control law within the range of the draft initial to intermediate draft and the intermediate draft to final draft. So, the maximum error never reaches the maximum variation and the maximum error is respected. So, the reference drafts are 21.0m, 18.21m and 15.42m for the FPWSO and 8.0m, 12.48m and 17.5m for the shuttle tanker.

Appendix C

Spectral Analysis

The hybrid concept applied to the offloading operation changes the nonlinear observer due to the sea state change. That modification is based on the peak-frequency of the response spectrum of the vessel first-order motion. In order to determinate which peak-frequency imposes significant change under the vessel motion, a detailed cross spectral analysis is carried out. Based on that, the number of the observers is determined.

C.1 Standard Spectrum

To evaluate the wave-frequency motion of the vessels, some sea spectra are generated based on the Beaufort scale. The relationship between the mean values of wind speed for each sea state and the wave height is used to generate sea spectra based on the Pierson-Moskowitz spectrum standard. This spectrum is given by

$$S(\omega) = A\omega^{-5}.e^{-B\omega^{-4}} \tag{C.1}$$

where S is the spectrum, ω is the frequency and the values A and B are equal to $A = 8.1e^{-3}.g^2$, $B = 0.74.(\frac{g}{V_{wind}})^4$, g and V_{wind} are the gravity acceleration and the wind velocity, respectively.

The significant wave height can be found as (FOSSEN, 1994).

$$H_s = 0.21.\frac{V_{wind}^2}{g} \tag{C.2}$$

where H_s is the significant wave height. The value of the constant B can be rewritten as

$$B = \frac{3.11}{H_s^2} \tag{C.3}$$

Taking the mean values of V_{wind} for each sea state, the parameters of the spectra are calculated using (C.2) and (C.3). The modal frequency ω_o and peak-period T_0 of the spectrum are found by

$$\omega_0 = \sqrt[4]{\frac{4B}{5}} \tag{C.4}$$

$$T_0 = 2\pi\sqrt[4]{\frac{5}{2B}} \tag{C.5}$$

Hence, the parameters of the spectra are determined using (C.4) and (C.5). Table C.1 presents the spectra for the cross spectral analysis. Figure C.1 presents the spectra of those table.

Table C.1: Considered spectra for cross analysis

Beaufort Number	Description	Wind Speed (knots)	Wave height [m]	Hs [m]	A	B	ω_0 [rad/s]	T_0 [s]
0	Calm	0-1	0	0	0.78	0	-	-
1	Light air	2-3	0-0.1	0.05	0.78	1244	8.94	0.70
2	Light breeze	4-7	0.1-0.5	0.3	0.78	34.55	3.65	1.72
3	Gentle breeze	8-11	0.5-1.25	0.87	0.78	4.06	2.14	2.94
4	Moderate breeze	12-16	1.25-2.5	1.87	0.78	0.88	1.46	4.30
5	Fresh breeze	17-21	2.5-4.0	2.62	0.78	0.45	1.23	5.09
6	Strong breeze	22-27	4.0-6.0	5	0.78	0.12	0.89	7.03
7	Moderate gale	28-33	6.0-9.0	7.5	0.78	0.05	0.73	8.61
8	Fresh gale	34-40	9.0-14.0	11.5	0.78	0.02	0.59	10.66
9	Strong gale	41-48	< 14.0	14	0.78	0.01	0.53	11.76

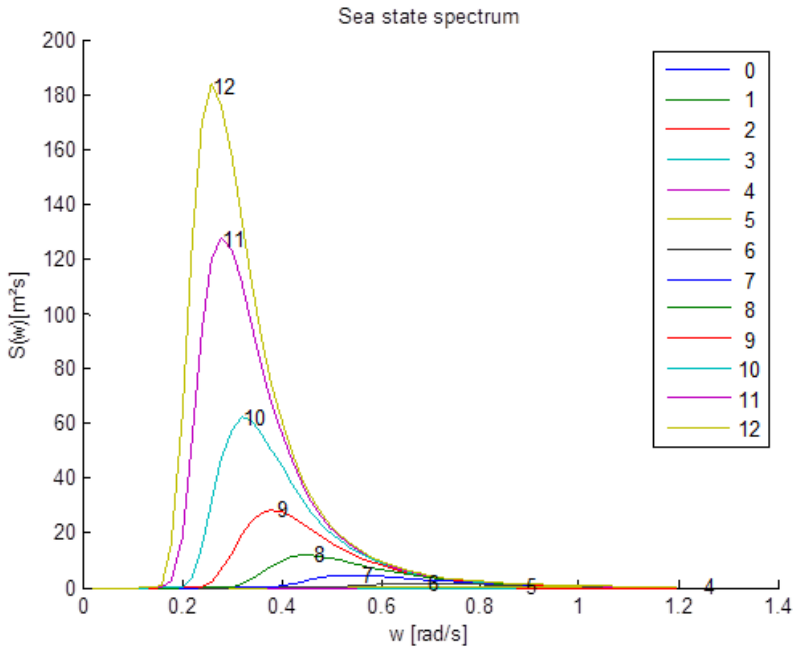

Figure C.1: Pierson-Moskowitz sea spectrum based on Beaufort scale

C.2 Response Amplitude Operator

The Response Amplitude Operators (RAO) are presented in Figures C.2 to C.13. The incidence angles vary from 180° to 135°. These angles are the operational variation angles for local sea state. A comparison is presented for three ship drafts of the FPWSO and the shuttle tanker: full draft, half draft and ballast condition. All RAO's have similar form in terms of response in period. This means they present the peak-frequency around the same value. However, they are different in terms of amplitude. In special, some great amplitude of yaw motion for the shuttle tanker is found in Figures C.7 and C.13, but the response in period is similar to the other drafts and to the FPWSO response.

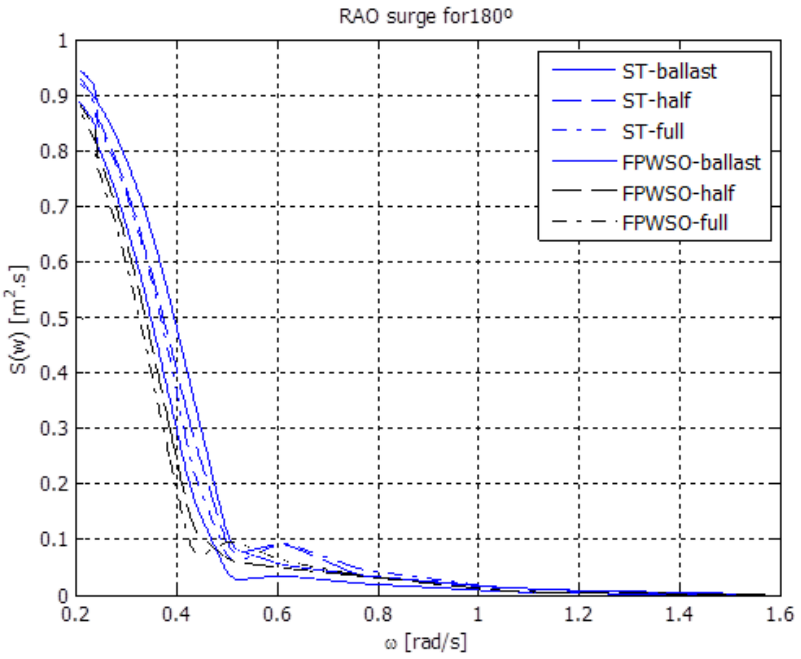

Figure C.2: Comparison between RAO for surge motion and 180° wave incidence

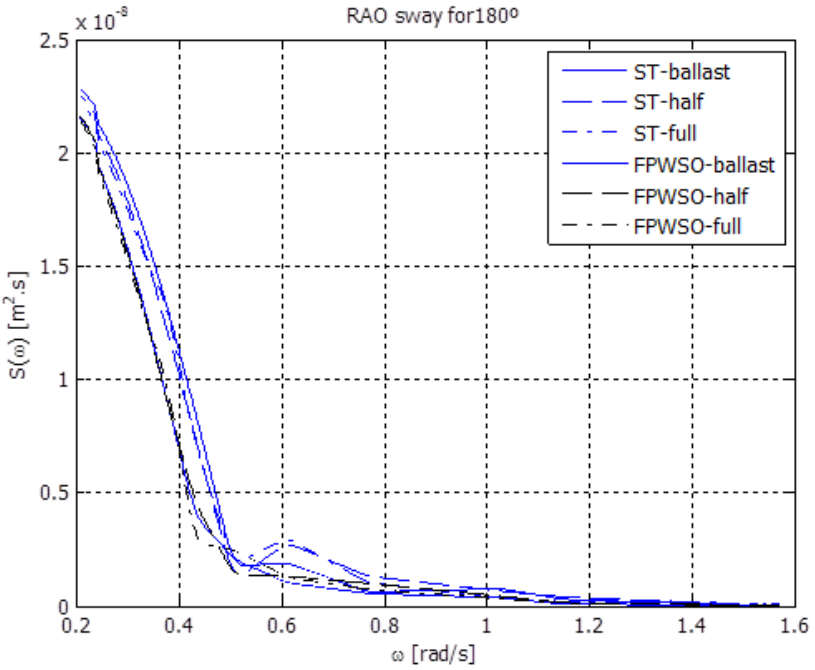

Figure C.3: Comparison between RAO for sway motion and 180° wave incidence

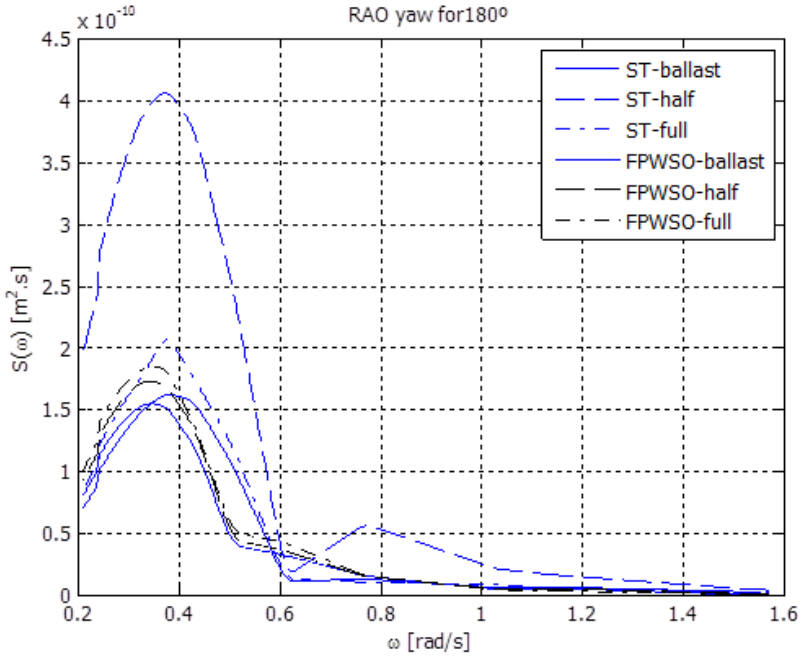

Figure C.4: Comparison between RAO for yaw motion and 180° wave incidence

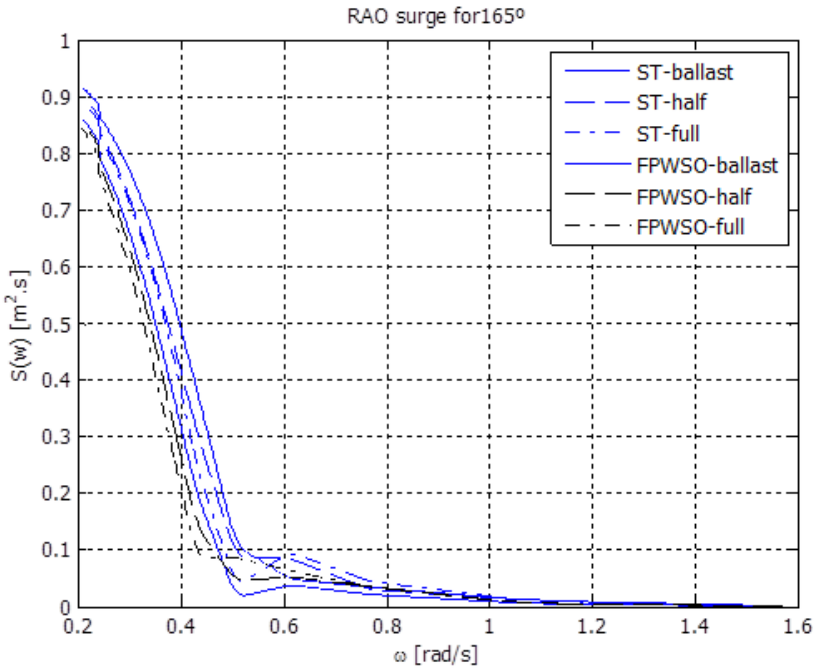

Figure C.5: Comparison between RAO for surge motion and 165° wave incidence

C.3 Ship Motion Spectrum

Once known the RAOs and the sea spectra, the response spectra of the wave-frequency motion of the vessel is determined as

$$S_r(\omega) = |RAO(\omega\beta)|^2 . S(\omega) \tag{C.6}$$

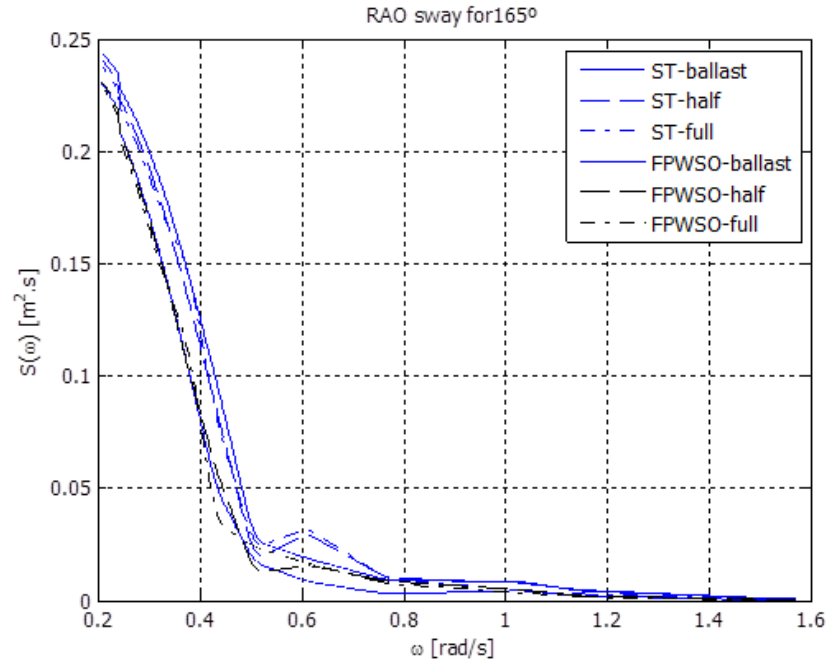

Figure C.6: Comparison between RAO for sway motion and 165° wave incidence

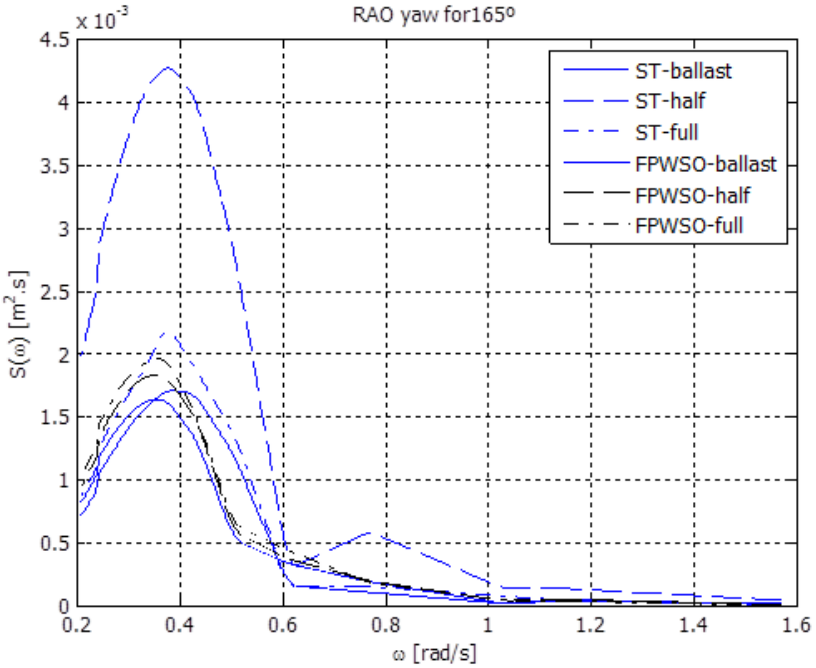

Figure C.7: Comparion between RAO for yaw motion and 165° wave incidence

where S_r is the response spectrum and β is the direction of the incident wave. Doing this calculation for the sea spectra for sea state 4 to 8 with the RAO's of the previous section, the motion spectra for the vessels in surge, sway and yaw are obtained. Figures C.14 to C.23 present the cross spectrum analysis. In these figures, there is a comparison between the response

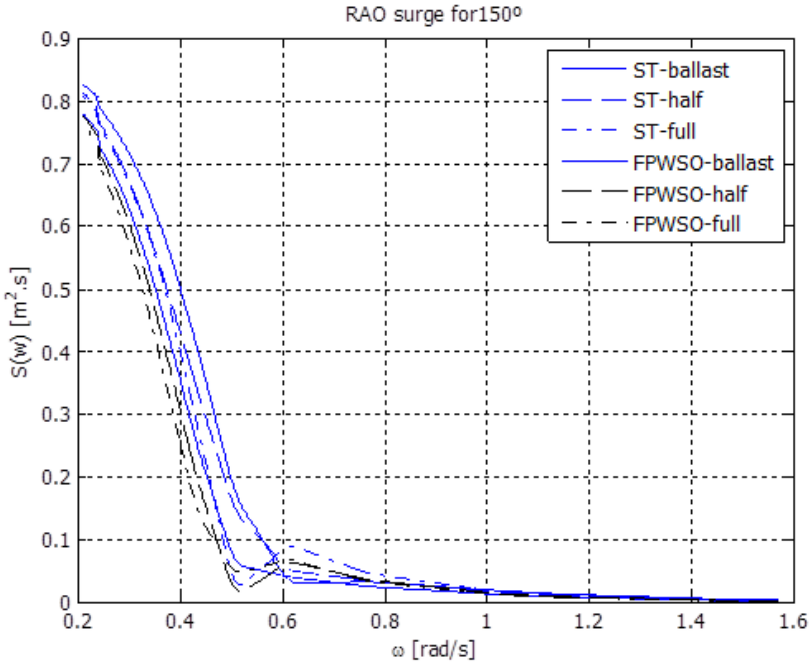

Figure C.8: Comparion between RAO for surge motion and 150° wave incidence

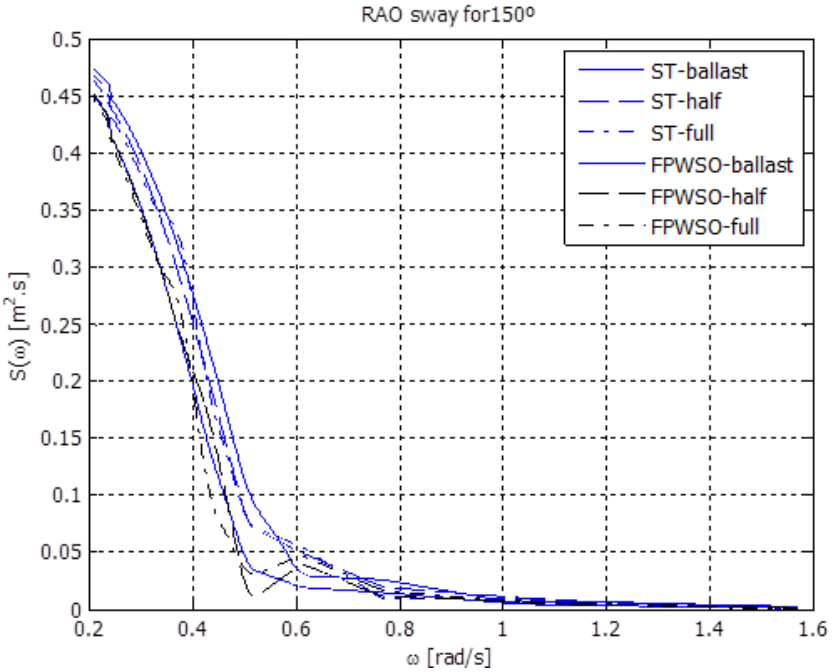

Figure C.9: Comparison between RAO for sway motion and 150° wave incidence

as function of the draft and the wave incidence angle for both vessels.

For sea state code 4, the cross spectra have very low amplitude and ω_p (peak frequency) around 1rad/s for both vessels. There is some bimodal response in 135° (Figure C.14), but still in high

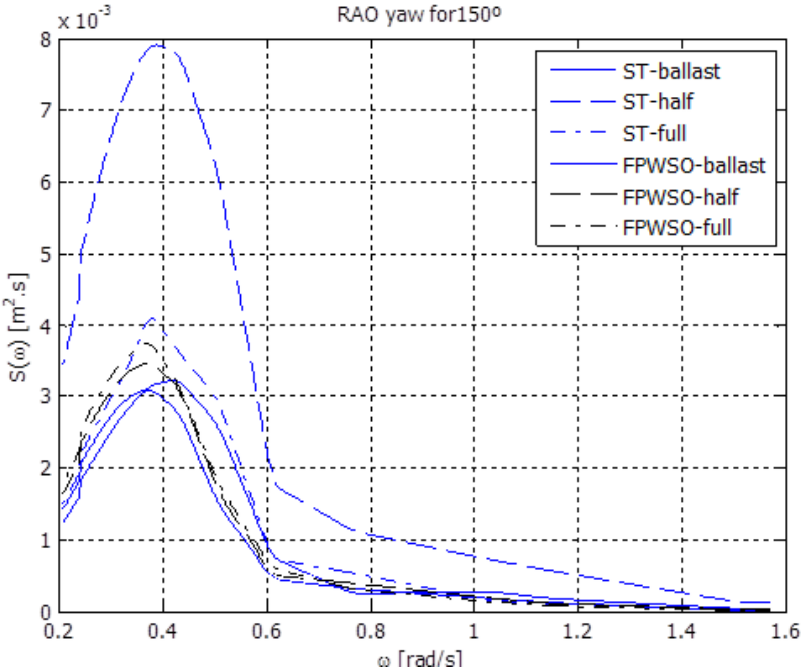

Figure C.10: Comparion between RAO for yaw motion and 150° wave incidence

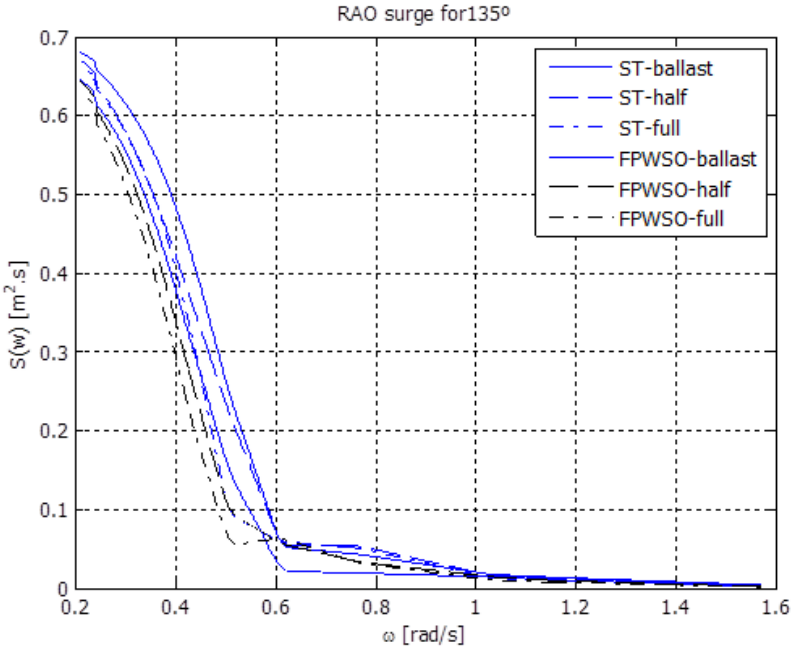

Figure C.11: Comparison between RAO for surge motion and 135° wave incidence

frequency. Sea state code 5 response presents little amplitude and ω_p between 0,6rad/s and 0,8rad/s. The wave incidence angle of 135° still shows bimodal response. Previous dynamical simulations have shown that some high frequency induces high frequency action of the thrusters

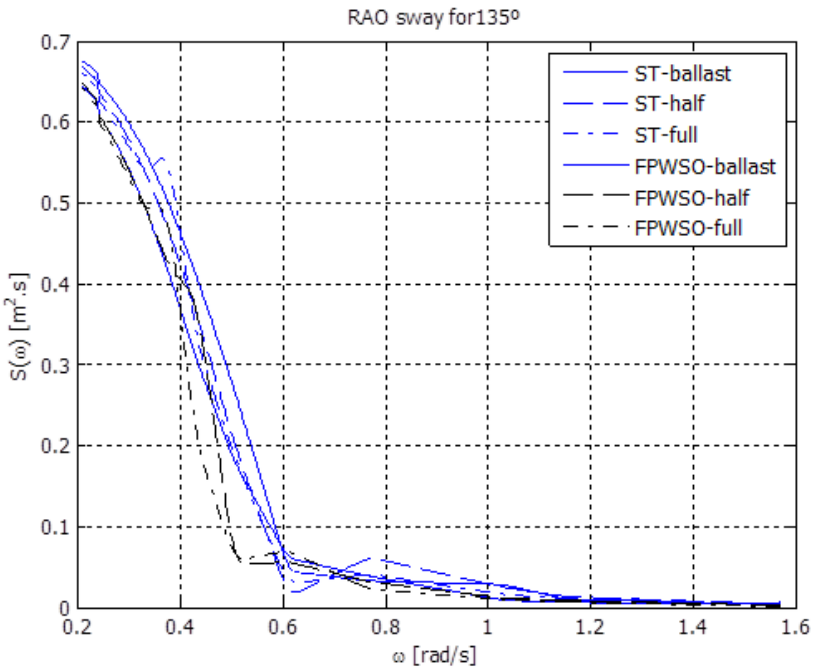

Figure C.12: Comparison between RAO for sway motion and 135° wave incidence

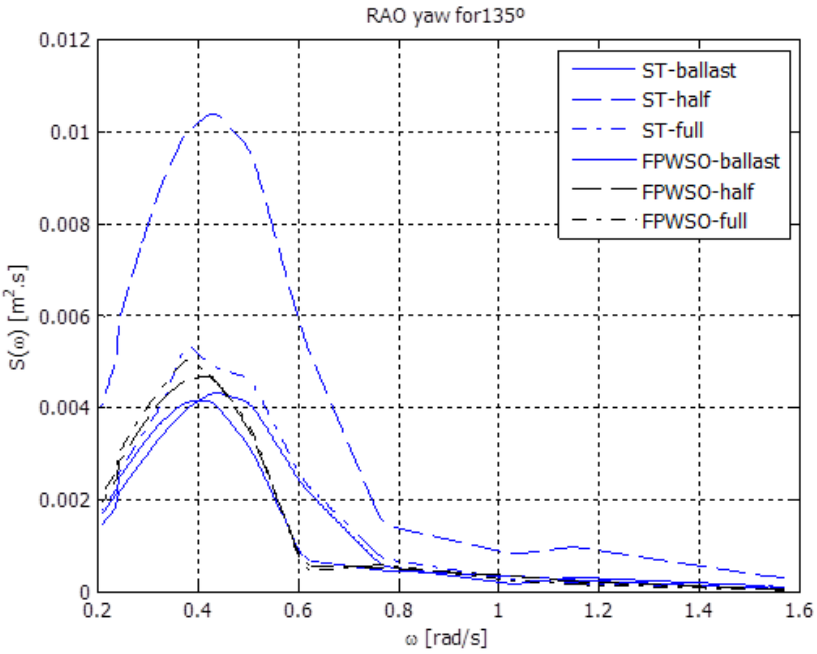

Figure C.13: Comparison between RAO for yaw motion and 135° wave incidence

for this range. Hence, the first cut-off frequency is around 0.8 rad/s.

The sea state 6 response has a higher amplitude than sea state 5 and the ω_p is a little more than 0.50rad/s. Due to the different amplitude between sea state code 5 and 6, some cross spectrum analyzes were carried out to investigate the high-frequency within this range. They have shown

that problems with filtering process have happened around ω_p between 0,6rad/s and 0,7rad/s. A simulation using a nonlinear observer with $\omega_p = 0.7 rad/s$ improved the thruster action filtering the high-frequency of thruster action. Hence, the second cut-off frequency is around 0.7 rad/s.

The response of the sea states 7 and 8 have the peak-frequency $\omega_p < 0.5$rad/s. Sorensen, Strand and Nyberg (2002) presented a study of a nonlinear observer for a shuttle tanker in extreme seas. In this work, the filter was shown within the bandwidth of the controller and the filter was no more necessary. Hence, the third-frequency of cut-off is around 0.5rad/s.

Dong (2005) presented a hybrid controller for a DP vessel in which the nonlinear observer parameters were modified due to the sea state variation. For $\omega_p < 0.45$rad/s, the author suggested the use of the nonlinear observer for extreme seas. For high values of the ω_p, the nonlinear observer proposed by Fossen and Strand (1999) was applied. In fact, the values of the ω_p used by Dong (2005) were used in previous simulations for the offloading operation and the results were very similar with the values found here by the cross spectral analysis. For convenience, the cut-off frequency for the offloading operation is assumed to be these values from Dong (2005). Table C.2 present these frequencies.

Some important facts need to be highlighted. The peak-frequency of the ship motion response does not change significantly due to the draft variation from full load to ballast condition for both vessels. Moreover, the peak-frequency also does not suffer the influence from the wave incidence angle within the considered incidence angle range, expect for some bimodal responses. However, these bimodal responses have the peak-frequency with higher energy around the wave peak-frequency and, for control applications, does not affect the cut-off frequency that has already chosen.

Table C.2: Nonlinear observer for offloading operation

Sea state	ω_p range [rad/s]	Observer
Calm seas	>0.79	Nonlinear with 1st order wave motion
Moderate seas	0.79-0.67	Nonlinear with 1st order wave motion
High seas	0.67-0.45	Nonlinear with 1st order wave motion
Extreme seas	<0.4	Nonlinear for extreme seas

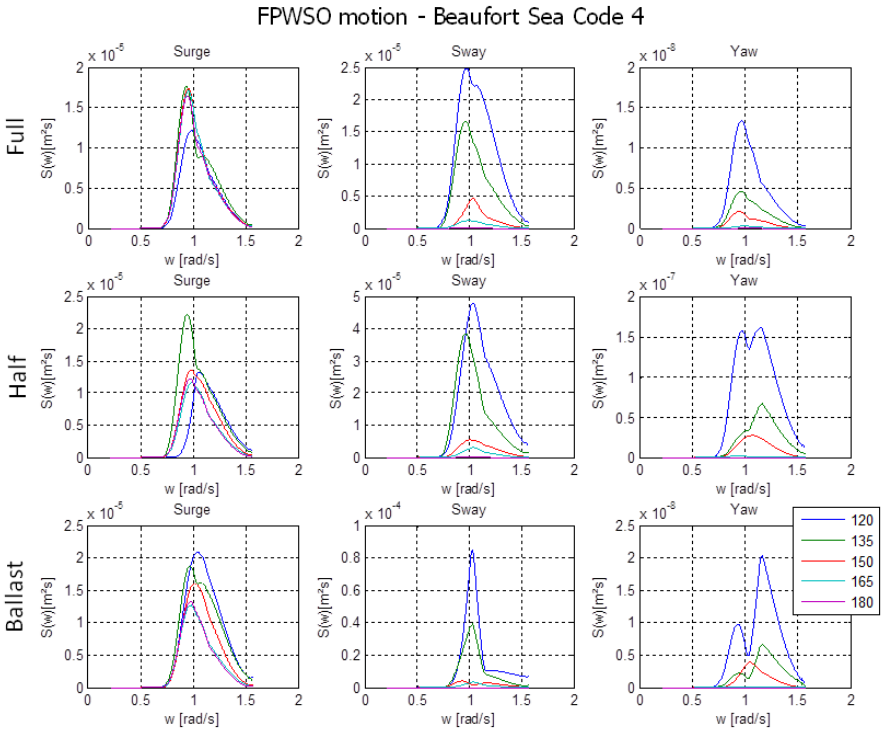

Figure C.14: Ship Motion Spectrum for FPWSO based on Beaufort seacode 4

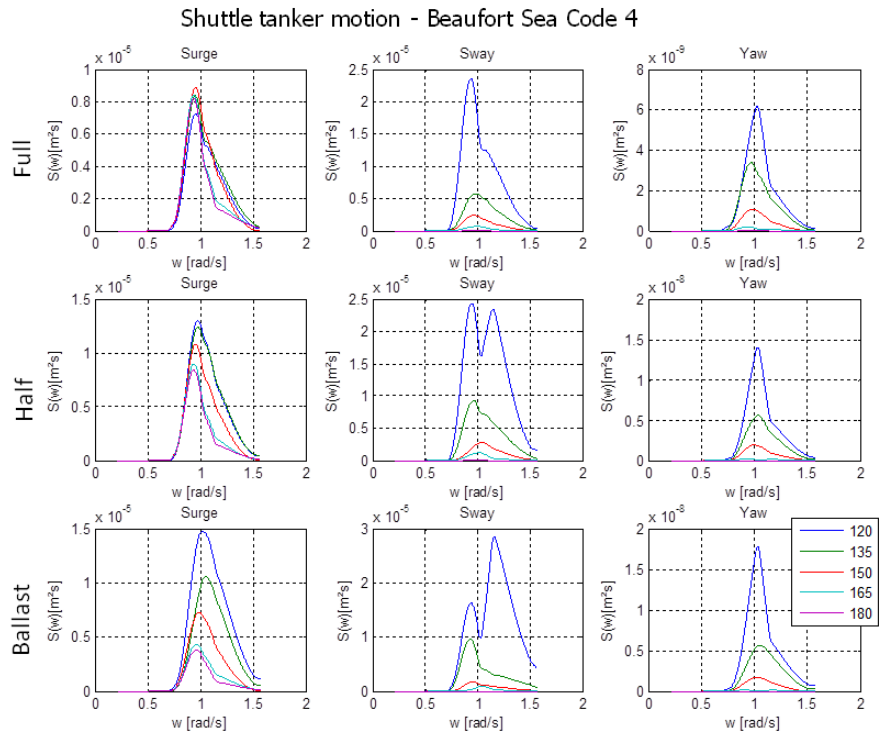

Figure C.15: Ship Motion Spectrum for ST based on Beaufort seacode 4

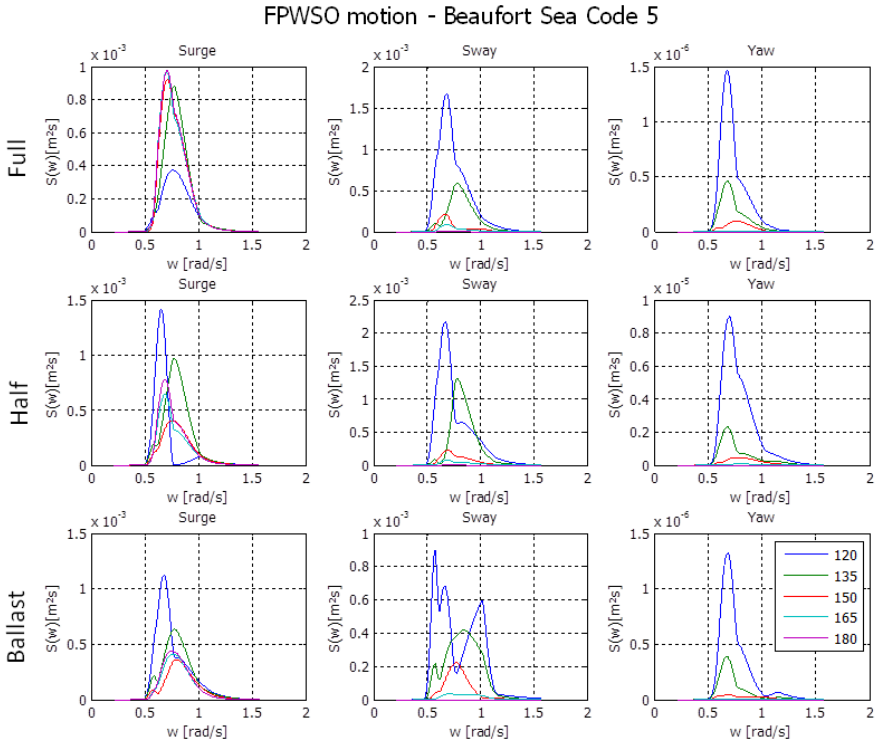

Figure C.16: Ship Motion Spectrum for FPWSO based on Beaufort seacode 5

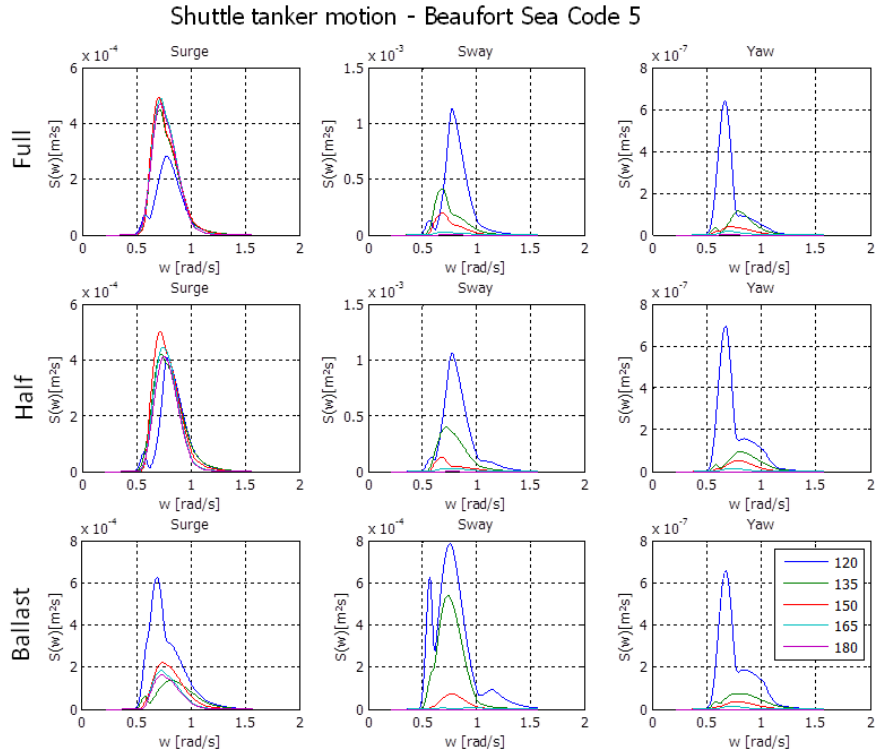

Figure C.17: Ship Motion Spectrum for ST based on Beaufort seacode 5

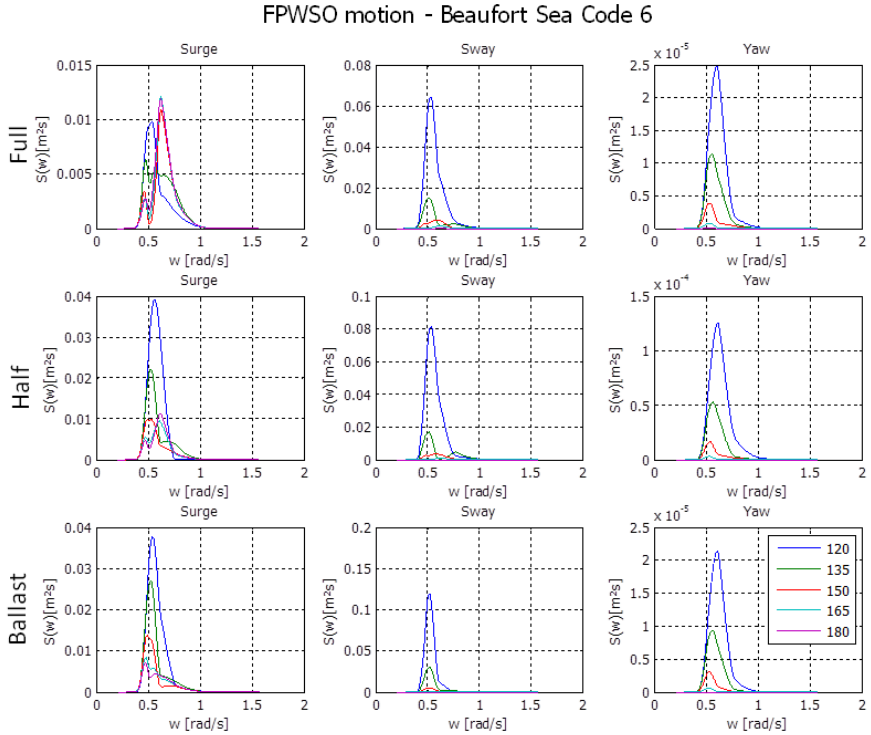

Figure C.18: Ship Motion Spectrum for FPWSO based on Beaufort seacode 6

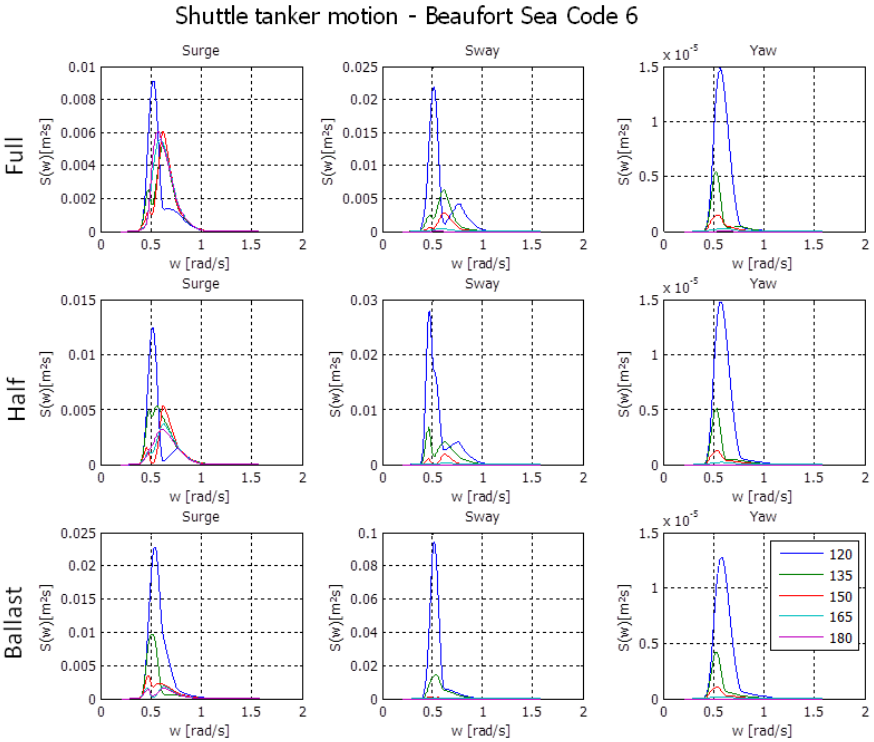

Figure C.19: Ship Motion Spectrum for ST based on Beaufort seacode 6

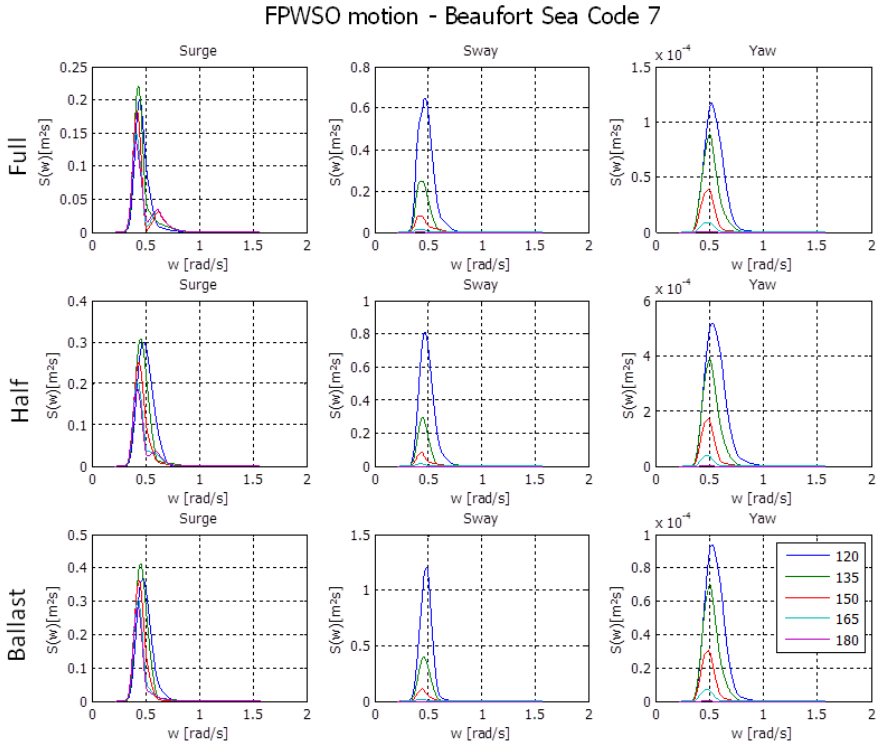

Figure C.20: Ship Motion Spectrum for FPWSO based on Beaufort seacode 7

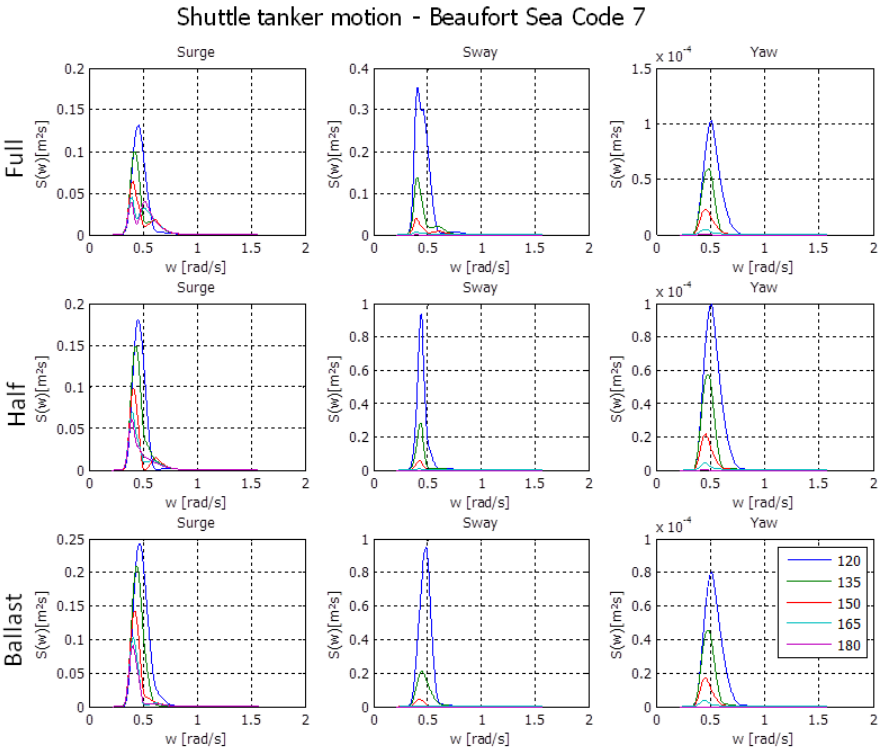

Figure C.21: Ship Motion Spectrum for ST based on Beaufort seacode 7

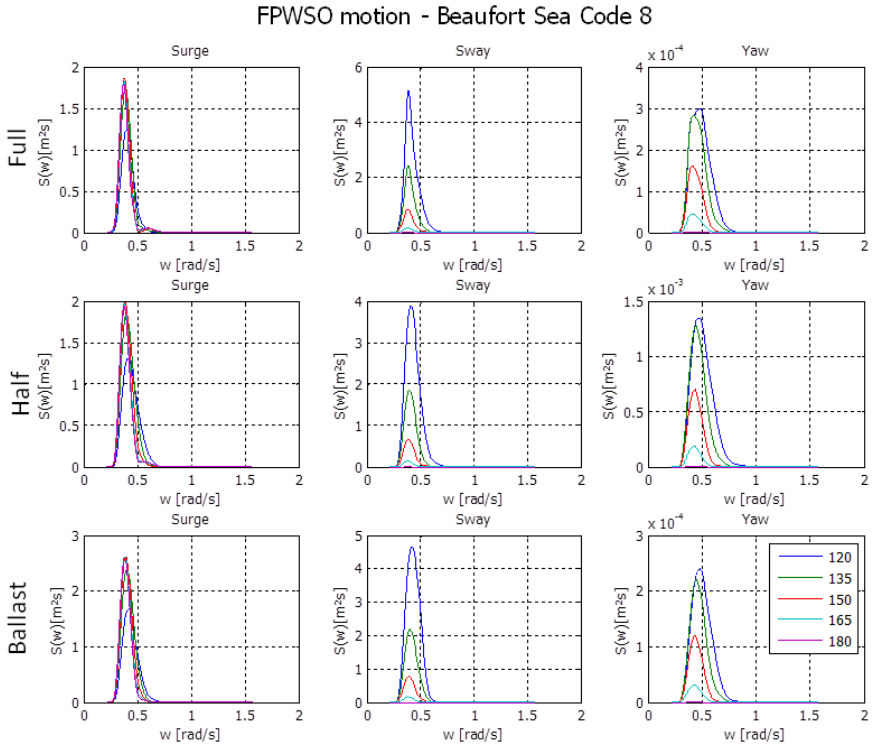

Figure C.22: Ship Motion Spectrum for FPWSO based on Beaufort seacode 8

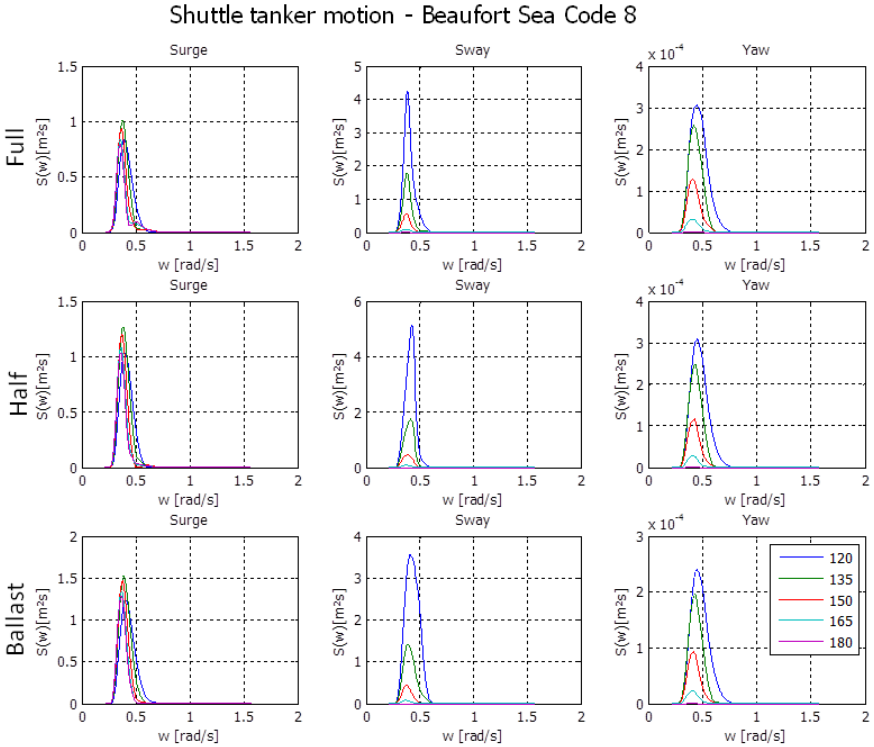

Figure C.23: Ship Motion Spectrum for ST based on Beaufort seacode 8

ANNEX

Annex A

Publications during the PhD Period

Journal Paper

TANNURI, E.A; AGOSTINHO, A.C.; MORISHITA, H.M.; MORATELLI, L.Jr. Dynamic positioning systems: experimental analysis of sliding mode control. **Control Engineering Practice**, p1-12, 2010.

Conference Papers

KUBOTA, L. MORISHITA, H.M., GREUELL, S., MORATELLI Jr, L. On the application of the empirical mode decomposition to dynamic positioning systems. **8th IFAC Conference on Control Applications in Marine Systems**, Rostock-Warnemünde, September 15-17, 2010.

MORATELLI. L. Jr.; MORISHITA, H.M.; TANNURI, E.A. Considerations on design of dynamic positioning system for shuttle tanker. **11th International Symposium on Practical Design of ships and Other floating structures** (PRADS2010), Rio de Janeiro, 2010.

MORATELLI, L. Jr.; COSTA, P.G.; De AMICIS, M. MORISHITA, H. M. Experimental evaluation of duct propellers in scale model. **23º Congresso Nacional de Transporte Aquaviário, Construção Naval e Offshore** (SOBENA 2010), Rio de Janeiro, 2010.

MORISHITA, H. M. et al. Avaliação de desempenho de posicionamento dinâmico em tanque de provas. **23º Congresso Nacional de Transporte Aquaviário, Construção Naval e Offshore** (SOBENA 2010), Rio de Janeiro, 2010.

MARANGONI, R. MORATELLI Jr., L. MORISHITA, H.M. Analysis of the Kalman Filter Performance and Tuning the Controller Parameters of a Dynamic Positioning System. **23º Congresso Nacional de Transporte Aquaviário, Construção Naval e Offshore** (SOBENA 2010), Rio de Janeiro, 2010.

RAMPAZZO. F.P., TANNURI, E.A., SILVA, J.L.B., PACIFICO, A.L., VIEIRA, D.P, MORATELLI, L. Jr. Numerical & Experimental tools for offshore DP operations. **Proceedings of the 30th International Conference on Ocean, Offshore and Arctic Engineering** (OMAE2011), June 19-24, Rotterdam, 2011.

MORISHITA, H.M., KUBOTA, L., VESTRI, M.S., GREUEL, S., MORATELLI, L. Jr. The Empirical Mode Decomposition Applied to Dynamic Positioning Systems. **Proceedings of the 30th International Conference on Ocean, Offshore and Arctic Engineering** (OMAE2011), June 19-24, Rotterdam, 2011.

TANNURI, E.A., MORATELLI, L. JR. VILETI, V.L., SILVA, J.L.B. Station Keeping and Propulsive Performance of a DP Crane Barge Close to a FPSO: A comprehensive set of experimental set. **Proceedings of the 31th International Conference on Ocean, Offshore and Arctic Engineering** (OMAE2012), July 1-6, Rio de Janeiro, Brazil, 2012.

TANNURI, E.A., MORISHITA, H.M., MIYAZAKI, M.R., MORATELLI, L. JR., MADUREIRA, R.M.L. Oil Transfer Between DP Shuttle and Conventional Tankers in Tandem Configuration: A Numerical Evaluation of Alternatives. **Proceedings of the 31th International Conference on Ocean, Offshore and Arctic Engineering** (OMAE2012), July 1-6, Rio de Janeiro, 2012.

MORISHITA, H.M.; MORATELLI Jr., L.; MARTINEZ, R.S. Performance comparison between linear and nonlinear controllers for a dynamic positioning system. **Proceedings of the 32th International Conference on Ocean, Offshore and Arctic Engineering (OMAE2013)**, June 9-14, Nantes, Brazil, 2013.

MORATELLI Jr., L.; MARANGONI, R.R.; MORISHITA, H.M; MARTINEZ, R.S. Observer-Lagrangian-based controller applied to two dynamically controlled vessels. **The 9th IFAC Conference on Control Applications in Marine Systems**, September 17-20, Osaka, Japan, 2013.

Remissive Index

V

W